

HYDROELASTIC ANALYSIS OF VERY LARGE FLOATING STRUCTURES

Alexey Andrianov

HYDROELASTIC ANALYSIS OF VERY LARGE FLOATING STRUCTURES

PROEFSCHRIFT

ter verkrijging van de graad van doctor
aan de Technische Universiteit Delft,
op gezag van de Rector Magnificus Prof. dr.ir. J.T. Fokkema,
in het openbaar te verdedigen ten overstaan van een commissie,
door het College voor Promoties aangewezen,

op vrijdag 9 september 2005 te 13.00 uur
door

Alexey (Olexiy) Igorevich ANDRIANOV,

Master of Science in Mechanics and Applied Mathematics
de Dnepropetrovsk Nationale Universiteit, Oekraïne,

geboren te Dnepropetrovsk, Oekraïne (Sovjet-Unie).

Dit proefschrift is goedgekeurd door de promotor:

Prof. dr.ir. A.J. Hermans

Samenstelling promotiecommissie:

Rector Magnificus,	voorzitter
Prof. dr.ir. A.J. Hermans,	EWI, Technische Universiteit Delft, promotor
Prof. dr.ir. J.A. Battjes,	CiTG, Technische Universiteit Delft
Prof. dr.ir. A.W. Heemink,	EWI, Technische Universiteit Delft
Prof. C.M. Linton,	Loughborough University, United Kingdom
Prof. M. Ohkusu,	Kyushu University, Japan
Prof. dr.ir. H.J. de Vriend,	CiTG, Technische Universiteit Delft
Prof. G. Zilman,	Tel Aviv University, Israel

ISBN 90-8559-081-7

Copyright © 2005 by Alexey Andrianov



This research was carried out in the section of Mathematical Physics at the Department of Applied Mathematics, Delft Institute of Applied Mathematics, Faculty of Electrical Engineering, Mathematics and Computer Science, Delft University of Technology, The Netherlands.

Keywords: diffraction, dispersion relation, elastic plate, fluid-structure interaction, free-surface elevation, hydroelastic analysis, hydroelastic response, incident surface waves, initiated wave pattern, integro-differential equation, offshore structure, plate deflection, plate-water interaction, reflection, transmission, very large floating platform (VLFP), very large floating structure (VLFS), water depth.

All rights reserved. No part of this publication may be reproduced, stored in a retrieval system or transmitted in any form or by any means, electronic, mechanical, photocopying, recording or otherwise, without the prior written permission of the author.

Typesetting system: L^AT_EX 2_ε.

Printed in The Netherlands by: Optima Grafische Communicatie, Rotterdam.

*To my parents,
my mother Valentina Lesnichaya
and my father Igor Andrianov*

Contents

Notations, abbreviations and keywords	xi
List of symbols	xiii
1 Introduction	1
1.1 The need for space	1
1.2 Very large floating structures	2
1.2.1 VLFS: pro et contra	3
1.2.2 Existing and proposed VLFSs and their applications	5
1.2.3 VLFS system	8
1.2.4 Mega-Float	9
1.3 Literature survey	9
1.3.1 VLFS analysis and basic assumptions	11
1.3.2 Methods	11
1.3.3 Water depth models	13
1.3.4 Related problems and applications	13
1.3.5 VLFS models and shapes	15
1.3.6 Mooring systems, breakwaters and anti-motion devices	16
1.4 Outline of thesis	17
1.5 Theory and method	18
2 General theory	21
2.1 Main information	21
2.2 General mathematical formulation	22
2.3 Thin plate theory	26
2.3.1 Free edge conditions	27
2.4 Water waves equations	28
2.4.1 General wave characteristics and equations	28
2.4.2 Infinite water depth	30
2.4.3 Finite water depth	31
2.4.4 Shallow water depth	31
2.5 Green's function	32
2.5.1 Green's function in Cartesian coordinates	33
2.5.2 Green's function in polar coordinates	35
2.6 Deflection	36

2.7	Integral and integro-differential equations	39
2.7.1	Formulation of integral equation	39
2.7.2	Integro-differential equation	40
2.7.3	General form of integro-differential equation	42
2.8	Additional information	43
2.8.1	The solution	43
2.8.2	Asymptotic expansions	43
3	Hydroelastic behavior of a semi-infinite plate and strip	45
3.1	Introduction	45
3.2	Formulation of the problem	46
3.3	Integro-differential equation	49
3.4	Finite water depth	50
3.4.1	Solution	51
3.5	Infinite water depth	55
3.6	Shallow water depth	57
3.7	Results, comparison and discussion	59
3.8	Conclusions	64
4	Hydroelasticity of a circular plate	67
4.1	Introduction	67
4.2	Formulation of the problem	68
4.3	Green's function and deflection	71
4.4	Infinite water depth	73
4.5	Finite water depth	77
4.6	Free-surface elevation and initiated wave pattern	79
4.7	Numerical results and discussion	80
4.8	Conclusions and summary	84
5	Hydroelastic behavior of a ring-shaped plate	87
5.1	Introduction and background	87
5.2	Mathematical formulation	89
5.3	Integro-differential equation	90
5.4	Green's function and deflection	92
5.5	Set of equations	94
5.6	Ring on water of infinite depth	96
5.7	Ring on water of finite depth	98
5.8	Free-surface elevation and initiated wave pattern	100
5.9	Numerical results	101
5.10	Conclusions	104
6	Hydroelasticity of a quarter-infinite plate	107
6.1	Introduction	107
6.2	Formulation of the problem	108
6.3	Solution in the main zone	110
6.4	Inner reflection	112

6.5	Matching conditions	113
6.6	Numerical results	116
6.7	Conclusions	117
6.8	Extensions	119
7	Hydroelastic behavior of a plate of finite draft	121
7.1	Introduction	121
7.2	Formulation	122
7.3	Solution	125
7.3.1	Deflection	125
7.3.2	Derivation and analysis of IDE	126
7.4	Zero draft order	129
7.5	First draft order	130
7.6	Numerical results and discussion	133
7.7	Extensions	136
7.8	Conclusions and discussion	137
8	General conclusions and recommendations	139
8.1	Main conclusions	139
8.2	Method	140
8.2.1	Extensions	141
8.3	Recommendations	142
8.4	Future of VLFS and VLFS for the future	143
	Bibliography	145
	Index	157
	Summary	159
	Samenvatting (summary in Dutch)	161
	Résumé (in Russian)	163
	Résumé (in Ukrainian)	165
	Acknowledgements	167
	Curriculum Vitae	171

Notations, abbreviations and keywords

VLFP	very large floating platform
VLFS	very large floating structure
VLMOs	very large mobile offshore structure
FWD	finite water depth
IWD	infinite water depth
SWD	shallow water depth
PFD	plate of finite draft
QIP	quarter-infinite plate
SIL	strip of infinite length
SIP	semi-infinite plate
SSIL	strip of semi-infinite length
IDE	integro-differential equation
IE	integral equation
BEM	boundary element method
FEM	finite element method
GOA	geometrical-optics approach
IDEM	integro-differential equation method
PLK	Poincaré-Lighthill-Kuo (Lindstedt) method
WHT	Wiener-Hopf technique
2D	two dimensional
3D	three dimensional

Keywords (general):

diffraction, dispersion relation, elastic plate, fluid-structure interaction, free-surface elevation, Green's function, Green's theorem, hydroelastic analysis, hydroelastic response, incident surface waves, initiated wave pattern, integro-differential equation, integro-differential equation method, offshore structure, plate deflection, plate-water interaction, reflection, transmission, very large floating platform, very large floating structure, water depth, zero-thickness assumption.

Keywords (additional):

chapter 3: semi-infinite plate, strip of infinite length;

chapter 4: circular plate, Bessel and Hankel functions;

chapter 5: ring-shaped plate, Bessel and Hankel functions;

chapter 6: matching conditions, quarter-infinite plate, ray method, wave modes;

chapter 7: finite draft, finite thickness, finite water depth, three-dimensional analysis.

References are given at the end of thesis and identified in the text by author(s) and number.

Summaries of this thesis in English, Dutch, Russian and Ukrainian are given at the end.

List of symbols

Common symbols, notations and definitions

x	horizontal coordinate, perpendicular to the plate edge
y	horizontal coordinate, along the plate edge
z	vertical coordinate, positive upwards from the free surface
ρ	polar coordinate, $\rho^2 = x^2 + y^2$
φ	polar coordinate, $\varphi = \arctan y/x$
\mathbf{x}	vector (x, y, z)
$\boldsymbol{\xi}$	vector (ξ, η, ζ)
\mathbf{n}	normal vector
s	arc-length along the edge
Δ, ∇^2	Laplacians
i	imaginary number, $i = \sqrt{-1}$
e	constant, $e = 2.7182818\dots$
π	constant, $\pi = 3.14159265\dots$
g	gravity acceleration, $g = 9.80663 \text{ m/s}^2$ (average)
t	time
ω	wave frequency
h	water depth
ρ_w	density of fluid (water)
A	wave amplitude of incident waves
H_w	wave height, $H_w = 2A$
K	wavenumber, IWD, $K = \omega^2/g$
k_0	wavenumber, FWD, positive real root of $k \tanh kh = K$
k_{sh}	wavenumber, SWD, $k_{\text{sh}} = \omega/\sqrt{gh}$
λ	wavelength of incident waves, $\lambda = 2\pi/K$
β	angle of incidence
β_{cr}	critical angle of incidence
ρ_p	density of the plate
h_p	plate thickness
d	plate draft

m	mass per unit area of the plate
D	flexural rigidity of the plate
E	Young's modulus
ν	Poisson's ratio
\mathcal{D}	introduced structural parameter, $\mathcal{D} = D/\rho_w g$, m^4
μ	introduced structural parameter, $\mu = m\omega^2/\rho_w g$
$\Phi(\mathbf{x}, t)$	total velocity potential
$\Phi(\boldsymbol{\rho}, t)$	total velocity potential, polar coordinates
$\phi(\mathbf{x})$	velocity potential, of harmonic waves
$\phi^{\text{inc}}(\mathbf{x})$	incident wave potential
$\phi^{\mathcal{P}}(\mathbf{x})$	potential in the plate area
$\phi^{\mathcal{F}}(\mathbf{x})$	potential in the open-water area
$\phi^{\text{dis}}(\mathbf{x})$	diffracted wave potential, in open water
$V(\mathbf{x}, t)$	fluid velocity vector
$V(\boldsymbol{\rho}, t)$	fluid velocity vector, in polar coordinates
$W(x, y, t)$	vertical free-surface elevation
$w(x, y)$	plate deflection
$\zeta(x, y)$	free-surface elevation
$\zeta^{\text{inc}}(x, y)$	free-surface elevation due to the incident wave
$\zeta^{\text{pm}}(x, y)$	free-surface elevation generated by the plate motion
$P(\mathbf{x}, t)$	pressure in the fluid
P_{atm}	atmospheric pressure
κ	general wavenumber, in the plate area
κ_n	reduced wavenumber, $\kappa_n^2 = \kappa^{(n)^2} - k_0^2 \sin^2 \beta$
$\kappa^{(n)}$	root of the plate dispersion relation
k	coordinate in the complex plane
k_i	root of the water dispersion relation
\mathcal{L}	contour of integration in the complex plane
\mathcal{L}'	contour of integration in the complex k -plane, FWD
\mathcal{FS}	free surface, $z = 0$
\mathcal{F}	open fluid region of \mathcal{FS}
\mathcal{P}	plate region of \mathcal{FS}
\mathcal{S}	dividing surface at \mathcal{FS}
$\mathcal{D}^{\mathcal{F}}$	open fluid domain
$\mathcal{D}^{\mathcal{P}}$	part of the fluid domain covered by the plate
$\partial\mathcal{D}$	vertical boundary surface, between $\mathcal{D}^{\mathcal{F}}$ and $\mathcal{D}^{\mathcal{P}}$
\mathcal{SB}	sea-bed (bottom surface)
\mathcal{S}_s	plate vertical side surface
$\mathcal{G}(\mathbf{x}, \boldsymbol{\xi})$	Green's function
$J_n(z)$	Bessel function with argument z of n -th order
$H_n^{(1)}(z)$	Hankel function of first kind of n -th order
$H_n^{(2)}(z)$	Hankel function of second kind of n -th order
$\delta(\mathbf{x}, \boldsymbol{\xi})$	Dirac function
R	horizontal distance to source, $R^2 = (x - \xi)^2 + (y - \eta)^2$

a_n, b_n	amplitudes of the wave modes, coefficients of the deflection
a_{mn}, b_{mn}	amplitudes of the wave modes
M, N	truncation parameters of the problem
R	reflection coefficient
T	transmission coefficient
R_∞	reflection coefficient, SIP
\mathcal{O}	order symbol

Chapter 3

l	width of the strip
\mathcal{F}	$x < 0$ ($\cup x > l$ for strip)
\mathcal{P}	$x > 0$ ($\cup x < l$ for strip)
\mathcal{S}	$x = 0$ ($\cup x = l$ for strip)
r	horizontal distance

Chapter 4

r_0	radius of the circle
\mathcal{F}	$\rho > r_0$
\mathcal{P}	$\rho < r_0$
\mathcal{S}	$\rho = r_0$

Chapter 5

r_0	outer radius of the ring
r_1	inner radius of the ring
\mathcal{F}	$\rho > r_0 \cup \rho < r_1$
\mathcal{F}_0	open water, outer free surface, $\rho > r_0$
\mathcal{F}_1	gap area, inner free surface, $\rho < r_1$
\mathcal{P}	$r_1 < \rho < r_0$
\mathcal{S}	$\rho = r_0 \cup \rho = r_1$

Chapter 6

θ, γ	angles of inner reflection
$w_s(x, y)$	deflection due to inner reflection

Chapter 7

$a_n^{(q)}$	amplitudes with respect to draft order, $q = 0, 1$
$\kappa_n^{(q)}$	reduced wavenumbers, $q = 0, 1$
$w^{(q)}(x)$	deflection term with respect to draft order

Chapter 1

Introduction

This thesis considers fluid-structure interaction, more specifically, the interaction between water waves and very large floating structures. A solution is derived for different problems of the hydroelastic motion of a very large floating structure in water waves. In this chapter the general introduction, literature survey and outline of thesis are given. First, the background of the fluid-structure interaction problem is presented. The concept of floating structures and their possible applications are described. A literature survey then gives the information about problems studied by researchers and engineers, methods developed, and results derived. Also, through the literature survey an overview is given of what has been already done in the analysis of very large floating structures and what problems remain. Next, the general problem, theories used and the main objectives of our study are given. Further, this introduction describes the direction of analysis and the method developed, and briefly reviews the mathematical operations applied. The information about six problems considered in the thesis is given.

1.1 The need for space

Buy land. They've stopped making it.

MARK TWAIN, XIX century.

N.B. Production is resumed.

VLFS RESEARCHERS, XXI century.

Wanted! A comfortably-appointed, well-drained desert island, neighbourhood of South Pacific Ocean preferred.

JEROME K. JEROME, Three Men in a Boat.

Seen from space, the Earth looks like a blue colored planet with constantly moving swirls of clouds of Earth's everchanging weather. The Earth is mostly blue because the main part of its surface is covered by oceans, seas, lakes, rivers, etc. The Earth's land surface measures 148,300,000 square kilometers, while the total area of the Earth's surface is 510,083,000 square kilometers. Thus the water surface area takes up 70 percent of the Earth's total surface area; the land only 30 percent, less than one third of the entire surface. We have only a very small part of the Earth to live on.

In the twentieth century, humanity ran into a new problem: lack of land. Now, in the beginning of the third millennium, this problem is becoming serious, with the fast growth of the Earth's population and corresponding expansion of industrial development and urban agglomeration. Countries such as Japan, China, Korea, the Netherlands, and Belgium have a very high population density. Many other countries in Europe and Asia are approaching the same density.

Many developed island countries and countries with long coastlines in need of land have for some time now been successfully reclaiming land from the sea to create new space and, correspondingly, to ease the pressure on their heavily-used land space. The Netherlands, Japan, Singapore and other countries have expanded their areas significantly through the land reclamation works. Such works are, however, subject to constraints, such as the negative environmental impact on the coastlines of the country and neighboring countries and marine ecological system, as well as huge economic costs in reclaiming land from deep coastal waters, especially when the sand for reclamation has to be bought from other countries [143]. Also, land reclamation is a good solution only for rather shallow waters with a depth of no more than 20 meters.

In response to the aforementioned needs and problems, researchers and engineers have proposed an interesting and attractive solution — the construction of very large floating structures (VLFS for short). These offshore structures can be located near the shore as well as rather far into the open sea. Very large floating structures, their behavior in and response to water waves (in other words, a hydroelastic analysis of the VLFS) are the main topics of this thesis.

1.2 Very large floating structures

Very large floating structures (or, as some literature refers to them, very large floating platforms, VLFP for short) can be constructed to create **floating** airports, bridges, breakwaters, piers and docks, storage facilities (for instance for oil), wind and solar power plants, for military purposes, to create industrial space, emergency bases, entertainment facilities, recreation parks, mobile offshore structures and even for habitation. Actually, the last could become reality sooner than one may expect: already different concepts have been proposed for building floating cities or huge living complexes.

VLFSs may be classified under two broad categories [143], namely the pontoon-type and the semi-submersible type. The former type is a simple flat box structure and features high stability, low manufacturing cost and easy maintenance and repair. In open sea, where the wave heights are relatively large, it is necessary to use the semi-submersible VLFS type to minimize the effects of waves while maintaining a constant buoyant force. VLFSs of the semi-submersible type are used for oil or gas exploration in sea and other purposes. They are fixed in place by column tubes, piles, or other bracing systems.

In contrast, the **pontoon-type VLFS** just floats (lies) on the sea surface. The pontoon-type VLFS is very flexible compared to other kinds of offshore structures, so that the elastic deformations are more important than their rigid body motions. Thus, hydroelastic analysis takes center stage in the analysis of the pontoon-type VLFSs. Together with the motion of the floating structure, the response of the structure to water waves and the impact on the entire fluid domain have to be studied.

Pontoon-type VLFSs are also known in the literature as mat-like VLFSs because of their small draft in relation to the length dimensions. Very large pontoon-type floating structure is often called Mega-Floats. As a rule, the Mega-Float is a floating structure having at least one length dimension greater than 60 meters. Horizontally large floating structures can be from 500 to 5000 meters in length and 100 to 1000 meters in width, while their thickness can be of the order of about 2—10 meters.

The largest offshore structure built so far is the Mega-Float, a floating runway prototype constructed in Tokyo Bay, which is shown in figure 1.1. The information about this structure is given in subsection 1.2.4. Other proposed and already existing VLFSs and their possible applications are described in subsection 1.2.2.



Figure 1.1: The Mega-Float, a floating airport prototype, Tokyo Bay, Japan.

Unlike the top surface of vessels, that of a VLFS is used as the ground, and therefore the floating structure should provide a very large surface area. It can be constructed by joining the necessary number of floating units together. The design of the floating structure must obey safety and strength requirements, operating conditions, etc. Steel, concrete (prestressed or reinforced hybrid) or steel-concrete composite materials may be used to build the floating structure. The motions of the floating structure must be less than those allowed to ensure the safety of people and facilities on a VLFS. Generally, floating structures shall be moored at the same site for a long time.

In the next subsection the advantages and disadvantages of VLFSs are discussed.

1.2.1 VLFS: pro et contra

Very large floating structures have the following advantages over traditional land reclamation:

- they are easy and fast to construct (components may be made at shipyards and then be

transported to and assembled at the site), thus, the sea space can be quickly exploited;

- VLFSs can easily be relocated (transported), removed, or expanded;
- VLFSs are cost effective when the water depth is large;
- the construction of VLFSs is not greatly affected by the depth of the water, sea bed profile, etc.;
- the position of VLFSs with respect to the water surface is constant; hence VLFSs can be used for airports, piers, etc.;
- they are environmentally friendly as they do not damage the marine ecological system, or silt up deep harbors or disrupt the ocean/sea currents;
- the structures and people on VLFSs are protected from seismic shocks since the energy is dissipated by the sea.

However, the pontoon-type floating structure is only suitable for use in calm waters, associated with naturally sheltered (by islands and peninsulas) coastal formations, often in bays, lakes or sea areas near the shoreline. To reduce the impact of waves on pontoon-type VLFS, breakwaters are usually constructed nearby. Also special anti-motion devices, anchoring or mooring systems can be used to stabilize the behavior of the VLFSs.

The very large floating structure is a reliable structure. The interior of the VLFS is divided into many buoyancy air chambers; hence, even if water leaks into one or two chambers, the neighboring chambers will provide sufficient buoyancy for the complete structure.

In contrast to ship behavior in waves, the VLFS, due to its large dimensions, covers many cycles of wave crests and wave troughs, causing the waves to cancel each other out, and it is therefore not affected by the movement of waves under it. A very small local deflection phenomenon, which is obscured by overall movement in the case of ships, occurs in the structure. This phenomenon, known as elastic response, is an oscillatory propagation of local deflection caused by waves from one end of the floating structure to the other and studied in this thesis. The movement caused by this phenomenon is so slight that it can hardly be noticed; nevertheless it must be investigated to ensure the functionality and stability of the offshore structure.

The safety design of the VLFS obeys the multistage reliability principle, see [104]: the measures required against airplane accidents and extreme marine and meteorological conditions. Floating unit joining, floating execution and environmental assessment technologies, safety regulations, trends of development of new technologies are described in, e.g., [104, 143].

The lifetime of floating structures of the proposed concepts is about 100 years (at least 50 years), so the structure can be used for a very long time (with maintenance if any is needed).

Various measurements were done to study the impact of a VLFS on the marine ecological system. The results showed that the installation of a VLFS has only a small effect on the natural ecosystem.

The overview of VLFSs constructed worldwide and those proposed is given in the next section. Further, subsection 1.2.3 describes the basic concept of a VLFS system.

1.2.2 Existing and proposed VLFSs and their applications

Very large floating structures have already been used for different purposes for quite some time in Japan, Canada, Norway, USA, UK, Brazil, Saudi Arabia, and Vietnam. China, Korea, Israel, the Netherlands, Germany, New Zealand, and Singapore are going to do so in the near future. Here we give a brief overview of already completed VLFSs and describe the most interesting proposed VLFS applications.

Japan, the world's leader in constructing VLFSs, constructed the Mega-Float [157, 158, 47, 104], a VLFS test model for floating airport terminals and airstrips in Tokyo Bay. Also in Japan, recently the following offshore structures have been constructed: the floating oil storage systems Kamigoto and Shirashima, the Yumemai floating swing bridge in Osaka [140], the floating emergency rescue bases in Yokohama, Tokyo and Osaka, and floating bridges, piers, amusement facilities, and many other offshore structures. The Mega-Float is shown in figure 1.1 and the Kamigoto Oil Storage Base in figure 1.2.

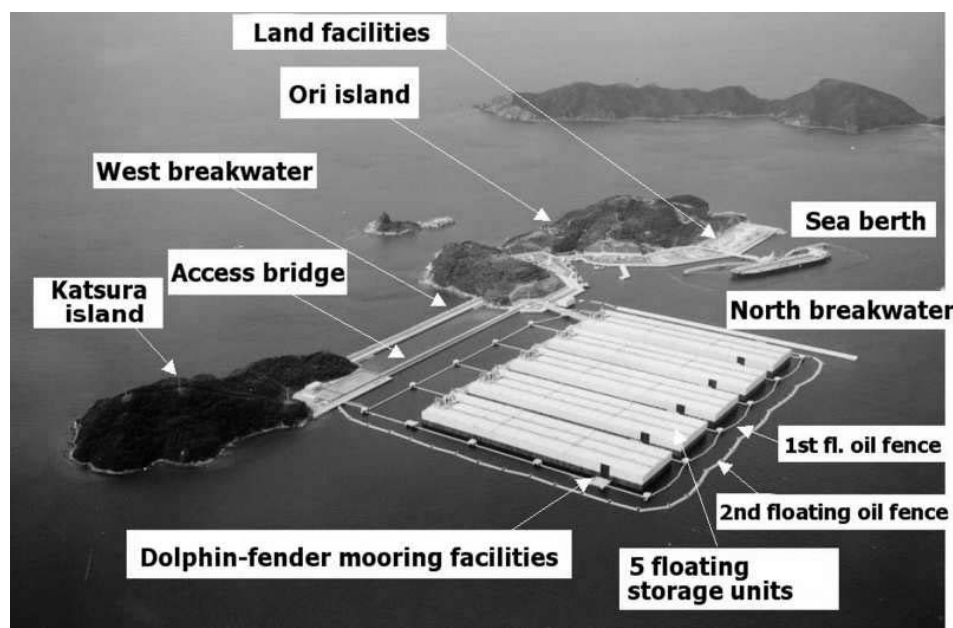


Figure 1.2: Kamigoto Floating Oil Storage Base, Nagasaki Prefecture, Japan.

Canada built a floating heliport in Vancouver and the Kelowna floating bridge. Norway has the Bergsøysund floating bridge and the Nordhordland bridge, which has a floating part. The United States has the floating bridges in Washington state. The United Kingdom, Saudi Arabia, Brazil and other countries also use floating structures for bridges and other purposes. The 'previous generation' of VLFSs are ships moored to the shore or reefs and are widely used in various countries. There are many proposals concerning the design, use and purposes of newly constructed VLFSs.

The earliest application of the pontoon-type VLFS is the **pontoon (floating) bridge** [144, 159]. Watanabe et al. [141, 144] described the history and worldwide development of floating bridges. The most famous bridges constructed in different countries are: the Galata Floating Bridge (1912) in Istanbul, the First (1940), the Second (1963), and the Third Bridge (1989, Lacey Murrow), on Lake Washington, and Hood Canal Bridge (1961)

near Seattle in Washington state, the Kelowna Floating Bridge (1958) in British Columbia, Canada, the Bergsøysund Bridge (1992) and the Nordhordland Bridge (1994) over the deep fjords in Norway, a West India Quay Footbridge in the Docklands, London (1996), the Admiral Clarey Bridge in Hawaii (1998), Seebrücke (2000) in Saxony-Anhalt, Germany, a new swing floating arch bridge, Yumemai Bridge, in Osaka (2000), and pontoon bridges on the rivers Amudarya and Syrdarya rivers in Uzbekistan and Turkmenistan (1989–2005). Also, floating bridges were built in Austria, France, India, the Netherlands (Antilles), Russia, etc. A complete list of the pontoon bridges still in use and demolished can be found at [159].



Figure 1.3: Yumemai floating bridge, Osaka, Japan.

The Yumemai Bridge [140, 151] shown in figure 1.3 was constructed to connect the reclaimed islands Yumeshima and Maishima across the North Waterway in the Port of Osaka. The bridge is a movable floating arch bridge standing on two floating pontoons, which can swing around the pivot with the assistance of tugboats. It has a total length of 940 meters with a floating part length of 410 meters and a width of 38.8 meters for six traffic lanes.

In addition, large floating offshore structures can also be used for **floating docks, piers and container terminals**. Many floating docks, piers, and berths are already in use. Floating piers have been constructed in Hiroshima, Japan, and Vancouver, Canada. In Valdez, Alaska, a floating pier was designed for berthing the 50000-ton container ships. The main advantage of a floating pier is its constant position with respect to the waterline. Thus, floating piers allow smooth loading and unloading of cargo because of the equal tidal rise and fall of the pier and ship/ferry. Floating docks have been constructed in the USA and other countries. In case of rather deep water, floating structures are a good alternative to traditional harbor facilities. Research on floating harbor facilities, their design and analysis is going on in many countries [144].

One of the applications of very large floating structures is the **floating storage facility**. VLFSs have already been used for storing fuel. An offshore oil storage facility is constructed like flat box-shaped tankers connected to each other and to other compo-

nents of the VLFS system, as shown in figure 1.2. Japan has two (the only two in the world so far) floating oil storage systems: Kamigoto (1990, near Nagasaki) and Shirashima (1996, near Kitakyusyu) with a capacity of 4.4 and 5.6 million kiloliters, respectively. The Kamigoto Oil Storage Base, figure 1.2, is the first oil storage base of the floating type. It consists of five huge connected barges, each having a capacity of 880 thousands kiloliters, moored with large dolphins and rubber fenders. Complete information on the design, experiments and mooring of the oil storage bases is given, e.g., in [151].

As floating structures are well protected from seismic shocks and can be moved, they can be used as convenient and functional **floating emergency bases**. Three Floating Disaster Prevention Bases were completed in Japan in 2000 in bays near Yokohama (Tokyo Bay), Osaka (Osaka Bay) and Nagoya (Ise Bay). All the bases have mooring facilities, a heliport, interior storage spaces for cargo, and a track crane. Three bases are of the movable type and used as floating piers at normal times. Specifications of the floating rescue bases can be found in [151, 144].

Floating plants are also possible applications of VLFSs. There are proposals to use VLFSs for wind and solar power plants [120, 122] and studies on this are already underway. The Floating Structure Association of Japan has presented concept designs of a clean power plant. Floating power plants for various types of energy are already being used in Brazil, Japan, Bangladesh, Saudi Arabia, Argentina, and Jamaica.

Certainly, VLFS can also be used for **floating entertainment facilities**. Very large floating structures of different dimensions and design are and can be used for hotels, restaurants, shopping centers, amusement and recreation parks, exhibition centers, theaters, cinemas, fishing piers, etc. VLFSs having been or being constructed are for example the Aquapolis exhibition center in Okinawa (1975, already removed), the Floating Island near Onomichi, and another one resembling the Parthenon near Hiroshima, all in Japan, and floating hotels in Australia, Vietnam and North Korea, floating restaurants in Japan, Hong Kong, Russia, Ukraine and other countries. An attractive panoramic view is one of the advantages floating entertainment facilities offer.

One of the most attractive applications of a VLFS is the **floating airport**. For some time now, scientists and engineers have been studying the possibility of constructing a floating airport in coastal waters. With the growth of cities and increase in air traffic, there is a need for airport expansion. In Asia, great progress is being made in constructing airports or airport facilities in the sea. Kansai International Airport (1994), Osaka, Japan, is the first airport in the world completely constructed in the sea, although on an artificial island. Airports with runways on reclaimed islands in the sea are Chek Lap Kok International Airport (1998), Hong Kong, China; Incheon International Airport (2001), Seoul, Korea; Changi airport, Singapore; and Central Japan International Airport (CentAir, 2005), Nagoya. Kobe Airport, Japan, will finish construction of runway in the sea in 2006, Haneda Airport, Tokyo, Japan, has decided to build one soon. However, the intensive research on floating airports is continued in Japan (Tokyo, Osaka), USA (San Diego) and many other countries. In the past, military engineers have constructed floating airfields for temporary use consisting of connected pontoons, and nowadays, research is being conducted going on the floating airport for military purposes. The first large runway constructed was the Mega-Float, figure 1.1; further information is given in subsection 1.2.4.

Henceforward in the thesis, we will mainly consider floating platform with the dimen-

sions and other parameters required for the floating airport. Floating helicopter ports have already been constructed in Vancouver, Canada and other places.

The **very large mobile offshore structure** (VLMOS) is the 'next generation' of very large floating structures. Another name for VLMOS is mobile offshore base (MOB). VLMOSs can also be used for different purposes in the sea, and their mobility is their main advantage compared to other sea-usage solutions. In Japan, proposals have been made to use VLMOSs for disaster prevention bases [151], wind and solar power plants [120, 122], while the Office of Naval Research, USA, initiated studies in order to provide logistic support for military operations when fixed bases are not available.

In response to Mark Twain and Jerome K. Jerome (see the beginning of this chapter), we may say that **floating cities** are not only dreams in the beginning of the third millennium. Perhaps, already in the 21st century, the first floating city/cities will become a reality. Architects and engineers have recently proposed different configurations and designs for floating cities. There are proposals/projects of the Japanese Society of Steel Construction, of the Nishimatsu and Shimizu corporations [144] in Japan, the Seasteading Project in the USA and plans of other companies/institutions.

Thus, already a lot of VLFSs are being used for various purposes, but even more applications have been proposed for use in the future. The major floating structures proposed or constructed up to now are also described in [144, 151].

1.2.3 VLFS system

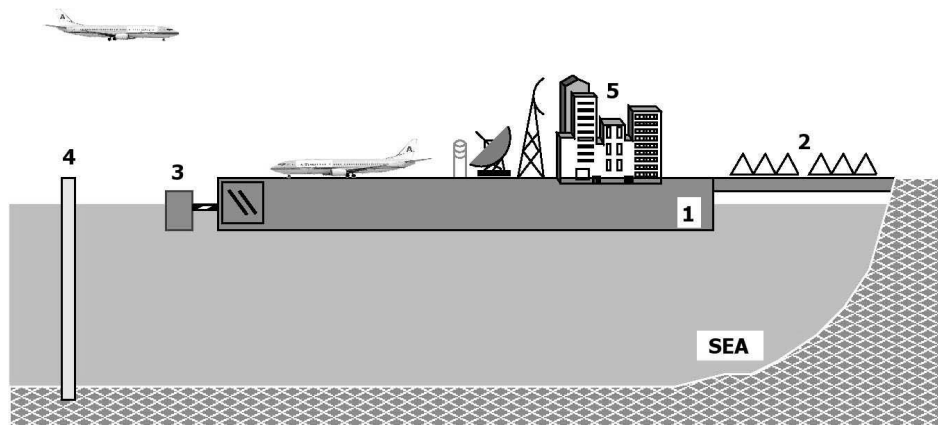


Figure 1.4: VLFS system.

The components of the VLFS system (general concept) are shown in figure 1.4. The VLFS system consists of: the very large (mat-like) floating structure (1) itself; an access bridge or a floating road to the floating structure from the shore (2); a mooring facility to keep the floating structure in a specific place (3); and a breakwater (4) for reducing the impact of wave forces on the floating structure (usually needed if the wave height is greater than 4 meters), which can be floating as well; structures, facilities and communications (5) located on a VLFS. For a real large offshore structure, Kamigoto Oil Storage Base, all the components are shown in figure 1.2.

1.2.4 Mega-Float

The **Mega-Float**, a floating airport model, was completed in 1998-99 near Yokosuka in Tokyo Bay, where it has been used till the end of 2000. The Technological Research Association of Mega-Float, a consortium of 17 Japanese companies, carried out the research and development of Mega-Float during the six-year period from 1995 to 2000 [157, 104]. The principal dimensions of Mega-Float shown in figure 1.1 are: length 1000.0 m, breadth 60.0 m (121.0 m maximum), depth 3.0 m, draft 1.0 m, deck area 84,000 m², weight of steel materials used 40,000 t, deck strength 6 t in distributed load.

The Mega-Float is the world's largest floating object ever built, in particular the largest artificial floating island. It consisted of six units, which were welded into one huge structure of 1000 m in length and 60 m (partially 121 m) in width. The largest unit of the structure was 383 m x 60 m. The Mega-Float was constructed to verify taking off and landing tests with use of rather light aircraft, and to verify commercialization. All reports of the tests show that the results are even better than expected. The platform has behaved very stably, with basically no movement caused by waves or planes landing or taking off. The unit was constructed of steel with walls or pillars inside a box structure designed for a lifetime of 100 years.

Additional information about the Mega-Float can be found in papers and overviews [47, 104, 157, 158]. Although the Mega-Float has been used to land (small) planes on, its size is only about a quarter of the real proposed airport runway. The floating runway proposed for Tokyo International Airport Haneda has a length of 3600 m. The name introduced in Japan for such structures is ultra large floating structure.

1.3 Literature survey

This survey covers books, papers, reports and abstracts that both give the basic theory for wave propagation and diffraction and study the interaction between floating bodies and water waves and related problems. Different methods used for the problem are described, for example VLFS models and shapes, wave and other forces, mooring systems, breakwaters, anti-motion devices, and sea bed profiles. Also, we review what has been done already, what is currently being investigated and the future directions to study for the problem of interaction between the water waves and VLFSs.

Fluid-structure interaction is not a new problem of hydrodynamics. In fact, there are two categories of this problem: the interaction between large floating structures and water waves, and the interaction between large ice fields and surface waves. Ice-water interaction problems can be solved with the use of the approaches applied for VLFS analysis, using the physical properties of ice instead of those of the platform.

Since the pioneering works of John [48, 49] and Stoker [107] on the motion of a floating rigid thin plane slab, plate-water interaction has been intensively studied by many authors across Europe, Asia, America and Oceania: in Japan, the Netherlands, Russia, the United Kingdom, the United States, New Zealand, China, India, Korea, Greece, Norway and other countries. Kashiwagi [52] presented a review of the most recent (at that time) studies on the prediction of hydroelastic responses of the VLFS. Recently, Watanabe et al. [143, 144] presented very detailed surveys on the research work on pontoon-type

VLFSs. The numerous publications reported in offshore structures/VLFS conference proceedings, journals, books and websites confirm the interest in and importance of these structures to engineers and scientists. Many papers on the analysis of very large floating structures were published in the following international journals: *Applied Ocean Research*, *Engineering Structures*, *Journal of Engineering Mathematics*, *Journal of Fluid Mechanics*, *Journal of Fluids and Structures*, *Marine Structures*, *Ocean Engineering*, *Wave Motion*; in the *Proceedings of the International Workshops on Water Waves and Floating Bodies (IWWF)* [156], *International Offshore and Polar Engineering Conferences (ISOPE)* [155] and other conferences, workshops and seminars. Also, many publications about VLFSs have been published in non-scientific or scientific-popular journals and newspapers and on the internet. Thus, the attention to and interest in the problems of the behavior of floating plates in waves has recently increased.

Compared to its horizontal parameters the thickness of the very large floating structure is small and therefore the structure may be modelled as a thin elastic plate. The water depth plays an important role in this kind of problem, and the theory is divided into three cases: very deep water (depth is considered as an infinite value), water of finite depth, and shallow water. This field of hydrodynamics, fluid-structure interaction, has well been studied by numerical approaches while some difficulties in analytical study remain, especially for the case of finite depth.

To start with the survey, we will refer to the most famous books of hydrodynamics which are commonly used in fluid-structure interaction research. These are: "Hydrodynamics" by Lamb [64], which gives general information about hydrodynamics; "Water Waves" by Stoker [107], describing water waves and their interaction with floating objects; "Surface Waves" by Wehausen and Laitone [146], which treats the various problems of fluid motion; "Marine Hydrodynamics" by Newman [88], which describes wave motion and deals with various problems of hydrodynamics. For the thesis we used the following parts of the theory presented in the aforementioned books. The theory of and solution examples for plates floating on shallow water are given in [107]. Basic theory, equations and conditions for finite and infinite water-depth models are described in [88]. For the equations of wave motion and a description of the Green's functions involved we will refer to [146]. With the pioneering works [48, 49, 107, 146, 88], the full three-dimensional hydroelasticity theory can be derived to proceed further with VLFS analysis. In the first works on VLFS analysis the Green's function method was used to model the fluid, and the finite element method to model the VLFS.

In addition, we have to mention the following books on hydrodynamics and fluid mechanics [59, 65, 66, 69, 99, 102, 147] that give basic theory, equations and describe wave propagation, diffraction and radiation in fluids. Also, the general books on wave propagation, diffraction and scattering [12, 22, 23, 50, 58, 67, 72, 106] should be listed in our survey. The famous works on theory of plates [34, 57, 71, 80, 124, 125] are used when we model VLFS as a thin elastic plate and, further, when plate motion must be described. Also, basic and specific mathematical literature is used for VLFS analysis, viz. [1, 20, 21, 33, 67, 73, 83, 84, 89, 112, 123, 131, 137, 145]. All of the aforementioned books are referred to in the thesis.

1.3.1 VLFS analysis and basic assumptions

In the hydroelastic analysis of VLFSs of the mat-like type, usually the following assumptions are made [88, 107, 143, 144, 146]:

- the VLFS is modelled as a thin elastic (isotropic/orthotropic) plate with free edges;
- the fluid is ideal, incompressible, inviscid, the fluid motion is irrotational, so that the velocity potential exists;
- the amplitude of the incident wave and the motions of the VLFS are both small, and only the vertical motion of the structure is considered;
- there is no gap (any space) between the VLFS and the free surface of the fluid;
- the sea bottom is assumed to be flat.

We will use these assumptions in this thesis. The VLFS will be modelled by a thin elastic isotropic plate; in principle, our method can be extended to an anisotropic plate. The governing equations and boundary conditions for the VLFS analysis are given in detail in sections 2.2–2.4. The origin of the coordinate system is on the undisturbed free surface, and z -axis is pointing upwards.

The main aim of the problem is to determine the deflection of the VLFS under the action of wave forces. Also, the hydroelastic response of the VLFS is often studied to measure the influence of the floating structure on water waves.

The analysis may be carried out in the frequency domain or in the time domain. More often, the hydroelastic analysis is carried out in the frequency domain. However, for transient responses and for nonlinear equations of motion due to the effects of a mooring system or nonlinear wave, it is necessary to perform the analysis in the time domain.

1.3.2 Methods

There are many approaches for problems of interaction between VLFSs and surface water waves. Two commonly used basic methods for the analysis of VLFS in the frequency domain are the modal expansion method and the direct method. In detail, we can distinguish the following approaches: the eigenfunction expansion method with numeric determination of the eigenfunctions [56, 98, 149]; the asymptotic theory for short waves [12, 91]; the geometrical-optics approach [41, 42, 43]; and the corresponding ray method, e.g., [116, 118] and, furthermore, the parabolic approximation method [117, 119, 95]; the variational equation method [78]; the Wiener-Hopf technique [30, 126, 127, 128, 129, 130]; the Galerkin method [51]; the accelerated Green's function method [135]; the boundary element method [40]; the finite element method; the hybrid FEM–BEM method [103]; the higher-order-coupled BEM–FEM method [138]; the fast multipole method [136], etc.

The modal expansion method consists of separating the hydrodynamic analysis and the dynamic response analysis of the plate, as was done by Mei and Black [76]. The deflection of the plate with free edges is decomposed into vibration modes that can be chosen arbitrarily. In this regard, researchers have adopted different modal functions such as products of free-free beam modes [51, 86, 134, 149], of a vibration of a free plate [77, 78], Green's functions [28], B-spline functions [51], two-dimensional polynomial functions, and finite element solutions of freely vibrating plates. The hydrodynamic radiation forces are evaluated for unit amplitude motions of each mode. The Galerkin method, by which the

governing equation of the plate is approximately satisfied, is used to calculate the modal amplitudes, and the modal responses are collected to obtain the total response. The eigenfunction expansion method was also used to study the behavior of the floating structures amongst others, in [56, 98]. The modes may be of the dry or wet type. While most researchers use the dry-mode approach because of its simplicity and numerical efficiency, some studies use the wet-mode approach, e.g., [38].

In the direct method, the deflection of the VLFS is determined by solving the equations directly without expanding the plate motion into eigenmodes. The solution can be derived for both a two-dimensional geometry and a three-dimensional geometry. Mamidipudi and Webster [74] pioneered this direct method for a VLFS. In their solution procedure, the potentials of the diffraction and radiation are established first, and the deflection of VLFS is determined by solving the combined hydroelastic equation using the finite difference scheme. Applying the pressure distribution method, the equation of motion can be solved using the finite element method.

Ohkusu and Namba [91, 92] proposed a different type of direct method. Their approach is based on the idea that the thin plate is part of the free water surface but with different physical characteristics than those of the free surface. The problem is considered as a boundary value problem [33] in hydrodynamics rather than a problem of determining the elastic response of the body to hydrodynamic action. This approach was used to analyze similar problems of two-dimensional ice floe dynamics by Meylan and Squire [77] and of a circular floating plate by Zilman and Miloh [153]. The deflections are estimated from the resulting velocity potential. The advantage of this method is that a closed-form solution may be obtained in the case of shallow water. For shallow water, the solution can be obtained with the approximation theory of Stoker [107], who derived the matching conditions along vertical boundaries in the fluid domain.

In the direct method of Kashiwagi [51], the pressure distribution method is applied and the deflection is derived from the vibration equation of the structure. In order to achieve high accuracy in a very short wavelength regime as well as short computational times, he uses bi-cubic B-spline functions to represent the unknown pressure and the Galerkin method to satisfy the body boundary conditions. The principal difference between the modal superposition method and the direct method lies in the treatment of the radiation motion for determining the radiation pressure.

The asymptotic theory for short waves has been described by Babich and Buldyrev [12] and is applied for VLFS analysis by Ohkusu and Namba [91]. Tkacheva [126, 127, 128, 129, 130] have solved various problems of plate-water interaction using the Wiener-Hopf technique [89, 83]. Meylan developed the variational equation method [78].

Hermans solved the problem of diffraction of incident surface waves on the floating flexible plate using the geometrical-optics approach (GOA) [41, 42, 43], while Takagi solved the problem using the corresponding ray method [116]. Takagi [117, 119] and Takagi and Nagayasu [118] improved the ray method by introducing and applying the parabolic approximation for plate-water interaction. The basic ideas of geometrical optics can be found in [12, 13, 58, 67, 72]. The VLFS hydroelastic motion is treated in the GOA or ray theory as wave propagation in the plate. The wave field around and in the floating plate is represented as a summation of the wave rays. We will use an asymptotic theory of the geometrical optics approach, which is discussed in section 1.5.

The corners of a VLFS (when a structure of finite extent is considered) are singular

points if the ray theory is applied. The corner effect was found to be inversely proportional to the square root of the distance from the corner; therefore, the corner effect is restricted to the (plate) area around the plate corner points. The wave amplitude can be changed essentially along a ray which passes the corner, but Takagi [117, 118, 119] found that this may be overcome by the parabolic approximation method. In chapter 6 we also will use the ray method for the quarter-plane problem.

Many numerical techniques were proposed by other researchers in the last ten years, so many experimental studies have been carried out, e.g., [68, 96, 103].

The commonly used approaches for the time-domain analysis of VLFS are the direct time integration method and the method that uses Fourier transforms, e.g., [29]. In the direct time integration method, the equations of motion are discretized for both the structure and the fluid domain. In the Fourier transform method, first the frequency domain solutions are obtained for the fluid domain and then the results are inserted into the differential equations for elastic motion.

1.3.3 Water depth models

There are three different models (cases) of water depth in hydrodynamics: infinite water depth (IWD), finite water depth (FWD), and shallow water depth (SWD) models. Correspondingly, when the fluid-structure problem is under consideration, one of the three models must be used. For the first and third cases, approximation theories were developed, while the finite water depth model is the general case (which is also most difficult to study analytically). In fact, the infinite and shallow depth cases are the limiting cases of the finite water depth theory. Taking the limits infinity and zero for the depth, we arrive at the IWD and SWD models, respectively. Main works on wave propagation and diffraction for 'infinitely' deep water were produced by Kochin [59], for water of finite depth by John [48, 49], and for both infinite and finite depth by Wehausen and Laitone [146] and later by Newman [88]. Shallow-water problems are treated by Stoker [107], who derived the approximation theory for the case of shallow depth.

For the problems for floating bodies in water waves solved for the IWD, see, e.g., [77, 40, 126, 119, 127, 98]. The FWD case is treated, for example, in the following papers [75, 32, 15, 115, 41, 78, 5, 31, 130, 44, 101, 121]. Sometimes, authors solve a problem for the IWD case first and then improve/extend their technique to the FWD case, e.g., [8, 9, 37]. For the problems in the SWD case, solutions were derived in, e.g., [30, 92, 95, 153, 108, 109, 132], mainly using Stoker theory. In [4, 5], the solution for the general shapes of the VLFP is derived for all three depth models.

In the next chapter we will describe three water depth models. The problems treated in the thesis are solved for all models; analytical and numerical results obtained are compared. However, the case of finite depth is of main interest for us. Using this model, problems for any depth may be solved exactly.

1.3.4 Related problems and applications

Very large floating structures have many different possible applications. Therefore, different research is underway to study, for instance, the effect of aircraft landing on and

taking off from the floating structure, the effect of different loads on VLFS, the problems of several connected or disconnected floating structures, etc.

Analytical studies of planes landing on or taking off from VLFSs were carried out and presented, e.g., in [29, 37]. Translating load applied on the floating structure has been investigated by Yeung and Kim [150]. The case of an external load on a platform floating in shallow water has been studied by Sturova [110, 111].

Recently studies were presented for alternative concepts of the floating structure. For instance, Pinkster et al. [100] and Guéret and Hermans [36, 37] have studied the motion of air-cushioned VLFP and compared their results to those for the usual mat-like VLFP. A pneumatic floating platform was considered by Cheung et al. [18]. The buoyancy force to carry the weight of the structure is provided by air pressure acting on the underside of the deck. The trapped air introduces a compressible element between the platform and the water that might modify the dynamic characteristics of the system.

Usually, VLFSs are modelled by flat thin plates having constant thickness, and the sea bottom is assumed to be flat so that the depth remains constant in the region underneath the plate. If the VLFS is located near the coastline, the shallow water depth usually varies at the very shallow end near the shore. A changing water depth and seabed topography affect the wave parameters, such as the wavelength, wave height, wave direction, wave reflection, radiation and scattering forces. However, some researchers have already modified theories for a realistic non-uniform sea bed and a non-flat VLFS bottom surface. Takagi and Kohara [116] studied the problem of the VLFS's hydroelastic motion with changing water depth. Murai et al. [85] have developed a prediction method which includes the topographical effects of the sea bed to extend the eigenfunction expansion method. Porter and Porter [101] have derived the solution for a plate of variable thickness floating on a fluid of variable depth for the case of finite water depth. Athanassoulis and Belibassakis [11, 16, 17] have studied the effect of variable depth on floating structures. Varying water depth and sea bed topography was also studied by other authors, see [143] for details.

VLMOS is abbreviation of very large mobile offshore structure (the next generation of VLFSs), which can also be used for different purposes in oceans/seas. In Japan, for instance, there are proposals to use VLMOSs for power plants — for wind or solar power conversion [120, 122, 144]. These structures are very convenient to use, but their moving increases the complexity of analysis. The first step of the analysis might be taking zero speed of mobile structures with the following extension of the technique derived.

The VLFSs can also be used for military purposes, ocean exploration [14], meteorology, and studies on regarding these applications have been carried out.

The problem of interaction between fluids and structures not only includes the hydroelastic motion of VLFS. For a long time researchers have studied the behavior of large ice sheets or fields in water waves. Nowadays, in principle, VLFS studies and approaches can be applied to study ice-water interaction and vice versa: one may use the results of ice studies for VLFS analysis. In general, these two problems are very close to each other, and hence, all VLFS studies have this second application.

The different information about the motion of ice fields, reflection and transmission of incoming waves can be found in [15, 27, 30, 32, 35, 70, 77, 101, 105]. There are different techniques used for this problem, including the eigenfunction method, the Wiener-Hopf technique and many others.

The diffraction of waves is not a new subject at all. It has been studied intensively, for

instance, in optics, acoustics, electromagnetism, etc. Hence, studies on the diffraction of various kinds of waves on objects can be used when considering the plate-water interaction problem, e.g. [50, 58, 62, 63, 67, 72, 106].

Literature surveys of Watanabe et al. [143, 144] and Kashiwagi [52] also give information about the many different approaches used for the hydroelastic analysis of VLFS.

1.3.5 VLFS models and shapes

In this subsection we discuss the different shapes of very large floating structures and their models proposed and analyzed by researchers and engineers worldwide.

Mainly, the mat-like VLFS is modelled as a thin plate. There are three well-known and commonly-used plate theories, namely, the Kirchhoff (also known as Gehring-Kirchhoff or Kirchhoff-Love) theory [34, 57, 71], the Timoshenko (or Timoshenko-Reissner) theory [124, 125], and the Mindlin theory [80].

Most researchers apply the Kirchhoff plate theory for the problem considering the isotropic thin plate, see [5, 8, 9, 10, 51, 55, 56, 78, 91, 115, 128, 153]. Kirchhoff's assumptions and theory are described in section 2.3. The plate freely vibrates on the water surface, i.e. it has free edges. For a refined analysis that includes varying plate mass and stiffness, the VLFS is modelled as an orthotropic plate, for example in [43, 74]. To obtain accurate stress resultants, the first-order shear deformation plate theory of Mindlin [80] has been used [38, 139, 142]. Some researchers model the VLFS as a floating beam. Such a model may be suitable for a ship, but it does not properly describe the two-dimensional action of the pontoon-type VLFS.

VLFSs have also been modelled as a module linked floating structure, as a two-dimensional articulated plate, as a plane grillage mode, as sandwich grillage model, etc.

In principle, the floating structure may be of any horizontal planform, i.e. shape [143, 151]. The choice of VLFS shape depends on its purpose, the ocean/sea currents, the wave behavior on a site, etc.

Mainly, the VLFS having a rectangular planform has been studied, see for example [5, 29, 43, 61, 74, 91, 93, 115, 134]. The analytical solution for plates having one or two infinite dimensions, which simplifies the complexity of analysis significantly, can be derived with any of the approaches described in subsection 1.3.2 and in the surveys [52, 143]. For finite plates numerical methods are often used. Numerous papers consider a half-plane problem, e.g. [5, 41, 70, 126], and the problem of a strip of infinite length, e.g. [5, 41, 115]. A quarter-infinite plate has been considered by Andrianov and Hermans [6], Ohkusu and Namba [95], and Takagi [121].

Not many papers consider arbitrarily shaped structures, although non-rectangular VLFSs may be used for purposes like floating airports, cities, storage facilities, power plants, etc. [143, 144], and the behavior of such VLFS could be analyzed by the methods developed. VLFSs having circular planform were studied by Meylan and Squire [77], Zilman and Miloh [153], Tsubogo [132], Peter et al. [97], Watanabe et al. [142], Andrianov and Hermans [7, 8], and Sturova [111]. A ring-shaped floating plate has been considered by Andrianov and Hermans [9].

Hermans [41], Takagi [118] and Meylan [78, 79] derived the solution for the general geometry of a VLFS; several interesting shapes of the structure are discussed in these

papers. L-shaped, T-shaped, C-shaped and X-shaped VLFSs were studied by Hamamoto and Fujita [38]. The case of multiple floating plates has been treated by Hermans [44]; the corresponding case is a finite gap between two plates, which was studied by Chung and Linton [19]. Evans and Porter [31] considered the case of narrow cracks in ice.

Also, VLFS designs have been proposed of hexagonal and other shapes, so that the floating structures can be expanded easily.

1.3.6 Mooring systems, breakwaters and anti-motion devices

A topic very important in VLFS analysis and for the design of floating structures is positioning, that is, holding a VLFS in place and reducing its motions. To keep them in place special mooring systems can be used, for instance dolphin-fender facilities, or chain or anchor lines. To further reduce the energy of incoming waves, breakwaters are usually constructed nearby. Special anti-motion devices can be used for these purposes as well. All the components of VLFS system are shown in figures 1.2 and 1.4.

Mooring systems are used to keep the VLFS in a specified place. If a mooring system is used, the responses of a VLFS in waves do not only include hydroelastic vertical motions, but also horizontal motions and the reaction forces of the mooring system. The hydroelastic behavior of VLFSs with a jointed mooring system has frequently been analyzed in the last years [143, 151]. Also the elastic deformation and mooring force of a VLFS on Tsunami waves has been studied, e.g., [113]. Studies on a mooring system for a VLFS moored in a reef or shore have also been conducted. The vertical displacement of the VLFS can be controlled by a special mooring system consisting of a combination of dolphins with rubber fenders as in the case of Kamigoto Oil Storage Base, figure 1.2. The floating structure must be safely moored, even during windstorms such as typhoon.

The **breakwaters** surrounding a floating structure can be used to reflect or reduce incoming water waves, which will decrease the motion of the structure. The effect of the breakwater on the motion of an elastic floating plate has been studied, e.g., by Nagata et al. [86, 87], Ohmatsu [96], and Utsunomiya et al. [134]. In the first paper, an analytical method is developed to determine the motion of an elastic mat-like VLFS in waves in a sea with a breakwater, where the domain decomposition method is used to analyze the fluid region. In the second paper, the presence of the breakwaters surrounding the VLFS is analyzed using the higher-order boundary element method (HOBEM). Seto and Ochi [103] have presented a numerical method for predicting the hydroelastic behavior of VLFS in a complex water area shape that is sheltered by breakwaters and land. For the free-surface flow, they employ a hybrid finite/infinite element formulation to reduce the computational effort. Ohmatsu [96] have developed an effective method for the hydroelastic analysis of VLFS, taking into consideration the mutual interaction effect between the VLFS and the breakwater where the partial reflection coefficient is included.

Results obtained demonstrate that breakwaters effectively reduce the plate response for long waves, but in case of short waves, the reduction is not always prominent. In the above papers, the breakwaters considered are of the gravity type, moored into the bottom. Although breakwaters of such a type break the waves most effectively, they interrupt water flows around the VLFS and thus are not environmentally friendly. Moreover, the construction costs of bottom-mounted breakwaters may be high for large installation

depths. To reduce costs as well as to maintain the environmentally friendly space, breakwaters are proposed which allow water to flow through openings at the bottom. Various types of breakwaters have been proposed recently, such as the oscillating water column (OWC) type and structure embedded by the OWC type breakwater, a system consisting of a floating breakwater using a submerged plate, vertical barriers, multi-layered wave barriers, etc. One of the examples is the twin-plate breakwater for the case of deep water studied by Usha and Gayelthri [133].

By analyzing the elastic motion of the Mega-Float it was found that elastic motion appears as propagation of water waves beneath a thin elastic platform and that its amplitude is not as small as was expected. Therefore, **anti-motion devices** were developed for the VLFS. One such device is a box-shaped body attached to the edge of the VLFS. Takagi et al. [115, 117] carried out numerical analysis as well as experimental studies and showed that the anti-motion performance of this device is good, reducing both the deformation, the shearing force and bending moment of the floating platform.

As an anti-motion device, a floating (or submerged) plate can be attached to the VLFS as well. Experimental and analytical (e.g., [54]) studies have been carried out to investigate the use of either a horizontal plate attached to the VLFS using vertical connectors or a vertical plate attached at the edge of the VLFS in order to reduce displacements of the structure. The horizontal plate proved to be more effective if it protrudes from one end of the VLFS and is not placed very deep. The vertical plate reduces the effect of displacement more with increasing plate depth and decreasing wave period.

Japanese researchers have reported that if the mooring system is used together with the plate attachments as anti-motion devices, this sufficiently reduces the motion of the VLFS; there is no need to use breakwaters, too. Very recently, a flat vertical plate (with horizontal slits) was attached to the edge of the IT base Mega-Float to reduce the drift force. Other forms of plate attachments such as L-shape and reverse L-shape plates have also been proposed. These additional attachments reduce the hydroelastic response and motions of the offshore structure and the wave drift force.

Further details on anti-motion devices, mooring systems, breakwaters, and on wave and other forces involved can be found in [143, 144].

1.4 Outline of thesis

Various problems of hydrodynamics treated in this thesis have in common that they concern interaction between a very large floating structure and water waves. A VLFS floating in an offshore zone can be used as an artificial island, airport, power plant, ferry pier, storage facility, rescue base, etc. The main subjects of the thesis are the hydroelastic behavior of a VLFS in waves and diffraction of surface waves by a VLFS. The main idea in the proposed concepts is to build a very large mat-like structure. Compared to its horizontal parameters, the thickness of a VLFS is very small; in a practical situation, the horizontal dimensions are about several kilometers by several hundred meters while the thickness and draft are of the order of several meters.

The main objective of our study is derivating an analytical solution and numerical results for various shapes and dimensions of a floating plate. The geometrical shapes of the plate considered are rectangular (half-plane, strip, quarter-plane, half-plane plate

with finite thickness), rotational (circle, ring) and arbitrary horizontal planforms. The wavelength is smaller than the width of the floating plate and there is no space between the plate and the water. The solutions for the plate's deflection and free surface elevation (vertical displacements in the plate and open-water regions, respectively), the reflection and transmission of waves are derived with different methods from applied mathematics, mechanics and fluid mechanics. New approaches for hydroelastic analysis of VLFSs are proposed. We study the problem for different water depth models: very shallow water when the floating structure is located near the coast, the general and universal case of finite water depth, and very deep water when the structure floats very far out in the sea or ocean.

The research reported in this thesis might be applied to predict the hydroelastic response of the VLFS to water waves and the general behavior of the VLFS for different values of wavelength, water depth, plate characteristics and other physical parameters of the problem. To obtain numerical results, several program packages were developed.

Chapter 2 gives the general theory on plate-water interaction, basic equations and conditions, our method and an introduction to particular problems. The following models and horizontal shapes of the very large floating platform are considered in the thesis: a semi-infinite plate and a strip of infinite length (chapter 3), a circular plate (chapter 4), a ring-shaped plate (chapter 5), a quarter-infinite plate (chapter 6), and a plate of finite small thickness (chapter 7). Analytical studies derived for specific cases are described in corresponding chapters. Numerical results and comparisons are presented in chapters 3–7 for practically important and relevant situations. Also, in chapters 3–7 we give concluding remarks, possible extensions and suggestions for other plate planforms. General conclusions and a discussion on the future of VLFSs and the VLFSs of the future are given in chapter 8. Our recommendations for the mathematical study of the problem, as well as for the VLFS design and shape, are collected in chapters 3–8.

1.5 Theory and method

The thesis considers the hydroelastic behavior of a floating elastic plate and its response to incident surface water waves. Simple time-harmonic motions are considered and the VLFS's behavior is analyzed in the frequency domain.

The motion of the floating plate and the plate's hydroelastic response to surface waves is studied. A new method, the integro-differential equation method, is developed and justified in the thesis. Solutions are presented for six different shapes of a thin elastic plate, which is a model of the very large floating structure. Analytical and numerical studies are presented for three water depth models: for infinite, finite and shallow depth.

The thickness of the plate and, correspondingly, the plate draft are small compared to the horizontal dimensions of the very large floating platform. The horizontal dimensions of a VLFP are about several kilometers by several hundred meters, while the thickness and draft are of the order of several meters. Also, VLFPs have mat-like dynamic behavior which can be described by the equation of thin-plate motion. Therefore, a thin elastic plate serves as a model for a VLFP; henceforward in the thesis, we will use the standard theory of plates of Kirchhoff. Such a model can also be applied to study the interaction between huge ice fields and water waves.

The physical and mathematical formulation of the problem are given in chapter 2. There we also describe the main equations and boundary conditions, which are the governing equations for the (boundary-value) problem of the interaction between the floating plate and water waves. The two-dimensional platform of different horizontal geometry is under consideration in chapters 3–6. In chapter 7, we take a finite plate thickness and, correspondingly, a finite draft into account. In this situation the wave amplitude is assumed to be smaller than the plate draft.

In practical situations, the horizontal dimensions of the floating plate might be of the order of a thousand meters, while the wavelength is of the order of ten or a hundred meters. Therefore, we consider and study numerically the situation where the wavelength is less than the length (diameter) of the plate. However, our approach is also valid for the case of small floating plates whose length is less than the wavelength.

First, we wish to determine the vertical displacements of the floating plate and the free surface of water. An integro-differential equation is derived for the deflection of a VLFP on deep water and water of finite depth applying the Green's theorem for the velocity potential and using the boundary conditions in chapter 2. The approach proposed in the thesis includes the integro-differential formulation and method (IDEM) and, in addition, a modified geometrical-optics approach (GOA). The information about the GOA and the corresponding ray method is given in [12, 13, 58, 67, 72]. Then, we proceed with an analysis; analytical studies are varied for particular problems. However, an integro-differential equation derived can be solved numerically, e.g., by means of a boundary element method and a mode expansion. The boundary conditions can be derived to apply the ray method for short-wave diffraction.

In chapter 3 we derive and use an asymptotic theory of the geometrical-optics approach. According to the standard GOA, the motion of the floating plate is treated as wave propagation (in the plate). The deflection is then represented as a superposition of wave modes (rays). Each term of the series consists of an amplitude of the corresponding wave mode multiplied by an exponential function with an argument which depends on the roots of the dispersion relation. If the problem is considered in polar coordinates, Bessel functions are used instead of exponential ones, see chapters 4–5.

The floating plate having a quarter-infinite horizontal planform is considered in chapter 6. There we also derive a solution using geometrical optics. The following investigation of the propagation of the main ray (ray Ansatz) is the main element of an analysis for this situation. In case of a quarter-infinite plate, the effect of inner reflection at the far (relative to the front of incoming waves) edge of the plate has to be considered. This can be done using the Ansatz ray. Hence, in chapter 6, we first use an asymptotic theory of the GOA and then the standard ray method.

The final case we study is that of a floating plate of finite thickness and draft, considered in chapter 7. To solve the problem, we first use our solutions for the previous problems derived with the IDEM and GOA. Next, the plate deflection is represented as a power series with respect to the draft order, as in the Lindstedt method.

The integro-differential formulation and method developed may be applied to study the interaction between VLFSS and water waves and the behavior of middle-sized and small-sized floating offshore structures (e.g., floating breakwaters), because the approach is valid for both short and long incident waves. Hence, the approach can be used to describe the interaction of water waves and large ice fields, either in the form of one large

plate or field, consisting of many different ice pieces. To do so, one needs to use the physical properties of ice in the equations instead of the plate parameters.

Thus, the solution of the problems treated in the thesis is based on the integro-differential equation method and asymptotic theory of the geometrical optics approach. The complete general theory and solution method proposed are described in chapter 2. In the other chapters we consider specific cases.

Chapter 2

General theory

Several plate-water interaction problems are studied in the thesis. This chapter presents the general theory and equations for all problems considered. First, the general mathematical formulation for the problem of the plate-water interaction is given. Governing equations and boundary conditions are presented in the second section. Subsequently, the thin plate theory is used in the third section, where it is described and verified. Because of simple harmonic motion, main water wave equations may be rewritten and then the analysis can be carried out in the frequency domain. This is presented in the fourth section, together with information on infinite, finite and shallow water depth theories. Furthermore, the Green's function is described and its different forms are in use for the problems treated in chapters 3–7. The plate's deflection is discussed and deflection representations are given for each particular case in the sixth section. The seventh section gives our method to study the problems. The main integro-differential equation for the potential, plate and free surface elevation are derived using the Green's theorem and free surface conditions. The section also shows how the analysis is continued in the rest of the thesis and points the solution.

2.1 Main information

This thesis studies the hydroelastic behavior of large floating flexible platforms in waves. The main objective of the study is to describe the motion of the plate itself and its hydroelastic response to incident waves.

Here we present the mathematical and physical formulation of the problem and give governing equations, boundary conditions, and formulas for the wave potential. Then, an approach to study the problem of interaction of very large floating flexible plates with water waves is developed and discussed. The method is based on the use of the Green's theorem and thin plate theory, which are described in this chapter. Furthermore, we will derive the main integro-differential equations for the vertical displacements in the plate and open-water regions. The integral equation for the potential is derived, which is the intermediate step of our analysis. The following chapters will provide further details on the approach developed and the use of the integro-differential equation method for particular problems. Hence, this chapter is a key to the solution of each particular problem considered elsewhere in this thesis.

Our analysis is restricted to floating structures whose dynamic behavior can be described by a thin plate model. We are mainly interested in the applications of large flexible floating structures for the purpose of floating airports, storage facilities, ferry piers, bridges, power plants, industrial space, emergency bases, parks or stadiums, etc. However, the approach and model presented may be used to study the interaction between water waves and middle- or small-sized floating platforms, such as floating breakwaters, pontoon bridges, and platforms for other purposes. Our approach and solutions can also be used to study the behavior of large ice fields and their interaction with water waves.

2.2 General mathematical formulation

This section describes main mathematical equations of hydrodynamics for fluid-structure interaction. The general physical problem is the following: **interaction** between a **very large floating flexible platform** of general shape, floating in open sea, and incoming **surface waves**. The platform considered is of the pontoon type, which is also known as the mat-like VLFS, see chapter 1.

The floating platform covers part of the water surface. Regular incident waves are coming in from the open-water region and are diffracted by the platform. The very large floating platform (VLFP) under consideration is modeled as a thin elastic plate. We can do this because of the small thickness and shallow draft of the platform, compared to its horizontal dimensions. Therefore, we can use thin plate theory to describe the plate motion. The VLFP is assumed to be a thin layer at the free surface $z = 0$, where z is assumed to point vertically upward. This means that we assume zero thickness, i.e., we assume the thickness h_p and draft d of the plate to be zero. This assumption is used to solve the problems studied in chapters 3–6, whereas in chapter 7 we consider the plate of finite thickness. The formulation of the problem in the latter case is a bit different from that of the other problems and is discussed in chapter 7 itself.

The general geometry of the problem and coordinate system are shown in figure 2.1. The part of the water-free surface $z = 0$, covered (occupied) by the plate, is denoted by

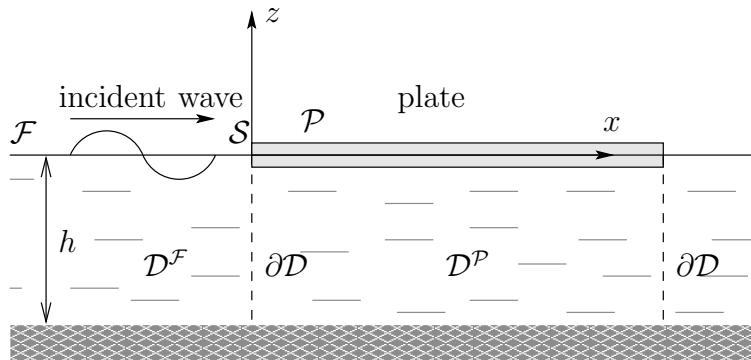


Figure 2.1: Definition sketch of the problem.

\mathcal{P} and the open free surface, surrounding the platform, towards infinity, by \mathcal{F} . The free surface is divided by the interface line — the plate contour \mathcal{S} . Henceforward for simplicity we will often use only the notation \mathcal{P} for the plate region $x, y \in \mathcal{P}$, $z = 0$, and \mathcal{F} for

the open fluid region $x, y \in \mathcal{F}$, $z = 0$. The fluid domain is also split up into two regions. The region underneath the platform is defined as \mathcal{D}^P and the region towards infinity, not covered by the plate, as \mathcal{D}^F , while the interface vertical surface is denoted by $\partial\mathcal{D}$.

The parameters of the problem are described below. The water and wave parameters are: h – depth, constant, λ – wavelength, A – wave amplitude, k_0 – wavenumber, β – angle of incidence, ω – wave frequency, ρ_w – density. The water depth is constant, so the sea bed is flat. The wave height is defined as twice the amplitude. The wavenumber k_0 is the phase change per unit distance in the propagation direction (x -axis in case of normal incidence). It has different values for three cases with different water depth. Further, we denote the wavenumber for the IWD case as K , for the FWD case as k_0 , and for the SWD case as k_{sh} . Complete information about the wavenumber is given in section 2.4.

The parameters of the plate and characteristics of the material are the following: ρ_p – density, m – mass per unit area, D – flexural rigidity, ν – Poisson's ratio, h_p – thickness, d – draft, which is a size of the wetted part of the plate vertical surface. The last two are assumed to be zero, except in chapter 7. Further, $\mathcal{D} = D/\rho_w g$, $\mu = m\omega^2/\rho_w g$ are structural parameters introduced, which are constant as an isotropic plate is considered. The flexural rigidity and bending stiffness of the plate are constant.

The fluid is assumed to be ideal, incompressible and inviscid, having irrotational motion. The water depth h is varied for different cases. The main theory is divided in three cases, each with a different water depth: infinite water depth (IWD), finite water depth (FWD), and shallow water depth (SWD). In section 2.4 we describe the theory for each case; differences are also demonstrated. In the first case, only one root of the water dispersion relation and three roots of the dispersion relation in the plate area are considered. This serves as a demonstration of how the method will be used in the finite depth case. On the other hand it also gives rather accurate results in the case of long waves. In the shallow water case we follow the standard depth averaging technique, which leads to approximate results. FWD is the general and universal case; with the theory for this case we may also study the IWD and SWD cases. For the IWD case — the case of very deep water in reality — the depth is assumed to be infinite. So, the water depth h is finite and constant for the FWD and SWD cases, and for the IWD case $h \rightarrow \infty$.

The plate deflection is generated by incoming surface waves propagating with an angle of incidence β to the positive x -direction without loss of generality. Mainly, we study the situation where the wavelength λ is smaller than the smallest horizontal dimension, e.g., the width of the strip l . The amplitude of the incident wave A is assumed to be small in comparison with other parameters of the problem. It is assumed that the plate is in contact with the water at all points and at every instant of time. Therefore, there is no cavity between the lower (wetted) surface of the plate and the water.

We assume that waves propagate in otherwise still water and have simple harmonic motion. The fluid velocity $\mathbf{V}(x, y, z, t)$ is expressed by the gradient of a velocity potential Φ , $\nabla\Phi(x, y, z, t) = \mathbf{V}(x, y, z, t)$. The effects of the free surface must be expressed in terms of appropriate surface boundary conditions. The physical nature of the free surface requires both a kinematic and a dynamic boundary condition: the normal velocities of the fluid and of the boundary surface must be equal, and the pressure on the free surface is the atmospheric pressure.

The total potential $\Phi(x, y, z, t)$ is a solution of the governing Laplace equation

$$\Delta\Phi = 0 \quad (2.1)$$

in the fluid, $-h < z < 0$. Equation (2.1) expresses conservation of fluid mass for potential flows and provides the governing partial differential equation to be solved for the function Φ .

The Laplace equation is supplemented by the boundary conditions at the free surface and bottom. The linearized kinematic condition, see, e.g., Newman [88], in the plate and water regions, at $z = 0$, has the form

$$\frac{\partial\Phi}{\partial z} = \frac{\partial W}{\partial t}, \quad (2.2)$$

where $W(x, y, t)$ denotes the free surface elevation, either the deflection of the plate in \mathcal{P} , or the free surface elevation in \mathcal{F} , and t is the time.

The dynamic condition is derived from the linearized Bernoulli equation [88]. The linearized equation for the free surface elevation is written as

$$-\frac{P - P_{\text{atm}}}{\rho_w} = \frac{\partial\Phi}{\partial t} + gw, \quad (2.3)$$

at $z = 0$, where ρ_w is the density of the water, g is gravitational acceleration, $P(x, y, t)$ is the pressure in the fluid, and P_{atm} is the atmospheric pressure. The relations (2.2) and (2.3) are kinematic and dynamic boundary conditions at the free surface, respectively.

At the fluid free surface, $P = P_{\text{atm}}$ and the dynamic boundary condition (2.3) can be differentiated with respect to time and combined with the kinematic condition (2.2). This gives a single boundary or the linearized free surface condition at $z = 0$

$$\frac{1}{g} \frac{\partial^2\Phi}{\partial t^2} + \frac{\partial\Phi}{\partial z} = 0. \quad (2.4)$$

The bottom condition at $z = -h$, another boundary condition, is the zero of normal derivative, and it is written in the following form

$$\frac{\partial\Phi}{\partial z} = 0. \quad (2.5)$$

The Laplace equation (2.1) and boundary conditions (2.2–2.5) are the governing equations of the problem. This formulation is valid for all three models, IWD, FWD and SWD. In addition, the Sommerfeld radiation condition for the potential must hold at infinity, see subsection 2.4.1.

The general (vertical) geometry sketch of the problem is shown in figure 2.1. First, we take a half-plane and a strip as the planforms of the floating thin plate, see chapter 3. In case of a strip of width l and infinite length $0 \leq x \leq l$, $-\infty < y < \infty$ the open (or free) fluid area at the free surface \mathcal{F} is $-\infty < x < 0 \cup l < x < \infty$, the plate area — part of the free surface, covered by the plate — \mathcal{P} is $0 < x < l$ and the dividing contour \mathcal{S} is $x = 0 \cup x = l$, as is shown in figure 2.1. For the semi-infinite platform (SIP) $0 \leq x < \infty$, $-\infty < y < \infty$, \mathcal{F} is $x < 0$, \mathcal{P} is $x > 0$ and \mathcal{S} is $x = 0$.

In case of a circular plate, the free surface is divided into the plate \mathcal{P} ($\rho \leq r_0$; $\varphi = [0, 2\pi]$) and open fluid \mathcal{F} ($\rho > r_0$; $\varphi = [0, 2\pi]$) regions. The dividing line \mathcal{S} is the plate contour ($\rho = r_0$; $\varphi = [0, 2\pi]$). In case of a ring-shaped plate, also the surface of the fluid domain is divided. The plate region \mathcal{P} is $r_1 \leq \rho \leq r_0$, and the open water region \mathcal{F} , which includes the open water region outside the plate \mathcal{F}_0 , $\rho > r_0$, and the gap area \mathcal{F}_1 , $\rho < r_1$. The dividing lines are at the inner $\rho = r_1$ and outer $\rho = r_0$ edges of the plate. In detail and for other horizontal planforms of the plate, \mathcal{F} , \mathcal{P} and \mathcal{S} are given in chapters 3–6.

For chapter 7, the free surface \mathcal{FS} is $z = 0$, the bottom surface, the sea bed or \mathcal{SB} , is $z = -h$, the bottom surface of the plate \mathcal{P} is $z = -d$, and the vertical side surface at $x = 0$ is denoted by \mathcal{S}_s .

Along the vertical boundaries $\partial\mathcal{D}$, we have the approximate transition (or matching) conditions for the total potential [107], denoting the continuity of the pressure and the mass flow. Then Φ_n and Φ_t are continuous at $\partial\mathcal{D}$, so that

$$\Phi_n^{\mathcal{P}} = \Phi_n^{\mathcal{F}}, \quad \Phi_t^{\mathcal{P}} = \Phi_t^{\mathcal{F}}, \quad x, y, z \in \partial\mathcal{D}. \quad (2.6)$$

Here, the potential in the fluid domain $\mathcal{D}^{\mathcal{P}}$ is denoted by $\Phi^{\mathcal{P}}$, and the potential in the fluid domain $\mathcal{D}^{\mathcal{F}}$ by $\Phi^{\mathcal{F}}$.

We will now describe the operators used in thesis. In Cartesian coordinates, the three-dimensional Laplacian is

$$\Delta_{(3)} = \nabla_{(3)}^2 = \frac{\partial^2}{\partial x^2} + \frac{\partial^2}{\partial y^2} + \frac{\partial^2}{\partial z^2},$$

where the subscript (3) is used to distinguish three-dimensional operators from two-dimensional operators Δ and ∇ at the free surface, which are expressed in the following way

$$\Delta = \nabla^2 = \frac{\partial^2}{\partial x^2} + \frac{\partial^2}{\partial y^2}.$$

The problem for a circular plate (see chapter 4) and a ring-shaped plate (chapter 5) is considered in polar coordinates, their relations to Cartesian coordinates are: $\rho^2 = x^2 + y^2$, $\varphi = \arctan y/x$, $z = z$. In cylindrical coordinates, the three-dimensional Laplacian is defined as

$$\Delta_{(3)} = \nabla_{(3)}^2 = \frac{\partial^2}{\partial \rho^2} + \frac{1}{\rho} \frac{\partial}{\partial \rho} + \frac{1}{\rho^2} \frac{\partial^2}{\partial \varphi^2} + \frac{\partial^2}{\partial z^2},$$

while the two-dimensional Laplacian is

$$\Delta = \nabla^2 = \frac{\partial^2}{\partial \rho^2} + \frac{1}{\rho} \frac{\partial}{\partial \rho} + \frac{1}{\rho^2} \frac{\partial^2}{\partial \varphi^2}.$$

Below we will mainly use two-dimensional operators.

The waves are monochromatic and have the frequency ω and wavenumber k_0 . With the usual assumptions of an ideal fluid and small amplitudes, the time can be excluded from the expression for the potential. The time dependence can be excluded for the

vertical displacement and pressure as well. In such a way, the potential Φ , the vertical elevation W and the pressure P have harmonic time dependence and may be replaced by

$$\Phi(x, y, z, t) = \phi(x, y, z) e^{-i\omega t}, \quad (2.7)$$

$$W(x, y, t) = w(x, y) e^{-i\omega t}, \quad (2.8)$$

$$P(x, y, t) = p(x, y) e^{-i\omega t}. \quad (2.9)$$

Analogously, the potential, the vertical displacement, and the pressure may be rewritten in polar coordinates.

Hence, we consider waves of a single frequency ω and further analysis is carried out in the frequency domain. In the previous text, W denotes the vertical displacement either in the open fluid area, the free surface elevation, or in the plate area, the plate deflection. Henceforward we will denote the free surface elevation in \mathcal{F} as $\zeta(x, y)$ and the plate deflection in \mathcal{P} as $w(x, y)$.

2.3 Thin plate theory

The floating flexible platform is modeled by a **thin elastic linear plate**. Such a model can be applied due to the fact that the plate thickness h_p is much smaller than the minimal dimension of the VLFP planform. Also, the minimal wavelength in special variables is much larger than the thickness of the platform. The use of the linear theory is justified because the vertical displacement of the platform is less than its thickness. The absence of the residual displacements in a practical situation is verified with the use of an elastic model. To describe the motion of the thin plate, one of the theories of Kirchhoff [57], Timoshenko [124] or Mindlin [80] may be used.

For the problems considered in chapters 3–6, the platform is assumed to be a thin layer at the free surface $z = 0$. That seems to be a good model for a shallow draft platform, which is then modeled as a thin elastic plate with zero thickness. In chapter 7, we use the zero-thickness assumption as a first step of the complete analysis; the total solution is represented as the series with respect to the draft order.

The classical theory of plate vibration is based on the hypotheses of Kirchhoff. These hypotheses are: (1) linear filaments of the plate initially normal to the middle-surface remain straight and normal to the middle surface after strain, and (2) all the elements of the middle surface remain unstretched. These assumptions allow expressing the potential energy of the bent plate in terms of the curvatures produced in its middle surface.

The equations of motion and the boundary conditions were first derived and applied by Kirchhoff in his theory of thin rods. Gehring investigated the problem of plate motion using this method [34] and his approach was afterwards adopted in an improved form by Kirchhoff [57]. The work is very similar to Kirchhoff's theory of thin rods, and it leads to an expression for the potential energy per unit area of the middle surface of the plate.

Hence, we chose the Gehring-Kirchhoff theory to describe the dynamic behavior of the elastic plate. A complete description of and requirements for this theory can be found in [57, 124, 125, 71]. The Gehring-Kirchhoff equation of plate motion, or the differential

equation for plate deflection, is written in the following form

$$D \left(\frac{\partial^2}{\partial x^2} + \frac{\partial^2}{\partial y^2} \right)^2 w(x, y) + m \frac{\partial^2 w(x, y)}{\partial t^2} = P(x, y, t) - P_{\text{atm}} \quad (2.10)$$

at $z = 0$ for the plate area $x, y \in \mathcal{P}$, where m is the mass per unit area of the plate, $m = \rho_p h_p$, D is the flexural rigidity, which is the characteristic of the material, expressed in terms of the Young's modulus E , Poisson's ratio ν and the plate thickness h_p as follows:

$$D = \frac{E h_p^3}{12(1 - \nu^2)}.$$

Equation (2.10) is dynamic; the corresponding statical equation (the time is excluded) is the Sophie Germain equation. The boundary horizontal (free edge) conditions are given in the following subsection.

Next we apply the operator $\partial/\partial t$ to (2.10) and use the surface conditions (2.2–2.4) to arrive at the following equation for the total potential Φ for our problem

$$\left\{ \frac{D}{\rho_w g} \left(\frac{\partial^2}{\partial x^2} + \frac{\partial^2}{\partial y^2} \right)^2 + \frac{m}{\rho_w g} \frac{\partial^2}{\partial t^2} + 1 \right\} \frac{\partial \Phi}{\partial z} + \frac{1}{g} \left\{ \frac{\partial^2}{\partial t^2} \right\} \Phi = 0. \quad (2.11)$$

at $z = 0$ in the plate area \mathcal{P} . Here and in the rest of this thesis the notation $\{\dots\}$ is used for operators.

As we consider harmonic waves, their potential can be written in the form (2.7). In the same way, the deflection can be rewritten in accordance to (2.8). Then the time dependence is reduced, and we consider the waves of a single frequency ω , obtaining from equation (2.11) for the plate region \mathcal{P} at $z = 0$

$$\{\mathcal{D}\Delta^2 - \mu + 1\} \frac{\partial \phi}{\partial z} - K\phi = 0, \quad (2.12)$$

where the structural parameters \mathcal{D} and μ are constant because the elastic plate considered is isotropic, and $K = \omega^2/g$. For the open-water region \mathcal{F} , from condition (2.4) we obtain

$$\frac{\partial \phi}{\partial z} - K\phi = 0. \quad (2.13)$$

All definitions given above are valid for all three water depth cases. Further, we use the zero-thickness assumption for some of the problems treated (where $h_p \ll A$) and, therefore $h_p = 0$. But, despite this, we take realistic values of the rigidity D and mass m for the floating structure or ice, so h_p is not used to calculate these structural parameters, which are finite.

2.3.1 Free edge conditions

Here we describe the boundary conditions at the horizontal edge (or edges) of the plate. For simplicity, below, free edge boundary conditions are denoted as free edge conditions.

The edge(s) of the plate is (are) free of vertical shear forces, bending and twisting moments. Taking into account (2.8), we have the following free edge conditions, see, e.g., [124, 125], at the plate edge(s)

$$\frac{\partial^2 w}{\partial n^2} + \nu \frac{\partial^2 w}{\partial s^2} = 0, \quad (2.14)$$

$$\frac{\partial^3 w}{\partial n^3} + (2 - \nu) \frac{\partial^3 w}{\partial n \partial s^2} = 0, \quad (2.15)$$

$x, y \in \mathcal{S}$, where n is the normal to the plate edge (the normal direction in the horizontal plane), s is the transversal direction, the arc coordinate of the plate contour \mathcal{S} . The conditions (2.14) and (2.15) express that the bending moment and generalized shear force, respectively, vanish at the plate edge, see for more details [124].

We rewrite the free edge conditions in Cartesian coordinates

$$\frac{\partial^2 w}{\partial x^2} + \nu \frac{\partial^2 w}{\partial y^2} = 0, \quad (2.16)$$

$$\frac{\partial^3 w}{\partial x^3} + (2 - \nu) \frac{\partial^3 w}{\partial x \partial y^2} = 0, \quad (2.17)$$

when $x, y \in \mathcal{S}$.

The free edge conditions in polar coordinates have the following form:

$$\left\{ \nabla^2 - \frac{(1 - \nu)}{\rho} \left(\frac{\partial}{\partial \rho} + \frac{1}{\rho} \frac{\partial^2}{\partial \varphi^2} \right) \right\} w = 0, \quad (2.18)$$

$$\left\{ \frac{\partial}{\partial \rho} \nabla^2 + \frac{(1 - \nu)}{\rho^2} \left(\frac{\partial}{\partial \rho} - \frac{1}{\rho} \right) \frac{\partial^2}{\partial \varphi^2} \right\} w = 0. \quad (2.19)$$

2.4 Water waves equations

General water theory is divided into three cases: infinite water depth (IWD), finite water depth (FWD), and shallow water depth (SWD). For the first and third case there are approximation theories, while the finite water depth model is general, universal case which is the most difficult to study. With this model one may study and solve problems for any depth. In this section, we give the general forms for the Laplace equation, the boundary and radiation conditions for a frequency-domain analysis. Then we will describe all different forms for the velocity potential and wavenumber for each water depth.

The general equations of hydrodynamics and detailed information on water waves and diffraction of waves by floating bodies are given in [64, 107, 146, 88].

2.4.1 General wave characteristics and equations

To describe waves with simple harmonic behavior, we take the potential ϕ , which in view of formula (2.7) does not depend on time. The Laplace equation is written then as

$$\Delta \phi = 0 \quad (2.20)$$

for the potential in the entire fluid domain $-h < z < 0$. The boundary conditions at the free surface and bottom are also rewritten. The condition at the bottom $z = -h$ takes the form

$$\frac{\partial \phi}{\partial z} = 0. \quad (2.21)$$

The free surface conditions take the following forms at $z = 0$

$$\frac{\partial \phi}{\partial z} = -i\omega w, \quad x, y \in \mathcal{P}, \quad (2.22)$$

$$\frac{\partial \phi}{\partial z} = K\phi, \quad x, y \in \mathcal{F}, \quad (2.23)$$

where

$$K = \frac{\omega^2}{g}. \quad (2.24)$$

Condition (2.22) is henceforward often used to describe the relation between the potential and plate deflection. The parameter K in condition (2.23) is the wavenumber. Further in this subsection the notation k_0 is used for the wavenumber for any water depth; the difference between K and k_0 is discussed in the following subsections.

In addition, the body vertical surface condition for the potential must be fulfilled

$$\frac{\partial \phi}{\partial x} = 0, \quad (2.25)$$

details are given in chapter 7. In chapters 3–6 we do not use the condition (2.25) because of (assumed) zero thickness of the floating plate.

The potential $\phi^{\mathcal{F}}$ must satisfy the Sommerfeld radiation condition [146]

$$\lim_{R \rightarrow \infty} \sqrt{R} \left(\frac{\partial \phi^{\mathcal{F}}}{\partial R} - ik_0 \phi^{\mathcal{F}} \right) = 0,$$

where R is the horizontal distance, and $R^2 = x^2 + y^2$ here. The radiation condition also may be written in the following form

$$\sqrt{R} \left(\frac{\partial}{\partial R} - ik_0 \right) (\phi - \phi^{\text{inc}}) = 0. \quad (2.26)$$

Hence, the potential ϕ must satisfy the Laplace equation (2.20), the boundary conditions at the sea bed (2.21) and the free surface (2.22–2.23), and the Sommerfeld radiation condition (2.26) in the far field.

The matching conditions (2.6), after use of the representation (2.7), take the form

$$\phi^{\mathcal{P}} = \phi^{\mathcal{F}}, \quad \frac{\partial \phi^{\mathcal{P}}}{\partial n} = \frac{\partial \phi^{\mathcal{F}}}{\partial n}, \quad x, y, z \in \partial \mathcal{D}. \quad (2.27)$$

These conditions express that the mass of the water is conserved and the energy flux is continuous. In fact, they may be used for the solution in the entire fluid, three-dimensional,

domain for any water depth. For the case where the plate has a rectangular shape, the normal derivative becomes an x -derivative.

The solution for the potential $\phi(x, y, z)$ in the domains $\mathcal{D}^{\mathcal{F}}$ and $\mathcal{D}^{\mathcal{P}}$ may be obtained from the Laplace equation (2.20) subject to boundary conditions at the free surface (2.22–2.23) and at the sea bed (2.21) and the radiation condition (2.26). For this we can use the eigenfunctions method or separation of the variables. However, three zones have to be considered separately: $\mathcal{D}^{\mathcal{F}_0}$, $x < 0$, where the wave motion consists of incident and reflected waves, $\mathcal{D}^{\mathcal{P}}$, and $\mathcal{D}^{\mathcal{F}_1}$, $x > l$, where the transmitted wave is moving; and matching conditions (2.27) are used along the vertical boundaries between these domains. We wish to develop an approach based on which the solution for the vertical displacements and the potential can be derived with one general set of equations.

The length of incoming waves is

$$\lambda = \frac{2\pi}{k_0}. \quad (2.28)$$

The wavelength λ is the distance between successive points on the wave with the same phase.

Generally, we consider the situation where the wavelength is less than the width (or diameter) of the plate. In a practical situation, the width of the strip l or radius of the circle r_0 , the horizontal dimensions of the plate, might be of the order of a thousand meters, while the wavelength λ is of the order of a hundred meters.

The deep-water limit of the theory is $k_0 h \gg 1$. The shallow-water limit is $k_0 h \ll 1$, the opposite.

2.4.2 Infinite water depth

The potential of the incident wave for water of infinite depth, see, e.g., [88], has the form

$$\phi^{\text{inc}}(x, y, z) = \frac{gA}{i\omega} e^{iK(x \cos \beta + y \sin \beta) + Kz}, \quad (2.29)$$

where the wavenumber K (k_0 in general theory) is given by formula (2.24).

The potential (2.29) is written for undisturbed incident field. If perpendicular waves are considered, the angle of incidence $\beta = 0$ and the potential is written in the simplified form

$$\phi^{\text{inc}}(x, z) = \frac{gA}{i\omega} e^{iKx + Kz}. \quad (2.30)$$

In polar coordinates, the potential ϕ^{inc} takes the form

$$\phi^{\text{inc}}(\rho, \varphi, z) = \frac{gA}{i\omega} e^{iK\rho \cos \varphi + Kz}. \quad (2.31)$$

The case of infinite water depth is a good intermediate step in developing the method as the outcome to derive the solution for the finite water depth case, which is our main interest. The infinite water depth model is also used for problems with very deep water where the depth is so large, that it can be assumed to be infinite.

2.4.3 Finite water depth

The potential of the incident wave ϕ^{inc} for water of finite depth is written in the following form

$$\phi^{\text{inc}}(x, y, z) = \frac{\cosh k_0(z+h)}{\cosh k_0 h} \frac{gA}{i\omega} e^{ik_0(x \cos \beta + y \sin \beta)}. \quad (2.32)$$

The wavenumber k_0 is the only positive real solution of the water dispersion relation

$$k \tanh kh = K, \quad (2.33)$$

where $K = w^2/g$. The water dispersion relation (2.33) has one real root, k_0 , the wavenumber, and many imaginary roots k_i , $i > 0$, located on the imaginary axis of the complex k -plane.

If we consider perpendicular waves, the angle of incidence $\beta = 0$ and geometry of our problem becomes two-dimensional. Therefore, the potential of incident field $\phi(x, z)$ takes the form:

$$\phi^{\text{inc}}(x, z) = \frac{\cosh k_0(z+h)}{\cosh k_0 h} \frac{gA}{i\omega} e^{ik_0 x}. \quad (2.34)$$

In the same way, we rewrite the deflection as $w(x)$.

The incident potential ϕ^{inc} in polar coordinates is given by

$$\phi^{\text{inc}}(\rho, \varphi, z) = \frac{\cosh k_0(z+h)}{\cosh k_0 h} \frac{gA}{i\omega} e^{ik_0 \rho \cos \varphi}. \quad (2.35)$$

2.4.4 Shallow water depth

For water of shallow depth the approximation theory of Stoker [107] can be used. The solution is derived with the use of the matching conditions (2.27) and plate free edge conditions. In accordance to the theory, the approximation condition is obtained for the potential

$$\Phi_z = -h\Delta\Phi,$$

which, after taking the potential of the harmonic wave in the form (2.7), becomes

$$\frac{\partial \phi}{\partial z} = -h \left(\frac{\partial^2}{\partial x^2} + \frac{\partial^2}{\partial y^2} \right) \phi. \quad (2.36)$$

Then, from the free surface conditions (2.22) and (2.23), using (2.36) and (2.7), we can obtain the following expressions for the potential in both the plate and open-water regions

$$\left(\frac{\partial^2}{\partial x^2} + \frac{\partial^2}{\partial y^2} \right) \phi - \frac{i\omega}{h} w = 0, \quad x, y \in \mathcal{P}, \quad (2.37)$$

$$\left(\frac{\partial^2}{\partial x^2} + \frac{\partial^2}{\partial y^2} \right) \phi + k_{\text{sh}}^2 \phi = 0, \quad x, y \in \mathcal{F}, \quad (2.38)$$

where k_{sh} is the wavenumber, which is

$$k_{\text{sh}} = \frac{\omega}{\sqrt{gh}} \quad (2.39)$$

in the case of shallow water.

The potential of incident waves for shallow water has the form

$$\phi^{\text{inc}}(x, y, z) = \frac{gA}{i\omega} e^{ik_{\text{sh}}(x \cos \beta + y \sin \beta)}. \quad (2.40)$$

We denote A^* as follows:

$$A^* = -\frac{igA}{\omega}.$$

The general solution of (2.38) and the conditions at infinity lead us to

$$\phi(x, y) = A^* e^{ik_{\text{sh}}(x \cos \beta + y \sin \beta)} + R^* e^{ik_{\text{sh}}(-x \cos \beta + y \sin \beta)}, \quad x < 0, \quad (2.41)$$

where the first term represents a progressed wave moving to the right and the second a reflected wave moving to the left, while $R = R^*/A^*$ is the coefficient of the reflected wave, the reflection coefficient, and

$$\phi(x, y) = T^* e^{ik_{\text{sh}}(x \cos \beta + y \sin \beta)}, \quad x > l, \quad (2.42)$$

where the right part represents the transmitted wave, and $T = T^*/A^*$ is the transmission coefficient.

Inserting the condition (2.3) for the pressure in modified form into the differential equation for the thin plate (2.10) and using condition (2.37), we obtain the following differential equation for the potential $\phi^{\mathcal{P}}$ in the plate area

$$\mathcal{D}\Delta^3\phi^{\mathcal{P}} + (1 - \mu)\Delta\phi^{\mathcal{P}} + k_{\text{sh}}^2\phi^{\mathcal{P}} = 0, \quad x, y \in \mathcal{P}. \quad (2.43)$$

For the open fluid surface, we have (2.38).

According to Stoker theory, the solution for shallow water can be derived using the transition (matching) conditions for the potential, which are valid along the vertical interface boundary, and the free edge conditions for the plate. This simplifies the problem significantly compared to the FWD and IWD cases. The complete description of the shallow water depth case, so a solution, is given in section 3.5.

2.5 Green's function

The main objective of this thesis is to determine the plate deflection, free surface elevation, reflection and transmission coefficients by solving a set of equations which is derived along the plate contour. For the FWD and IWD cases, we apply the Green's theorem to the potential and vertical displacement to obtain, as will be shown later, an integral and an integro-differential equation, respectively. In the latter case, the set of equations to determine the deflection can be obtained from the integro-differential equation (IDE),

supplemented by the plate free edge conditions. As we apply the Green's theorem, the Green's function is an important part of our study.

In this section we describe the Green's function, its derivation, different forms for water of finite or infinite depth in Cartesian and polar coordinates, required conditions, and operations applied to the Green's function. Also, corresponding contours of an integration are described, and an exponential, Bessel and Hankel functions are given. It then points out the direction of further analysis for particular problems.

The general expressions for the Green's function for water of infinite and finite depth can be found in Wehausen and Laitone [146]. In this section we develop modified Green's functions to be used in further analysis. Other forms for the free surface Green's function were given by Havelock [39] for the IWD case, John [49] for the IWD and FWD cases, Noblesse [90], Eatock Taylor and Ohkusu [28] for the FWD case, and Peter and Meylan [98] for the IWD case.

2.5.1 Green's function in Cartesian coordinates

We introduce the Green's function for a source within the fluid that fulfills, in Cartesian coordinates,

$$\Delta \mathcal{G}(\mathbf{x}, \boldsymbol{\xi}) = 4\pi \delta(\mathbf{x} - \boldsymbol{\xi}), \quad (2.44)$$

where \mathbf{x} is a source point, $\boldsymbol{\xi}$ is an observation (field) point, and δ is the Dirac δ -function

$$\delta(\mathbf{x} - \boldsymbol{\xi}) = \delta(x - \xi)\delta(y - \eta)\delta(z - \zeta).$$

The Green's function, as well as the velocity potential, obeys the boundary conditions at the free surface

$$\mathcal{G}_z = K\mathcal{G}, \quad z = 0, \quad (2.45)$$

and at the bottom

$$\mathcal{G}_z = 0, \quad z = -h, \quad (2.46)$$

and the radiation condition at infinity

$$\lim_{R \rightarrow \infty} \sqrt{R} \left(\frac{\partial}{\partial R} - iK \right) \mathcal{G} = 0, \quad -h < z < 0. \quad (2.47)$$

First we describe and derive the Green's function for the IWD case, and then for the FWD case.

For deep water, the three-dimensional Green's function can be written in the following form

$$\mathcal{G}(\mathbf{x}, \boldsymbol{\xi}) = -\frac{1}{\varrho} + \frac{1}{\varrho_1} - 2 \int_{\mathcal{L}} \frac{k}{k-K} J_0(kR) e^{k(z+\zeta)} dk, \quad (2.48)$$

where $\varrho^2 = R^2 + (z - \zeta)^2$; $\varrho_1^2 = R^2 + (z + \zeta)^2$, here R is the horizontal distance, so that $R^2(x, y; \xi, \eta) = (x - \xi)^2 + (y - \eta)^2$. Further, \mathcal{L} is the contour of an integration in the

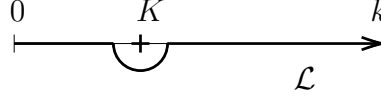


Figure 2.2: Contour of integration in the complex plane.

complex k -plane, from 0 to $+\infty$, underneath the singularity $k = K$, as shown in figure 2.2, chosen to satisfy the radiation condition, and $J_0(kR)$ is the Bessel function.

The Green's function $\mathcal{G}(x, y, z; \xi, \eta, \zeta)$ for the source and observation points at $z = \zeta = 0$ is written as

$$\mathcal{G}(x, y; \xi, \eta) = -2 \int_{\mathcal{L}} \frac{k}{k - K} J_0(kR) dk, \quad (2.49)$$

and henceforward we will use this form in our analysis.

For the case of finite water depth, the three-dimensional Green's function has the following form at $z = \zeta = 0$

$$\mathcal{G}(x, y; \xi, \eta) = -2 \int_{\mathcal{L}} \frac{k \cosh kh}{k \sinh kh - K \cosh kh} J_0(kR) dk. \quad (2.50)$$

In the case of FWD, we have additional poles $k = k_i$ for $i = 1, 2, \dots, M-3$ on the imaginary axis of the complex plane.

At $z = \zeta = 0$, the two-dimensional Green's function for infinite water depth has the form

$$\mathcal{G}(x; \xi) = -2 \int_{\mathcal{L}} \frac{\cos k(x - \xi)}{k - K} dk. \quad (2.51)$$

This expression of the Green's function is used for the case of zero angle of incidence, i.e., when we deal with perpendicular waves.

For the FWD case, the two-dimensional Green's function has the form

$$\mathcal{G}(x; \xi) = - \int_{\mathcal{L}'} \frac{\cosh kh}{k \sinh kh - K \cosh kh} e^{ik(x-\xi)} dk \quad (2.52)$$

at $z = \zeta = 0$. The contour \mathcal{L}' has two singularities: the poles of the integrand at $k = K$, which pass underneath due to the radiation condition, and at $k = -K$, passing above.

The general form of the three-dimensional Green's function for the source and observation points at $z = \zeta = 0$ is as follows

$$\mathcal{G}(x, y; \xi, \eta) = -2 \int_{\mathcal{L}} F(k) J_0(kR) dk, \quad (2.53)$$

where \mathcal{L} is the contour of the integration in the complex k -plane from 0 to $+\infty$, underneath the singularity $k = K$, as shown in figure 2.2, chosen to satisfy the radiation condition.

It is the same for the IWD and FWD case. The function $F(k)$ is given by

$$F(k) = \begin{cases} \frac{k}{k-K} & \text{for IWD,} \\ \frac{k \cosh kh}{k \sinh kh - K \cosh kh} & \text{for FWD.} \end{cases} \quad (2.54)$$

The Green's functions for IWD and FWD written above are used for plates of rectangular shape. These problems are solved in chapters 3, 6, 7.

2.5.2 Green's function in polar coordinates

The problems for plates of rotationally symmetric configuration, circular and ring-shaped ones in the thesis, have to be considered in polar coordinates. In this subsection we obtain the Green's function in polar coordinates.

The general form (2.53) of the Green's function is rewritten. In polar coordinates, the Green's function $\mathcal{G}(\rho, \varphi, z; r, \theta, \zeta)$ for the source and observation points at $z = \zeta = 0$ takes the form

$$\mathcal{G}(\rho, \varphi; r, \theta) = -2 \int_{\mathcal{L}} F(k) J_0(kR) dk, \quad (2.55)$$

where the horizontal distance R in polar coordinates is $R^2(\rho, \varphi; r, \theta) = \rho^2 + r^2 - 2\rho r \cos(\theta - \varphi)$, and the function $F(k)$ is given by (2.54). In (2.55), ρ and r are the distance from the center of the plate to the source and to the observation points, respectively, and $\theta - \varphi$ is the angle between r and ρ .

If we apply Graf's addition theorem [131] to the Bessel function $J_0(kR)$, i.e., Neumann's formula in the case of Bessel function of zero order, it can be replaced by the series in the following way

$$J_0(kR) = \sum_{q=-\infty}^{\infty} J_q(kr) J_q(k\rho) \cos q(\theta - \varphi), \quad (2.56)$$

which may be represented at once as

$$J_0(kR) = \sum_{q=0}^{\infty} \delta_q J_q(kr) J_q(k\rho) \cos q(\theta - \varphi), \quad (2.57)$$

where $\delta_0 = 1$ and $\delta_q = 2$ if $q > 0$. For numerical computations the upper limit of q can be taken as a finite number N , which then becomes the truncation parameter of the problem. This is permitted due to the decaying behavior of Bessel functions with respect to their order for finite values of the argument. All terms of an order higher than N are negligible. If the argument of the Bessel function equals zero, then $J_0(0) = 1$ and $J_q(0) = 0$ for $q > 0$.

In such a way, we represent the Bessel function $J_0(kR)$ as a combination of Bessel functions $J_q(kr)$ and $J_q(k\rho)$, and the Green's function takes the following form

$$\mathcal{G}(r, \theta; \rho, \varphi) = -2 \int_0^{\infty} F(k) \sum_{q=0}^N \delta_q J_q(kr) J_q(k\rho) \cos q(\theta - \varphi) dk \quad (2.58)$$

at $z = \zeta = 0$ in polar coordinates. The Green's function (2.58) obeys the conditions at the free surface and the bottom, and the radiation condition at infinity.

Specifically, for infinite water depth, the Green's function has the following form

$$\mathcal{G}(\rho, \varphi; r, \theta) = -2 \int_0^\infty \frac{k}{k - k_0} \sum_{q=0}^\infty \delta_q J_q(kr) J_q(k\rho) \cos q(\theta - \varphi) dk, \quad (2.59)$$

and for finite water depth it takes the form

$$\mathcal{G}(\rho, \varphi; r, \theta) = -2 \int_0^\infty \frac{k \cosh kh}{k \sinh kh - K \cosh kh} \sum_{q=0}^\infty \delta_q J_q(kr) J_q(k\rho) \cos q(\theta - \varphi) dk. \quad (2.60)$$

The analysis for the Green's function, represented in this subsection, is suitable for a plate of rotational configuration. The Green's function in the form (2.59) for IWD and in the form (2.60) for FWD are used for circular and ring-shaped plates. The problems of interaction between circular and ring-shaped VLFP and water waves are considered in chapters 4 and 5, respectively.

2.6 Deflection

Here we represent the different forms of plate deflection for each of the plate horizontal planforms studied in the thesis. Choosing a specific form for deflection is a key idea of our method.

Plate deflection can be written as the superposition of exponential functions with coefficients containing the amplitudes of the wave modes. This applies when the plate has a rectangular planform. For plates having a rotationally symmetric planform the deflection can be represented as a series of Bessel or Hankel functions. In general, the idea is similar to the geometrical-optics approach [67, 72, 12, 41] as well as to the eigenfunction approach, see, e.g., [56] for finite depth and [77] for infinite depth.

For a **semi-infinite plate** (SIP), the deflection can be represented in the following form

$$w(x, y) = \sum_{n=1}^\infty a_n e^{i(\kappa_n x + k_0 y \sin \beta)}, \quad (2.61)$$

where a_n are unknown amplitudes of corresponding wave modes, and κ_n are reduced wavenumbers. It will be shown later that κ_n are related to the roots of the dispersion relation in the plate area, and in case of perpendicular waves, they are simply the roots of the plate dispersion relation.

Due to the convergence of the series in (2.61) and, correspondingly, final results with respect to n , a finite number, N , can be taken as the upper limit. This makes N , which is the number of the wave modes considered, the truncation parameter of the problem. In such a way, the deflection of the semi-infinite plate takes the form

$$w(x, y) = \sum_{n=1}^N a_n e^{i(\kappa_n x + k_0 y \sin \beta)}, \quad (2.62)$$

where N is the number of reduced wavenumbers κ_n which are taken into account.

Analogously to the SIP case, for the rest of the problems we can introduce the finite upper limit of the series at once. The details about the chosen form of the deflection and the series convergence are given in the next chapters for different problems. The convergence of the deflection function is also justified by numerical tests.

For a **strip** of infinite length and width l , the deflection can be represented in the form

$$w(x, y) = \sum_{n=1}^N (a_n e^{i\kappa_n x} + b_n e^{-i\kappa_n x}) e^{ik_0 y \sin \beta}. \quad (2.63)$$

Here, a_n and b_n are the amplitudes of corresponding wave modes. The second term in (2.63) decreases with the growth of n ; this term is also small when $n \gg 1$ as the amplitudes b_n are small. However, the strip deflection may also be represented in the form

$$w(x, y) = \sum_{n=1}^N (a_n e^{i\kappa_n x} + b_n e^{-i\kappa_n (x-l)}) e^{ik_0 y \sin \beta}.$$

The truncation parameter N obeys the ratio $N < l/h_p$.

The representations (2.62), (2.63) (and the following ones) can be used if we consider dry modes (or 'dry plate'), where we have a finite number of modes. In our case the number of modes will be infinite, hence we truncate the series at N . Thus, a solution of the boundary value problem, equation (2.20) and boundary conditions (2.16–2.17), may be sought in the form, e.g., (2.63). Details on a number of modes taking into account are given for particular problems and water depth models.

The deflection of a **circular plate** of radius r_0 , written in polar coordinates, can be represented as a series of Bessel functions with corresponding coefficients in the following form

$$w(\rho, \varphi) = \sum_{m=1}^M \sum_{n=0}^N a_{mn} J_n(\kappa_m \rho) \cos n\varphi, \quad (2.64)$$

where a_{mn} are unknown amplitudes and κ_m the reduced wavenumbers, the roots of the dispersion relation in the plate region. Here, M is the number of reduced wavenumbers, $m = 1..M$, and N is the truncation parameter, described in the previous section.

The deflection of a **ring-shaped plate** of radii r_1 and r_0 , written in polar coordinates, can be represented as a series of Hankel functions with corresponding coefficients in the following form

$$w(\rho, \varphi) = \sum_{m=1}^M \sum_{n=0}^N [a_{mn} H_n^{(1)}(\kappa_m \rho) + b_{mn} H_n^{(2)}(\kappa_m \rho)] \cos n\varphi, \quad (2.65)$$

where a_{mn} and b_{mn} are unknown amplitudes, and κ_m , M and N are the same as for the circular plate. Analogously to the strip case, the amplitudes b_{mn} become small for $m \gg 1$.

The total deflection of a **quarter-infinite plate** (QIP) is written as the sum

$$w(x, y) = \sum_{n=1}^N a_n e^{i(\kappa_n x - k_0 y \sin \beta)} + w_s, \quad (2.66)$$

for the whole platform area (we assume that waves propagate from second to fourth quadrant). The first term is the main part of the solution, corresponding to the solution for the semi-infinite plate, and the second term represents the solution along the rays by stretching the coordinates; it is written in the following form

$$w_s(x, y) = \frac{i}{\omega} \phi_{z'}(x, y). \quad (2.67)$$

Further details are given in chapter 6.

The deflection of a semi-infinite **plate of finite draft** and thickness is written in the form

$$w(x) = \sum_{n=0}^M (a_n^{(0)} + da_n^{(1)}) e^{i\kappa_n^{(0)}(1+d\kappa_n^{(1)})x}, \quad (2.68)$$

where $a_n^{(0)}$, $a_n^{(1)}$ are the unknown amplitudes and $\kappa_n^{(0)}$, $\kappa_n^{(1)}$ the reduced wavenumbers. The superscripts 0 and 1 show the draft order. The terms of zero order represent the solution for a semi-infinite plate with zero-thickness assumption; the other terms are correction ones, derived for the first draft order. In this case we consider only perpendicular waves.

For SWD, three roots of the dispersion relation in the plate area are used, $N = 3$. This is the result of the approximation theory for shallow water. For IWD, we also use three roots of the dispersion relation; further information is given in chapters 3–5. For FWD, more roots, namely N , are taken into account in accordance with the water dispersion relation (2.33), which has one real root k_0 , corresponding to only one wavenumber for deep water, and a number of imaginary roots, k_i , where $i = 1, 2, \dots, N - 3$.

So, for plates having a rectangular planform with one infinite (horizontal) dimension, the deflection is represented as the superposition of exponential functions, while for plates having a rotationally symmetric rotational configuration it is represented as the superposition of Bessel or Hankel functions.

The deflection forms for specific problems (2.62–2.68) are good approximations of the geometrical-optics solutions for realistic values of the plate parameters \mathcal{D} and μ . This is for the case when these parameters are constant, otherwise the more general ray method can be applied for the problem.

The representation of the free surface vertical displacement, the plate deflection and water surface elevation, presented above, was validated in [3, 4, 5, 6, 7, 8, 9, 40, 41, 42, 43, 44] for a number of different problems. More information and details on the deflection function for particular problems may be found in the following chapters. Taking the finite limit in the series in (2.62) for the SIP, (2.63) for the strip, (2.64) for the circular plate, (2.65) for the ring-shaped plate, (2.66) for the QIP, and (2.68) for the plate of finite draft is justified by the theory and by numerical tests.

2.7 Integral and integro-differential equations

In this section we continue our analysis and derive main equations for the potential and vertical displacements in the plate region and open water region. We apply the Green's theorem to the potential in each respective region and, doing some operations, derive the general equation for the potential. Next, using of the relation between the potential and vertical displacement, we derive the general equations for the displacements. The main equation for the total potential is an integral, while for the plate deflection and the free surface elevation it is an integro-differential.

The main equation for the plate-water interaction problem is derived in this section. The derivation is the same for finite and infinite water depth models. The application of the Green's theorem and the derivation of the integro-differential equation are described here. The general forms of the integral and integro-differential equations are given in subsection 2.7.3. In the following chapters we will insert the specific forms of the deflection and Green's function into the plate equation to solve it. These chapters also describe further steps of the analysis and differences for other cases.

2.7.1 Formulation of integral equation

The free surface is split up into two regions \mathcal{P} and \mathcal{F} with the interface \mathcal{S} . The potential function in the open water region \mathcal{F} is written as a superposition of the incident wave potential and $\phi^{\text{dis}}(\mathbf{x})$, which is the sum of classical diffraction potential and radiation potential (scattering and radiation potential), as follows

$$\phi^{\mathcal{F}}(\mathbf{x}) = \phi^{\text{inc}}(\mathbf{x}) + \phi^{\text{dis}}(\mathbf{x}), \quad (2.69)$$

while the total potential in the plate region \mathcal{P} is denoted by $\phi^{\mathcal{P}}$. It will be shown that this choice leads to an interesting way to derive an integral equation for the potential.

The Green's theorem is applied to the potentials ϕ^{dis} and $\phi^{\mathcal{P}}$ at $z = \zeta = 0$. We obtain for the open fluid $x, y \in \mathcal{F}$:

$$4\pi\phi^{\text{dis}} = - \int_{\mathcal{S} \cup \mathcal{F}} \left(\phi^{\text{dis}} \frac{\partial \mathcal{G}}{\partial n} - \mathcal{G} \frac{\partial \phi^{\text{dis}}}{\partial n} \right) dS; \quad (2.70)$$

$$0 = \int_{\mathcal{S} \cup \mathcal{P}} \left(\phi^{\mathcal{P}} \frac{\partial \mathcal{G}}{\partial n} - \mathcal{G} \frac{\partial \phi^{\mathcal{P}}}{\partial n} \right) dS, \quad (2.71)$$

and for the plate region $x, y \in \mathcal{P}$:

$$0 = - \int_{\mathcal{S} \cup \mathcal{F}} \left(\phi^{\text{dis}} \frac{\partial \mathcal{G}}{\partial n} - \mathcal{G} \frac{\partial \phi^{\text{dis}}}{\partial n} \right) dS; \quad (2.72)$$

$$4\pi\phi^{\mathcal{P}} = \int_{\mathcal{S} \cup \mathcal{P}} \left(\phi^{\mathcal{P}} \frac{\partial \mathcal{G}}{\partial n} - \mathcal{G} \frac{\partial \phi^{\mathcal{P}}}{\partial n} \right) dS. \quad (2.73)$$

In the expressions (2.70–2.73), dS is the surface element with respect to the coordinates (ξ, η) .

We have applied the Green's theorem at $z = \zeta = 0$. Application of the Green's theorem at $z < 0$ together with an expansion of the deflection gives rise to the standard eigenfunction expansion for the potential function, which can be found in [56] or [77].

The integrals over \mathcal{F} become zero, due to the zero-current free-surface condition for the Green's function \mathcal{G} and diffraction potential ϕ^{dis} . Next, we add up the two expressions (2.72) and (2.73) and use the free surface conditions for the Green's function and the potential, which leads to

$$4\pi\phi^{\mathcal{P}} = \int_{\mathcal{S}} \left([\phi] \frac{\partial \mathcal{G}}{\partial n} - \mathcal{G} \left[\frac{\partial \phi}{\partial n} \right] \right) dS + \int_{\mathcal{P}} (K\phi^{\mathcal{P}} - \phi_{\zeta}^{\mathcal{P}}) \mathcal{G} dS \quad (2.74)$$

for $x, y \in \mathcal{P}$, where the notation [...] is used for the jump of the function concerned. Furthermore, we use the jump condition between the potentials ϕ^{dis} and $\phi^{\mathcal{P}}$, so that

$$[\phi] = \phi^{\mathcal{P}} - \phi^{\text{dis}} = \phi^{\text{inc}}, \quad (2.75)$$

and their normal derivatives. For the total potential, the jumps are zero and, therefore, we obtain

$$4\pi\phi^{\mathcal{P}} = \int_{\mathcal{S}} \left(\phi^{\text{inc}} \frac{\partial \mathcal{G}}{\partial n} - \mathcal{G} \frac{\partial \phi^{\text{inc}}}{\partial n} \right) dS - \int_{\mathcal{P}} \left(\mu\phi_{\zeta}^{\mathcal{P}} - \mathcal{D} \left(\frac{\partial^2}{\partial \xi^2} + \frac{\partial^2}{\partial \eta^2} \right)^2 \phi_{\zeta}^{\mathcal{P}} \right) \mathcal{G} dS, \quad (2.76)$$

where the relation (2.12) has been used for $\phi^{\mathcal{P}}$. The relation (2.76) is suitable for further manipulation to end up with an integro-differential equation. The Green's function itself has a weak singularity, so we may take the limit $z \rightarrow 0$ and use (2.12) to express $\phi^{\mathcal{P}}$ in terms of an operator acting on $\phi_z^{\mathcal{P}}$.

The analysis presented in this subsection, including equations (2.69–2.76), is valid in the entire fluid domain $-z < h < 0$. Then $\phi^{\mathcal{F}}$ is the potential in the domain $\mathcal{D}^{\mathcal{F}}$ and $\phi^{\mathcal{P}}$ that in the domain $\mathcal{D}^{\mathcal{P}}$. If we consider the entire fluid domain, the continuity of the total potential and its normal derivative is guaranteed at the dividing surface $\partial\mathcal{D}$, conditions (2.27).

2.7.2 Integro-differential equation

In this subsection the integro-differential is derived for the vertical displacements: the plate deflection and the free surface elevation.

The first integral on the right-hand side of (2.76) can be simplified significantly. This term is independent of the plate (platform) parameters, hence it is the same if there is no plate present. Therefore, it equals $4\pi\phi^{\text{inc}}$, which can be verified by manipulating the integrals. Finally, we derive the following integral (or integro-differential) equation for

the potential derivative $\phi_z^{\mathcal{P}}$

$$4\pi \left(\phi_z^{\mathcal{P}} - \mu \phi_z^{\mathcal{P}} + \mathcal{D} \left(\frac{\partial^2}{\partial x^2} + \frac{\partial^2}{\partial y^2} \right)^2 \phi_z^{\mathcal{P}} \right) = K \int_{\mathcal{P}} \left(\mathcal{D} \left(\frac{\partial^2}{\partial \xi^2} + \frac{\partial^2}{\partial \eta^2} \right)^2 \phi_{\xi}^{\mathcal{P}} - \mu \phi_{\xi}^{\mathcal{P}} \right) \mathcal{G} \, dS + 4\pi \phi_z^{\text{inc}}, \quad (2.77)$$

which is valid at $z = 0$. For the last term, which represents the potential of the incident waves, we have used condition (2.13).

Next, we obtain the following equation for the deflection of the plate w from (2.77), taking into account (2.22),

$$\left(\mathcal{D} \left(\frac{\partial^2}{\partial x^2} + \frac{\partial^2}{\partial y^2} \right)^2 - \mu + 1 \right) w(x, y) = \frac{K}{4\pi} \int_{\mathcal{P}} \mathcal{G}(x, y; \xi, \eta) \left(\mathcal{D} \left(\frac{\partial^2}{\partial \xi^2} + \frac{\partial^2}{\partial \eta^2} \right)^2 - \mu \right) w(\xi, \eta) \, d\xi \, d\eta + A e^{ik_0 x \cos \beta} \quad (2.78)$$

at $z = 0$, for $x, y \in \mathcal{P}$. Equation (2.78) is the general **integro-differential equation** for plate deflection.

We can directly use the derivation presented and equations (2.77) and (2.78) for the strip and for the semi-infinite plate cases. For other plate shapes, as well as for the problem in polar coordinates, some minor modifications are required.

In such a way, we can determine the potential in the plate area with (2.77), and the plate deflection with (2.78). In a similar way, we may derive the integral (integro-differential) equation to be solved in the open fluid region \mathcal{F} . Adding up expressions (2.70) and (2.71) and following the analysis given for $\phi_z^{\mathcal{P}}$, we obtain for ϕ^{dis}

$$\phi^{\text{dis}} = \frac{1}{4\pi} \int_{\mathcal{P}} \mathcal{G} \left(\mathcal{D} \left(\frac{\partial^2}{\partial \xi^2} + \frac{\partial^2}{\partial \eta^2} \right)^2 \phi_{\xi}^{\mathcal{P}} - \mu \phi_{\xi}^{\mathcal{P}} \right) \, dS. \quad (2.79)$$

The total potential in the open water region \mathcal{F} is written in the form (2.69). Thus, we have for $\phi^{\mathcal{F}}$

$$4\pi \phi^{\mathcal{F}} = K \int_{\mathcal{P}} \mathcal{G} \left(\mathcal{D} \left(\frac{\partial^2}{\partial \xi^2} + \frac{\partial^2}{\partial \eta^2} \right)^2 \phi_{\xi}^{\mathcal{P}} - \mu \phi_{\xi}^{\mathcal{P}} \right) \, dS + 4\pi \phi_z^{\text{inc}}. \quad (2.80)$$

The total potential in \mathcal{F} is represented as the sum of the incident wave potential and the potential of waves which appear due to the vibration of the plate. Analogously, the free surface elevation ζ in the open fluid region equals to the sum of the incident wave elevation and the additional wave elevation generated by the plate motion

$$\zeta = \zeta^{\text{inc}} + \zeta^{\text{pm}}, \quad (2.81)$$

where the value of elevation ζ^{inc} is known because it is the parameter of the incident wave field, whereas the value of ζ^{pm} may be obtained from the analysis of the integro-differential equation (2.80) for the region \mathcal{F}

$$\zeta(x, y) = \frac{K}{4\pi} \int_{\mathcal{P}} \mathcal{G}(x, y; \xi, \eta) \{ \mathcal{D}\Delta^2 - \mu \} w(\xi, \eta) dS + A e^{ik_0(x \cos \beta + y \sin \beta)}. \quad (2.82)$$

The term, containing the integral in (2.82), represents the displacement of the free surface which takes place due to the motion of the plate.

We may find the difference between the plate deflection w and the free-surface elevation ζ , i.e. the difference of the vertical displacement in \mathcal{P} and \mathcal{F} , at the plate contour \mathcal{S} . Using (2.78) and (2.82), we found it to be

$$\zeta = \{ \mathcal{D}\Delta^2 - \mu + 1 \} w \quad (2.83)$$

at $x, y \in \mathcal{S}$.

2.7.3 General form of integro-differential equation

This subsection describes the general forms of the integral equation for the potential, and integro-differential equations for the plate deflection and free surface elevation.

The main integral equation for the potential may be written in the general form

$$4\pi\phi(X) = 4\pi\phi^{\text{inc}}(X) + \int_{\mathcal{P}} (K\phi(\Xi) - \phi_n(\Xi)) \mathcal{G}(X; \Xi) dS, \quad (2.84)$$

in accordance to (2.77), where ϕ is the total potential, ϕ_n is its normal derivative, ϕ^{inc} is the incident wave potential, X and Ξ are the coordinates, \mathcal{P} is the unit plate on the surface of the water, and dS is the surface element with respect to Ξ coordinates. The coordinates are $X = (x, y, z)$, $\Xi = (\xi, \eta, \zeta)$ in Cartesian coordinates and $X = (\rho, \varphi, z)$, $\Xi = (r, \theta, z)$ in polar coordinates. The normal derivative of the potential, ϕ_n , at the free surface $z = 0$ becomes $\partial\phi/\partial z$, which we denote by ϕ_z . The integral equation (2.84) is valid in both areas of the free surface \mathcal{P} and \mathcal{F} .

We obtain for the normal derivative of the potential at the free surface $z = 0$

$$\{ \mathcal{D}\Delta_X^2 - \mu + 1 \} \phi_z(X) = \frac{K}{4\pi} \int_{\mathcal{P}} \mathcal{G}(X; \Xi) \{ \mathcal{D}\Delta_{\Xi}^2 - \mu \} \phi_{\zeta}(\Xi) dS + \phi_z^{\text{inc}}, \quad (2.85)$$

where Δ_X and Δ_{Ξ} are the Laplacians in corresponding coordinates. Using the expression (2.84) for the potential or the expression for the potential normal derivative (2.85) we can obtain expressions for both vertical displacements: the plate deflection in \mathcal{P} , and the free-surface elevation in \mathcal{F} .

The main integro-differential equation for the plate deflection has the following general form

$$\{ \mathcal{D}\Delta_X^2 - \mu + 1 \} w(X) = \frac{K}{4\pi} \int_{\mathcal{P}} \mathcal{G}(X; \Xi) \{ \mathcal{D}\Delta_{\Xi}^2 - \mu \} w(\Xi) dS + \zeta^{\text{inc}}. \quad (2.86)$$

For the free-surface elevation ζ , we obtain

$$\zeta(X) = \frac{K}{4\pi} \int_{\mathcal{P}} \mathcal{G}(X; \Xi) \{ \mathcal{D}\Delta_{\Xi}^2 - \mu \} w(\Xi) dS + \zeta^{\text{inc}}. \quad (2.87)$$

In such a way, the general equation for the potential ϕ is written in the form (2.84); that for the plate deflection w in the form (2.86), and that for the free-surface elevation ζ in the form (2.87).

2.8 Additional information

2.8.1 The solution

Our method is based on the integro-differential equation derived and an asymptotic theory of the geometrical-optics approach. Complete analytical and numerical studies for each problem are given in chapters 3–7. The next step of our method is insertion of the Green's and deflection functions, which are different for each problem, into the corresponding integro-differential equation. Then, from the integro-differential equation, we can derive the equations to determine the plate deflection, free-surface elevation, velocity potential, reflection and transmission coefficients, etc. The equations derived from the IDE are supplemented by relations obtained from the free edge conditions. These are presented in the following chapters, together with a theoretical explanation and numerical results, details and a discussion.

2.8.2 Asymptotic expansions

The phase velocity V_p can be expressed in the following form

$$V_p = \frac{\omega}{k_0} = \sqrt{\frac{g}{k_0} \tanh k_0 h}, \quad (2.88)$$

using (2.33).

It is possible to derive the asymptotic expression for the potential in the open-water region $\phi^{\mathcal{F}}$ at infinity, $R \rightarrow \infty$,

$$4\pi\phi^{\text{dis}} = i\sqrt{\frac{k_0}{R}} \int_{\mathcal{P}} \{ \mathcal{D}\Delta^2 - \mu \} \phi_{\zeta}^{\mathcal{P}} e^{-ik_0\rho \cos(\psi-\theta)} dS. \quad (2.89)$$

Also, doing some operations and considering the contour of the integration, one can derive the asymptotic form for the Green's function \mathcal{G} at infinity

$$\mathcal{G} \sim i\pi k_0 e^{k_0(z+\zeta)} H_0^{(1)}(k_0 R). \quad (2.90)$$

The description of nonlinear effects, neglected in the given linearized theory, may be found in [147, 88, 46] and other literature.

Chapter 3

Hydroelastic behavior of a semi-infinite plate and strip

This chapter considers first two problems of the interaction between a very large floating platform and water waves treated in the thesis. We consider two general geometric forms of the plate, which is the model of VLFP, namely a half-plane and a strip. The hydroelastic response of the two-dimensional plate to a plane incident wave is investigated for three different water depths: infinite, finite and shallow. An integro-differential equation is derived to describe the plate deflection due to the incident waves for the current case. Then, the plate deflection is determined using a derived set of equations for both geometrical forms. The expressions for the reflection and transmission coefficients are determined as well. Numerical results are obtained for various values of the parameters. The results for the strip and for the half-plane are compared for different values of depth and other parameters. In addition, a comparison of our results with those obtained by other approaches is presented.

3.1 Introduction

This chapter solves two problems of the interaction between a very large floating structure and water waves. Here, we consider two geometrical forms of the plate: a semi-infinite plate and a strip of infinite length. A VLFS is modeled by a thin elastic plate.

In general, a floating structure may have any shape. Mainly researchers have analyzed VLFSs of a rectangular planform. The case of half-plane was recently intensively studied by many researchers across Europe, Asia, America and Oceania. It is a good starting point for hydroelastic analysis of the interaction between VLFSs and water waves. Ohkusu and Namba [91] presented an asymptotic theory to describe the deflection of a platform on shallow water due to relatively short incident waves while it is positioned at shallow water. Hermans [40] derived an exact integral-differential equation for the deflection of a VLFP on deep water. The equation was solved numerically by means of a boundary element method and a mode expansion. Later Hermans [42, 43] used this formulation to derive boundary conditions to apply the ray method for short wave diffraction. The short wave expansion of Takagi et al. [115], who used the eigenfunction expansion method, leads to similar results. Khabakhpasheva and Korobkin [55] derived a set of equations

to obtain asymptotic results. Tkacheva [126, 127, 128, 129] solved this problem using the Wiener-Hopf technique. The shallow-water problem was solved by Sturova [108], who used boundary integral equations. Kim and Ertekin [56] applied the eigenfunction expansion method to solve the problem.

The following assumptions are invoked, as in a basic hydroelastic analysis of mat-like VLFSs, chapters 1–2. The fluid is incompressible, inviscid, and has irrotational motion, so that the velocity potential exists. A VLFS is modeled as a thin elastic isotropic plate with free edges. The amplitude of the incident wave and the motion of the VLFS are both small. Then only the vertical elevation of the structure is considered. There are no gaps between the VLFS and the fluid free surface.

The diffraction of surface waves by a large floating flexible plate (FFP) of general geometric form is studied. The plate, which is the model of a VLFS, floats on the surface of an ideal incompressible fluid. We consider three cases: infinite (IWD), finite (FWD) and shallow (SWD) water depth. Differences between these three cases shall be indicated in this chapter. The problem is solved for oblique incident waves, which includes the case of normal incidence: perpendicular incoming waves. The integro-differential formulation is applied; we derive the main integro-differential equation for the problem. The integro-differential equation can be used more flexibly to derive asymptotic results compared to other methods. The approach is developed for and applied to two different forms of the plate: an infinitely long strip of finite width and a semi-infinite plate. For both forms of the plate we obtain and compare an analytical solution and numerical results for the plate deflection. Reflection and transmission of incoming waves are studied as well.

The theory and approach described in this chapter were previously presented and published in [40, 3, 4, 43, 5] together with some results. Our approach is based on the integro-differential equation derived and an asymptotic theory of the geometrical-optics approach. The main equations and physical parameters are described in chapter 2; here we only give specific information if needed.

3.2 Formulation of the problem

The mathematical formulation is derived for the diffraction of waves by the floating flexible plate, floating on the surface of an ideal incompressible fluid of constant depth h . The numerical value of the water depth is varied for the IWD, FWD and SWD models.

The geometry of the problem and coordinate system are shown in figure 3.1. Incoming waves are propagated from the open fluid with an angle β to the positive x -direction. In the case of a strip of width l and infinite length $0 \leq x \leq l$, $-\infty < y < \infty$ we define the open fluid area $-\infty < x < 0 \cup l < x < \infty$ as \mathcal{F} , the plate area, part of the free surface, covered by the plate $0 < x < l$ as \mathcal{P} and the dividing line, the plate contour $x = 0 \cup x = l$, as \mathcal{S} ; whereas for the semi-infinite platform (SIP) $0 \leq x < \infty$, $-\infty < y < \infty$, \mathcal{F} is $x < 0$, \mathcal{P} is $x > 0$, and \mathcal{S} is $x = 0$.

We assume waves in otherwise still water and introduce the velocity potential by $\nabla\Phi(\mathbf{x}, t) = \mathbf{V}(\mathbf{x}, t)$. As was described in chapter 2, see formulas (2.1–2.5), $\Phi(x, y, z, t)$ is a solution of the Laplace equation

$$\Delta\Phi = 0 \tag{3.1}$$

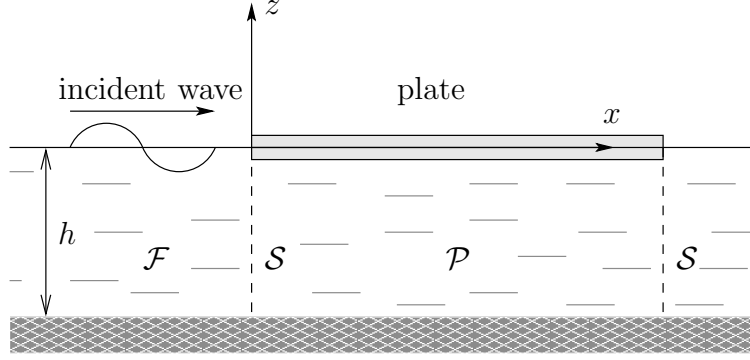


Figure 3.1: Geometry and coordinate system of the problem.

in the fluid ($z < 0$), supplemented by the boundary conditions and the radiation condition (2.26). The boundary conditions at the free surface conditions, $z = 0$, are:
at the plate area $x, y \in \mathcal{P}$

$$\frac{\partial \Phi}{\partial z} = \frac{\partial W}{\partial t}, \quad (3.2)$$

and at the fluid area $x, y \in \mathcal{F}$

$$\frac{\partial \Phi}{\partial z} = -\frac{1}{g} \frac{\partial^2 \Phi}{\partial t^2}; \quad (3.3)$$

and the boundary condition at the bottom $z = -h$ is:

$$\frac{\partial \Phi}{\partial z} = 0. \quad (3.4)$$

The function $W(x, y, t)$ denotes either the deflection in the plate area \mathcal{P} or the free surface elevation in the open water region \mathcal{F} . The boundary conditions are the same for all water depths.

The matching conditions at the vertical boundaries \mathcal{S} are:

$$\Phi_x \text{ and } \Phi_t \text{ are continuous at } \mathcal{S}, \quad (3.5)$$

as the direction of the normal n to the plate edge coincides with the x -direction. Physically these conditions express that the mass of the water is conserved and the energy flux is continuous.

The platform is assumed to be a thin layer at the free surface $z = 0$. A shallow draft platform can be modeled as an elastic plate with zero thickness. To describe the deflection of the plate, we use the thin plate theory, which leads to a differential equation of the following form:

$$D \left(\frac{\partial^2}{\partial x^2} + \frac{\partial^2}{\partial y^2} \right)^2 W + m \frac{\partial^2 W}{\partial t^2} = P(x, y, t) \quad (3.6)$$

at $z = 0$ for the plate area $x \in \mathcal{P}$. The linearized pressure P is written in the following form

$$P = -\rho_w \frac{\partial \Phi}{\partial t} - \rho_w g W \text{ at } z = 0, \quad (3.7)$$

where ρ_w is the density of the fluid.

For infinite and finite water depth, we apply the operator $\partial/\partial t$ to (3.7) and use the surface condition (3.2) to derive from (3.6) the following equation for Φ at $z = 0$ in the plate area $(x, y) \in \mathcal{P}$

$$\left\{ \frac{D}{\rho_w g} \left(\frac{\partial^2}{\partial x^2} + \frac{\partial^2}{\partial y^2} \right)^2 + \frac{m}{\rho_w g} \frac{\partial^2}{\partial t^2} + 1 \right\} \frac{\partial \Phi}{\partial z} + \frac{1}{g} \left\{ \frac{\partial^2}{\partial t^2} \right\} \Phi = 0. \quad (3.8)$$

As harmonic motion is considered, we can represent the potential of the incident wave in the following form

$$\Phi(x, y, z, t) = \phi(x, y, z) e^{-i\omega t}. \quad (3.9)$$

Then, the potential ϕ must satisfy the Laplace equation (2.20), the boundary conditions at the sea bed (2.21) and at the free surface (2.22–2.23), and the Sommerfeld radiation condition (2.26) in the far field. The deflection and the pressure can be represented in the same way as the potential, see formulas (2.8) and (2.9), respectively. Using these three representations, we work in the frequency domain and obtain the relations for the potential (2.12) at the plate area \mathcal{P} and (2.13) at the open fluid area \mathcal{F} .

The incident wave potential for a fluid of infinite depth equals, see subsection 2.4.2 (p.30),

$$\phi^{\text{inc}} = -\frac{igA}{\omega} e^{iK(x \cos \beta + y \sin \beta) + Kz}, \quad (3.10)$$

where A is the wave amplitude of the undisturbed incident wave, ω is the frequency, and K is the wavenumber, which equals $K = \omega^2/g$ for IWD.

In the case of shallow depth, subsection 2.4.4 (p.31), the wavenumber is $k_{\text{sh}} = \omega/\sqrt{gh}$ and the incident wave potential is written as

$$\phi^{\text{inc}} = -\frac{igA}{\omega} e^{ik_{\text{sh}}(x \cos \beta + y \sin \beta)}. \quad (3.11)$$

For finite water depth, subsection 2.4.3 (p.31), the potential of the incident waves is written in the following form

$$\phi^{\text{inc}} = -\frac{\cosh k_0(z+h)}{\cosh k_0 h} \frac{igA}{\omega} e^{ik_0(x \cos \beta + y \sin \beta)}, \quad (3.12)$$

and the wavenumber k_0 is the only positive real solution of the water dispersion relation

$$k_i \tanh k_i h = K, \quad (3.13)$$

where $K = \omega^2/g$. The imaginary roots k_i , $i > 0$ of the dispersion relation (3.13) are discussed later on in this thesis.

The wavelength of the incoming waves is $\lambda = 2\pi/k_0$. In this chapter, for the strip we consider the waves to be smaller than the strip width l .

The free edge(s) of the plate is (are) free of shear forces, bending and twisting moments. Hence, the free edge conditions are:

$$\frac{\partial^2 w}{\partial x^2} + \nu \frac{\partial^2 w}{\partial y^2} = 0, \quad (3.14)$$

$$\frac{\partial^3 w}{\partial x^3} + (2 - \nu) \frac{\partial^3 w}{\partial x \partial y^2} = 0, \quad (3.15)$$

when $x, y \in \mathcal{S}$ at $z = 0$.

3.3 Integro-differential equation

The main integro-differential equation for the problem is derived in this section. The IDE for the plate deflection was derived in chapter 2. Following the analysis given in section 2.7, we split the fluid domain into two regions with an interface surface \mathcal{S} . The free surface at $z = 0$ is split into a plate \mathcal{P} and open fluid \mathcal{F} areas by the plate contour \mathcal{S} .

The potential function in \mathcal{F} is written as a superposition of the incident wave potential ϕ^{inc} and a ϕ^{dis} , which is the sum of classical diffraction potential and radiation potential, as follows

$$\phi^{\mathcal{F}}(\mathbf{x}) = \phi^{\text{inc}}(\mathbf{x}) + \phi^{\text{dis}}(\mathbf{x}), \quad (3.16)$$

while the total potential in \mathcal{P} is denoted by $\phi^{\mathcal{P}}$. It will be shown that this choice leads to an interesting way to derive an integral equation.

We introduce the Green's function $\mathcal{G}(\mathbf{x}, \boldsymbol{\xi})$, which fulfills $\Delta \mathcal{G} = 4\pi\delta(\mathbf{x} - \boldsymbol{\xi})$, where δ is the Dirac δ -function, the boundary conditions at the free surface and the bottom, and the radiation condition. Next, the Green's theorem is applied to the potentials ϕ^{dis} and $\phi^{\mathcal{P}}$, respectively. Then, the equations (2.70–2.71) are obtained for open fluid $x, y \in \mathcal{F}$, and equations (2.72–2.73) at the plate region $x, y \in \mathcal{P}$.

The integrals over \mathcal{F} become zero, due to the zero-current free-surface condition for \mathcal{G} and ϕ^{dis} . Adding up the two expressions in (2.72–2.73) and using the free-surface condition for the Green's function (2.45) and the potential ϕ^{dis} (2.13), we derive

$$4\pi\phi^{\mathcal{P}} = \int_{\mathcal{S}} \left([\phi] \frac{\partial \mathcal{G}}{\partial n} - \mathcal{G} \left[\frac{\partial \phi}{\partial n} \right] \right) dS + \int_{\mathcal{P}} (K\phi^{\mathcal{P}} - \phi_{\zeta}^{\mathcal{P}}) \mathcal{G} dS, \quad (3.17)$$

for $x, y \in \mathcal{P}$, where the notation [...] is used for the jump of the function concerned and dS is the surface element with respect to the coordinates (ξ, η) . The jump conditions between the potentials ϕ^{dis} and $\phi^{\mathcal{P}}$ (2.75) and their normal derivatives are used. In addition, we use relation (3.8) for $\phi^{\mathcal{P}}$ and obtain

$$4\pi\phi^{\mathcal{P}} = \int_{\mathcal{S}} \left(\phi^{\text{inc}} \frac{\partial \mathcal{G}}{\partial n} - \mathcal{G} \frac{\partial \phi^{\text{inc}}}{\partial n} \right) dS - \int_{\mathcal{P}} \left(\mu \phi_{\zeta}^{\mathcal{P}} - \mathcal{D} \left(\frac{\partial^2}{\partial \xi^2} + \frac{\partial^2}{\partial \eta^2} \right)^2 \phi_{\zeta}^{\mathcal{P}} \right) \mathcal{G} dS, \quad (3.18)$$

where the structural parameters $\mathcal{D} = D/\rho_w g$, $\mu = m\omega^2/\rho_w g$ are introduced. These parameters are constant as we are investigating an isotropic plate.

Relation (3.18) is suitable for further manipulation to end up with an integral equation for the potential and then an integro-differential equation for the plate deflection that can be solved numerically. We notice that the first integral on the right-hand side of (3.18) can be simplified significantly as this term is independent of the parameters of the plate

(platform). Hence, it would be the same if no platform were present and, therefore, it equals $4\pi\phi^{\text{inc}}$. Next, we may take the limit $z \rightarrow 0$ and use (3.8) to express $\phi^{\mathcal{P}}$ in terms of an operator acting on $\phi_z^{\mathcal{P}}$ because the Green's function itself has a weak singularity. Then we obtain the following integro-differential equation for the potential derivative $\phi_z^{\mathcal{P}}$

$$4\pi \left(\phi_z^{\mathcal{P}} - \mu \phi_z^{\mathcal{P}} + \mathcal{D} \left(\frac{\partial^2}{\partial x^2} + \frac{\partial^2}{\partial y^2} \right)^2 \phi_z^{\mathcal{P}} \right) + K \int_{\mathcal{P}} \left(\mu \phi_{\xi}^{\mathcal{P}} - \mathcal{D} \left(\frac{\partial^2}{\partial \xi^2} + \frac{\partial^2}{\partial \eta^2} \right)^2 \phi_{\xi}^{\mathcal{P}} \right) \mathcal{G} \, dS = 4\pi \phi_z^{\text{inc}}, \quad (3.19)$$

at the surface $z = 0$.

Taking into account relation (2.22), we move from the velocity potential to the deflection of the plate w and obtain the following equation

$$\left(\mathcal{D} \left(\frac{\partial^2}{\partial x^2} + \frac{\partial^2}{\partial y^2} \right)^2 - \mu + 1 \right) w(x, y) = \frac{K}{4\pi} \int_{\mathcal{P}} \mathcal{G}(x, y; \xi, \eta) \left(\mathcal{D} \left(\frac{\partial^2}{\partial \xi^2} + \frac{\partial^2}{\partial \eta^2} \right)^2 - \mu \right) w(\xi, \eta) \, d\xi \, d\eta + A e^{ik_0(x \cos \beta + y \sin \beta)}. \quad (3.20)$$

This is the governing integro-differential equation (IDE) for problem considered. It has the same form for FWD and IWD. However, next we will need to use the Green's and deflection functions, different for these two depths, and insert them into IDE (3.20) to continue our analysis.

3.4 Finite water depth

In this section we derive the solution for a strip and semi-infinite plate on FWD. The finite water-depth model is the most important, but also the most difficult to study. First, we insert specific forms of the Green's function and deflection into the integro-differential equation. The following analysis results in a solution of the problem. A set of equations to determine the plate deflection is obtained, as well as expressions for the reflection and transmission of incident waves.

The Green's function obeys the boundary conditions at the free surface and the bottom and the radiation condition; further particulars are given in section 2.5. For FWD, the Green's function has the following form at $z = 0$

$$\mathcal{G}(x, y; \xi, \eta) = -2 \int_{\mathcal{L}} \frac{k \cosh kh}{k \sinh kh - K \cosh kh} J_0(kr) \, dk, \quad (3.21)$$

where \mathcal{L} is the integration contour in the complex k -plane, as seen in figure 2, from 0 to $+\infty$ underneath the singularity $k = k_0$, chosen for fulfilling the radiation condition, $J_0(kr)$ is Bessel function, while r is horizontal distance, so $r^2 = (x - \xi)^2 + (y - \eta)^2$.

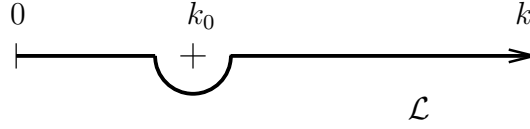


Figure 3.2: Contour of the integration.

3.4.1 Solution

First, we consider the **strip** shape. The deflection of the plate is represented as a superposition of exponential functions in the following form at $z = 0$

$$w(x, y) = \sum_{n=1}^M (a_n e^{i\kappa_n x} + b_n e^{-i\kappa_n x}) e^{ik_0 y \sin \beta} \quad (3.22)$$

for $0 \leq \beta \leq \beta_{cr} \leq \pi/2$, where unknown amplitudes a_n , b_n and reduced wavenumbers κ_n have to be determined. The critical angle of incidence β_{cr} will be discussed later in this section; mainly in the thesis we consider the situation when $\beta \leq \beta_{cr}$. We will see later that because the inhomogeneous term behaves like $e^{ik_0 x}$ does not mean that the solution behaves accordingly. Initially the upper limit of the series (3.22) is infinite, but as discussed in section 2.6, it can be replaced by the finite number M . The value of M is chosen and discussed later on in this chapter. To describe the connection between the plate deflection and the potential we use the condition (2.22).

Next, we insert the Green's function (3.21) and the plate deflection (3.22) into IDE (3.20). To carry out the integration with respect to η , we use the following formula [73]

$$\int_0^\infty \cos(bt) J_0(k\sqrt{a^2 + t^2}) dt = \begin{cases} 0 & \text{if } k < b, \\ \frac{\cos a\sqrt{k^2 - b^2}}{\sqrt{k^2 - b^2}} & \text{if } k > b, \end{cases} \quad (3.23)$$

for the Bessel function $J_0(kr)$. After the integration with respect to ξ and decomposition by $e^{ik_0 y \sin \beta}$ we obtain the following equation

$$\begin{aligned} \sum_{n=1}^M \left(\mathcal{D}\kappa^{(n)4} - \mu + 1 \right) (a_n e^{i\kappa_n x} + b_n e^{-i\kappa_n x}) &= i \sum_{n=1}^M \frac{K}{2\pi} \left(\mathcal{D}\kappa^{(n)4} - \mu \right) \times \\ &\int_{\mathcal{L}} \frac{\cosh kh}{k \sinh kh - K \cosh kh} \left(a_n \left[\frac{e^{ix\sqrt{k^2 - k_0^2 \sin^2 \beta}}}{\sqrt{k^2 - k_0^2 \sin^2 \beta} - \kappa_n} - \frac{e^{-ix\sqrt{k^2 - k_0^2 \sin^2 \beta}}}{\sqrt{k^2 - k_0^2 \sin^2 \beta} + \kappa_n} \right] \right. \\ &+ b_n \left[\frac{e^{ix\sqrt{k^2 - k_0^2 \sin^2 \beta}}}{\sqrt{k^2 - k_0^2 \sin^2 \beta} + \kappa_n} - \frac{e^{-ix\sqrt{k^2 - k_0^2 \sin^2 \beta}}}{\sqrt{k^2 - k_0^2 \sin^2 \beta} - \kappa_n} \right] \Bigg) \frac{k dk}{\sqrt{k^2 - k_0^2 \sin^2 \beta}} + A e^{ik_0 x \cos \beta}, \end{aligned} \quad (3.24)$$

where $\kappa^{(n)}$ is defined as

$$\kappa^{(n)} = \sqrt{\kappa_n^2 + k_0^2 \sin^2 \beta} \quad \text{for } n = 1, \dots, M. \quad (3.25)$$

The coefficient b in expression (3.23) corresponds to $k_0 \sin \beta$ in our analysis.

The contribution of the integral along the branch cut must be zero, which results in the choice of two different contours for the integrand in the expanded IDE (3.24). For the first part of the integrand with the plus signs in the exponential, the contour is chosen above the branch cut, whereas for the second part with the minus signs in the exponential, the contour is chosen underneath the branch cut. Adding up the two integrals results in a zero, required by formula (3.23). The first part of the integral (terms with the plus signs) can be closed in the upper half-plane. The final result is an integral, which can be written as a sum of residues [5, 43] at the poles described below.

We assume that the poles at $\kappa_n = \sqrt{k^2 - k_0^2 \sin^2 \beta}$ are in the upper half-plane and apply the residue lemma at these poles. Then, the coefficients of $e^{i\kappa x}$ are considered to derive the dispersion relation for $\kappa^{(n)}$

$$(\mathcal{D}\kappa^4 - \mu + 1) \kappa \tanh \kappa h = K \quad (3.26)$$

for finite water depth. The dispersion relation (3.26) has the following solutions in the complex plane: two at the real axis $\pm\kappa^{(1)}$, four complex roots $\pm\kappa^{(2)}$, $\pm\kappa^{(3)}$; the position of these six roots is shown in figure 3.3, and $\pm\kappa^{(n)}$, $n = 4, 5, \dots$ at the imaginary axis. The four complex roots are symmetrically placed with respect to both the real and imaginary axes, so that $\pm\kappa^{(2,3)} = \pm(\kappa_{\text{Re}} \pm i\kappa_{\text{Im}})$. We take into account M roots of the dispersion relation due to the form of the plate deflection (3.22).

Three roots are physically realistic solutions for κ , so for IWD and SWD. They are situated in the upper complex half-plane, namely: real positive root $\kappa^{(1)}$, which represents a traveling wave mode, and two complex roots $\kappa^{(2)}$ and $\kappa^{(3)}$ with equal imaginary parts and equal but opposite-signed real parts, which represent damped wave modes.

Also, we can determine the critical angle of incidence. The angle becomes critical when κ_1 , the value corresponding to the real positive root $\kappa^{(1)}$ of the dispersion relation, equals 0, therefore

$$\sin \beta_{\text{cr}} = \kappa^{(1)} / k_0. \quad (3.27)$$

Next, we consider the zeros of the dispersion relation for the water surface (3.13). We take into account $M - 2$ roots k_i of the water dispersion relation, one real k_0 and $M - 3$ imaginary k_i , $i = 1, \dots, M - 3$, which are also poles of the integrand in (3.24) with the integration contour being closed in the complex plane. These roots lead us to the relations for determining the amplitudes a_n and b_n , which are coefficients of the deflection function.

The contribution of the pole $k = k_0$ give us two linear relations:

$$\begin{aligned} & \sum_{n=1}^M \left(\mathcal{D}\kappa^{(n)4} - \mu \right) \frac{k_0 K}{(K(1 - Kh) + k_0^2 h)} \\ & \times \left(\frac{a_n}{(\kappa_n - k_0 \cos \beta) \cos \beta} - \frac{b_n}{(\kappa_n + k_0 \cos \beta) \cos \beta} \right) + A = 0, \end{aligned} \quad (3.28)$$

and

$$\begin{aligned} & \sum_{n=1}^M \left(\mathcal{D}\kappa^{(n)4} - \mu \right) \frac{k_0 K}{(K(1 - Kh) + k_0^2 h)} \\ & \times \left(-\frac{a_n e^{i\kappa_n l}}{(\kappa_n + k_0 \cos \beta) \cos \beta} + \frac{b_n e^{-i\kappa_n l}}{(\kappa_n - k_0 \cos \beta) \cos \beta} \right) = 0. \end{aligned} \quad (3.29)$$

The contribution of the imaginary poles $k = k_i$ leads to $2(M - 3)$ equations for $i = 1, \dots, M - 3$

$$\sum_{n=1}^M \left(\mathcal{D}\kappa^{(n)^4} - \mu \right) \frac{k_i^2 K}{(K(1 - Kh) + k_i^2 h) k_i^*} \left(\frac{a_n}{(\kappa_n - k_i^*)} - \frac{b_n}{(\kappa_n + k_i^*)} \right) = 0, \quad (3.30)$$

$$\sum_{n=1}^M \left(\mathcal{D}\kappa^{(n)^4} - \mu \right) \frac{k_i^2 K}{(K(1 - Kh) + k_i^2 h) k_i^*} \left(-\frac{a_n e^{i\kappa_n l}}{(\kappa_n + k_i^*)} + \frac{b_n e^{-i\kappa_n l}}{(\kappa_n - k_i^*)} \right) = 0, \quad (3.31)$$

where $k_i^* = \sqrt{k_i^2 - k_0^2 \sin^2 \beta}$. Terms containing b_n do not result in numerical computation problems for the current case; if so, it is possible to choose another form of the deflection, which is given in section 2.6.

For the strip-shaped plate we may obtain four relations from the free edge conditions at both edges $x = 0$ and $x = l$. These four relations are required to complete the set of equations for determining the plate deflection. The zero-moment condition (3.14) leads to:

$$\sum_{n=1}^M (\kappa_n^2 + \nu k_0^2 \sin^2 \beta) (a_n + b_n) = 0 \quad (3.32)$$

and

$$\sum_{n=1}^M (\kappa_n^2 + \nu k_0^2 \sin^2 \beta) (a_n e^{i\kappa_n l} + b_n e^{-i\kappa_n l}) = 0. \quad (3.33)$$

The zero condition for generalized shear force (3.15) leads to:

$$\sum_{n=1}^M (\kappa_n^3 + (2 - \nu) \kappa_n k_0^2 \sin^2 \beta) (a_n - b_n) = 0 \quad (3.34)$$

and

$$\sum_{n=1}^M (\kappa_n^3 + (2 - \nu) \kappa_n k_0^2 \sin^2 \beta) (a_n e^{i\kappa_n l} - b_n e^{-i\kappa_n l}) = 0. \quad (3.35)$$

In this way, we have completed the set of $2M$ equations (3.28–3.35). The solution of this set gives us the values of the deflection components a_n and b_n and, correspondingly, the value of the deflection itself computed by (3.22).

Next, we study the reflection and transmission of incoming waves. Adding up the two expressions (2.70–2.71), we can compute the reflection and transmission coefficients as a contribution of the pole $k = k_0$ in the regions $x < 0$ and $x > l$, respectively. For the reflection coefficient R , which is the amplitude of the reflected wave, we obtain:

$$R = \frac{k_0 K}{(K - K^2 h + k_0^2 h)} \left(\sum_{n=1}^M \frac{(\mathcal{D}\kappa^{(n)^4} - \mu) a_n}{(\kappa_n + k_0 \cos \beta) \cos \beta} (e^{i(k_0 + \kappa_n)l} - 1) + \sum_{n=1}^M \frac{(\mathcal{D}\kappa^{(n)^4} - \mu) b_n}{(\kappa_n - k_0 \cos \beta) \cos \beta} (e^{i(k_0 - \kappa_n)l} - 1) \right). \quad (3.36)$$

For the transmission coefficient T , the amplitude of the transmitted wave, we derive the following result

$$T = 1 + \frac{k_0 K}{(K - K^2 h + k_0^2 h)} \left(\sum_{n=1}^M \frac{(\mathcal{D}\kappa^{(n)^4} - \mu) a_n}{(\kappa_n - k_0 \cos \beta) \cos \beta} (e^{-i(k_0 - \kappa_n)l} - 1) + \sum_{n=1}^M \frac{(\mathcal{D}\kappa^{(n)^4} - \mu) b_n}{(\kappa_n + k_0 \cos \beta) \cos \beta} (e^{-i(k_0 + \kappa_n)l} - 1) \right). \quad (3.37)$$

The coefficients R and T are determined for each depth and compared later.

For the **semi-infinite** plate, the method described above is used. The Green's function has the same form (it does not depend on the floating object), whereas the deflection is written in the form

$$w(x, y) = \sum_{n=1}^M a_n e^{i\kappa_n x + ik_0 y \sin \beta}. \quad (3.38)$$

Inserting (3.21) and (3.38) into the IDE (3.20), we obtain an expanded integro-differential equation for the half-plane problem in the form (3.24) without b_n -terms; see also [43].

The dispersion relation (3.26), its roots $\kappa^{(n)}$, reduced wavenumbers κ_n , and angle β_{cr} are the same as for the strip-shaped plate. Doing the same operations as for the strip, we derive relations (3.28) and (3.30) without b_n -terms and two edge conditions at $x = 0$, which are:

$$\sum_{n=1}^M (\kappa_n^2 + \nu k_0^2 \sin^2 \beta) a_n = 0, \quad (3.39)$$

$$\sum_{n=1}^M (\kappa_n^3 + (2 - \nu) \kappa_n k_0^2 \sin^2 \beta) a_n = 0. \quad (3.40)$$

After solving the system of M equations we obtain M amplitudes a_n , which allows us to find the deflection. The reflection coefficient for the semi-infinite plate R_∞ can be computed by formula (3.36) without the b_n -term.

In a situation where $\beta \geq \beta_{\text{cr}}$, our model remains valid. In this case we have three damped modes, the coefficients are $R = 1$ and $T = 0$, and the plate is deflected only near the edge $x = 0$.

The case of perpendicular waves — the case of normal incidence — is the particular case of the analysis presented. Taking $\beta = 0$, we can easily derive the equations for the plate deflection and the coefficients of the incident field in a simplified form.

Finite water depth is the general case. Taking the limit $h \rightarrow \infty$ we arrive at IWD and with the limit $h \rightarrow 0$ at SWD including the transition from dispersion relation (3.26) for finite water to dispersion relations for infinite and shallow water, respectively.

3.5 Infinite water depth

This chapter derives the solution for infinite water depth. The solution is based on the analysis of the previous chapter, but here we have some differences. The wavenumber, the potential of incoming waves and the Green's function are different from FWD, whereas the deflection is represented in the same form for the geometries of the plate: (3.22) for the strip and (3.38) for the half-plane.

In the same way, we split the fluid domain and do following operations described in section 3.3, we introduce the Green's function and obtain the expressions (3.17–3.18) and, then, (3.19). Finally, we obtain the integro-differential equation for the plate deflection (3.20), which has exactly the same form as that for FWD.

The Green's function obeys the boundary conditions at the free surface and at the bottom, and the radiation condition. For infinitely deep water, according to section 2.5, the Green's function has the form

$$\mathcal{G}(x, y; \xi, \eta) = -2 \int_{\mathcal{L}} \frac{k}{k - K} J_0(kr) dk \quad (3.41)$$

at $z = 0$, where \mathcal{L} and $J_0(kr)$ are as in section 3.4.

First we consider the **strip** shape. The plate deflection is described by (3.22), $M = 3$, the amplitudes a_n , b_n , reduced wavenumbers κ_n , roots $\kappa^{(n)}$ and β_{cr} are of the same order as for FWD.

Next, we insert the expressions for the Green's function (3.41) and deflection (3.22) into the IDE (3.20). Integrating with respect to ξ and η , we obtain the following equation

$$\begin{aligned} \sum_{n=1}^3 \left(\mathcal{D}\kappa^{(n)4} - \mu + 1 \right) (a_n e^{i\kappa_n x} + b_n e^{-i\kappa_n x}) = i \sum_{n=1}^3 \frac{K}{2\pi} \left(\mathcal{D}\kappa^{(n)4} - \mu \right) \times \\ \int_{\mathcal{L}} \frac{k}{(k - K) \sqrt{k^2 - K^2 \sin^2 \beta}} \left(a_n \left[\frac{e^{ix \sqrt{k^2 - K^2 \sin^2 \beta}}}{\sqrt{k^2 - K^2 \sin^2 \beta} - \kappa_n} - \frac{e^{-ix \sqrt{k^2 - K^2 \sin^2 \beta}}}{\sqrt{k^2 - K^2 \sin^2 \beta} + \kappa_n} \right] \right. \\ \left. + b_n \left[\frac{e^{ix \sqrt{k^2 - K^2 \sin^2 \beta}}}{\sqrt{k^2 - K^2 \sin^2 \beta} + \kappa_n} - \frac{e^{-ix \sqrt{k^2 - K^2 \sin^2 \beta}}}{\sqrt{k^2 - K^2 \sin^2 \beta} - \kappa_n} \right] \right) dk + A e^{iKx \cos \beta}. \end{aligned} \quad (3.42)$$

Following the analysis, we consider the integrand of the expanded IDE (3.42). The integral has to be evaluated for positive values of x . We transform the integral into integrals along the vertical axis in the complex k -plane. The path of integration of the first part of the integral can be closed in the first quadrant of the complex plane, while the integration contour for the second part is closed in the fourth quadrant [41].

We consider two situations separately and obtain, collecting the coefficients of the exponential function $e^{i\kappa x}$,

$$(\mathcal{D}\kappa^4 - \mu + 1) \kappa = \pm K, \quad (3.43)$$

where the plus sign corresponds to the first integral, having the poles in the first quadrant, and the minus sign to the second integral, having the poles in the fourth quadrant. Three roots of (3.43) meet the requirements, and they coincide with the roots of the plate

dispersion relation. The dispersion relation at the plate area for infinite water depth is written as

$$(\mathcal{D}\kappa^4 - \mu + 1)\kappa = K. \quad (3.44)$$

We take into account three roots for κ : one real root $\kappa^{(1)}$ and two complex roots $\kappa^{(2)}$, $\kappa^{(3)}$. All six roots of the dispersion relation (3.44) are shown in figure 3.3. As for finite depth, the three roots represent the traveling (real root) and damped (complex roots) wave modes. For IWD we ignore the contribution along the imaginary axis of the k -plane, after closing the integration contour.

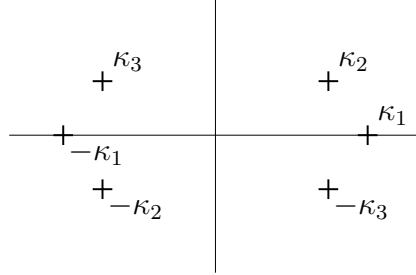


Figure 3.3: Zeros of the dispersion relation for deep water.

The contribution of the zeros of the dispersion relation for the water results in relations to determine the amplitudes a_n and b_n . Computing the contribution of the pole $k = k_0$, we obtain two linear relations:

$$\sum_{n=1}^3 (\mathcal{D}\kappa^{(n)4} - \mu) K \left(\frac{a_n}{(\kappa_n - K \cos \beta) \cos \beta} - \frac{b_n}{(\kappa_n + K \cos \beta) \cos \beta} \right) + A = 0 \quad (3.45)$$

and

$$\sum_{n=1}^3 (\mathcal{D}\kappa^{(n)4} - \mu) K \left(-\frac{a_n e^{i\kappa_n l}}{(\kappa_n + K \cos \beta) \cos \beta} + \frac{b_n e^{-i\kappa_n l}}{(\kappa_n - K \cos \beta) \cos \beta} \right) = 0. \quad (3.46)$$

Together with the free edge conditions (3.32–3.35) we have obtained the set of six equations needed to find the amplitudes a_n and b_n . Next, the deflection can be computed.

For the reflection and transmission coefficients, the following relations are obtained:

$$R = \sum_{n=1}^3 \frac{(\mathcal{D}\kappa^{(n)4} - \mu) K a_n}{(\kappa_n + K \cos \beta) \cos \beta} (e^{i(K+\kappa_n)l} - 1) + \sum_{n=1}^3 \frac{(\mathcal{D}\kappa^{(n)4} - \mu) K b_n}{(\kappa_n - K \cos \beta) \cos \beta} (e^{i(K-\kappa_n)l} - 1), \quad (3.47)$$

$$T = 1 + \sum_{n=1}^3 \frac{(\mathcal{D}\kappa^{(n)4} - \mu) K a_n}{(\kappa_n - K \cos \beta) \cos \beta} (e^{-i(K-\kappa_n)l} - 1) + \sum_{n=1}^3 \frac{(\mathcal{D}\kappa^{(n)4} - \mu) K b_n}{(\kappa_n + K \cos \beta) \cos \beta} (e^{-i(K+\kappa_n)l} - 1). \quad (3.48)$$

For the **semi-infinite** plate, the deflection is written in the form (3.38), $M = 3$. Using the same method, we derive (3.45) without the b_n -term and two free edge conditions at $x = 0$ (3.39) and (3.40). The reflection coefficient can be computed by (3.47) without the b_n -term.

3.6 Shallow water depth

Here we derive the solution for shallow water. The solution is based on transition conditions, that is different from the analysis for FWD and IWD. According to Stoker [107], the solution for the plate elevation, reflection and transmission of the incident wave can be derived using the transition (matching) and the free edge conditions.

In this section, the wavenumber k_{sh} is given by (2.39), and the plate deflection is represented by (3.22) for a strip of width l and by (3.38) for a semi-infinite plate, respectively. The amplitudes a_n , b_n , reduced wavenumbers κ_n and critical angle β_{cr} are the same as these parameters in sections 3.4–3.5.

For the plate, which floats on a fluid of shallow depth, in accordance with the shallow-water theory of Stoker [107], we have the approximation condition

$$\Phi_z = -h \left(\frac{\partial^2}{\partial x^2} + \frac{\partial^2}{\partial y^2} \right) \Phi. \quad (3.49)$$

Representing the potential in the form (3.9), the approximation condition takes the form

$$\frac{\partial \phi}{\partial z} = -h \left(\frac{\partial^2}{\partial x^2} + \frac{\partial^2}{\partial y^2} \right) \phi. \quad (3.50)$$

From the free surface conditions (3.2–3.3) using (3.50) we can obtain the following conditions:

$$\left(\frac{\partial^2}{\partial x^2} + \frac{\partial^2}{\partial y^2} \right) \phi - \frac{i\omega}{h} w = 0 \quad (3.51)$$

at the plate area $x, y \in \mathcal{P}$, and

$$\left(\frac{\partial^2}{\partial x^2} + \frac{\partial^2}{\partial y^2} \right) \phi + k_{\text{sh}}^2 \phi = 0 \quad (3.52)$$

at the open fluid $x, y \in \mathcal{F}$. For SWD, the relation between the plate deflection and the potential is described by (3.51).

Transition conditions (3.5) are rewritten in the following form:

$$\phi^{\mathcal{P}} = \phi^{\mathcal{F}}, \quad \frac{\partial \phi^{\mathcal{P}}}{\partial n} = \frac{\partial \phi^{\mathcal{F}}}{\partial n}, \quad (3.53)$$

where $x, y \in \mathcal{S}$. In the expression for the incident potential (3.11), we introduce the amplitude parameter

$$A^* = -\frac{igA}{\omega}. \quad (3.54)$$

As follows from (2.41), the general solution of (3.52) has the form in the water region $x < 0$:

$$\phi(x, y) = A^* \left(e^{ik_{sh}(x \cos \beta + y \sin \beta)} + R e^{ik_{sh}(-x \cos \beta + y \sin \beta)} \right), \quad (3.55)$$

where the first term represents a progressed wave moving to the right and the second a reflected wave moving to the left. In the water region $x > l$ we have:

$$\phi(x, y) = A^* T e^{ik_{sh}(x \cos \beta + y \sin \beta)}, \quad (3.56)$$

where right part represents the transmitted wave. The reflection R and the transmission T coefficients are still to be determined.

The differential equation of the plate motion has the form (3.6). With condition (3.7), equation (3.8) was derived for the total potential. For shallow water, the use of (3.9) and (3.51) lead to the following differential equation for the potential $\phi^{\mathcal{P}}$

$$\mathcal{D} \Delta^3 \phi^{\mathcal{P}} + (1 - \mu) \Delta \phi^{\mathcal{P}} + k_{sh}^2 \phi^{\mathcal{P}} = 0, \quad (3.57)$$

at the plate area \mathcal{P} .

From equation (3.57) we can derive the dispersion relation in the plate region, that proves the correctness of our approach. We can derive the expression for the potential using the relation (3.51) and (3.22) for the strip. Then, inserting the derived expression into (3.57) and collecting the coefficients of $e^{i\kappa x}$, we derive the dispersion relation for shallow water

$$(\mathcal{D} \kappa^4 - \mu + 1) \kappa^2 = k_{sh}^2. \quad (3.58)$$

Three roots of the dispersion relation (3.58) are taken into account. Real root $\kappa^{(1)}$ represents the traveling (propagating) wave mode, and two complex roots κ_2 and κ_3 represent damped (decaying-propagating) wave modes. All three roots are in the upper complex half-plane. As in the previous chapters, the roots of the dispersion relation can be represented in the form $\kappa^{(n)2} = \kappa_n^2 + k_0^2 \sin^2 \beta$.

The coefficients, or amplitudes, of the reflection and transmission of the incident wave can be found at once with the deflection components in the SWD case. Hence, for the definition of six amplitudes a_n and b_n and the reflection R and transmission T coefficients, we need a set of eight equations. We already have derived four relations (3.32–3.35) from the free edge conditions (3.14–3.15).

The other four equations can be obtained from the transition conditions (3.53) at both edges of the plate. We use the expressions for the potential $\phi^{\mathcal{F}}$ derived from (3.55) when $x < 0$ and from (3.56) when $x > l$ and for the potential $\phi^{\mathcal{P}}$ derived from (3.51) and (3.22). Then, we obtain from the first of the transition conditions (3.53) at the edge $x = 0$

$$-\frac{i\omega}{h} \sum_{n=1}^3 \frac{1}{\kappa^{(n)2}} (a_n + b_n) = A^* (1 + R), \quad (3.59)$$

and at the edge $x = l$

$$-\frac{i\omega}{h} \sum_{n=1}^3 \frac{1}{\kappa^{(n)2}} (a_n e^{i\kappa_n l} + b_n e^{-i\kappa_n l}) = T e^{ik_{sh} l \cos \beta}. \quad (3.60)$$

From the second of the transition conditions (3.53) at $x = 0$, we obtain

$$\frac{\omega}{h} \sum_{n=1}^3 \frac{\kappa_n}{\kappa^{(n)^2}} (a_n - b_n) = -iA^* k_{\text{sh}} \cos \beta (1 - R), \quad (3.61)$$

and at $x = l$

$$\frac{\omega}{h} \sum_{n=1}^3 \frac{\kappa_n}{\kappa^{(n)^2}} (a_n e^{i\kappa_n l} - b_n e^{-i\kappa_n l}) = -iA^* k_{\text{sh}} \cos \beta T e^{ik_{\text{sh}} l \cos \beta}. \quad (3.62)$$

Solving the set of eight equations (3.32–3.35), (3.59–3.62) we obtain the values of the plate deflection w , and of the coefficients R and T .

The plate deflection and reflection coefficient for the semi-infinite plate can be obtained analogously. The deflection is represented in the form (3.38). From transition conditions (3.53) and (3.55) we obtain the conditions (3.59) and (3.61) at the edge $x = 0$ without b_n -terms. The last two equations are obtained from the free edge conditions (3.39–3.40). After solving of the derived set of four equations we obtain three components of the deflection and the reflection coefficient R_∞ for the SIP.

3.7 Results, comparison and discussion

Numerical results are given for the deflection of the strip and of the semi-infinite plate for all three water depth models. In all figures, the left subplot is denoted as (a), and the right as (b). The results for the deflection are shown for \mathcal{W} , which is absolute real value of the deflection, normalized by the wave amplitude A , $|w|/A$. For the half-plane, we use the notation l for the part of plate considered, which is equal to the strip width taken. Thus, the results are demonstrated for the first l meters of the semi-infinite plate.

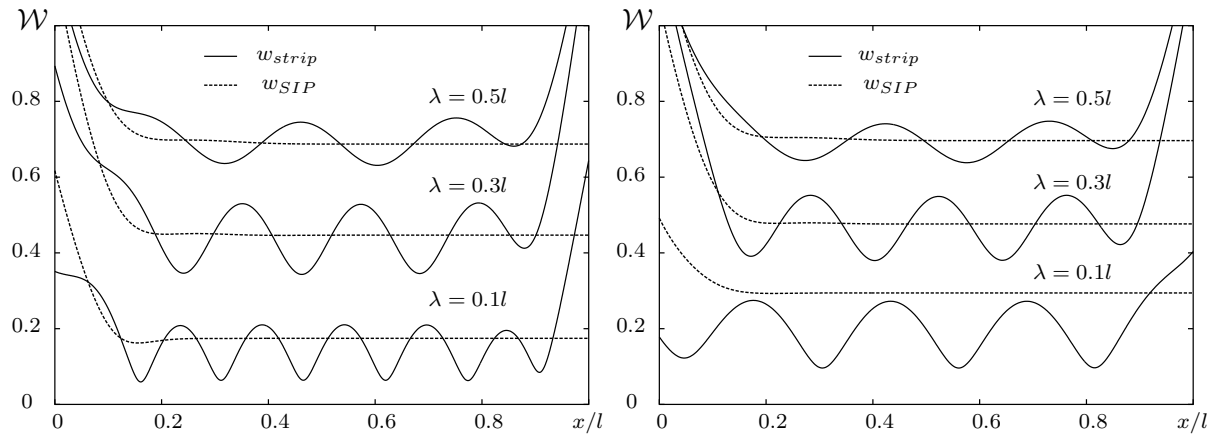


Figure 3.4: Comparison of the results for the deflection w for the strip and SIP for $D/\rho_w g = 10^5 \text{ m}^4$, $\beta = 0^\circ$ (a), and $\beta = 15^\circ$ (b), IWD.

The following values of the constant parameters were computed numerically: the wave amplitude $A = 1 \text{ m}$, the Poisson ratio $\nu = 0.25$, the ratio $m/\rho_w = 0.25 \text{ m}$ and the width of

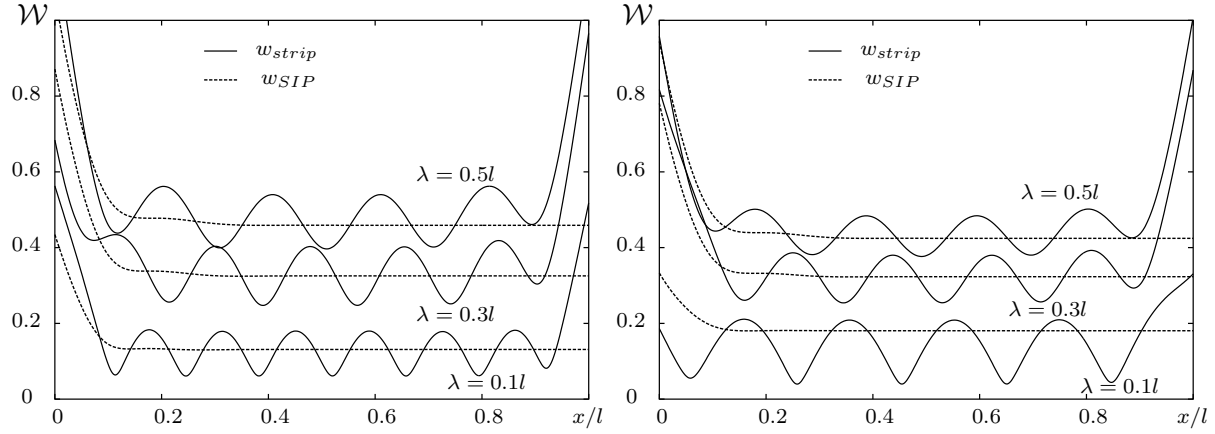


Figure 3.5: Comparison of the results for the deflection w for the strip and SIP for $D/\rho_w g = 10^5 \text{ m}^4$, $\beta = 0^\circ$ (a), and $\beta = 15^\circ$ (b), FWD, $h = 10 \text{ m}$.

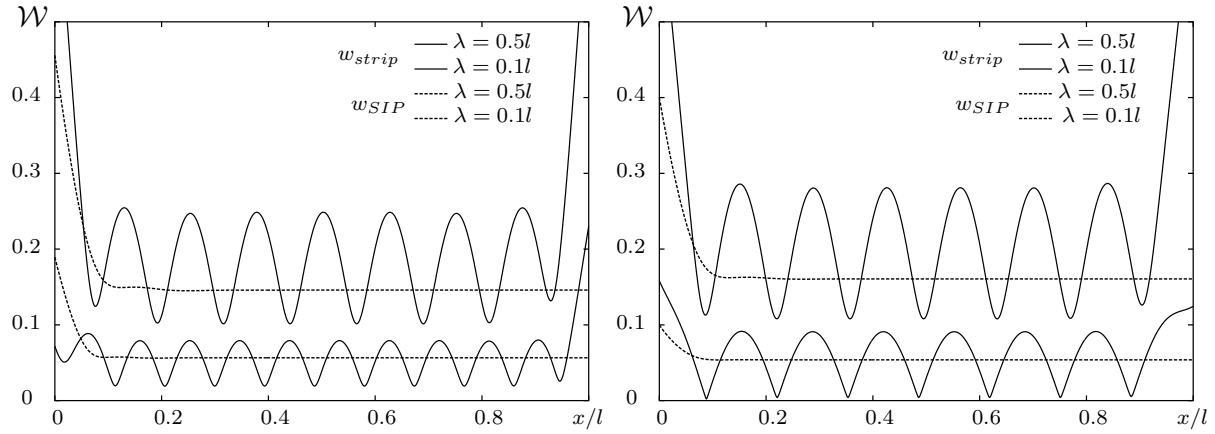


Figure 3.6: Comparison of the results for the deflection w of the strip and SIP for $D/\rho_w g = 10^5 \text{ m}^4$, $\beta = 0^\circ$ (a), and $\beta = 10^\circ$ (b), SWD, $h = 1 \text{ m}$.

the strip $l = 300 \text{ m}$. The results are given for various values of the water depth, incident wavelength, angle of incidence, and plate flexural rigidity. As the wavelength is varied, the wavenumber k_0 and of the frequency ω vary as well.

The number of roots of the plate dispersion relation for the finite water-depth case (3.26) which are taken into account is $M = 30$.

Figures 3.4–3.6 show the results for both forms of the plate for different values of the incidence angle β while other parameters are constant. Results are given for IWD, FWD and SWD, respectively.

The results for strip deflection at different wavelengths are presented in figure 3.7. Results are shown for three depths at zero angle of incidence. With growth of the water depth the value of plate deflection increases and lengths of 'wave in the plate' increase as well. Then the number of wave peaks in subplots in figures 3.4–3.6 becomes smaller with increasing depth, that is especially well prominent in figure 3.7.

In figures 3.8–3.9 we compare the results for the deflection of the strip and the semi-infinite plate for the same wavelength and depth for FWD and IWD. For each form of

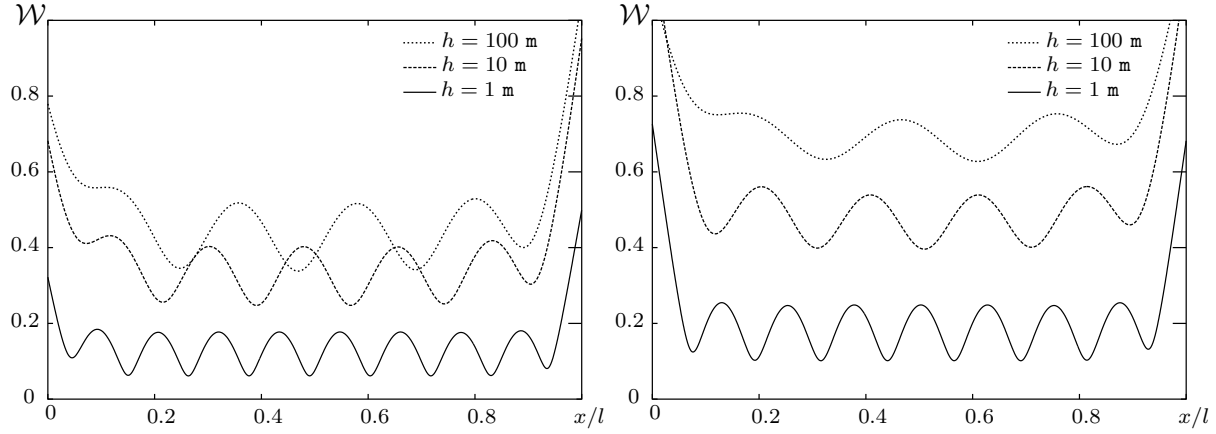


Figure 3.7: Results for strip deflection for $D/\rho_w g = 10^5 \text{ m}^4$, $h = 1, 10, 100 \text{ m}$, for $\lambda = 0.3l$ (a) and $\lambda = 0.5l$ (b).

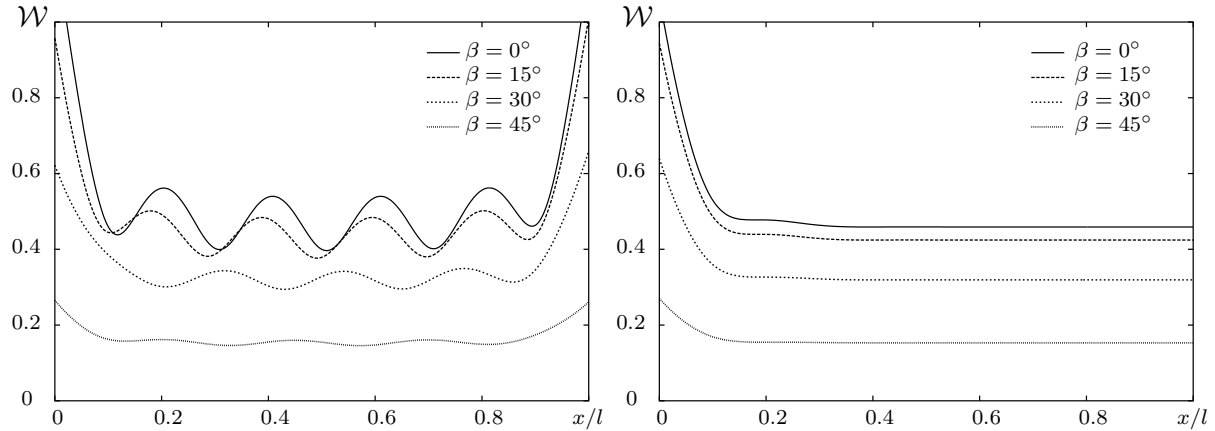


Figure 3.8: Results for the deflection for $D/\rho_w g = 10^5 \text{ m}^4$, $h = 10 \text{ m}$, $\lambda = 0.5l$ for the strip (a) and for the SIP (b), different angles, finite water depth.

the plate, results are presented for four values of the angle of incidence.

Figure 3.10 shows results for IWD and FWD for the plate flexural rigidity $D/\rho_w g = 10^7 \text{ m}^4$. It is seen that plate having larger rigidity is less dependent on the depth.

In figure 3.11, we show results for water of finite depth for different values of β including $\beta \geq \beta_{\text{cr}}$. As we have noted before, in such cases our model remains valid: the plate is deflected only near the edge.

Figure 3.12 gives the results for the reflection and transmission coefficients for FWD and SWD. Results are given for absolute values of the coefficients. The peaks of the plot for the reflection coefficient in SWD are significantly higher than in FWD; numerically this coefficient is quite close to that for IWD. Wave energy is conserved up to a high degree of accuracy $|R|^2 + |T|^2 = 1$.

In figure 3.13, we demonstrate the influence of the number of dispersion relation roots on the results. The figures are shown for the depths 200 m and 10 m, respectively, and compared for three wavelengths. The lower graph in figure 3.13(a) can be a model of the

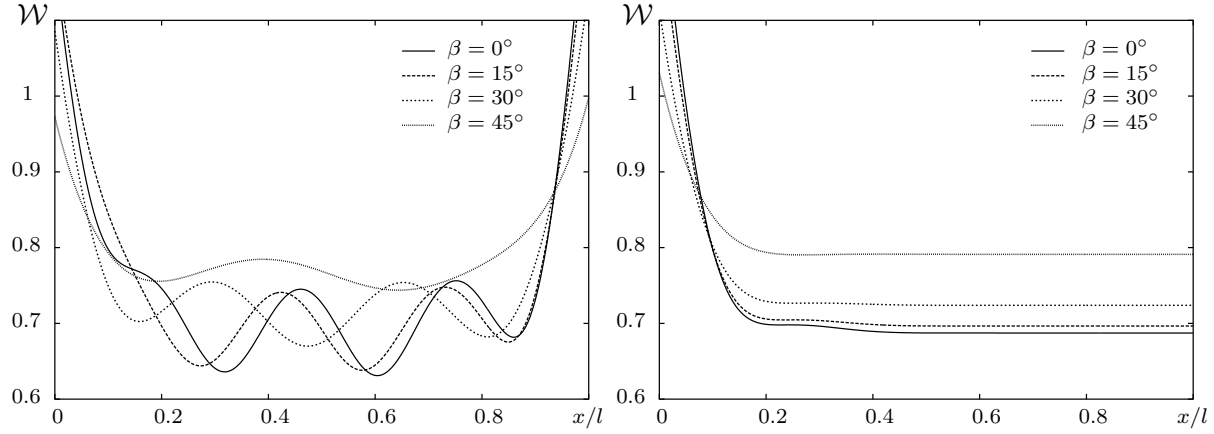


Figure 3.9: Results for the deflection for $D/\rho_w g = 10^5 \text{ m}^4$, $\lambda = 0.5l$ for the strip (a) and for the SIP (b), different angles, infinite water depth.

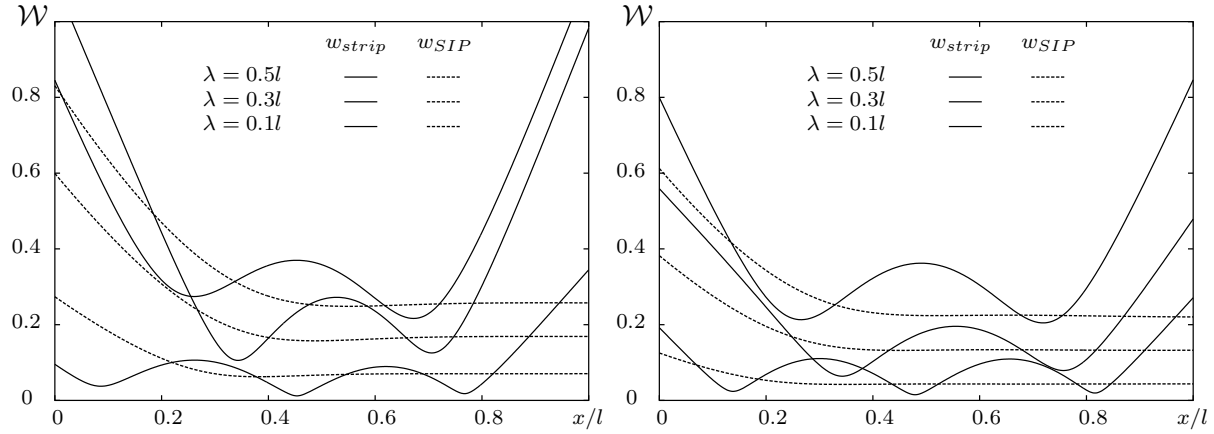


Figure 3.10: Comparison of the results for the deflection for the strip and SIP for $D/\rho_w g = 10^7 \text{ m}^4$, $\beta = 0^\circ$ on water of infinite (a) and finite, $h = 100 \text{ m}$, (b) depth.

IWD case — the wavelength is 30 m while the depth is 200 m with relevant behavior of the plate. The difference between results is large near the edges of the strip. All other graphs correspond to finite water depth. In this case, differences between the results are small, especially if we consider rather shallow depth.

Also, we found that when the depth becomes larger than 200 m, the roots of dispersion relation are convergent and the numerical results are close to those for IWD.

Results for the propagation of the rays are shown in figure 3.14 for zero reflection (this case corresponds to a semi-infinite plate); it also shows the contribution of one (first) reflection at $x = l$ separately, the combined result after one reflection at $x = l$, and one at $x = 0$, and finally the result after multiple reflection. The result after two reflections is an overestimation of the final result.

In figures 3.15 we show that numerical results obtained by different approaches and computational programs for the same values of depth are very close. It is shown that the FWD solution can be used to obtain results for IWD and SWD.

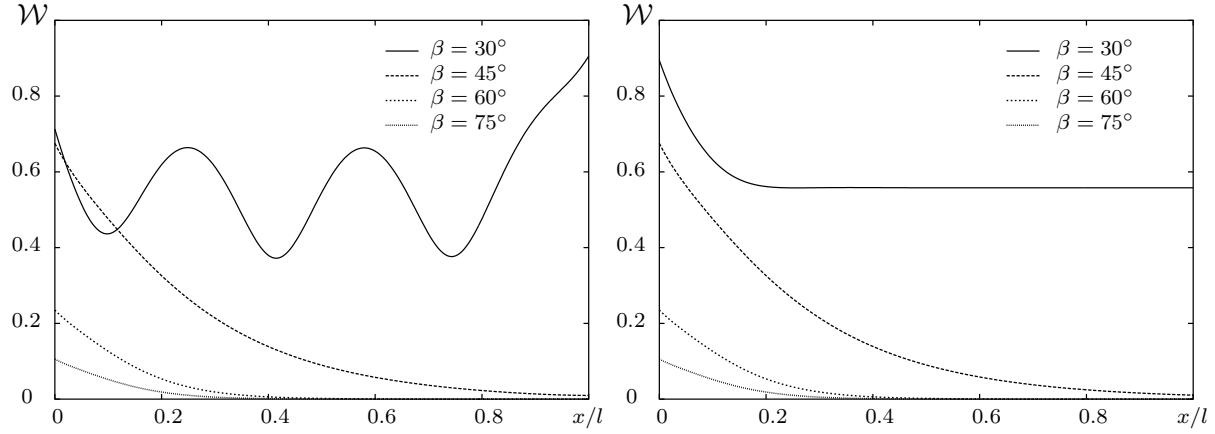


Figure 3.11: Results for the deflection for $D/\rho_w g = 10^5 \text{ m}^4$, $h = 100 \text{ m}$, $\lambda = 0.3l$ for the strip (a) and for the SIP (b), finite water depth.

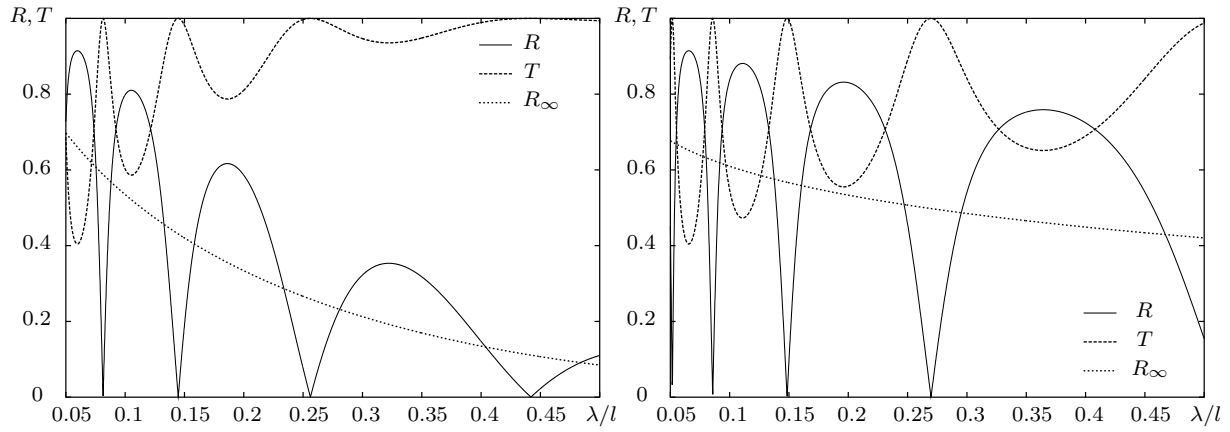


Figure 3.12: Reflection and transmission coefficients for $D/\rho_w g = 10^5 \text{ m}^4$, $\beta = 0^\circ$ for $h = 100 \text{ m}$ (a) and $h = 1 \text{ m}$ (b).

We already mentioned that the case of finite water depth is general. By taking the limit $h \rightarrow \infty$, we arrive at IWD, and by the limit $h \rightarrow 0$ at SWD, including transition from the dispersion relation for finite water to that for infinite and shallow water, respectively.

The comparison of our results derived for the strip-shaped plate with the results of Takagi et al. [115] and Yoshimoto et al. [152] is shown in figure 3.16, subplots (a) and (b), respectively. The comparison is provided for the general case of finite water depth. In the first subplot we compare our results with ones of Takagi et al. [115], who used an eigenfunction expansion method. Then, results are compared with those obtained by a modal analysis by Yoshimoto et al. [152], in the second subplot. The comparisons presented show very good agreement of all three different methods. For infinite depth, we compare numerical results with those obtained of Tkacheva [126] by the Wiener-Hopf technique, and with the results of Hermans [40] obtained by boundary element computations. These comparisons also proves the accuracy of the method presented in this chapter.

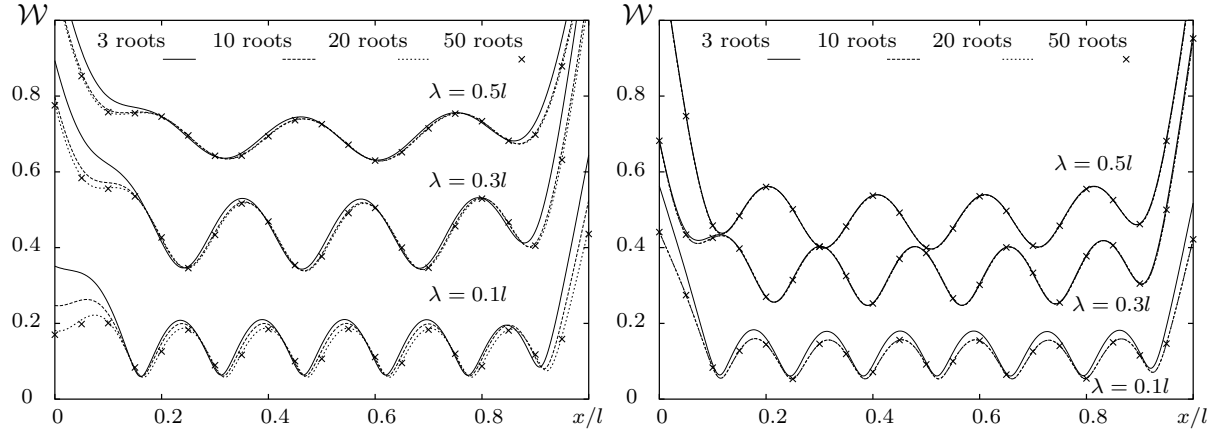


Figure 3.13: Comparison of the results for $D/\rho_w g = 10^5 \text{ m}^4$, $\beta = 0^\circ$ for 3, 10, 20 and 50 wave modes, $h = 200$ m (a) and $h = 10$ m (b).

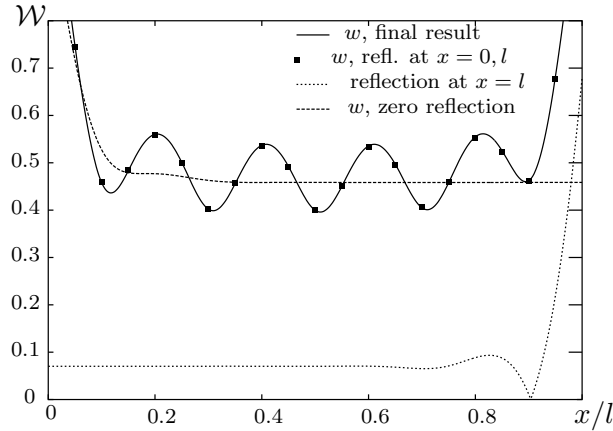


Figure 3.14: Multiple reflection for $\lambda = 0.3l$, $D/\rho_w g = 10^5 \text{ m}^4$, $\beta = 0^\circ$, $h = 10$ m.

3.8 Conclusions

The problem of the hydroelastic behavior of a floating plate has been solved for two plate planforms: a half-plane and a strip. The motion of the plate and its hydroelastic response to incoming waves were studied analytically and numerically. The problem has been solved and results are shown for three different models: infinite, finite, and shallow water depth. The comparison of results obtained for different models has been provided. Also, we have presented the comparison with the results obtained by other approaches, which shows a good agreement of different methods.

For IWD and FWD, the results were obtained by analysis of the derived integro-differential equation for the plate deflection and asymptotic theory of the geometrical-optics approach. For SWD, the major simplification is the Stoker shallow-water approximation.

Three modes of deflection were considered for all depths, one traveling (propagating) wave mode, and two damped (decaying-propagating) wave modes. Our numerical results showed that all these approximations are consistent with each other. In the transition

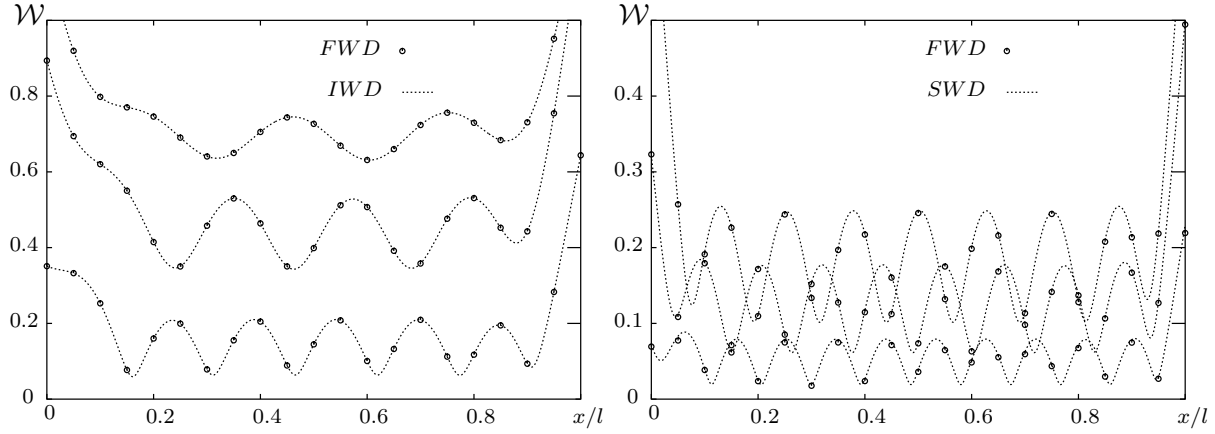


Figure 3.15: Comparison of numerical results for the strip deflection for $D/\rho_w g = 10^5 \text{ m}^4$, $\lambda = 0.5l, 0.3l, 0.1l$: IWD & FWD, $h = 250$ m, (a), SWD & FWD, $h = 1$ m, (b).

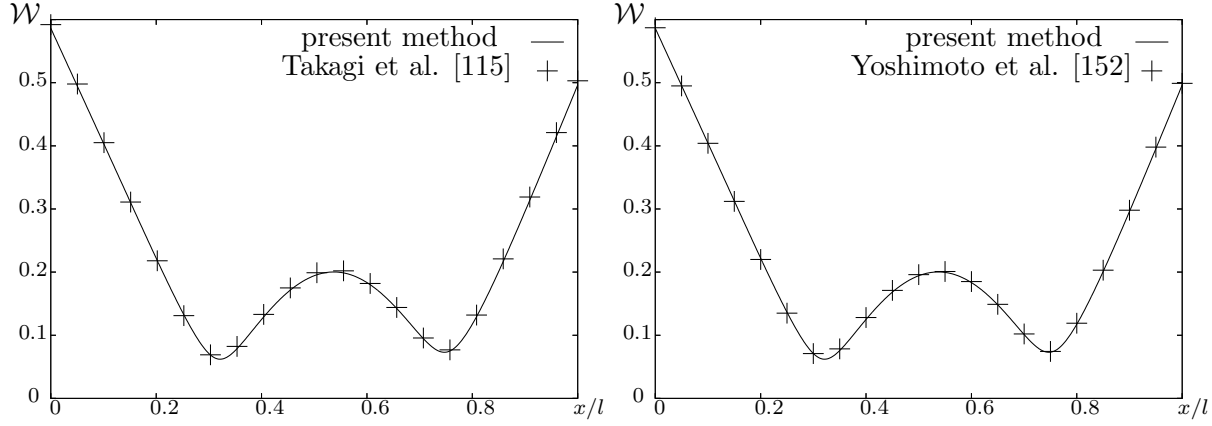


Figure 3.16: Comparison with the results of Takagi et al. [115] (a) and Yoshimoto et al. [152] (b), the strip case, for $h = 107$ m, $D = 1.411 \times 10^7 \text{ m}^4$, $\lambda = 0.278l$.

from one case to the other, the numerical values show a continuous behavior.

In the next chapters we will often refer to the analysis presented here. The solution of the problems in chapters 4–7 is partially based on our approach and solution for the half-plane and strip.

One of the possible extensions for the method and solution presented in this chapter is the case of multiple floating strip-shaped plate; such real object is the Kamigoto Oil Storage Base shown in figure 1.2. The solution for this problem is derived by Hermans [44].

Chapter 4

Hydroelasticity of a circular plate

In this chapter we consider the diffraction of incident surface waves by a floating elastic circular plate. We investigate the hydroelastic response of the plate to a plane incident wave for two water depths. An analytic and numerical study is presented. An integro-differential equation is derived for the problem, and an algorithm for its numerical solution is proposed. The representation of the solution as a series of Bessel functions is the key idea of the approach. After a brief introduction and formulation of the problem, we derive the main integro-differential equation by using the thin plate theory and the Green's theorem. The plate deflection, free-surface elevation, and the Green's function are expressed in cylindrical coordinates as series of Bessel functions. For the coefficients, a set of algebraic equations is obtained, yielding the approximate solution for infinite water depth. Then a solution is obtained analogously for the general case of finite water depth. The exact solution is approximated by taking into account a finite number of roots of the dispersion relation. Numerical results for the plate deflection, initiated wave pattern and free-surface elevation are presented for various physical parameters of the problem, together with some remarks on the computation and discussion.

4.1 Introduction

Recently, a number of papers has been published on the hydroelastic motion of VLFS. A detailed literature surveys for this problem are given by Watanabe et al. [143] and Kashiwagi [52]. Our literature survey is given in section 1.3. Many different problems related to fluid-structure interaction are treated in the books, articles and abstracts these three surveys refer to.

The analytical solution for plates having one or two infinite dimensions, which significantly simplifies the complexity of analysis, can be derived with any of the approaches described in the aforementioned surveys. For plates of finite extent (length), often numerical methods are used. Mainly, the indicated articles study the VLFSs of rectangular planforms. There are only few papers considering arbitrarily shaped structures, although non-rectangular VLFSs may be used for floating airports, cities, storage facilities, power plants, etc. [143, 144], section 1.3.

Several papers studying circular plates were presented recently at international conferences. For the circular ice floe, Meylan and Squire solved the problem for deep water

using the eigenfunction method [77]. A closed-form solution for a buoyant circular plate floating on shallow water has been developed by Zilman and Miloh [153] with the shallow water theory of Stoker [107]. This problem had also been solved by Tsubogo [132] by an advanced boundary element method. A plate floating on shallow water under an external load had been considered by Sturova [111]. For finite water depth, the problem was solved by Watanabe et al. [142], who used the Galerkin method and Mindlin plate theory [80]. Peter et al. [97] presented a solution for the same problem based on decomposing the solution into angular eigenfunctions. Andrianov and Hermans solved the problem of hydroelastic response of a circular plate for water of finite and infinite depth; some preliminary results were published in [7, 8].

Here we consider the problem for a floating disk-shaped plate for two different cases: deep water and water of finite depth. An analytical study is presented for both cases. The circular plate floats on the surface of an ideal fluid. We consider a plate with constant flexural rigidity and homogeneous stiffness. The edge of the plate is free of shear forces, bending and twisting moments. We use the Green's theorem and an integro-differential formulation for the deflection, as derived and described in sections 2.5 and 2.7 and in papers by Hermans [43] and Andrianov and Hermans [5, 8]. The plate deflection generated by incoming surface waves is represented as a series of Bessel functions, multiplied by cosine functions. The approach presented allows us to study the plate deflection, the initiated wave pattern generated by the plate motion, and the free-surface elevation.

The main objective of our study is to determine the plate deflection by solving a set of equations. An integro-differential equation can be derived if we apply the Green's theorem as in chapter 3. To complete a set of equations for determining the plate deflection, we use the plate free edge conditions.

First, we study the behavior of the circular plate floating on the surface of water of infinite depth. It seems a rather theoretical problem, but this is a good starting point to find a solution for the general and most important case of finite water depth. Then, we consider finite water depth, where the general analysis and set of equations are more complicated, as more roots of the water dispersion relation have to be taken into account. The numerical results obtained are presented and discussed with regard to various physical parameters of the problem. The conclusions and the information about possible extensions of the approach are given in the last section.

4.2 Formulation of the problem

In this section we derive the general mathematical formulation for the problem under consideration. A thin elastic circular floating plate of radius r_0 covers part of the surface of the water, where water is assumed to be an ideal incompressible fluid. The value of the water depth h is infinite for the IWD model and finite and constant for the FWD model. We assume that no space exists between the free surface and the plate. The flexural rigidity of circular plate is constant.

The plate deflection is generated by incoming surface waves. We assume that these waves propagate in otherwise calm water. Also, it is assumed that the incoming waves propagate in the positive x -direction without loss of generality. The wave amplitude is assumed to be small in comparison to the other length parameters of the problem.

The problem is considered in polar coordinates; these are related to Cartesian coordinates by $\rho^2 = x^2 + y^2$, $\varphi = \arctan y/x$. The geometric sketch of the plate is shown in figure 4.1. At the free surface $z = 0$, we denote the plate region as \mathcal{P} ($\rho \leq r_0$; $\varphi = [0, 2\pi]$), the plate contour as \mathcal{S} ($\rho = r_0$; $\varphi = [0, 2\pi]$) and the open fluid region as \mathcal{F} ($\rho > r_0$; $\varphi = [0, 2\pi]$). Hence, we formulate the problem in polar coordinates.

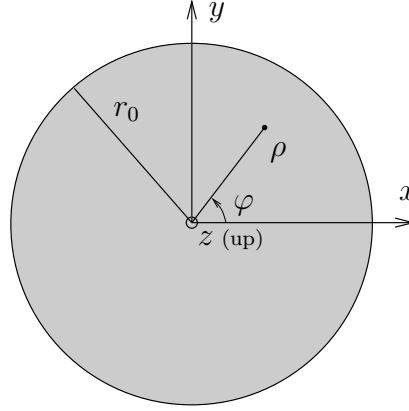


Figure 4.1: The geometry and coordinate system of the problem.

The velocity potential is introduced by $\nabla_{(3)}\Phi(\rho, \varphi, z, t) = \mathbf{V}(\rho, \varphi, z, t)$, where $\mathbf{V}(\rho, \varphi, z, t)$ is the fluid velocity vector. The Laplacian in cylindrical coordinates is defined as

$$\nabla_{(3)}^2 = \Delta_{(3)} = \frac{\partial^2}{\partial \rho^2} + \frac{1}{\rho} \frac{\partial}{\partial \rho} + \frac{1}{\rho^2} \frac{\partial^2}{\partial \varphi^2} + \frac{\partial^2}{\partial z^2},$$

where the subscript (3) is used for three-dimensional operators, to distinguish them from two-dimensional operators Δ and ∇ at the free surface. The velocity potential $\Phi(\rho, \varphi, z, t)$ is a solution of the governing Laplace equation in the fluid, $z < 0$,

$$\Delta_{(3)}\Phi = 0, \quad (4.1)$$

together with the boundary conditions at the free surface and the bottom. The linearized kinematic condition in the plate and water regions, $z = 0$, has the form

$$\frac{\partial \Phi}{\partial z} = \frac{\partial W}{\partial t}, \quad (4.2)$$

where $W(\rho, \varphi, t)$ denotes either the deflection of the plate in \mathcal{P} , or the free-surface elevation in \mathcal{F} , and t is the time. The linearized dynamic condition, derived from the linearized Bernoulli equation, is written as

$$\frac{P - P_{\text{atm}}}{\rho_w} = -\frac{\partial \Phi}{\partial t} - gW, \quad (4.3)$$

at $z = 0$, where ρ_w is the density of the fluid, g is gravitational acceleration, $P(\rho, \varphi, t)$ is the pressure in the fluid, and P_{atm} is the atmospheric pressure. The relations (4.2–4.3) are kinematic and dynamic conditions at the free surface, and the linearized free-surface condition in the open water region \mathcal{F} , $z = 0$, takes the form

$$\frac{\partial \Phi}{\partial z} = -\frac{1}{g} \frac{\partial^2 \Phi}{\partial t^2}. \quad (4.4)$$

The normal potential equals zero at the bottom $z = -h$

$$\frac{\partial \Phi}{\partial z} = 0. \quad (4.5)$$

The platform is modeled as an elastic plate of zero thickness. Such a model can be applied, as described above, because of the small thickness and shallow draft of the platform. To describe the deflection of the plate $W(\rho, \varphi)$, we apply the isotropic thin plate theory, see section 2.3, which leads to a differential equation at $z = 0$ in the plate area \mathcal{P} , known as the Gehring-Kirchhoff equation of plate motion

$$D\Delta^2 W + m \frac{\partial^2 W}{\partial t^2} = P - P_{\text{atm}}, \quad (4.6)$$

where m is the mass per unit area of the platform, and D is the flexural rigidity. Both parameters are constant because the plate considered is isotropic. From now on, the Laplacian will be a two-dimensional operator

$$\nabla^2 = \Delta = \frac{\partial^2}{\partial \rho^2} + \frac{1}{\rho} \frac{\partial}{\partial \rho} + \frac{1}{\rho^2} \frac{\partial^2}{\partial \varphi^2}.$$

Following the procedure described in chapters 2–3 and in Andrianov and Hermans [5], we apply the operator $\partial/\partial t$ to (4.6) and use the surface conditions (4.2) and (4.3) to arrive at the following differential equation for the potential Φ acting on the plate at $z = 0$:

$$\left\{ \frac{D}{\rho_w g} \Delta^2 + \frac{m}{\rho_w g} \frac{\partial^2}{\partial t^2} + 1 \right\} \frac{\partial \Phi}{\partial z} + \frac{1}{g} \frac{\partial^2 \Phi}{\partial t^2} = 0. \quad (4.7)$$

Considering harmonic motion of the waves, we can write the potential of the incident wave in the form

$$\Phi(\rho, \varphi, z, t) = \phi(\rho, \varphi, z) e^{-i\omega t}, \quad (4.8)$$

where ω is the wave frequency. In the same way, the deflection is written as

$$W(\rho, \varphi, t) = w(\rho, \varphi) e^{-i\omega t}. \quad (4.9)$$

Then we reduce the time dependence and consider waves of a single frequency ω and obtain at $z = 0$ for the plate region \mathcal{P}

$$\left\{ \mathcal{D} \Delta^2 - \mu + 1 \right\} \frac{\partial \phi}{\partial z} - K \phi = 0, \quad (4.10)$$

where $K = \omega^2/g$ and the introduced structural parameters $\mathcal{D} = D/\rho_w g$, $\mu = m\omega^2/\rho_w g$, which are constant. For the open-water region \mathcal{F} , we have

$$\frac{\partial \phi}{\partial z} - K \phi = 0. \quad (4.11)$$

All the definitions given above are valid for water of both infinite and finite depth.

The potential of the incident wave for water of finite depth has the form

$$\phi^{\text{inc}}(\rho, \varphi, z) = \frac{\cosh k_0(z+h)}{\cosh k_0 h} \frac{gA}{i\omega} e^{ik_0 \rho \cos \varphi}, \quad (4.12)$$

where k_0 is the wavenumber, and A is the amplitude of the incident wave. The wavenumber k_0 is the positive real solution of the water dispersion relation

$$k \tanh kh = K. \quad (4.13)$$

For deep water, the potential is represented in the form

$$\phi^{\text{inc}}(\rho, \varphi, z) = \frac{gA}{i\omega} e^{ik_0 \rho \cos \varphi + k_0 z}. \quad (4.14)$$

In this case, the wavenumber is $k_0 = K = \omega^2/g$.

The wavelength of the incoming waves is $\lambda = 2\pi/k_0$. In a practical situation, the radius of the floating circular plate r_0 might be of the order of a thousand meters, while the wavelength λ may be of the order of ten or a hundred meters. Therefore, we consider and compute numerically the situation where the wavelength is less than the diameter of the plate ($\lambda < 2r_0$), but the approach presented in this chapter is also valid for small circular disks ($\lambda > 2r_0$).

The edge of the circular plate is free of vertical shear forces, bending and twisting moments. Hence, the free edge conditions at the plate contour \mathcal{S} are written as

$$\left\{ \nabla^2 - \frac{(1-\nu)}{\rho} \left(\frac{\partial}{\partial \rho} + \frac{1}{\rho} \frac{\partial^2}{\partial \varphi^2} \right) \right\} w = 0, \quad (4.15)$$

$$\left\{ \frac{\partial}{\partial \rho} \nabla^2 + \frac{(1-\nu)}{\rho^2} \left(\frac{\partial}{\partial \rho} - \frac{1}{\rho} \right) \frac{\partial^2}{\partial \varphi^2} \right\} w = 0. \quad (4.16)$$

4.3 Green's function and deflection

In this section we describe the Green's function and deflection function and the operations on the corresponding Bessel functions for the circular plate. The expressions for the Green's function for water of infinite and finite depth can be found in Wehausen and Laitone [146], and the modified forms for the Green's function are given in section 2.5. In subsection 2.5.2 we present the expressions for the Green's function in polar coordinates.

We introduce the Green's function for a source within the fluid which in Cartesian coordinates satisfies $\Delta_{(3)} \mathcal{G} = 4\pi \delta(\mathbf{x} - \boldsymbol{\xi})$, where δ is the Dirac δ -function, \mathbf{x} is a source point, and $\boldsymbol{\xi}$ is an observation point. The Green's function obeys the boundary conditions at the free surface (2.45) and at the bottom (2.46), and the radiation condition (2.47).

For deep water, the three-dimensional Green's function can be written in the following form:

$$\mathcal{G}(\mathbf{x}, \boldsymbol{\xi}) = -\frac{1}{\varrho} + \frac{1}{\varrho_1} - 2 \int_{\mathcal{L}} \frac{k}{k - k_0} J_0(kR) e^{k(z+\zeta)} dk, \quad (4.17)$$

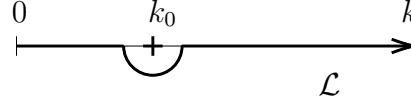


Figure 4.2: Contour of the integration.

where $\varrho^2 = R^2 + (z - \zeta)^2$, $\varrho_1^2 = R^2 + (z + \zeta)^2$, R is the horizontal distance, and $J_0(kR)$ is the Bessel function. The contour of integration \mathcal{L} is shown in figure 4.2. It passes underneath the singularity $k = k_0$ to fulfill the radiation condition.

The Green's function in polar coordinates $\mathcal{G}(\rho, \varphi, z; r, \theta, \zeta)$ for the source and observation points at $z = \zeta = 0$ is written as

$$\mathcal{G}(\rho, \varphi; r, \theta) = -2 \int_{\mathcal{L}} \frac{k}{k - k_0} J_0(kR) dk, \quad (4.18)$$

where the horizontal distance R in polar coordinates is $R^2(\rho, \varphi; r, \theta) = \rho^2 + r^2 - 2\rho r \cos(\theta - \varphi)$. Here, ρ and r are the distances from the center of the plate to the source and to the observation points, respectively, and $\theta - \varphi$ is the angle between r and ρ .

We apply Graf's addition theorem to the Bessel function $J_0(kR)$ in expression (4.18). Following Tranter [131], we write

$$J_0(kR) = \sum_{q=0}^{\infty} \delta_q J_q(kr) J_q(k\rho) \cos q(\theta - \varphi), \quad (4.19)$$

where $J_0(kR)$ is represented as a combination of the Bessel functions $J_q(kr)$ and $J_q(k\rho)$, $\delta_0 = 1$ and $\delta_q = 2$ for $q > 0$. Finally, the Green's function in polar coordinates for deep water takes the form

$$\mathcal{G}(\rho, \varphi; r, \theta) = -2 \int_0^{\infty} \frac{k}{k - k_0} \sum_{q=0}^{\infty} \delta_q J_q(kr) J_q(k\rho) \cos q(\theta - \varphi) dk. \quad (4.20)$$

The Green's function for finite water depth obeys the conditions at the free surface (2.45), at the bottom (2.46), and the radiation condition (2.47). The three-dimensional Green's function at $z = \zeta = 0$ has the following form in polar coordinates:

$$\mathcal{G}(\rho, \varphi; r, \theta) = -2 \int_{\mathcal{L}} \frac{k \cosh kh}{k \sinh kh - K \cosh kh} J_0(kR) dk, \quad (4.21)$$

where \mathcal{L} is the contour of the integration in the complex k -plane, given in figure 4.2. Again we apply Graf's addition theorem to the Bessel function in the integrand, and the Green's function takes the form

$$\mathcal{G}(\rho, \varphi; r, \theta) = -2 \int_0^{\infty} \frac{k \cosh kh}{k \sinh kh - K \cosh kh} \sum_{q=0}^{\infty} \delta_q J_q(kr) J_q(k\rho) \cos q(\theta - \varphi) dk. \quad (4.22)$$

As in the eigenfunction approach, see, e.g., Kim and Ertekin [56] for finite water depth and Meylan and Squire [77] for infinite water depth, we represent the plate deflection as a series of Bessel functions with corresponding coefficients of the form

$$w(\rho, \varphi) = \sum_{m=1}^M \sum_{n=0}^{\infty} a_{mn} J_n(\kappa_m \rho) \cos n\varphi, \quad (4.23)$$

where a_{mn} are unknown amplitude functions and κ_m are the wavenumbers in the plate region. It will be shown later that κ_m , $m = 1, \dots, M$ obeys the plate dispersion relation. M is the number of wave modes taken into account, i.e., the number of roots of the plate dispersion relation.

For numerical computations, we will take the upper limit of q in expressions (4.20) or (4.22) and n in expression (4.23) as N , which is a truncation parameter of the problem. We can do this because the Bessel functions decay with increasing order. Convergence of the final results is verified in the numerical computations. All terms of an order higher than N are negligible.

In the next section, we will apply the Green's theorem at $z = \zeta = 0$. An application of the Green's theorem at $z < 0$ together with the expansion (4.23) gives rise to the standard eigenfunction expansion as can be found in Meylan and Squire [77] for the potential in the entire fluid domain.

4.4 Infinite water depth

Here we apply Green's theorem to obtain the integro-differential equation for the potential and vertical displacements. Then an approximate solution is derived for the more theoretical and less complicated case of deep water. The deep-water case is a good intermediate step for deriving the solution for finite water depth, which is our main interest. The main integro-differential equation has been derived for the general three-dimensional situation described in chapter 2 and applied in chapter 3, see also Hermans [41] and Andrianov and Hermans [5]. Now we rederive it in polar coordinates.

The application of the Green's theorem leads to the following expression for the total potential at $z = \zeta = 0$:

$$4\pi\phi(\rho, \varphi) = 4\pi\phi^{\text{inc}}(\rho, \varphi) + \int_{\mathcal{P}} \mathcal{G}(\rho, \varphi; r, \theta) \left(K\phi(r, \theta) - \frac{\partial\phi(r, \theta)}{\partial\zeta} \right) r \, dr \, d\theta, \quad (4.24)$$

where the free-surface condition (2.45) for the Green's function has been used.

We use the notation $\phi^{\mathcal{F}}$ for the potential function in the open water region \mathcal{F} . The potential $\phi^{\mathcal{F}}$ is the superposition of the incident wave potential ϕ^{inc} and ϕ^{dis} , which is the sum of the classical diffraction potential and the radiation potential, as follows:

$$\phi^{\mathcal{F}} = \phi^{\text{inc}} + \phi^{\text{dis}}. \quad (4.25)$$

The potential ϕ^{dis} must satisfy the Sommerfeld radiation condition

$$\sqrt{\rho} \left(\frac{\partial}{\partial\rho} - ik_0 \right) \phi^{\text{dis}} = 0 \quad (4.26)$$

as $\rho \rightarrow \infty$. The total potential in the area covered by the plate \mathcal{P} is denoted by $\phi^{\mathcal{P}}$.

Using the dynamic condition (4.10) for the plate region \mathcal{P} to express $\phi^{\mathcal{P}}$ in terms of an operator acting on $\phi_z^{\mathcal{P}}$, we obtain the following equation:

$$\{\mathcal{D}\Delta^2 - \mu + 1\} \phi_z^{\mathcal{P}} = \frac{K}{4\pi} \int_{\mathcal{P}} \mathcal{G}(\rho, \varphi; r, \theta) \{\mathcal{D}\Delta^2 - \mu\} \phi_z^{\mathcal{P}} r dr d\theta + \phi_z^{\text{inc}}, \quad (4.27)$$

where condition (4.11) has been used for the last term, which represents the potential of the incoming waves. The relation (4.27) is suitable for further analysis to derive the integro-differential equation for the plate deflection. We switch from the potential to the deflection function by using the expression

$$\phi_z^{\mathcal{P}} = -i\omega w, \quad (4.28)$$

derived from the kinematic condition (4.2). Hence, the following equation is obtained:

$$\{\mathcal{D}\Delta^2 - \mu + 1\} w(\rho, \varphi) = \frac{K}{4\pi} \int_{\mathcal{P}} \mathcal{G}(\rho, \varphi; r, \theta) \{\mathcal{D}\Delta^2 - \mu\} w(r, \theta) r dr d\theta + A e^{ik_0 \rho \cos \varphi} \quad (4.29)$$

for the plate deflection w . Equation (4.29) can be considered as the governing equation for the problem of diffraction of incident water surface waves on a circular plate which floats in deep water.

We insert the relations for the deflection (4.23) and Green's function (4.20) into IDE (4.29) and obtain the expanded integro-differential equation:

$$\begin{aligned} & \{\mathcal{D}\Delta^2 - \mu + 1\} \sum_{m=1}^M \sum_{n=0}^N a_{mn} J_n(\kappa_m \rho) \cos n\varphi \\ & + \frac{K}{2\pi} \int_0^{2\pi} \int_0^{r_0} \{\mathcal{D}\Delta^2 - \mu\} \sum_{m=1}^M \sum_{n=0}^N a_{mn} J_n(\kappa_m r) \cos n\theta \\ & \times \left(\int_0^\infty \frac{k}{k - k_0} \sum_{q=0}^N \delta_q J_q(kr) J_q(k\rho) \cos q(\theta - \varphi) dk \right) r dr d\theta = A \sum_{n=0}^N \epsilon_n J_n(k_0 \rho) \cos n\varphi, \end{aligned} \quad (4.30)$$

where $\epsilon_n = \delta_n i^n$. Due to the orthogonality relation for the cosine functions we only get a nonzero contribution in the integrand for $n = q$. Next, we work out the integration with respect to r and θ . The integration over r , in accordance with Korn and Korn [60], gives us

$$\int_0^{r_0} J_n(kr) J_n(\kappa_m r) r dr = \frac{r_0}{(k^2 - \kappa_m^2)} [kJ_{n+1}(kr_0) J_n(\kappa_m r_0) - \kappa_m J_n(kr_0) J_{n+1}(\kappa_m r_0)], \quad (4.31)$$

while the integration over θ gives us 2π for $n = 0$ and $\delta_n \pi \cos n\varphi$ for $n > 0$, and then $2\pi \cos n\varphi$ for all n .

In such a way, we also obtain the following set of $N + 1$ equations from the integro-differential equation (4.30):

$$\sum_{m=1}^M (\mathcal{D}\kappa_m^4 - \mu + 1) a_{mn} J_n(\kappa_m \rho) + Kr_0 \int_0^\infty \sum_{m=1}^M (\mathcal{D}\kappa_m^4 - \mu) a_{mn} J_n(k\rho) \times \frac{k}{(k - k_0)(k^2 - \kappa_m^2)} [kJ_{n+1}(kr_0)J_n(\kappa_m r_0) - \kappa_m J_n(kr_0)J_{n+1}(\kappa_m r_0)] dk = A\epsilon_n J_n(k_0 \rho), \quad (4.32)$$

where $n = 0, \dots, N$. Here, $k = \kappa_m$ is not a singularity of the integrand. For plates with one infinite dimension, the deflection can be represented as a superposition of exponential functions, as shown in section 2.6. Therefore, it is easier to work out the integration over k in the integro-differential equation for those problems. For a circular plate, however, the integration in the complex plane needs special attention, which is described below.

For the plate region \mathcal{P} ($\rho < r_0$), we represent the Bessel function $J_q(kr_0)$ — where q is n or $n + 1$ — as the half-sum of Hankel functions of the first and second kind

$$J_q(kr_0) = \frac{H_q^{(1)}(kr_0) + H_q^{(2)}(kr_0)}{2}. \quad (4.33)$$

Then the integral in equation (4.32) is split up in two; these two parts we transform into integrals along the vertical axis in the complex k -plane plus the sum of the residues. All poles in the complex plane are shown in figure 4.3. For the first integral with $H_q^{(1)}(kr_0)$, the contour can be closed in the upper half-plane with the poles $k = \kappa_m$, and for the second one with $H_q^{(2)}(kr_0)$, it can be closed in the lower half-plane, where the poles are $k = -\kappa_m$.

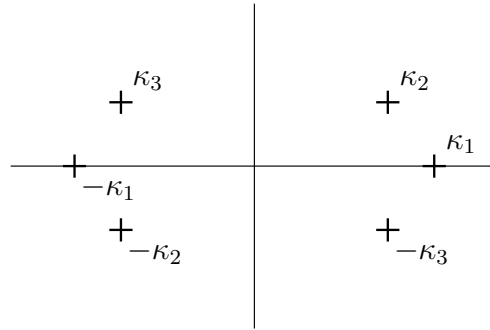


Figure 4.3: Zeros of the dispersion relation for deep water.

Next, we consider two separate situations to derive the plate dispersion relation. In the first integral, each of the Bessel functions with the argument $\kappa_m r_0$ is represented as the half-sum of Hankel functions of first and second kind. After application of the Cauchy residue theorem to the integrand at the poles $k = \kappa_m$, the Wronskian W can be used, see e.g. Abramowitz and Stegun [1], in those poles for the combination of Hankel functions:

$$W \{H_n^{(1)}(\kappa_m r_0), H_n^{(2)}(\kappa_m r_0)\} = H_{n+1}^{(1)}(\kappa_m r_0)H_n^{(2)}(\kappa_m r_0) - H_n^{(1)}(\kappa_m r_0)H_{n+1}^{(2)}(\kappa_m r_0) = -\frac{4i}{\pi \kappa_m r_0}. \quad (4.34)$$

For the second integral, we apply the procedure described above and use the fact that $H_q^{(2)}(-\kappa_m r_0) = -e^{q\pi i} H_q^{(1)}(\kappa_m r_0)$. Then, the coefficients of $J_n(\kappa r_0)$ are considered to derive the dispersion relation for deep water

$$(\mathcal{D}\kappa^4 - \mu + 1) \kappa = \pm k_0, \quad (4.35)$$

where the plus sign on the right-hand side corresponds to the first situation, and the minus sign to the second. The roots of the plate dispersion relation (4.35) are shown in figure 4.3: two real roots $\pm\kappa_1$, and four complex roots $\pm\kappa_2$ and $\pm\kappa_3$, which are symmetrically placed with respect to both the real and imaginary axes. Due to the symmetry of the Bessel function, three roots of the plate dispersion relation (4.35) are taken into account: real positive κ_1 , complex κ_2 and κ_3 with equal imaginary parts and equal real parts but of opposite sign. The real root κ_1 represents the main traveling wave mode and the two complex roots damped wave modes.

In this way, for infinite water depth, we use three roots of the plate dispersion relation, as for the semi-infinite plate in chapter 3, and in the equations of this section the upper limit of the summation M is equal to 3. For finite depth, more than three roots are taken into account.

In the first integral we also obtain a contribution of the pole $k = k_0$ of the integrand. This contribution has to cancel the term on the right-hand side of the expanded IDE (4.32). Because we use the deep water case to introduce the finite water-depth case, we do not consider the contribution of the integral along the imaginary axis, which makes our solution for the IWD case approximate. The application of the Jordan's lemma and the contribution of the pole $k = k_0$ leads to $N + 1$ relations:

$$\begin{aligned} \pi i r_0 \sum_{m=1}^M \frac{k_0^2}{k_0^2 - \kappa_m^2} \left[k_0 H_{n+1}^{(1)}(k_0 r_0) J_n(\kappa_m r_0) - \kappa_m H_n^{(1)}(k_0 r_0) J_{n+1}(\kappa_m r_0) \right] \\ \times (\mathcal{D}\kappa_m^4 - \mu) a_{mn} = A \epsilon_n. \end{aligned} \quad (4.36)$$

The system for determining the unknown amplitudes a_{mn} can be completed by the free edge conditions. We obtain $N + 1$ equations from each of the free edge conditions (4.15–4.16) at $\rho = r_0$:

$$\sum_{m=1}^M \left[J_n(\kappa_m r_0) \left(-\kappa_m^2 + \frac{(1-\nu)n(n-1)}{r_0^2} \right) + J_{n+1}(\kappa_m r_0) \kappa_m \frac{(1-\nu)}{r_0} \right] a_{mn} = 0, \quad (4.37)$$

$$\begin{aligned} \sum_{m=1}^M \left[J_n(\kappa_m r_0) \left(-\frac{n}{r_0} \kappa_m^2 + \frac{(1-\nu)n^2(1-n)}{r_0^3} \right) \right. \\ \left. + J_{n+1}(\kappa_m r_0) \left(\kappa_m^3 + \frac{(1-\nu)n^2}{r_0^2} \kappa_m \right) \right] a_{mn} = 0. \end{aligned} \quad (4.38)$$

In such a way we have derived the system of $3N + 3$ equations (4.36–4.38), as $M = 3$ for the IWD case, for the determination of $3N + 3$ amplitudes a_{mn} . When the amplitudes are known, the plate deflection can be calculated with formula (4.23).

4.5 Finite water depth

In this section we consider the general case where the plate floats on water of finite depth. The governing integro-differential equation can be derived similarly as in the previous section. It takes the form of IDE (4.29), the same as in the deep water case, where we use expression (4.22) for the Green's function for the finite water-depth case.

Inserting the relations for the plate deflection (4.23) and Green's function (4.22) into IDE (4.29), we obtain the following expanded integro-differential equation for water of finite depth:

$$\begin{aligned} & \left\{ \mathcal{D}\Delta^2 - \mu + 1 \right\} \sum_{m=1}^M \sum_{n=0}^N a_{mn} J_n(\kappa_m \rho) \cos n\varphi \\ &= \frac{K}{2\pi} \int_0^{2\pi} \int_0^{r_0} \left\{ \mathcal{D}\Delta^2 - \mu \right\} \sum_{m=1}^M \sum_{n=0}^N a_{mn} J_n(\kappa_m r) \cos n\theta \left(\int_0^\infty \frac{k \cosh kh}{K \cosh kh - k \sinh kh} \right. \\ & \quad \left. \times \sum_{q=0}^N \delta_q J_q(kr) J_m(k\rho) \cos q(\theta - \varphi) dk \right) r dr d\theta + A \sum_{n=0}^N \epsilon_n J_n(k_0 \rho) \cos n\varphi \end{aligned} \quad (4.39)$$

at the free surface $z = 0$. Only the case $q = n$ has to be considered, as was done for infinitely deep water. First we close the contour of the integration. Then the integration with respect to r and θ in equation (4.39) leads us to the set of $N + 1$ equations

$$\begin{aligned} & \sum_{m=1}^M (\mathcal{D}\kappa_m^4 - \mu + 1) a_{mn} J_n(\kappa_m \rho) + K r_0 \int_{\mathcal{L}} \sum_{m=1}^M (\mathcal{D}\kappa_m^4 - \mu) a_{mn} J_n(k\rho) \\ & \quad \times \frac{k \cosh kh}{(K \cosh kh - k \sinh kh)(k^2 - \kappa_m^2)} [k J_{n+1}(kr_0) J_n(\kappa_m r_0) - \kappa J_n(kr_0) J_{n+1}(\kappa_m r_0)] dk \\ & = A \epsilon_n J_n(k_0 \rho), \end{aligned} \quad (4.40)$$

where $n = 0, \dots, N$.

Next, we consider the function

$$F(k) = \frac{k \cosh kh}{K \cosh kh - k \sinh kh}. \quad (4.41)$$

The poles of function $F(k)$ are the roots of the dispersion relation for water region (4.13) $k = \pm k_i$, $i = 0, \dots, M-3$, where k_0 is the positive real root, and k_i , for $i \neq 0$, is the positive imaginary root, as shown in figure 4.4. The function $F(k)$ is meromorphic as it is bounded for all roots. For our problem, the meromorphic function $F(k)$ can be represented in the following way:

$$F(k) = \sum_{i=0}^{M-3} \frac{k_i^2}{k_i^2 h - K^2 h + K} \left(\frac{1}{k + k_i} + \frac{1}{k - k_i} \right). \quad (4.42)$$

This procedure is described by Whittaker and Watson [148] and applied in John [48]. The upper bound in the summation is chosen in accordance with the number of imaginary roots of the water dispersion relation (4.13).

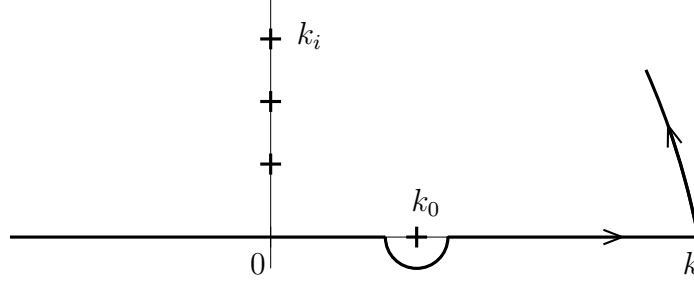


Figure 4.4: Closure of the integration contour in the upper half-plane.

Next, we insert relation (4.42) into equation (4.40), where two integrals in the complex k -plane are considered, which can be combined into one integral from $-\infty$ to $+\infty$ with only the poles $k = k_i$. Finally, we derive the governing integro-differential equation for finite water depth

$$\begin{aligned} & \sum_{m=1}^M (\mathcal{D}\kappa_m^4 - \mu + 1) a_{mn} J_n(\kappa_m \rho) + Kr_0 \int_{-\infty}^{\infty} \sum_{m=1}^M (\mathcal{D}\kappa_m^4 - \mu) a_{mn} \frac{J_n(k\rho)}{(k^2 - \kappa_m^2)} \\ & \times \sum_{i=0}^{M-3} \frac{k_i^2}{(k_i^2 h - K^2 h + K)(k - k_i)} [kJ_{n+1}(kr_0)J_n(\kappa_m r_0) - \kappa_m J_n(kr_0)J_{n+1}(\kappa_m r_0)] dk \\ & = A\epsilon_n J_n(k_0 \rho) \end{aligned} \quad (4.43)$$

at $z = 0$. Now the integration in the complex plane has to be carried out, which can be done analogously to the deep water case. The contour of the integration is depicted in figure 4.4.

We split up the Bessel functions with the argument kr_0 into half-sums of Hankel functions by formula (4.33), which turns the integral in equation (4.43) into the sum of the integrals in the upper and lower half-planes. The sum of the residues gives us the same result in both situations due to the property of the meromorphic function. Also, the Wronskian (4.34) can be used for the combination of the Hankel functions. The residue lemma is applied at the poles $k = \kappa_m$, that leads to the standard dispersion relation for water of finite depth if we consider the coefficients of $J_n(\kappa_m r_0)$.

The plate dispersion relation has the following form:

$$(\mathcal{D}\kappa^4 - \mu + 1) \kappa \tanh \kappa h = K. \quad (4.44)$$

The dispersion relation (4.44) has two real roots $\pm\kappa_1$, and four complex roots $\pm\kappa_2$ and $\pm\kappa_3$, symmetrically placed with respect to both the real and imaginary axes, those six being of the same order as in the deep-water case; this relation also has infinitely many pure imaginary roots. Here, we take into account M roots of relation (4.44): one real positive root κ_1 , and two complex roots κ_2 and κ_3 , with equal imaginary and real parts where the latter are of opposite sign, as well as $M - 3$ imaginary roots, all located in the upper half-plane. We notice that the positions of the roots κ_m in the complex k -plane are similar to those of the roots of the water dispersion relation (4.13), except for those of the two complex roots κ_2 and κ_3 . Deriving the dispersion relation (4.44) from IDE (4.43) is a good way to check the correctness of the approach.

Then we consider the contribution of the roots of the water dispersion relation, plotted in figure 4.4. The contour of integration for the integrals with $H_q^{(1)}(kr_0)$ and with $H_q^{(2)}(kr_0)$ may be closed in the upper and lower half-plane, respectively. In the latter case we get a zero contribution because the poles are as indicated in figure 4.4. The application of the Cauchy theorem to the integral closed in the upper half-plane gives the following $N + 1$ equations to determine the amplitudes a_{mn} :

$$\pi i K r_0 \sum_{m=1}^M \frac{k_0^2}{(k_0^2 - \kappa_m^2)(k_0^2 h - K^2 h + K)} \times \left[k_0 H_{n+1}^{(1)}(k_0 r_0) J_n(\kappa_m r_0) - \kappa_m H_n^{(1)}(k_0 r_0) J_{n+1}(\kappa_m r_0) \right] (\mathcal{D}\kappa_m^4 - \mu) a_{mn} = A\epsilon_n, \quad (4.45)$$

and the poles at the imaginary axis $k = k_i$ result in a set of $(M - 3)(N + 1)$ equations:

$$\pi i K r_0 \sum_{m=1}^M \frac{k_i^2}{(k_i^2 - \kappa_m^2)(k_i^2 h - K^2 h + K)} \times \left[k_i H_{n+1}^{(1)}(k_i r_0) J_n(\kappa_m r_0) - \kappa_m H_n^{(1)}(k_i r_0) J_{n+1}(\kappa_m r_0) \right] (\mathcal{D}\kappa_m^4 - \mu) a_{mn} = 0, \quad (4.46)$$

where $i = 1, \dots, M - 3$. The free edge conditions (4.37–4.38) give us $2(N + 1)$ equations, as in the previous section. Hence, we derive a system of $M(N + 1)$ equations (4.45–4.46), (4.37–4.38) to determine the amplitudes a_{mn} for the plate floating in water of finite depth. After solving this system, we can compute the deflection of the circular plate with formula (4.23).

The finite depth model can be used for problems of shallow water, and the results obtained are more accurate than those obtained by the shallow water approximation because more roots of the water and plate dispersion relations are taken into account.

4.6 Free-surface elevation and initiated wave pattern

Here we study the total free-surface elevation and wave pattern generated by the plate motion. The free-surface elevation can be determined with our approach for the plate-water interaction and integro-differential equation. The wave field initiated by the motion of the plate is the sum of the scattered and diffracted wave fields.

The total potential in \mathcal{F} ($r > r_0$) is represented in equation (4.25) as the sum of the incident wave potential and the potential of waves which appeared due to the vibration of the plate. Therefore, the free-surface elevation ζ in the open fluid region \mathcal{F} equals the sum of the incident wave elevation and the additional wave elevation generated by the motion of the plate,

$$\zeta(\rho, \varphi) = \zeta^{\text{inc}}(\rho, \varphi) + \zeta^{\text{pm}}(\rho, \varphi), \quad (4.47)$$

where the value of elevation ζ^{inc} is known, as it is the parameter of the incident wave field, while the value of ζ^{pm} may be obtained from analysis of an integro-differential equation.

For the region \mathcal{F} we can derive from equation (4.27), analogously to the analysis for the plate area \mathcal{P} , the following integro-differential equation

$$\zeta = Ae^{ik_0\rho\cos\varphi} + \frac{K}{4\pi} \int_{\mathcal{P}} \mathcal{G}(\rho, \varphi; r, \theta) \{ \mathcal{D}\Delta^2 - \mu \} w(r, \theta) r \, dr \, d\theta. \quad (4.48)$$

From the IDE (4.48), with the residue lemma at the pole $k = k_0$, we obtain the following expression for the free-surface elevation for water of infinite depth

$$\begin{aligned} \zeta(\rho, \varphi) = & Ae^{ik_0\rho\cos\varphi} - \pi i r_0 \sum_{m=1}^M \frac{k_0^2}{(k_0^2 - \kappa_m^2)} (\mathcal{D}\kappa_m^4 - \mu) \\ & \times \sum_{n=0}^N a_{mn} [k_0 J_{n+1}(k_0 r_0) J_n(\kappa_m r_0) - \kappa_m J_n(k_0 r_0) J_{n+1}(\kappa_m r_0)] H_n^{(1)}(k_0 \rho) \, dk. \end{aligned} \quad (4.49)$$

For finite water depth, after using the residue lemma at the poles $k = k_i$, we obtain the following expression for the free-surface elevation:

$$\begin{aligned} \zeta(\rho, \varphi) = & Ae^{ik_0\rho\cos\varphi} - \pi i K r_0 \sum_{m=1}^M \sum_{i=0}^{M-3} \frac{k_i^2}{(k_i^2 - \kappa_m^2)(k_i^2 h - K^2 h + K)} (\mathcal{D}\kappa_m^4 - \mu) \\ & \times \sum_{n=0}^N a_{mn} [k_i J_{n+1}(k_i r_0) J_n(\kappa_m r_0) - \kappa_m J_n(k_i r_0) J_{n+1}(\kappa_m r_0)] H_n^{(1)}(k_i \rho) \, dk. \end{aligned} \quad (4.50)$$

The expressions (4.49) and (4.50) are used to calculate the total free-surface elevation.

To study the initiated wave pattern, i.e., to see the consequence of the presence of floating plate, we may subtract the incident field from these expressions. The second terms on the right-hand side of formulas (4.49) and (4.50) represent ζ^{pm} for the cases of infinite and finite water depth, respectively. The numerical computation details are given in the next section.

4.7 Numerical results and discussion

This section gives numerical results for the deflection of the circular plate, free-surface elevation and initiated wave pattern for different values of the physical parameters. Results are presented for relevant and practically important cases. Also some comments are made on the numerical calculation and about the results obtained. In all figures, the left subplot is denoted as (a), and the right as (b); if there are four subplots, then the lower left is denoted as (c) and lower right as (d).

The Bessel functions of a complex argument, including κ_2 and κ_3 , have to be calculated carefully. The amplitudes a_{mn} of each wave mode behave as decaying functions because of the decay of the Bessel functions with respect to the order n , common for Bessel functions and amplitudes. Similar behavior of these amplitudes is reported by Zilman and Miloh [153] for shallow water. If we increase the value of flexural rigidity or radius, the decay is faster. Taking into account the first 30 terms of the series resulted in sufficient accuracy for realistic rigidity values. Even for very low rigidity, it is sufficient to choose this number of terms.

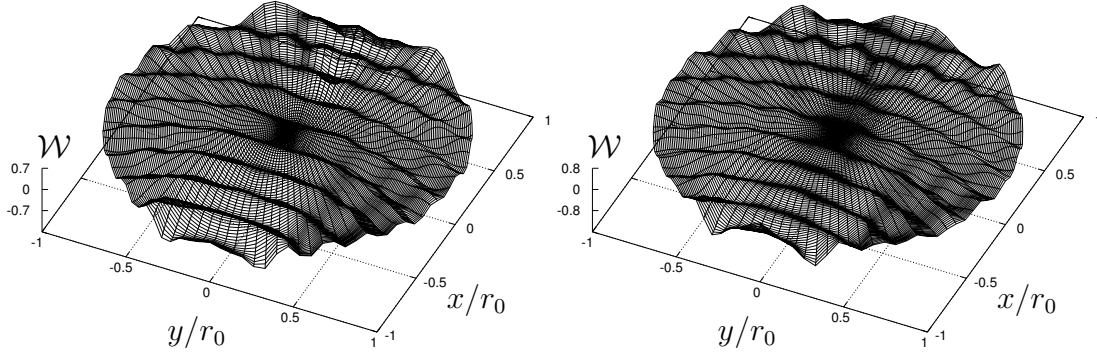


Figure 4.5: Deflection of the circular plate, for $\lambda = 50$ m, $r_0 = 500$ m, $\mathcal{D} = 10^5$ m⁴: a) infinite depth, b) finite depth, $h = 20$ m.

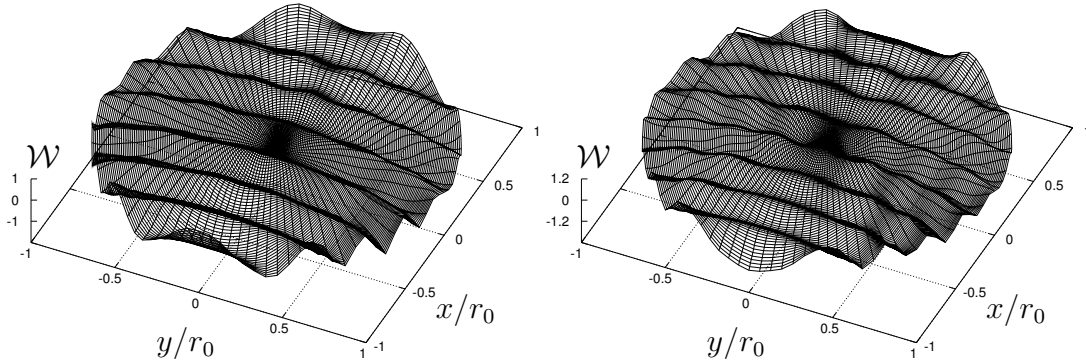


Figure 4.6: Deflection of the circular plate, as figure 4.5, for $\lambda = 100$ m.

To avoid difficulties in numerical computation when the argument of the function is small, it is possible in principle to use the recurrence relation described in Abramowitz and Stegun [1],

$$\mathcal{C}_{n+1}(z) = \frac{2n}{z}\mathcal{C}_n(z) - \mathcal{C}_{n-1}(z), \quad (4.51)$$

where \mathcal{C} denotes functions J , $H^{(1)}$ or $H^{(2)}$, and z denotes the arguments in the corresponding functions.

Numerical calculations were performed for various values of the plate radius and flexural rigidity, while Poisson's ratio $\nu = 0.25$ and ratio $m/\rho_w = 0.25$ m are remained constant. Taking the wave amplitude as $A = 1$ m, we varied the water depth and incident wavelength, which leads to different values of the wavenumber k_0 and of the frequency ω . As was described above, the number of Bessel function modes which were taken into account is $N = 30$. The number of roots of the plate dispersion relation for finite water depth (4.44) which were taken into account was $M = 10$. Especially for shallow water, there was

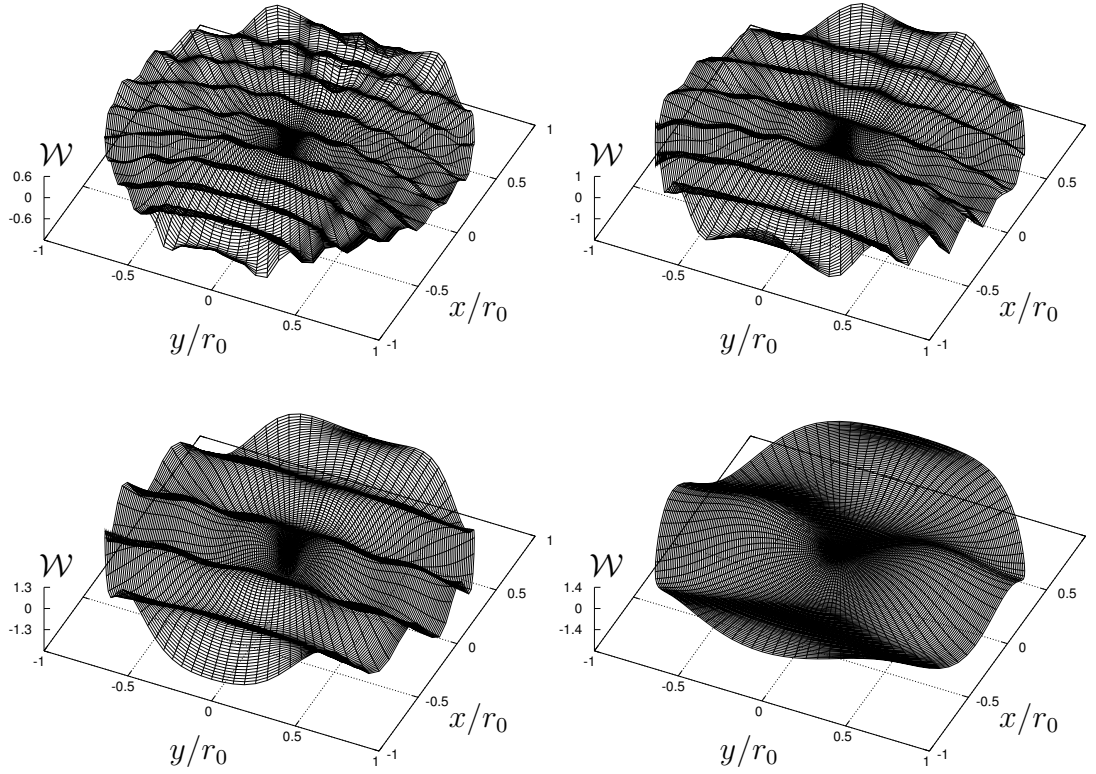


Figure 4.7: Deflection of the circular plate, for $h = 100$ m, $r_0 = 500$ m, $\mathcal{D} = 10^5$ m⁴: a) $\lambda = 50$ m, b) $\lambda = 100$ m, c) $\lambda = 200$ m, d) $\lambda = 500$ m.

hardly any difference in the results due to the number of roots M , while for deep water, the influence of the number of roots can be seen in the area close to the plate edge. The choice of such values of truncation parameters M and N was also justified by numerical tests. More details about the number of roots were given in chapter 3.

The numerical results are plotted for the real part of the plate deflection normalized by the wave amplitude $Re(w)/A$, denoted by \mathcal{W} in the figures. The results for both water depths are shown in the figures for a constant plate radius and rigidity and different wavelengths and water depths. The results for the circular plate on water of infinite depth are shown in subplots (a) of figures 4.5–4.6. The results for finite water depth are shown in all other subplots of figures 4.5–4.8. We can see clearly the wave propagation through the plate area.

The figures shown demonstrate that the wave traveling through the plate propagates with a curved wave front. This is especially prominent for cases where the wavelength is much smaller than the diameter of the circle. The plate deflection highly depends on the ratio between its radius r_0 and the wavelength λ . We found that for the rigidity parameter $\mathcal{D} > 10^7$ m⁴, the plate behaves like a very rigid body, whereas for $\mathcal{D} < 10^3$ m⁴, the plate has hardly any influence on the surface waves. Realistic values of the reduced flexural rigidity \mathcal{D} are of the order of about 10^7 m⁴ for the plate, while for ice, it can be of an order of about 10^5 m⁴. Certainly, the rigidity of the floating platform, the Young's

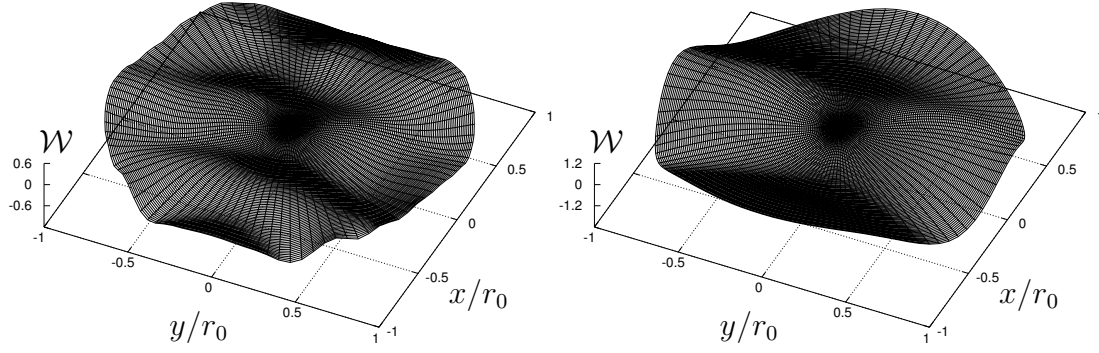


Figure 4.8: Deflection of the circular plate, for $h = 100$ m, $r_0 = 500$ m, $\mathcal{D} = 10^7$ m⁴: a) $\lambda = 100$ m, b) $\lambda = 500$ m.

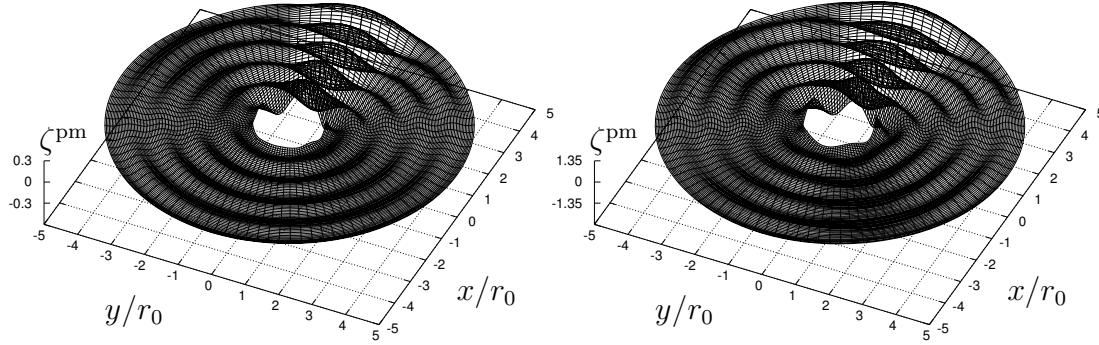


Figure 4.9: Initiated wave pattern, for $h = 100$ m, $\lambda = 500$ m, $r_0 = 500$ m, $r_f = 2500$ m: a) $\mathcal{D} = 10^6$ m⁴, b) $\mathcal{D} = 10^7$ m⁴.

modulus and Poisson's ratio highly depend on the structure material used. In a zone close to the plate edge, the deflection displays special behavior and can be quite different from the deflection in the center zone for a floating plate with low rigidity.

We also found that computational results for large depths, $h > 100$ m, remained almost the same with a growth of water depth. So, for such deep water, the depth does not strongly influence the results, and for this situation it is sufficient to take $M = 10$ as well. With decreasing water depth, the results for the plate deflection and free-surface elevation change gradually, i.e., the smaller the water depth, the larger its influence on the results. In addition the deflection of the plate is influenced by the rigidity (or stiffness) of the plate and by the wavelength: it increases with both of them. It also increases numerically with the water depth.

In figure 4.9 we show the results for the initiated wave pattern, i.e. for the free-surface elevation ζ^{pm} , generated by the motion of the circular plate. The subplots are given for the surface of a fluid domain of radius r_f , for water of finite depth. The initiated wave pattern highly depends on the water depth h and physical plate properties.

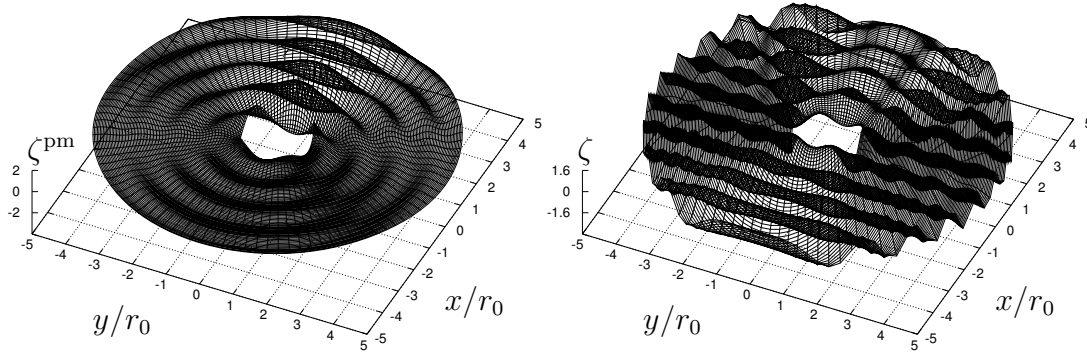


Figure 4.10: Initiated wave pattern (a) and free-surface elevation (b), for $\lambda = 500$ m, $r_0 = 500$ m, $r_f = 2500$ m, $\mathcal{D} = 10^8$ m⁴.

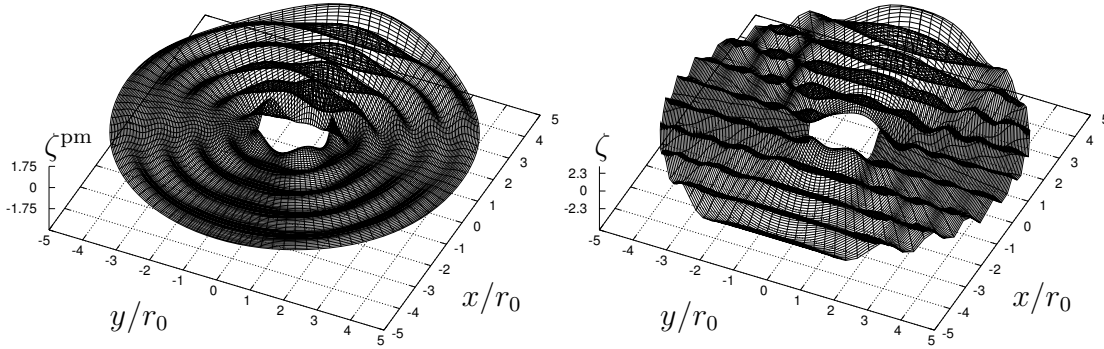


Figure 4.11: Initiated wave pattern (a) and free-surface elevation (b), for $h = 100$ m, $\lambda = 500$ m, $r_0 = 500$ m, $r_f = 2500$ m, $\mathcal{D} = 10^8$ m⁴.

In figures 4.10–4.11, numerical results are given for the initiated wave pattern, subplots (a), and the free-surface elevation, subplots (b), for infinite and finite water depth. The influence of the plate motion is clearly visible in the area behind the plate, where the propagation of the waves clearly changes. With the flexural rigidity of the plate (or its stiffness or Poisson's ratio), there is also an increase in the influence of the motion of the plate on the total elevation of the water surface. All figures are symmetric about the x -axis, because incoming plane waves propagate in the x -direction and their crests are parallel to the y -axis.

4.8 Conclusions and summary

The problem of interaction between a floating elastic circular plate and incident surface waves has been solved. The hydroelastic behavior of the plate was studied analytically and numerically. The integro-differential equation for the problem was derived, and an

algorithm of its numerical solution proposed. For finite water depth, a system of equations for the expansion coefficients was obtained analytically. For infinitely deep water, the problem was solved partly.

The finite water-depth model can be used to solve the plate-water interaction problem for the case of shallow water or water of infinite depth. Taking the limits $h \rightarrow \infty$ and $h \rightarrow 0$, we can derive the dispersion relations for deep or shallow water from the dispersion relation for water of finite depth. The floating structures are located in offshore zones, usually close to shore. Normally, the water is rather shallow in such zones, but as the wavelength could be short or long it is more universal to use finite water depth results to describe the motion of the structure and its hydroelastic response to ocean or sea waves.

The initiated wave pattern and the free-surface elevation in the open water region, the reflection and the transmission of incoming waves can also be described with the derived integro-differential equation. In contrast to other approaches, our approach can find the plate deflection and free-surface elevation using one set of equations. The approach presented can be extended to other rotationally symmetric configurations of the plate, e.g., the ring-shaped plate considered in the next chapter.

The approach is valid when the plate thickness and draft are assumed to be zero. To extend our method to plates of finite thickness, we may do the following. The deflection of the plate may be represented in the form

$$w = w^{(0)}(\kappa_m^{(0)}) + dw^{(1)}(\kappa_m^{(0)}, \kappa_m^{(1)}), \quad (4.52)$$

where $w^{(0)}$ is the solution obtained in the foregoing with the zero-thickness assumption, and $\kappa_m^{(0)}$ are the roots of the plate dispersion relation, also given in the foregoing, d is the draft of the plate, the superscripts denote the draft order. To avoid secular terms in $w^{(1)}$, $\kappa_m^{(0)}$ will be determined. The term $w^{(1)}$ can then be derived with the function $w^{(0)}$ and the extended dispersion relation for the first draft order, where the roots $\kappa_m^{(1)}$ are expressed via $\kappa_m^{(0)}$. Further details are presented in chapter 7.

One of possible applications of the method is its use for hydroelastic analysis of a VLFP for, say, a floating airport. The planform of a VLFP depends on the currents of the sea or ocean, in which it is to be installed, and on the distance from the coast, water depth, expected diffraction pattern, etc. In some cases it can make sense to give a VLFP an arbitrary horizontal shape, for instance a circular planform.

By inserting the physical properties of ice instead of those of the elastic plate, we can use the present approach to study the motion of large ice fields in water waves. There are so-called pancake ice fields with horizontal shape very close to a circle, whose ice-water interaction may be studied with the given method.

Chapter 5

Hydroelastic behavior of a ring-shaped plate

This chapter considers the diffraction of plane incident waves on a flexible ring-shaped floating plate and this plate's response to incident waves. An analytic and numerical study of the hydroelastic behavior of the plate is presented. An integro-differential equation is derived for the problem, and an algorithm of its numerical solution is proposed. The key ingredient of the approach is the representation of the solution as a series of Hankel functions. After an introduction, the problem is formulated. In section 5.3, the main integro-differential equation is derived on the basis of the Laplace equation and thin-plate theory. The plate deflection and free-surface elevation are expressed in polar coordinates as superpositions of Hankel functions, and the Green's function as a superposition of Bessel functions (as in previous chapter). These expressions, given in section 5.4, are used to analyze the integro-differential equation further. The problem is solved for two water depths: infinite and finite. For the coefficients for infinite depth, a set of algebraic equations is obtained, yielding an approximate solution in section 6. Then analogously a solution is obtained for the general and most important case of finite water depth in section 5.7. The exact solution might be approximated by taking into account a finite number of roots of the plate dispersion relation. Also, the influence of the plate's motion on wave propagation in the open water region and within the gap of the ring is studied. Numerical results are presented for illustrative purposes.

5.1 Introduction and background

This thesis studies the interaction between incident surface water waves and floating elastic plates. A literature survey for the problem was presented in section 1.3 and recently one has been published by Watanabe et al. [143]. Mainly plates having rectangular planforms have been studied. However, several papers studying the circular plate have been published recently as indicated in section 4.1. The problem for a circular plate on shallow water was solved by Zilman and Miloh [153] and Tsubogo [132]. For finite water depth, the problem was solved by Watanabe et al. [142] by use of the Galerkin method and Mindlin plate theory [80], and by Peter et al. [97], who presented a solution that is decomposed into angular eigenfunctions. In chapter 4, we solved the problem for a

circular disk on water of finite and infinite depth using an integro-differential formulation.

Here, the theory is extended to the case of a ring-shaped plate (or, as it is described in some of the literature, a circular plate with a circular hole). A floating structure of this form may be either of large dimensions, for VLFPs, or small, for other purposes. The hydroelastic behavior of the ring-shaped floating elastic plate and its response to incident surface waves are investigated. The ring floats on the surface of an ideal, incompressible fluid. We consider two water depths. First, we study the motion of a ring floating on the surface of water of infinite depth. Next, the case of water of finite depth is considered, where the general analysis and set of equations are more complicated as more roots of a water dispersion relation have to be taken into account. An analytical study is carried out and presented for both cases. The problem for water of shallow depth can be solved more easily by the use of the well-known Stoker approximation theory [107]. In the latter case, a set of equations is derived from free-edge and transition conditions at the inner and outer edges of the ring.

The integro-differential formulation which allows us to solve the diffraction problem for different geometrical configurations was developed in chapter 2, and, with modifications due to polar coordinates, in chapter 4. This formulation was used in chapters 3–4 and articles [8, 43, 5, 44]. The formulation might be applied to a plate of finite or infinite dimensions and even to the case of multiple plates. In addition we use the thin plate theory, the Laplace equation in the fluid supplemented by surface and boundary conditions, and the Green's theorem.

We consider an elastic plate of constant flexural rigidity and homogeneous stiffness. The edges of the ring are free of shear forces, bending and twisting moments. The plate deflection is generated by incoming plane surface waves. In general, in this section, we follow the analysis presented in chapter 4, for formulating the problem and deriving an IDE. However, an analysis for the case of the ring-shaped plate is more complicated. Nevertheless, we shall investigate the behavior of water waves in the ring gap as well. Hence, here we derive the solution for the plate deflection and free-surface elevation in the far field and ring gap.

The plate deflection is represented as a superposition of Hankel functions with corresponding coefficients, containing amplitudes. In a similar way, we represent the Green's function, obeying the boundary conditions at the free surface and at the sea bed, as a series of Bessel functions for both water depths. Further, as in chapter 4, we apply Graf's addition theorem to the Green's function.

Next, we derive the governing integro-differential equation. The problem involves two dispersion relations: one in the plate region, and one in the open water. An analysis of integrals in the complex plane and use of Cauchy's theorem lead us to the dispersion relation in the plate region. Furthermore, we derive from the integro-differential equation, supplemented by the free-edge conditions, a set of equations for the coefficients in the series expansion to determine the plate deflection. In addition, the free-surface elevation in the ring gap and in the open water field is studied. To analyze the influence of the plate on the propagation of incoming waves, we obtain results for the wave pattern generated by the plate's motion. Numerical results are obtained for different values of the physical parameters for practically important cases. Some details of the approach and the results have recently been published in [9].

5.2 Mathematical formulation

A thin elastic ring-shaped floating plate of inner radius r_1 and outer radius r_0 covers a part of the surface of an ideal, incompressible expanse of water. A plate with zero thickness can serve as a model of the VLFP, as described previously, due to the small thickness and shallow draft of the platform. The water depth h is infinite for deep water, and finite and constant for the other case. We assume that no space exists between the free surface and the plate. The flexural rigidity of the thin elastic isotropic plate is constant.

The plate deflection is generated by incoming surface waves of length λ . It is also assumed that incoming waves propagate in water that is still homogeneous in the positive x -direction. The wave amplitude A is rather small in comparison with other length parameters of the problem.

The horizontal geometry sketch of the plate is shown in figure 5.1. The radial coordinate ρ is measured from the center of the plate. We denote the surface of the fluid domain in the plate region ($r_1 \leq \rho \leq r_0$) as \mathcal{P} and in the open water as \mathcal{F} , where the open-water region outside the plate is \mathcal{F}_0 ($\rho > r_0$) and the gap area \mathcal{F}_1 ($\rho < r_1$). The three-dimensional Laplacian in polar coordinates is

$$\Delta = \nabla^2 = \frac{\partial^2}{\partial \rho^2} + \frac{1}{\rho} \frac{\partial}{\partial \rho} + \frac{1}{\rho^2} \frac{\partial^2}{\partial \varphi^2} + \frac{\partial^2}{\partial z^2}.$$

The relations between polar and Cartesian coordinates are the following: $\rho^2 = x^2 + y^2$, $\varphi = \arctan y/x$, $z = z$.

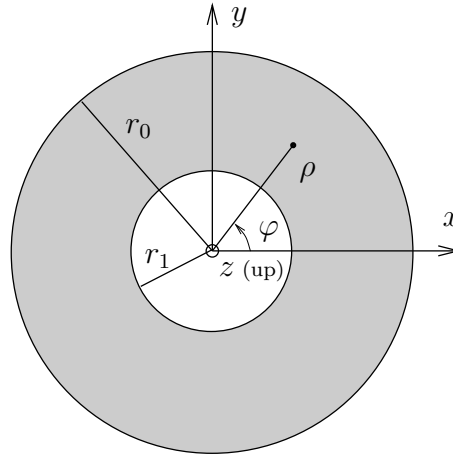


Figure 5.1: Geometry and coordinate system of the problem.

The velocity potential is introduced by $\nabla \Phi(\rho, \varphi, z, t) = \mathbf{V}(\rho, \varphi, z, t)$, where $\mathbf{V}(\rho, \varphi, z, t)$ is the fluid velocity vector. The velocity potential $\Phi(\rho, \varphi, z, t)$ is a solution of the governing Laplace equation in the fluid

$$\Delta \Phi = 0, \tag{5.1}$$

for $-h < z < 0$ in the FWD and IWD cases (in the IWD case, the fluid occupies the region $-\infty < z < 0$), supplemented by the boundary conditions at the free surface and

at the bottom. The linearized kinematic condition in the plate and water regions, at the surface $z = 0$, has the form

$$\frac{\partial \Phi}{\partial z} = \frac{\partial W}{\partial t}, \quad (5.2)$$

where $W(\rho, \varphi, t)$ denotes either the free-surface elevation or the deflection of the plate; t is the time. Later, to describe the vertical displacements, we will denote the free-surface elevation in the open-water region \mathcal{F} by ζ , while the plate deflection in \mathcal{P} will still be denoted by w . The dynamic condition, derived from the linearized Bernoulli equation, has the form

$$\frac{P - P_{\text{atm}}}{\rho_w} = -\frac{\partial \Phi}{\partial t} - gW, \quad (5.3)$$

at $z = 0$, where ρ_w is the density of the fluid, g is the gravitational acceleration, $P(\rho, \varphi, t)$ is the pressure in the fluid, and P_{atm} is the atmospheric pressure. Relations (5.2–5.3) are the kinematic and dynamic conditions at the free surface. The linearized free-surface condition in the water region \mathcal{F} takes the form

$$\frac{\partial \Phi}{\partial z} = -\frac{1}{g} \frac{\partial^2 \Phi}{\partial t^2} \quad (5.4)$$

at $z = 0$. The other boundary condition at the bottom, $z = -h$, is written in the following form

$$\frac{\partial \Phi}{\partial z} = 0. \quad (5.5)$$

The edges of the ring are free of vertical shear forces, bending and twisting moments. Therefore, the free-edge conditions at $\rho = r_1$ and $\rho = r_0$ are:

$$\left\{ \nabla^2 - \frac{(1-\nu)}{\rho} \left(\frac{\partial}{\partial \rho} + \frac{1}{\rho} \frac{\partial^2}{\partial \varphi^2} \right) \right\} w = 0, \quad (5.6)$$

$$\left\{ \frac{\partial}{\partial \rho} \nabla^2 + \frac{(1-\nu)}{\rho^2} \left(\frac{\partial}{\partial \rho} - \frac{1}{\rho} \right) \frac{\partial^2}{\partial \varphi^2} \right\} w = 0, \quad (5.7)$$

where the deflection $w(\rho, \varphi)$ does not depend on time, see (4.9). Here and in the rest of the thesis the Laplacian is two-dimensional, except when the Green's function is derived.

5.3 Integro-differential equation

In this section, the main integro-differential equation (IDE) is derived along the plate contour, consisting of the inner and outer edges of the ring. The approach for plates of rectangular shape in Cartesian coordinates is described in chapter 2 and applied in chapter 3 and with modifications in chapters 6–7. The derivation of IDE in polar coordinates is presented in chapter 4.

To describe the deflection of the plate W , we apply the isotropic thin-plate theory, see section 2.3, which leads to the Gehring-Kirchhoff differential equation at $z = 0$ in the plate area \mathcal{P}

$$D\Delta^2 W + m \frac{\partial^2 W}{\partial t^2} = P - P_{\text{atm}}, \quad (5.8)$$

where m is the mass per unit area of the plate, and D is the flexural rigidity. Like we did in chapters 3–4 for both the IWD and FWD cases, we apply the operator $\partial/\partial t$ to (5.8) and use the surface conditions (5.2–5.3) to arrive at the following equation for the total potential Φ

$$\left(\frac{D}{\rho_w g} \Delta^2 + \frac{m}{\rho_w g} \frac{\partial^2}{\partial t^2} + 1 \right) \frac{\partial \Phi}{\partial z} + \frac{1}{g} \frac{\partial^2 \Phi}{\partial t^2} = 0. \quad (5.9)$$

With the usual assumptions of an ideal fluid and small wave amplitude, the potential can be written in the form (4.8). The harmonic motion is considered, and from (5.2), it follows that the surface elevation has the same harmonic behavior, whence according to (4.9) we have the functions $w(\rho, \varphi)$ and $\zeta(\rho, \varphi)$ in \mathcal{P} and \mathcal{F} , respectively. Therefore, we consider waves of the single frequency ω and obtain the following differential equation for the potential ϕ at $z = 0$

$$(\mathcal{D}\Delta^2 - \mu + 1) \frac{\partial \phi}{\partial z} - K\phi = 0, \quad (5.10)$$

where $\mathcal{D} = D/\rho_w g$, $\mu = m\omega^2/\rho_w g$ are additional constant physical parameters, and $K = \omega^2/g$.

The potential of the undisturbed incident wave ϕ^{inc} in polar coordinates is

$$\phi^{\text{inc}}(\rho, \varphi, z) = \begin{cases} \frac{gA}{i\omega} e^{ik_0 \rho \cos \varphi + k_0 z} & \text{for IWD,} \\ \frac{\cosh k_0(z+h)}{\cosh k_0 h} \frac{gA}{i\omega} e^{ik_0 \rho \cos \varphi} & \text{for FWD,} \end{cases} \quad (5.11)$$

where A is the amplitude of the incident wave, and k_0 is the wavenumber. The wave height is defined as twice the amplitude. For deep water, the wavenumber is $k_0 = K$, and for water of finite depth, the wavenumber k_0 is the positive real solution of the water dispersion relation

$$k \tanh kh = K. \quad (5.12)$$

The length of the incoming waves is $\lambda = 2\pi/k_0$. In a practical situation, the outer diameter $2r_0$ of the ring-shaped VLFP is longer than the wavelength; the reverse case corresponds to extremely long waves.

The potential must satisfy the Sommerfeld radiation condition

$$\sqrt{\rho} \left(\frac{\partial}{\partial \rho} - ik_0 \right) (\phi - \phi^{\text{inc}}) = 0 \quad (5.13)$$

when $\rho \rightarrow \infty$.

The free-surface elevation ζ in the open water \mathcal{F} is equal to the sum of the incident wave elevation ζ^{inc} and the additional wave elevation ζ^{pm} , generated by the plate motion

$$\zeta = \zeta^{\text{inc}} + \zeta^{\text{pm}}. \quad (5.14)$$

The total potential in \mathcal{F} is also represented as the sum of the incident wave potential and the potential of waves arising because of the plate motion

$$\phi^{\mathcal{F}} = \phi^{\text{inc}} + \phi^{\text{dis}}, \quad (5.15)$$

where ϕ^{dis} is the diffraction potential plus the radiation potential. In fact, the potential ϕ^{dis} must satisfy radiation condition (5.13). The governing equations for the regions \mathcal{F}_0 and \mathcal{F}_1 are the same. Due to the fact that $\rho > r_0$ and $\rho < r_1$, respectively, differences will appear in the analysis which will be discussed later.

We introduce the Green's function $\mathcal{G}(r, \theta; \rho, \varphi)$, fulfilling the free-surface and the radiation conditions, and apply Green's theorem to the potentials in the water and plate regions $\phi^{\mathcal{F}}$ and $\phi^{\mathcal{P}}$, respectively. As for the circular plate problem, we analyze the relations obtained and use the dynamic (5.10) and kinematic (5.2) conditions to obtain the main integro-differential equation in general form at the free surface $z = 0$

$$\begin{aligned} & \{\mathcal{D}\Delta^2 - \mu + 1\} w(\rho, \varphi) \\ &= \frac{K}{4\pi} \int_{\mathcal{P}} \mathcal{G}(r, \theta; \rho, \varphi) \{\mathcal{D}\Delta^2 - \mu\} w(r, \theta) r \, dr \, d\theta + A e^{ik_0 \rho \cos \varphi}, \end{aligned} \quad (5.16)$$

where the last term represents the potential of the incoming waves. The IDE can be derived in polar and Cartesian coordinates, i.e., for plates of any geometrical shape. Chapter 4 gives detailed information on the derivation of IDE is given for polar coordinates and chapters 2–3 for Cartesian coordinates.

5.4 Green's function and deflection

In this section we describe the Green's function, plate deflection and the operations on corresponding Bessel and Hankel functions for the ring-shaped plate. The general expressions for the Green's function of a surface singularity for water of infinite and finite depth can be found in [146]. The description of the modified Green's function, which is used in the thesis, is given in section 2.5.

We introduce the Green's function for a source within the fluid that in Cartesian coordinates fulfills $\Delta \mathcal{G} = 4\pi \delta(\mathbf{x} - \boldsymbol{\xi})$, where δ is the Dirac δ -function, \mathbf{x} is a source point, and $\boldsymbol{\xi}$ is an observation point. The Green's function obeys the boundary conditions at the free surface (2.45) and at the sea bed (2.46) as well as the radiation condition (2.47). The three-dimensional Green's function at $z = \zeta = 0$ takes the following form:

$$\mathcal{G}(x, y; \xi, \eta) = -2 \int_{\mathcal{L}} F(k) J_0(kR) \, dk, \quad (5.17)$$

where $J_0(kR)$ is the Bessel function, R measures horizontal distance, viz. $R^2 = (x - \xi)^2 + (y - \eta)^2$ in Cartesian coordinates. \mathcal{L} is the integration contour in the complex k -plane from 0 to $+\infty$, passing beneath the singularity $k = k_0$, as shown in figure 5.2, and chosen such that the radiation condition is satisfied. The function $F(k)$ in (5.17) is given by

$$F(k) = \begin{cases} \frac{k}{k - k_0} & \text{for IWD, (a)} \\ \frac{k \cosh kh}{k \sinh kh - K \cosh kh} & \text{for FWD, (b).} \end{cases} \quad (5.18)$$

In the FWD case, we have additional poles $k = \pm k_i$ on the imaginary axis of the complex plane.

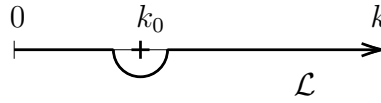


Figure 5.2: Contour of the integration.

In polar coordinates, the horizontal distance is written as $R^2(\rho, \varphi; r, \theta) = \rho^2 + r^2 - 2\rho r \cos(\theta - \varphi)$. Here ρ and r are the distance from the center of the plate to the source and to the observation points, respectively, and $\theta - \varphi$ is the angle between r and ρ .

If we apply Graf's addition theorem to the Bessel function $J_0(kR)$, which is also called Neumann's formula for the Bessel function of order zero, it can be replaced by the series [131]

$$J_0(kR) = \sum_{q=0}^{\infty} \delta_q J_q(kr) J_q(k\rho) \cos q(\theta - \varphi), \quad (5.19)$$

where $\delta_0 = 1$ and $\delta_q = 2$ if $q > 0$. We truncate the series in (5.19) at $q = N$, chosen such that convergence of the final results is guaranteed, where the decaying behavior of the Bessel functions with respect to the order has been taken into account. The value of N is chosen later; all terms of order higher than N are negligible. This is justified by invoking a computational test. Then, the Green's function in polar coordinates takes the form

$$\mathcal{G}(r, \theta; \rho, \varphi) = -2 \int_{\mathcal{L}} F(k) \sum_{q=0}^N \delta_q J_q(kr) J_q(k\rho) \cos q(\theta - \varphi) dk. \quad (5.20)$$

Further on in this chapter, the form (5.20) is used for the Green's function.

At the same time, the deflection function has to be chosen separately for each shape of the plate; our representations are given in section 2.6. For the circular plate, it is expressed by the superposition of Bessel functions (4.23). Analogously, for the ring-shaped plate, the deflection can be represented as a series of Hankel functions with corresponding coefficients of the following form

$$w(\rho, \varphi) = \sum_{m=1}^M \sum_{n=0}^N [a_{mn}^{(1)} H_n^{(1)}(\kappa_m \rho) + a_{mn}^{(2)} H_n^{(2)}(\kappa_m \rho)] \cos n\varphi, \quad (5.21)$$

where $a_{mn}^{(1)}$ and $a_{mn}^{(2)}$ are unknown amplitude functions, κ_m are the roots of the plate dispersion relation, which are reduced wavenumbers, and M is the number of these roots taken into account in the computations.

For the IWD case, we use three roots of the dispersion relation in the plate area:

$$(\mathcal{D}\kappa^4 - \mu + 1) \kappa = \pm k_0. \quad (5.22)$$

The roots of the plate dispersion relation (5.22), shown in figure 5.3, are the following: two real roots $\pm\kappa_1$, and four complex roots $\pm\kappa_2$ and $\pm\kappa_3$, which are symmetrically placed with respect to both the real and imaginary axes. Due to a property of Hankel functions, three roots are taken into account for the current situation: real positive root κ_1 and roots κ_2 and κ_3 , with equal imaginary parts and equal real parts but with opposite signs, all three located in the upper half-plane. The real root κ_1 represents the main traveling wave mode; the two complex roots represent damped wave modes.

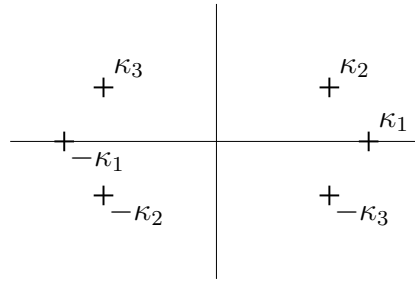


Figure 5.3: Zeros of the dispersion relation for deep water.

The plate dispersion relation for water of finite depth has the following form

$$(\mathcal{D}\kappa^4 - \mu + 1) \kappa \tanh \kappa h = K. \quad (5.23)$$

The dispersion relation (5.23) has two real roots $\pm\kappa_1$, and four complex roots $\pm\kappa_2$ and $\pm\kappa_3$ symmetrically placed with respect to both the real and imaginary axes, these six being of the same order as in the IWD case, and infinitely many pure imaginary roots. We take into account M roots of the dispersion relation (5.23): one real positive κ_1 , two complex roots κ_2 and κ_3 , having equal imaginary parts and equal but opposite-signed real parts, and $M - 3$ imaginary roots, all located in the upper half-plane.

The positions of the roots κ_m in the complex k -plane are similar to those of the roots of the water dispersion relation (5.12), which has one real root k_0 , corresponding to only one wavenumber of deep water, and a number of pure imaginary roots k_i , $i = 1, \dots, M - 3$, except for two complex roots κ_2 and κ_3 . Thus, in the FWD case, M is the truncation parameter, and we take into account M roots of the plate dispersion relation (5.23) κ_m , $m = 1, \dots, M$, and $M - 2$ roots of the water dispersion relation (5.12) k_i , $i = 0, \dots, M - 3$. In the IWD case the number of the roots is $M = 3$. The dispersion relations (5.22–5.23) can be derived from an analysis of the integro-differential equation.

5.5 Set of equations

At this point we have only equations resulting from the free-edge conditions to determine the unknown amplitudes $a_{mn}^{(1)}$ and $a_{mn}^{(2)}$. To complete the set of equations, we will derive

relations from the integro-differential equation.

If we insert the relations for the deflection (5.21) and Green's function (5.20) into (5.16), the integro-differential equation at the free surface $z = 0$ takes the expanded form

$$\begin{aligned} & \left\{ \mathcal{D}\Delta^2 - \mu + 1 \right\} \sum_{m=1}^M \left[\sum_{n=0}^N a_{mn}^{(1)} H_n^{(1)}(\kappa_m \rho) \cos n\varphi + \sum_{n=0}^N a_{mn}^{(2)} H_n^{(2)}(\kappa_m \rho) \cos n\varphi \right] \\ & + \frac{K}{2\pi} \int_0^{2\pi} \int_{r_1}^{r_0} \left\{ \mathcal{D}\Delta^2 - \mu \right\} \sum_{m=1}^M \left[\sum_{n=0}^N a_{mn}^{(1)} H_n^{(1)}(\kappa_m r) \cos n\theta + \sum_{n=0}^N a_{mn}^{(2)} H_n^{(2)}(\kappa_m r) \cos n\theta \right] \\ & \times \int_{\mathcal{L}} F(k) \sum_{q=0}^N \delta_q J_q(kr) J_q(k\rho) \cos q(\theta - \varphi) dk r dr d\theta = A \sum_{n=0}^N \epsilon_n J_n(k_0 \rho) \cos n\varphi, \quad (5.24) \end{aligned}$$

where $\epsilon_n = \delta_n i^n$. Due to the orthogonality relation for the cosine function, we only get a non-zero contribution in the integrand for $n = q$. Next, the integration with respect to θ in (5.24) is carried out. If only components dependent on θ are considered, the integration over θ gives 2π for $n = 0$ and $\delta_n \pi \cos n\varphi$ for $n > 0$, which means $2\pi \cos n\varphi$ for all n . Then, using the orthogonality of the cosine function, we end up with the following set of $N + 1$ equations derived from IDE (5.24):

$$\begin{aligned} & \sum_{m=1}^M (\mathcal{D}\kappa_m^4 - \mu + 1) [a_{mn}^{(1)} H_n^{(1)}(\kappa_m \rho) + a_{mn}^{(2)} H_n^{(2)}(\kappa_m \rho)] \\ & + K \int_{r_1}^{r_0} \sum_{m=1}^M (\mathcal{D}\kappa_m^4 - \mu) [a_{mn}^{(1)} H_n^{(1)}(\kappa_m r) + a_{mn}^{(2)} H_n^{(2)}(\kappa_m r)] \\ & \times \int_{\mathcal{L}} F(k) J_n(kr) J_n(k\rho) dk r dr = A \epsilon_n J_n(k_0 \rho), \quad (5.25) \end{aligned}$$

for $n = 0, \dots, N$. In accordance with [60, equation 21.8-22], the integration with respect to r leads us to the difference of two Lommel integrals at r_0 and r_1 . Therefore, equation (5.25) takes the form

$$\begin{aligned} & \sum_{m=1}^M (\mathcal{D}\kappa_m^4 - \mu + 1) [a_{mn}^{(1)} H_n^{(1)}(\kappa_m \rho) + a_{mn}^{(2)} H_n^{(2)}(\kappa_m \rho)] \\ & + K \int_{\mathcal{L}} \sum_{m=1}^M (\mathcal{D}\kappa_m^4 - \mu) \frac{F(k)}{(k^2 - \kappa_m^2)} [a_{mn}^{(1)} c_{mn}^{(1)} + a_{mn}^{(2)} c_{mn}^{(2)}] J_n(k\rho) dk = A \epsilon_n J_n(k_0 \rho), \quad (5.26) \end{aligned}$$

where we have introduced the function $c_{mn}^{(q)}$ as a combination of Bessel and Hankel functions of the form

$$\begin{aligned} c_{mn}^{(q)} = & r_0 \left[k J_{n+1}(kr_0) H_n^{(q)}(\kappa_m r_0) - \kappa_m J_n(kr_0) H_{n+1}^{(q)}(\kappa_m r_0) \right] \\ & - r_1 \left[k J_{n+1}(kr_1) H_n^{(q)}(\kappa_m r_1) - \kappa_m J_n(kr_1) H_{n+1}^{(q)}(\kappa_m r_1) \right], \quad q = 1, 2. \quad (5.27) \end{aligned}$$

From equation (5.26), we can derive $2(M-2)(N+1)$ relations to determine $2M(N+1)$ unknown amplitudes. The set of equations for both water depths is completed by the free-edge conditions (5.6–5.7) in which the deflection function is inserted. These conditions at the edges $\rho = r_1$ and $\rho = r_0$ give us $4(N+1)$ equations:

$$\sum_{m=1}^M a_{mn}^{(1)} d_{mn,ij}^{(1)} + a_{mn}^{(2)} d_{mn,ij}^{(2)} = 0, \quad (5.28)$$

where $n = 0, \dots, N$, $i = 0, 1$, $j = 1, 2$, and the functions $d_{mn,ij}^{(q)}$ are

$$\begin{aligned} d_{mn,i1}^{(q)} &= \left[H_n^{(q)}(\kappa_m r_i) \left(-\kappa_m^2 + \frac{(1-\nu)n(n-1)}{r_i^2} \right) + H_{n+1}^{(q)}(\kappa_m r_i) \kappa_m \frac{(1-\nu)}{r_i} \right], \\ d_{mn,i2}^{(q)} &= \left[H_n^{(q)}(\kappa_m r_i) \left(-\frac{n}{r_i} \kappa_m^2 + \frac{(1-\nu)n^2(1-n)}{r_i^3} \right) \right. \\ &\quad \left. + H_{n+1}^{(q)}(\kappa_m r_i) \left(\kappa_m^3 + \frac{(1-\nu)n^2}{r_i^2} \kappa_m \right) \right], \end{aligned} \quad (5.29)$$

where $q = 1, 2$ is the Hankel-function index, and r_i is either inner-ring contour r_1 or outer-ring contour r_0 .

From now on we consider IWD and FWD separately.

5.6 Ring on water of infinite depth

Here a ring floating on water of infinite depth is studied analytically. In the IWD case, we only consider part of the solution, namely that related to the water dispersion relation. The analysis given in this section is a good basis from which to derive a solution for the general and most complicated case of water of finite depth. To demonstrate the method we wish to use for the FWD case, we consider the contribution of the pole $k = k_0$ in the IWD case. Here, we ignore the contribution of the integral along the imaginary axis after closing the contour in (5.20). This means that local disturbances are disregarded.

The deflection of the plate, the Green's function, and the function $F(k)$ are represented by expressions (5.21), (5.20) and (5.18a), respectively. For deep water, the wavenumber k_0 equals K , so $k_0 = \omega^2/g$.

Now we will analyze the k -integral in IDE (5.26). The integrand has the poles $k = \pm \kappa_m$ shown in figure 5.3 and can be represented as a sum of four integrals

$$\begin{aligned} k_0 \int_0^\infty \frac{k}{(k - k_0)(k^2 - \kappa_m^2)} [a_{mn}^{(1)} c_{mn}^{(1)} + a_{mn}^{(2)} c_{mn}^{(2)}] J_n(k\rho) dk \\ = a_{mn}^{(1)} (I_{01} - I_{11}) + a_{mn}^{(2)} (I_{02} - I_{12}), \end{aligned} \quad (5.30)$$

where the path of integration in (5.31) is below the singularities $k = k_0$ and $k = \kappa_1$. The

integrals I_{iq} for $i = 0, 1$, $q = 1, 2$ are

$$I_{iq} = k_0 r_i \int_0^\infty \frac{k}{(k - k_0)(k^2 - \kappa_m^2)} \times \left[k J_{n+1}(kr_i) H_n^{(q)}(\kappa_m r_i) - \kappa_m J_n(kr_i) H_{n+1}^{(q)}(\kappa_m r_i) \right] J_n(k\rho) dk, \quad (5.31)$$

with r_i as r_1 or r_0 , $m = 1, \dots, M$ and $n = 0, \dots, N$. The contour of integration may be closed in the complex k -plane. In the integral I_{iq} , we split up the Bessel function of largest argument to be able to close the contour of integration and, furthermore, to use Jordan's lemma.

Let us consider the integral I_{01} . For further manipulation we use the fact that $\rho < r_0$ and write the Bessel function $J_t(kr_0)$ as the half-sum of the corresponding Hankel functions of the first and second kind

$$J_t(kr_0) = \frac{H_t^{(1)}(kr_0) + H_t^{(2)}(kr_0)}{2}, \quad (5.32)$$

where t is either n or $n+1$. Then I_{01} is decomposed into two integrals. These we transform into integrals along the vertical axis in the complex k -plane plus the sums of the residues at the poles as shown in figure 5.3, with factors $2\pi i$. Then the contour of integration for the first integral with $H_t^{(1)}(kr_0)$ is closed in the upper half-plane with the poles $k = \kappa_m$, and that for the second one with $H_t^{(2)}(kr_0)$ is closed in the lower half-plane, where the poles are at $k = -\kappa_m$. These two situations have to be considered separately.

If we apply the same procedure to the integral I_{02} , the contour for its first integral, obtained by (5.32) and containing $H_t^{(1)}(kr_0)$, can be closed in the upper half-plane; that for the integral with $H_t^{(2)}(kr_0)$, in the lower half-plane. For the integrals I_{11} and I_{12} , the same closure procedure is applied, but with one difference. In this case, $\rho > r_1$ and therefore, to close the contours of integration, we represent the Bessel functions $J_n(k\rho)$ as the half-sums of corresponding Hankel functions of the first and second kind, as was done in (5.32).

When the contours are closed for all integrals, we apply the Cauchy residue lemma at the poles $k = \kappa_m$ for the integrals with the contour closed in the upper half-plane and at the poles $k = -\kappa_m$ for the integrals with the contour closed in the lower half-plane. The Wronskian $W\{H_n^{(1)}(\kappa_m r_i), H_n^{(2)}(\kappa_m r_i)\}$ applies for the combination of Hankel functions, analogously to chapter 4,

$$H_{n+1}^{(1)}(\kappa_m r_i) H_n^{(2)}(\kappa_m r_i) - H_n^{(1)}(\kappa_m r_i) H_{n+1}^{(2)}(\kappa_m r_i) = -\frac{4i}{\pi \kappa_m r_i}. \quad (5.33)$$

Then, adding up the resulting terms and considering the coefficients of $J_n(\kappa r_i)$, we derive the plate dispersion relation for deep water (5.22), where the plus sign in the right-hand side corresponds to the integrals in the upper half-plane, and the minus sign to the integrals in the lower half-plane. The derivation of the plate dispersion relation from IDE is also a justification of our approach.

In the upper half-plane we also obtain a contribution of the pole $k = k_0$ of the integrand, as seen in figure 5.2. This contribution has to cancel the term in the right-hand

side of IDE (5.26). If we neglect the integral along the imaginary axis, application of Jordan's lemma and the contribution of the pole $k = k_0$ lead to $2(N + 1)$ relations

$$\pi i r_0 \sum_{m=1}^M (\mathcal{D}\kappa_m^4 - \mu) \frac{k_0^2}{k_0^2 - \kappa_m^2} \left[k_0 H_{n+1}^{(1)}(k_0 r_0) (a_{mn}^{(1)} H_n^{(1)}(\kappa_m r_0) + a_{mn}^{(2)} H_n^{(2)}(\kappa_m r_0)) \right. \\ \left. - \kappa_m H_n^{(1)}(k_0 r_0) (a_{mn}^{(1)} H_{n+1}^{(1)}(\kappa_m r_0) + a_{mn}^{(2)} H_{n+1}^{(2)}(\kappa_m r_0)) \right] = A \epsilon_n \quad (5.34)$$

and

$$\pi i r_1 \sum_{m=1}^M (\mathcal{D}\kappa_m^4 - \mu) \frac{k_0^2}{k_0^2 - \kappa_m^2} \left[k_0 J_{n+1}(k_0 r_1) (a_{mn}^{(1)} H_n^{(1)}(\kappa_m r_1) + a_{mn}^{(2)} H_n^{(2)}(\kappa_m r_1)) \right. \\ \left. - \kappa_m J_n(k_0 r_1) (a_{mn}^{(1)} H_{n+1}^{(1)}(\kappa_m r_1) + a_{mn}^{(2)} H_{n+1}^{(2)}(\kappa_m r_1)) \right] = 0. \quad (5.35)$$

We have now derived a system of $2M(N + 1)$ equations (5.34–5.35) and (5.28) for the determination of $2M(N + 1)$ amplitudes $a_{mn}^{(1)}$ and $a_{mn}^{(2)}$ for infinitely deep water, whereas $M = 3$. When the amplitudes are known, the plate deflection is calculated by formula (5.21).

5.7 Ring on water of finite depth

In this section we consider a ring on water of finite depth. In general, we follow the analysis for the IWD case presented in the previous section. For the FWD case, the deflection of the plate is represented by (5.21) and the Green's function is given by formulas (5.20) and (5.18b). Here, we take into account $M - 2$ roots of the water dispersion relation (5.12) and M roots of the plate dispersion relation (5.23).

Let us consider the function $F(k)$ which is given by (5.18b). For the FWD case, this function is meromorphic, as it is bounded for all poles. The poles are the roots of the dispersion relation for the water region (5.12) $k = \pm k_i$, $i = 0, \dots, M - 3$, where k_0 is the positive real root and k_i , for $i \neq 0$, is the pure imaginary root. Hence, the meromorphic function $F(k)$ for water of finite depth can be expressed as

$$F(k) = \sum_{i=0}^{M-3} \frac{k_i^2}{k_i^2 h - K^2 h + K} \left(\frac{1}{k + k_i} + \frac{1}{k - k_i} \right). \quad (5.36)$$

The relation (5.36) is inserted into IDE (5.26). There are two integrals in the complex k -plane; these can be combined into one integral from $-\infty$ to $+\infty$ with the poles $k = k_i$. The contour of integration is defined as \mathcal{L}' . Finally, we derive the governing integro-differential equation for the case of finite water depth

$$\sum_{m=1}^M (\mathcal{D}\kappa_m^4 - \mu + 1) [a_{mn}^{(1)} H_n^{(1)}(\kappa_m \rho) + a_{mn}^{(2)} H_n^{(2)}(\kappa_m \rho)] + K \int_{\mathcal{L}'} \sum_{m=1}^M (\mathcal{D}\kappa_m^4 - \mu) \\ \times \frac{J_n(k\rho)}{(k^2 - \kappa_m^2)} \sum_{i=0}^{M-3} \frac{k_i^2}{(k_i^2 h - K^2 h + K)(k - k_i)} [a_{mn}^{(1)} c_{mn}^{(1)} + a_{mn}^{(2)} c_{mn}^{(2)}] dk = A \epsilon_n J_n(k_0 \rho) \quad (5.37)$$

at $z = 0$, where $n = 0, \dots, N$ and the functions $c_{mn}^{(q)}$ are given by (5.27) for $q = 1, 2$.

To obtain the dispersion relation, we repeat the procedure we applied for the IWD case: the representation of k -integral as a sum of four integrals and, further, decomposition of each of those four into two integrals with contours closed in the different half-planes of the complex plane. In the FWD case, we have the poles given in figure 5.3, plus the poles at the imaginary axis $\pm \kappa_m$ for $m = 4, \dots, M$. The application of the residue lemma at the poles leads to the standard plate dispersion relation for water of finite depth (5.23).

Next, the contributions of the poles of the water dispersion relation (5.12) are considered. The closure of the contour is shown in figure 5.4. The contour for the integrals with $H_q^{(1)}(kr_i)$ might be closed in the upper half-plane, while the contour for the integrals with $H_q^{(2)}(kr_i)$ is closed in the lower half-plane. In the latter case, we get a zero contribution, because the poles $k = k_i$ are located as indicated in figure 5.4.

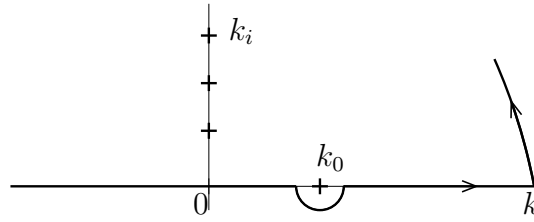


Figure 5.4: Closure of the contour of the integration in the upper half-plane.

Application of the Cauchy theorem to the integrals with the contour closed in the upper half-plane gives us equations to determine the amplitudes $a_{mn}^{(1)}$ and $a_{mn}^{(2)}$. The poles $k = k_i$, where $i = 0, \dots, M-3$, result in $2(M-2)(N+1)$ equations. The first $(M-2)(N+1)$ equations are derived along the outer ring edge $\rho = r_0$ which have the following form

$$\begin{aligned} & \pi i K r_0 \sum_{m=1}^M \frac{(\mathcal{D}\kappa_m^4 - \mu) k_i^2}{(k_i^2 - \kappa_m^2)(k_i^2 h - K^2 h + K)} \\ & \times \left[k_i H_{n+1}^{(1)}(k_i r_0) (a_{mn}^{(1)} H_n^{(1)}(\kappa_m r_0) + a_{mn}^{(2)} H_n^{(2)}(\kappa_m r_0)) \right. \\ & \left. - \kappa_m H_n^{(1)}(k_i r_0) (a_{mn}^{(1)} H_{n+1}^{(1)}(\kappa_m r_0) + a_{mn}^{(2)} H_{n+1}^{(2)}(\kappa_m r_0)) \right] = A_i, \end{aligned} \quad (5.38)$$

where

$$A_i = \begin{cases} A\epsilon_n, & i = 0, \\ 0, & i = 1, \dots, M-3, \end{cases}$$

as the case $i = 0$ corresponds to the pole $k = k_0$. The remaining $(M-2)(N+1)$ equations are derived along the inner edge of the ring $\rho = r_1$

$$\begin{aligned} & \pi i K r_1 \sum_{m=1}^M \frac{(\mathcal{D}\kappa_m^4 - \mu) k_i^2}{(k_i^2 - \kappa_m^2)(k_i^2 h - K^2 h + K)} \\ & \times \left[k_i J_{n+1}(k_i r_1) (a_{mn}^{(1)} H_n^{(1)}(\kappa_m r_1) + a_{mn}^{(2)} H_n^{(2)}(\kappa_m r_1)) \right. \\ & \left. - \kappa_m J_n(k_i r_1) (a_{mn}^{(1)} H_{n+1}^{(1)}(\kappa_m r_1) + a_{mn}^{(2)} H_{n+1}^{(2)}(\kappa_m r_1)) \right] = 0. \end{aligned} \quad (5.39)$$

Hence, the set of $2(M - 2)(N + 1)$ equations (5.38–5.39) is derived to determine the unknown amplitudes. Like in the previous section, the set of equations is completed by $4(N + 1)$ edge conditions (5.28). The deflection can now be computed with (5.21).

The finite-water-depth model can be used to solve the problem of shallow or infinitely deep water. Taking the limits $h \rightarrow 0$ and $h \rightarrow \infty$, we can derive the solutions for these situations including transition from the dispersion relation for water of finite depth to the dispersion relations for deep and shallow water, respectively.

5.8 Free-surface elevation and initiated wave pattern

In this section we continue the analysis of the plate-water interaction for current geometry and consider the open-water region, which consists of the main region \mathcal{F}_0 and the gap inside the ring \mathcal{F}_1 . The elevation $\zeta(\rho, \varphi)$ of the free surface can be computed with (5.14), where the value of ζ^{inc} may be obtained from the incident wave potential expression (5.11) using the kinematic condition (5.2) and the value of ζ^{pm} from the following analysis of IDE in the open-water area.

The integro-differential equation has the form (5.37) for the FWD case. Therefore, analogously to chapter 4, we obtain the following expression for the free-surface elevation

$$\begin{aligned} \zeta(\rho, \varphi) = & A e^{ik_0 \rho \cos \varphi} - K \int_{\mathcal{L}'} \sum_{m=1}^M (\mathcal{D}\kappa_m^4 - \mu) \frac{J_n(k\rho)}{(k^2 - \kappa_m^2)} \\ & \times \sum_{i=0}^{M-3} \frac{k_i^2}{(k_i^2 h - K^2 h + K)(k - k_i)} [a_{mn}^{(1)} c_{mn}^{(1)} + a_{mn}^{(2)} c_{mn}^{(2)}] dk. \end{aligned} \quad (5.40)$$

We notice that in the open-water region \mathcal{F}_0 , where $\rho > r_0 > r_1$, $J_n(k\rho)$ is split up into the half-sum of corresponding Hankel functions to close the contour of integration; to do so, at the gap area \mathcal{F}_1 the Bessel functions $J_t(kr_1)$, $t = n, n + 1$, are split up for $\rho < r_1 < r_0$. After using the residue lemma at the poles $k = k_i$, we obtain the following relation for the free-surface elevation

$$\begin{aligned} \zeta(\rho, \varphi) = & A e^{ik_0 \rho \cos \varphi} - \pi i \sum_{m=1}^M (\mathcal{D}\kappa_m^4 - \mu) \\ & \times \sum_{i=0}^{M-3} \frac{k_i^2 K}{(k_i^2 h - K^2 h + K)(k_i^2 - \kappa_m^2)} [a_{mn}^{(1)} f_{mni}^{(1)} + a_{mn}^{(2)} f_{mni}^{(2)}], \end{aligned} \quad (5.41)$$

where the functions $f_{mni}^{(q)}$ are expressed in the following way for the open water \mathcal{F}_0 and for the gap \mathcal{F}_1

$$f_{mni}^{(q)} = \begin{cases} r_0 H_n^{(1)}(k_i \rho) \left[k J_{n+1}(k_i r_0) H_n^{(q)}(\kappa_m r_0) - \kappa_m J_n(k_i r_0) H_{n+1}^{(q)}(\kappa_m r_0) \right] & \text{in } \mathcal{F}_0, \\ r_1 J_n(k_i \rho) \left[k H_{n+1}^{(1)}(k_i r_1) H_n^{(q)}(\kappa_m r_1) - \kappa_m H_n^{(1)}(k_i r_1) H_{n+1}^{(q)}(\kappa_m r_1) \right] & \text{in } \mathcal{F}_1, \end{cases} \quad (5.42)$$

for $q = 1, 2$ and $i = 0, \dots, M - 3$.

For infinitely deep water, the procedure is generally the same, but only the pole $k = k_0$ of the water dispersion relation is used. We derive the following equation for the free-surface elevation

$$\zeta(\rho, \varphi) = A e^{i k_0 \rho \cos \varphi} - \pi i \sum_{m=1}^M (\mathcal{D} \kappa_m^4 - \mu) \frac{k_0^2}{(k_0^2 - \kappa_m^2)} \left[a_{mn}^{(1)} f_{mn0}^{(1)} + a_{mn}^{(2)} f_{mn0}^{(2)} \right], \quad (5.43)$$

where the functions $f_{mn0}^{(q)}$, $q = 1, 2$ are defined by formula (5.42) for $i = 0$, for the water regions \mathcal{F}_0 and \mathcal{F}_1 .

The expressions (5.41) and (5.43) are used for the total free-surface elevation for the FWD and IWD cases. We can subtract the incident field and use the second terms in the right-hand sides of these expressions, representing ζ^{pm} , to study the resulting wave pattern which is generated by the plate motion.

5.9 Numerical results

In this section, numerical results are given for the problem of interaction between the floating ring-shaped plate and surface water waves. Results are presented for relevant and practically important cases. For both the IWD and the FWD models, results are shown for the plate deflection w , free-surface elevation ζ and initiated wave pattern elevation ζ^{pm} , all normalized by the wave amplitude A . Calculations are based on the varied flexural rigidity D , while the plate radii r_1 and r_0 , Poisson's ratio $\nu = 0.25$ and ratio $m/\rho_w = 0.25 \text{ m}$ are constant. The wave amplitude is $A = 1 \text{ m}$, the water depth and incident wavelength are varied, leading to different values of the wavenumber k_0 and frequency ω . In all figures given, the values of the inner and outer radii are $r_1 = 100 \text{ m}$ and $r_0 = 500 \text{ m}$.

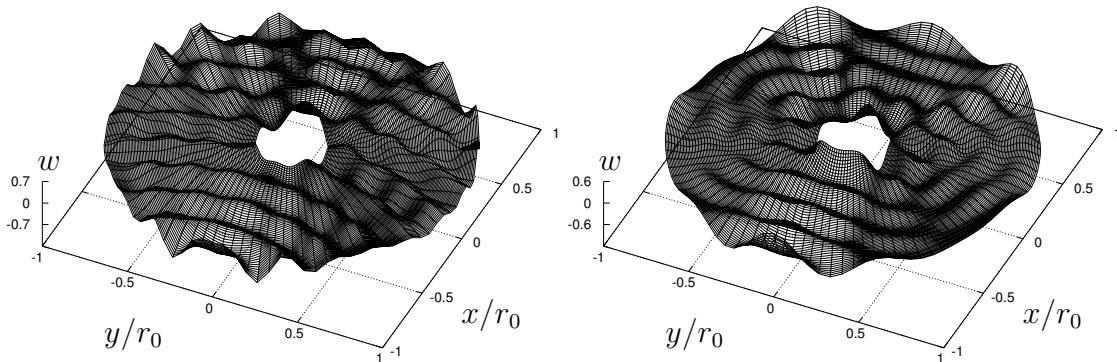


Figure 5.5: Deflection of the ring-shaped plate, for $\lambda = 50 \text{ m}$, $\mathcal{D} = 10^5 \text{ m}^4$: a) infinite depth, b) finite depth, $h = 20 \text{ m}$.

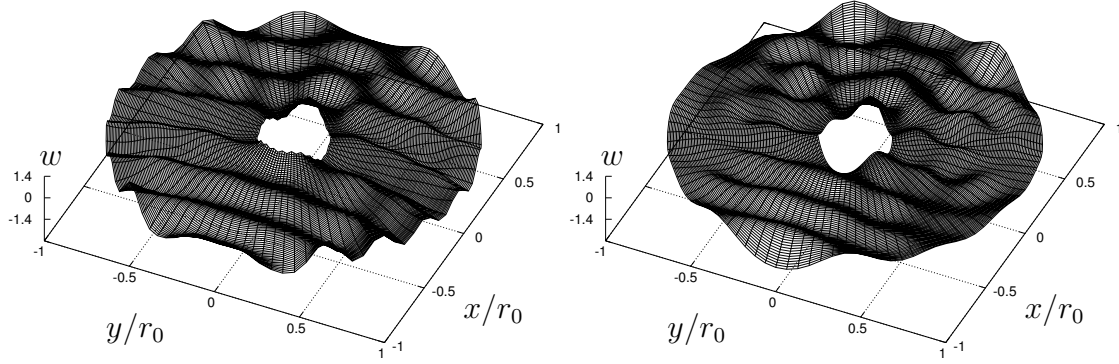


Figure 5.6: Plate deflection, as in figure 5.5, for $\lambda = 100$ m.

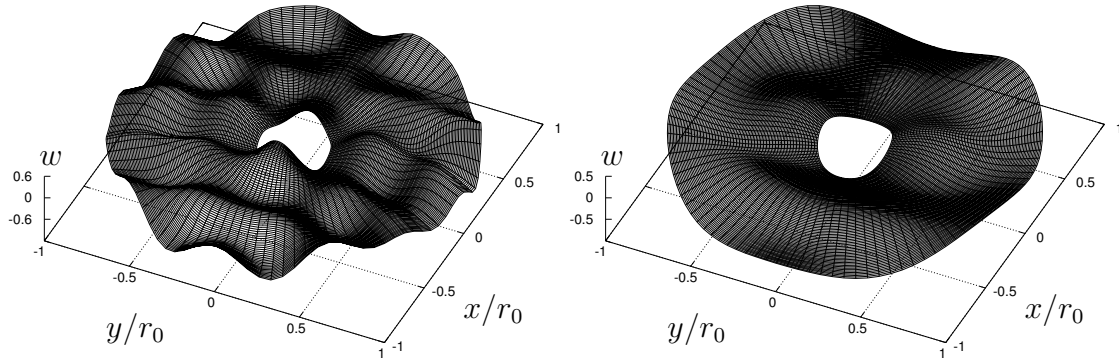


Figure 5.7: Plate deflection, for $\lambda = 100$ m, $h = 100$ m: a) $\mathcal{D} = 10^6 \text{ m}^4$, b) $\mathcal{D} = 10^7 \text{ m}^4$.

The number of roots of the plate dispersion relation taken into account for the FWD case is $M = 10$. The Bessel and Hankel functions of the complex argument must be computed accurately. Problems may appear when the argument is smaller than the order of the function and when the argument is too large or too small. Our algorithm is based on the Amos package [2], with some modifications to increase the accuracy, and computations were performed using the Fortran compiler. Scaled functions were used which remove the exponential behavior in both the upper and lower half-planes. The definitions and description may be found in [1]. For zero argument, table values of Bessel and Hankel functions were used.

We take $N = 30$ as the highest order of the modes of the Bessel functions; hence, Bessel and Hankel functions of order 0 to 30 are considered. The choice of the truncation parameters M and N was also validated by computational tests to ensure sufficient accuracy. More details related to the number of roots can be found in chapter 3 and in [4, 5] and details about the order of the Bessel functions, in chapter 4 and in [8].

The amplitude coefficients $a_{mn}^{(1)}$ and $a_{mn}^{(2)}$ decay rapidly because of the corresponding

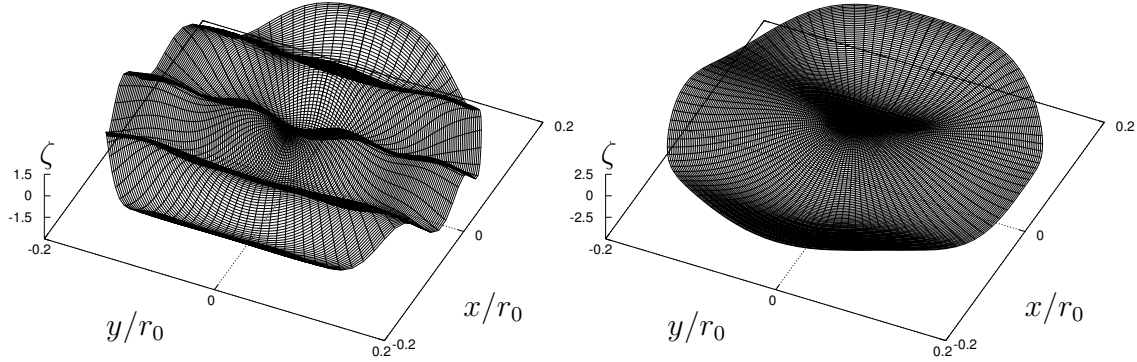


Figure 5.8: Free-surface elevation in the gap, for $h = 100$ m, $\mathcal{D} = 10^7$ m⁴: a) $\lambda = 50$ m, b) $\lambda = 100$ m.

Hankel functions. With the increase of the radii and, correspondingly, of the arguments of the functions or the flexural rigidity, the decay increases as well.

In all figures, the left subplot is denoted as (a), and the right as (b); if there are four subplots, then the lower left is denoted as (c) and lower right as (d). All figures are symmetric about the x -axis because incoming plane waves propagate in the x -direction and their crests are parallel to the y -axis.

In figures 5.5–5.6, numerical results are shown for the plate deflection for both water depths. The wavelength in the second figure is two times larger than in the first, while the plate parameters are constant. The plate deflection for larger values of rigidity is shown in figure 5.7.

Numerical results for the elevation of the free surface in the ring gap are given in figure 5.8 for different wavelengths. In figure 5.9 we show results for the initiated wave pattern, i.e., for the free-surface elevation ζ^{pm} generated by the motion of the plate, and the total free-surface elevation. The subplots for the open-water region \mathcal{F}_0 are given for the surface of the fluid domain of the radius r_f , for water of finite depth. In figures 5.10–5.11 we show a complete set of results for the unknown vertical elevations being studied in the chapter. Results are given for the plate deflection (a), free-surface elevation in \mathcal{F}_1 (b), initiated wave pattern (c) and the free-surface elevation in \mathcal{F}_0 (d) for the IWD and FWD cases, respectively.

The propagation of the wave through the plate area can clearly be seen, especially for small plate rigidity values. The wave propagates with a curved wave front, as can be clearly observed for cases where the wavelength is much smaller than the outer diameter of the ring. In a zone close to the plate edges, the deflection can differ quite a lot from that in the main zone of the plate.

The plate deflection and its hydroelastic response to the wave field are highly dependent on the ratio between outer radius r_0 and the wavelength λ . With decreasing water depth, the results for the plate deflection and free-surface elevation change gradually, where the water depth h itself has a growing influence on the results. For smaller plate

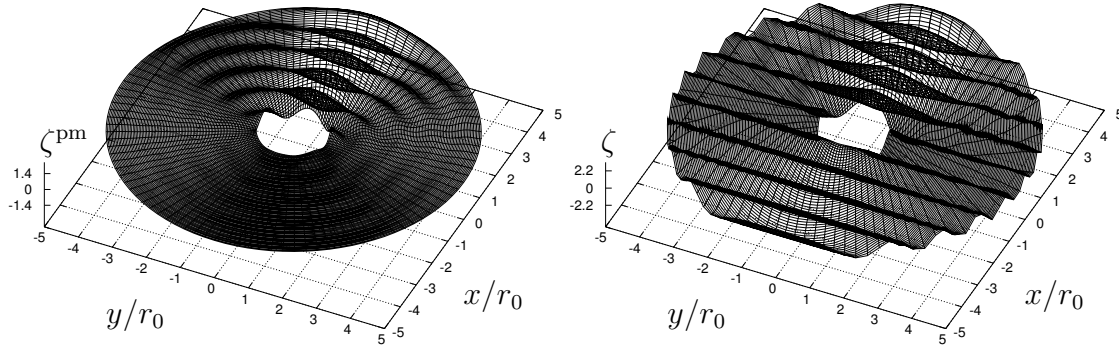


Figure 5.9: Initiated wave pattern (a) and free-surface elevation (b), for $\lambda = 500$ m, $h = 100$ m, $r_f = 2500$ m, $\mathcal{D} = 10^7$ m⁴.

rigidity or stiffness values the plate deflection increases, which is demonstrated in figures 5.5–5.7. If the wavelength decreases, then the value of the deflection grows. The plate deflection is also larger numerically when the water depth increases. Also, we found that computational results for large depths, $h > 100$ m, remained almost the same with a growth of the water depth. For this situation it is sufficient to take $M = 10$ as well.

As in previous chapters, we found that for a parameter $\mathcal{D} > 10^7$ m⁴ the plate behaves like a rigid body, having a significant influence on the surface waves, whereas for $\mathcal{D} < 10^3$ m⁴, the plate has hardly any influence on the incident surface waves. Realistic rigidity values for the floating structure can be of order of about 10^7 m⁴; here, many of the results shown for smaller values well demonstrate the nature of plate-water interaction effects; the rigidity of the ice is of an order of about 10^5 m⁴.

The influence of the ring gap on the results is also shown. The behavior of the propagated wave changes essentially after it has crossed the gap. The influence of the gap increases for smaller wavelengths, which can be expected.

The initiated wave pattern highly depends on the water depth and the physical properties of the plate. With growing values of the plate flexural rigidity, stiffness or Poisson's ratio, the influence of the plate's motion on the total elevation of the water surface grows as well.

5.10 Conclusions

The problem of interaction between a thin elastic floating plate of a ring-shaped planform and incident surface water waves has been solved. The hydroelastic behavior of the plate was studied analytically and numerically. The integro-differential equation of the problem was derived and an algorithm of its numerical solution proposed. For water of finite depth, we obtained a system of equations for the expansion coefficients analytically. For infinitely deep water, we partly solved the problem. Numerical results were presented for relevant

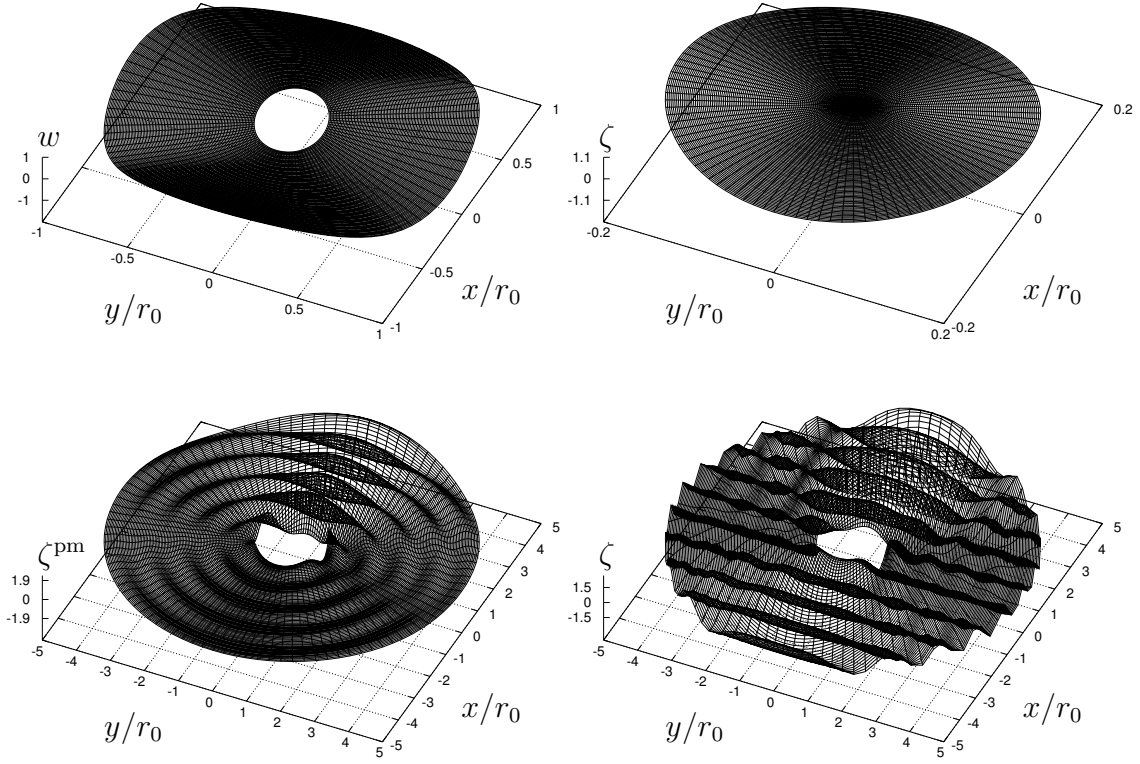


Figure 5.10: Deflection of the plate (a), free-surface elevation in \mathcal{F}_1 (b), initiated wave pattern (c) and free-surface elevation in \mathcal{F}_0 (d), for $\lambda = 500$ m, $h = 100$ m, $r_f = 2500$ m, $\mathcal{D} = 10^8$ m⁴.

cases.

The vertical displacements in the plate and water regions were studied, and we obtain the plate deflection and free-surface elevation caused by the waves' propagation and plate's motion, respectively. The influence of the plate motion on the solution in the water regions was analyzed by deriving the initiated wave pattern. Also, we analyzed the influence of the ring gap. For realistic values of the plate mass and rigidity, the behavior of a ring does not differ much from that of a circular plate, except for the area behind the ring gap. In the inner free surface area \mathcal{F}_1 , the resonant situation, that is, large free-surface elevation, is possible for some wavelength values, see figure 5.8, as was shown by Hermans [44] for a channel between two plates. This phenomenon is also demonstrated by Molin in his study of sloshing modes in a moonpool [82].

The solution for water of finite depth can be used to solve problems with shallow or very deep (infinite) water. The floating platform should be located in an offshore zone of the ocean or sea. The water depth is rather small in such zones, but as both short and long wavelengths can occur, it is more natural to use the finite-water-depth model to study the hydroelastic response of the plate to water waves.

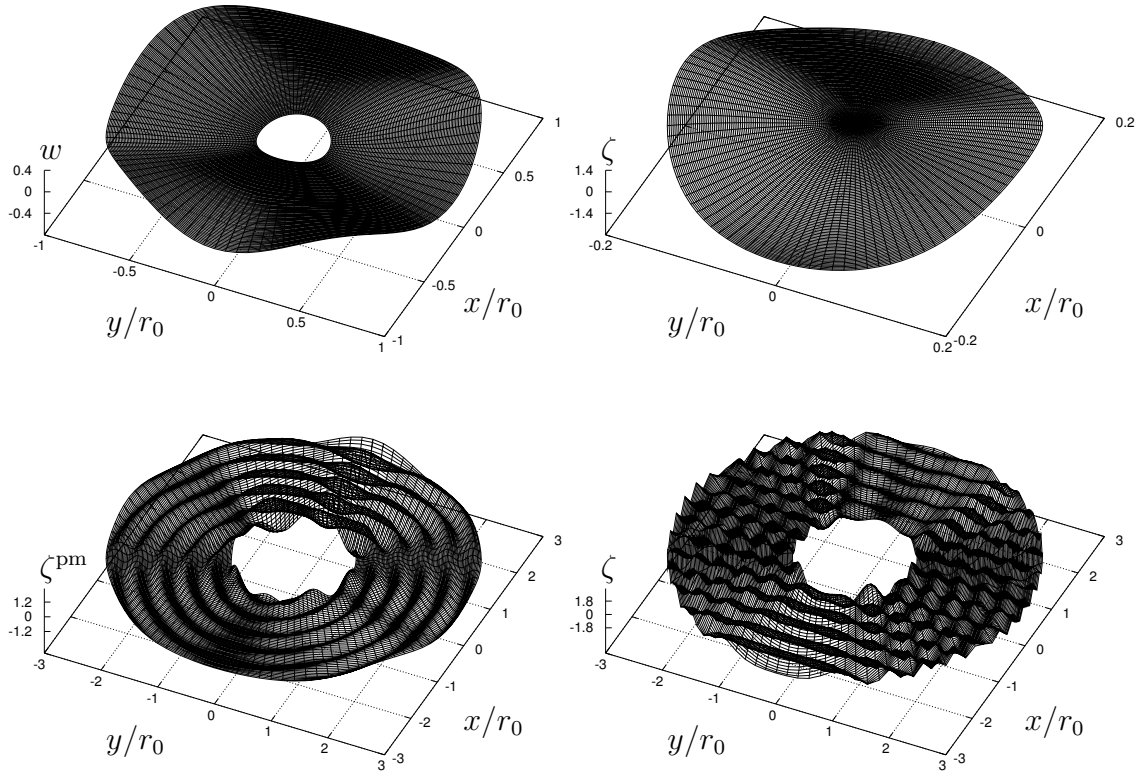


Figure 5.11: Deflection of the plate (a), free-surface elevation in \mathcal{F}_1 (b), initiated wave pattern (c) and free-surface elevation in \mathcal{F}_0 (d), for $\lambda = 200$ m, $r_f = 1500$ m, $\mathcal{D} = 10^8$ m⁴.

The solution presented above is a new application of the integro-differential formulation and integro-differential equation method. Using this formulation and method we solve all problems of the interaction between water waves and floating bodies treated in the thesis. The main goal of the method is a derivation of an integro-differential equation along the plate contour, followed by its analysis and solution. One of the advantages of our approach is that we may find both vertical displacements, the plate deflection in \mathcal{P} and the free-surface elevation in \mathcal{F} , using a common set of equations.

The presented approach is valid when the plate draft and thickness are assumed to be zero. A solution for a plate of non-zero thickness is derived in chapter 7.

A possible application of the method is the hydroelastic analysis of the VLFP. The planform of a VLFP depends on the water depth, the currents of the sea or ocean where the floating airport is to be located, the distance from the coast, etc. In some cases it can make sense to construct a VLFP with an arbitrary horizontal shape. The presented approach can also be used to study the motion of large ice fields in water waves, where the physical properties of the ice should replace those of the elastic plate. Mainly, results are obtained for large plates, $2r_0 > \lambda$, but the approach is also valid for small-sized floating plates $2r_0 < \lambda$, which may be used for different purposes in the sea.

Chapter 6

Hydroelasticity of a quarter-infinite plate

This chapter considers the interaction between surface water waves and a plate of quarter-infinite horizontal planform. It studies the hydroelastic motion of the plate and the diffraction of the incident waves by the plate. The problem is solved for the main case of finite water depth. The plate covers the first quadrant of the surface, while the waves are coming in from the second quadrant by our assumption. For the problem formulated, the asymptotic theory of the geometrical-optics approach and ray method are used. The propagation of the wave modes in the plate region is described sequentially. Solutions are obtained for different zones of the plate, supplemented by matching conditions derived along the interface between these zones. The wave propagation in the plate region is studied, as well as an inner reflection of the wave at the plate's far edge. Numerical results, conclusions, and recommendations for the method's extension are given, and a direction for analysis for other geometries of the problem is pointed out.

6.1 Introduction

In chapter 3, a solution was derived for two planforms of the plate: a semi-infinite plate and a strip of infinite length. Results were obtained for the deflection, reflection and transmission coefficients for three water depths: infinite, finite and shallow depth. The analysis applied and analytical and numerical results obtained were also published in papers [42, 43, 3, 5]. In this chapter, the theory is developed further for the case of a quarter-infinite plate. Some preliminary results were presented in [6]. As in the previous chapters, the platform draft is shallow and therefore the platform is assumed to be a thin plate laying at the free surface — the VLFP is modeled as an elastic plate with zero thickness. Here, we use all basic assumptions of chapters 2–5.

Hence, we study the diffraction of surface waves by a quarter-infinite plate (QIP). The plate floats on the surface of water of finite depth. Two situations may be considered separately: normal incidence and oblique incidence of the surface water waves. The case of normal incidence of the water waves on the quarter-infinite plate has been studied by Takagi [121] and Ohkusu and Namba [95], who used a parabolic approximation method with matching of the results in different zones of the plate. Therefore, we wish to obtain

the solution for the realistic case of oblique incident waves. However, the solution derived is also valid for the case of perpendicular waves. The plate covers the first quadrant of the free surface, which coincides with the horizontal zero-surface of our coordinate system. By our assumption, the surface waves are coming from the second quadrant.

The Green's theorem, the integro-differential formulation, the geometrical-optics approach and, further, the ray method are used to solve the problem. The information about the Green's function, the derivation of the integro-differential equation, and further steps of the analysis are presented in chapters 2–5. For information about the geometrical-optics (GOA) and ray approaches see, e.g., [72, 58, 67, 12]. Hermans [43] used the integro-differential formulation to derive boundary conditions to apply the ray method for short-wave diffraction. In a similar way, we use this formulation to apply the asymptotic theory of the GOA for the problem considered.

The problem is formulated in section 6.2. The solution consists of three parts, presented in sections 6.3–6.5. First, we apply the Green's theorem to obtain the integro-differential equation in the main zone of the plate. This part is presented in section 6.3, where we follow the analysis given in chapter 3 for SIP and use the GOA. The main wave mode involved is the traveling wave mode. In section 6.4, we study the propagation of this wave mode (ray Ansatz) and the additional deflection of the plate, generated by the vibration of the plate far edge, the so-called inner reflection (of the main traveling wave mode). We restrict ourselves to the inner reflection, in this case the method is well demonstrated. The inner reflection influences the plate area close to the edge. Next, using the ray method, we derive the matching conditions along the border between this zone and the main zone of the plate. This is presented in section 6.5. Adding up the deflection terms, which are obtained in sections 6.3–6.5, we derive the final result. Numerical results for the plate deflection and inner reflection are given in section 6.6, and concluding remarks in section 6.7. Using the approach derived, we also can solve the problem where the waves are coming from the third quadrant, see section 6.8. The method can also be extended to the case of a floating plate of finite dimensions.

6.2 Formulation of the problem

A flexible thin plate floats on the surface of an ideal incompressible fluid of constant depth h . The plate covers a quarter of the free surface, which coincides with the first quadrant, see figure 6.1; z is the positive upward coordinate. The plate area ($x > 0$, $y > 0$) is denoted as \mathcal{P} , and the open fluid area (second, third and fourth quadrants) as \mathcal{F} .

The plate deflection is generated by incoming surface waves of length λ and frequency ω . It is also assumed that incoming waves propagate in otherwise still water, from the second quadrant in the direction of the fourth quadrant. The wave amplitude A is rather small in comparison with other length parameters of the problem.

The velocity potential is introduced by $\nabla\Phi(x, y, z, t) = \mathbf{V}(x, y, z, t)$, where $\Phi(x, y, z, t)$ is a solution of the Laplace equation

$$\Delta\Phi = 0 \tag{6.1}$$

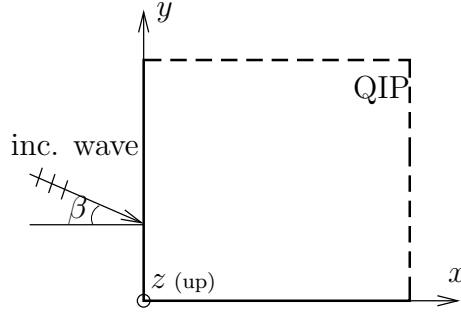


Figure 6.1: Geometry of the problem.

in the fluid $z < 0$, supplemented by the boundary conditions at the free surface $z = 0$

$$\frac{\partial \Phi}{\partial z} = \frac{\partial W}{\partial t}, \quad x, y \in \mathcal{P}, \quad (6.2)$$

$$\frac{\partial \Phi}{\partial z} = -\frac{1}{g} \frac{\partial^2 \Phi}{\partial t^2}, \quad x, y \in \mathcal{F}, \quad (6.3)$$

and at the bottom $z = -h$

$$\frac{\partial \Phi}{\partial z} = 0. \quad (6.4)$$

The dynamic condition, see p.24, has the following form at the free surface $z = 0$

$$\frac{P - P_{\text{atm}}}{\rho_w} = -\frac{\partial \Phi}{\partial t} - gw, \quad (6.5)$$

where $P(x, y, z, t)$ is the linearized pressure.

Incoming waves propagate from the open fluid in the direction which makes an angle β to the x -axis, shown in figure 6.1. The plate edges are defined by \mathcal{S}_y ($x = 0, 0 < y < \infty$) and by \mathcal{S}_x ($0 < x < \infty, y = 0$).

To describe the plate deflection W (vertical displacement of the plate), we apply the thin plate theory, p.26, which leads to the following differential equation

$$D \left(\frac{\partial^2}{\partial x^2} + \frac{\partial^2}{\partial y^2} \right)^2 W + m \frac{\partial^2 W}{\partial t^2} = P - P_{\text{atm}} \quad (6.6)$$

at $z = 0$ in the plate area \mathcal{P} . Applying the operator $\partial/\partial t$ to the equation of the plate motion (6.6) as in section 2.3 and using conditions (6.2) and (6.5), we arrive at the following equation for the potential Φ at the free surface $z = 0$

$$\left\{ \frac{D}{\rho_w g} \left(\frac{\partial^2}{\partial x^2} + \frac{\partial^2}{\partial y^2} \right)^2 + \frac{m}{\rho_w g} \frac{\partial^2}{\partial t^2} + 1 \right\} \frac{\partial \Phi}{\partial z} + \frac{1}{g} \frac{\partial^2 \Phi}{\partial t^2} = 0. \quad (6.7)$$

Due to the usual assumptions of an ideal fluid and small wave amplitude, the potential can be represented by (2.7). The harmonic motion is considered, and from (6.2) it follows

that the surface vertical elevation has the same harmonic behavior. Thus, according to (2.8), we consider waves of the single frequency ω and obtain the following differential equation for the potential $\phi(x, y, z)$ at $z = 0$

$$\left\{ \mathcal{D} \left(\frac{\partial^2}{\partial x^2} + \frac{\partial^2}{\partial y^2} \right)^2 - \mu + 1 \right\} \frac{\partial \phi}{\partial z} - K \phi = 0, \quad (6.8)$$

where we have introduced the parameters $\mathcal{D} = D/\rho_w g$, $\mu = m\omega^2/\rho_w g$, and $K = \omega^2/g$.

The potential of the incident waves for finite water depth is written for our problem as

$$\phi^{\text{inc}} = \frac{\cosh k_0(z+h)}{\cosh k_0 h} \frac{gA}{i\omega} e^{ik_0(x \cos \beta - y \sin \beta)}, \quad (6.9)$$

where A is the wave height; the wavenumber k_0 is the only real solution of the water dispersion relation

$$k \tanh kh = K. \quad (6.10)$$

The wavelength of incoming waves is $\lambda = 2\pi/k_0$.

The edges of the plate are free of vertical shear forces, bending and twisting moments. Therefore, the free-edge conditions for the plate deflection $w(x, y)$ at \mathcal{S}_y ($x = 0$) are:

$$\frac{\partial^2 w}{\partial x^2} + \nu \frac{\partial^2 w}{\partial y^2} = 0; \quad \frac{\partial^3 w}{\partial x^3} + (2 - \nu) \frac{\partial^3 w}{\partial x \partial y^2} = 0, \quad (6.11)$$

and at \mathcal{S}_x ($y = 0$), they are:

$$\frac{\partial^2 w}{\partial y^2} + \nu \frac{\partial^2 w}{\partial x^2} = 0; \quad \frac{\partial^3 w}{\partial y^3} + (2 - \nu) \frac{\partial^3 w}{\partial y \partial x^2} = 0. \quad (6.12)$$

6.3 Solution in the main zone

Here we derive the main part of the deflection of the quarter-infinite plate, which later will be added to additional terms. We follow the analysis presented in chapter 3 for the semi-infinite plate for the case of finite depth. Applying the integro-differential formulation, we derive the main integro-differential equation for the problem.

We consider the case where the incident waves are coming in from the second quadrant $x < 0, y > 0$, as shown in figure 6.1, with the angle of incidence β which is smaller than the critical angle of incidence $0 < \beta < \beta_{\text{cr}} < \pi/2$. As the localized effect of the corner point $(0, 0)$ is not considered, we can use the asymptotic theory of the geometrical-optics approach for an incident field of this geometry.

The deflection of the quarter-infinite plate due to the propagation of the waves is represented as a superposition of exponential functions in the following form:

$$w_1(x, y) = \sum_{n=1}^N a_n e^{i\kappa_n x - i k_0 y \sin \beta}, \quad (6.13)$$

where a_n are the amplitudes of wave modes, and κ_n are the reduced wavenumbers. Due to the convergence of the series in (6.13), a finite number can be taken as the upper limit of the series, like in the previous chapters. The value of the limit, the number of wave modes taken into account, is discussed later. The minus signs are in the exponential functions in (6.9) and (6.13) because the waves propagate from the second to the fourth quadrant by our assumption. The function w_1 is the largest part (numerically) of the total deflection corresponding to the situation where rays already cross the edge \mathcal{S}_y , but do not yet reach the edge \mathcal{S}_x . Henceforward we call the function w_1 the deflection in the main zone of the plate (or the main part of the deflection). The deflection form (6.13) for a QIP coincides with the deflection form (3.38) for a SIP. The form for the plate deflection in the case of perpendicular incoming waves can be derived from (6.13) if the y -term is neglected.

The reduced wavenumbers κ_n are defined in the following way as in chapter 3

$$\kappa_n^2 = \kappa^{(n)2} - k_0^2 \sin^2 \beta, \quad (6.14)$$

where $\kappa^{(n)}$ are the roots of the dispersion relation in the plate area

$$(\mathcal{D}\kappa^4 - \mu + 1) \kappa \tanh \kappa h = K. \quad (6.15)$$

We take into account N roots $\kappa^{(n)}$, $n = 1, \dots, N$ of the dispersion relation (6.15): one real root, two complex roots, and $N - 3$ imaginary roots. The real root $\kappa^{(1)}$ represents the traveling wave mode, and the imaginary roots $\kappa^{(2)}$ and $\kappa^{(3)}$ represent damped wave modes. So, we need to find $N + 2$ unknown amplitudes a_n . To obtain a set of equations for the amplitudes, we apply the integro-differential formulation and Green's theorem.

As in chapters 2–3, we split up the fluid domain in the plate region \mathcal{P} and the open-water region \mathcal{F} . We introduce the Green's function, p.32, and apply the Green's theorem to the potential in \mathcal{P} and \mathcal{F} . Following the method presented for the SIP, we obtain the following integro-differential equation for the deflection of the quarter-infinite plate:

$$\begin{aligned} & \left(\mathcal{D} \left(\frac{\partial^2}{\partial x^2} + \frac{\partial^2}{\partial y^2} \right)^2 - \mu + 1 \right) w_1(x, y) \\ &= \frac{K}{4\pi} \int_{\mathcal{P}} \left(\mathcal{D} \left(\frac{\partial^2}{\partial \xi^2} + \frac{\partial^2}{\partial \eta^2} \right)^2 - \mu \right) w_1(\xi, \eta) \mathcal{G}(x, y; \xi, \eta) d\xi d\eta + A e^{ik_0(x \cos \beta - y \sin \beta)}. \end{aligned} \quad (6.16)$$

The complete derivation of the IDE (6.16) is described in section 2.7. The Green's function has the following form, see section 2.5, at $z = \zeta = 0$

$$\mathcal{G}(x, y; \xi, \eta) = -2 \int_{\mathcal{L}'} \frac{k \cosh kh}{k \sinh kh - K \cosh kh} J_0(kR) dk, \quad (6.17)$$

where $J_0(kR)$ is the Bessel function and $R^2 = (x - \xi)^2 + (y - \eta)^2$. The contour \mathcal{L}' of an integration in the complex k -plane from 0 to $+\infty$ underneath the singularity $k = k_0$ is chosen to fulfill the radiation condition; it is shown in figure 6.2.

The deflection (6.13) and the Green's (6.17) functions are inserted into the IDE (6.16). Next, we do operations on the complex integration. The application of the residue lemma

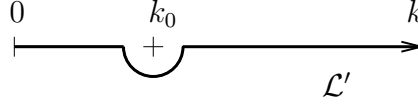


Figure 6.2: Contour of integration.

at the zeros of the water dispersion relation (6.10) results in equations to determine the amplitudes a_n . The contribution of the pole $k = k_0$ gives us

$$\sum_{n=1}^N a_n \mathcal{K}_0 \frac{(\mathcal{D}\kappa^{(n)4} - \mu)}{(\kappa_n - k_0 \cos \beta) \cos \beta} + A = 0, \quad (6.18)$$

and that of the pole $k = k_i$ for $i = 1, \dots, N - 3$

$$\sum_{n=1}^N a_n \mathcal{K}_i \frac{k_i}{k_i^*} \frac{(\mathcal{D}\kappa^{(n)4} - \mu)}{(\kappa_n - k_i^*)} = 0, \quad (6.19)$$

where

$$\mathcal{K}_i = \frac{k_i K}{K(1 - Kh) + k_i^2 h} \quad (6.20)$$

for $i = 0, \dots, N - 3$ and $k_i^* = \sqrt{k_i^2 - k_0^2 \sin^2 \beta}$. To complete the system of $N + 2$ equations, we obtain two equations from the free edge conditions (6.11), and they are written in the form (3.39–3.40). In such a way, the amplitudes a_n and the function w_1 can be determined.

6.4 Inner reflection

Next, we study the propagation of the traveling wave mode, or the main ray Ansatz. Because the reflection of the traveling wave mode has the amplitude a_1 on the edge \mathcal{S}_x with an angle θ , described in [12] and shown in figure 6.3, the QIP gets an additional deflection w_2 generated by the vibration of the plate edge \mathcal{S}_x .

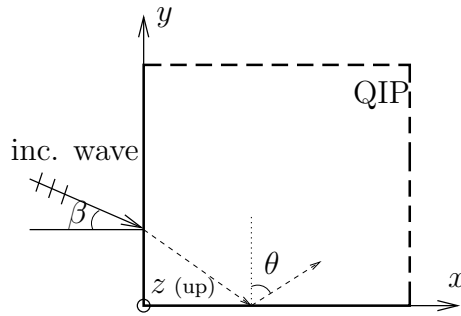


Figure 6.3: Reflection of traveling wave mode (Ansatz ray).

The reflected part of the deflection w_2 occurs in the region $x/\tan \theta > y$, which is denoted by \mathcal{P}_2 . The region $x < y \tan \theta$ is denoted by \mathcal{P}_1 ; the border between these zones is $x = y \tan \theta$. The angle of the ray reflection θ can be obtained from

$$\tan \theta = k_0/\kappa_1. \quad (6.21)$$

We represent the deflection function w_2 in the following way:

$$w_2(x, y) = \sum_{n=1}^N a_n^* e^{i\kappa_n^* y + i\kappa_1 x}, \quad (6.22)$$

where a_n^* are the amplitudes of the inner reflection at the edge \mathcal{S}_x and the corresponding wavenumbers are

$$\kappa_n^{*2} = \kappa^{(n)2} - \kappa_1^2. \quad (6.23)$$

In that way, $\kappa_1^* = -k_0 \sin \beta$, and the largest term of the reflected traveling wave is $a_1^* e^{-ik_0 y \sin \beta + i\kappa_1 x}$. In the mathematical plan, a_n^* are the solutions of a set of equations dependent on $a_1(\kappa_1)$. The equations of this set can be derived analogously those for the amplitudes a_n of the deflection in the main zone of the plate.

An integro-differential formulation leads to the following equations for the amplitudes a_n^* :

$$\sum_{n=1}^N a_n^* \mathcal{K}_0 \frac{(\mathcal{D}\kappa^{(n)4} - \mu)}{(\kappa_n - k_0 \cos \theta) \cos \theta} + a_1(\kappa_1) = 0 \quad (6.24)$$

as the contribution of the pole $k = k_0$, and

$$\sum_{n=1}^N a_n^* \mathcal{K}_i \frac{k_i}{k_i^*} \frac{(\mathcal{D}\kappa^{(n)4} - \mu)}{(\kappa_n - k_i^*)} = 0 \quad (6.25)$$

as the contribution of the pole $k = k_i$, $i = 1, \dots, N-3$; here, $k_i^* = \sqrt{k_i^2 - k_0^2 \sin^2 \theta}$. The set of $N + 2$ equations is completed by two equations derived from the free edge conditions (6.12). Then the amplitudes a_n^* and the function w_2 can be determined.

Hence, the deflection of the QIP can be represented as the sum

$$w(x, y) = w_1(x, y) + w_2(x, y), \quad (6.26)$$

where the functions $w_1(x, y)$ and $w_2(x, y)$ are already known. We have the following results for the total deflection $w(x, y)$ in the plate zones: $w = w_1$ in \mathcal{P}_1 and $w = w_1 + w_2$ in \mathcal{P}_2 . These results are intermediate. In the next section, the approach will be improved by the derivation of special matching conditions along the border between the zones \mathcal{P}_1 and \mathcal{P}_2 . Furthermore, we will derive a new deflection function to be used instead of w_2 .

6.5 Matching conditions

Here, we derive the matching conditions along the border $x = y \tan \theta$ which splits the plate area into two zones, \mathcal{P}_1 and \mathcal{P}_2 . By deriving and using these conditions, we find a new deflection function, which exists in both zones and will be used instead of the function w_2 . Then the solution for the whole plate area will be completed, which is described in this section. Here, we use the straightforward ray method, solving the problem for the potential.

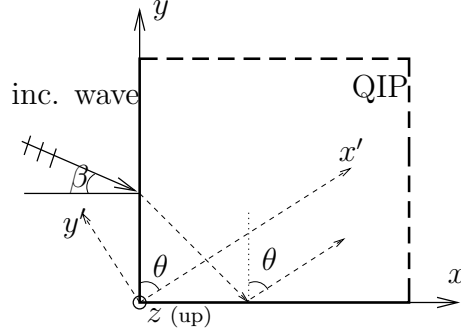


Figure 6.4: Geometry of current analysis, ray method and matching conditions.

The total potential $\Phi(\mathbf{x}, t)$, the solution of the Laplace equation (6.1), is rewritten in the form (2.7), and the potential of undisturbed incident wave ϕ^{inc} is given by (6.9).

Let us consider the new system of coordinates, $0x'y'$, which is derived by the rotation on angle $\pi/2 - \theta$ from the old system of coordinates $0xy$; the x' -axis is the border between the zones \mathcal{P}_1 and \mathcal{P}_2 . The direction of the x' -axis coincides with the direction of propagation of the ray Ansatz after the reflection at the edge $y = 0$.

We assume that the potential $\phi(x', y', z)$ can be written as a superposition of ray-mode solutions

$$\phi(x', y', z) = \sum_{n=1}^N \varphi_n(x', y') e^{i\kappa x' + \kappa z}, \quad (6.27)$$

where $\varphi_n(x')$ is the amplitude function of the n -th mode. Then, the deflection $w_s(x', y')$ is represented by

$$w_s(x', y') = \frac{i}{\omega} \phi_z(x', y'). \quad (6.28)$$

The dispersion relation is written in the form (6.15).

Our approximation is valid in the whole area of the plate. Relations (6.27) and (6.8) are used for further manipulations. Inserting the expression (6.27) into the Laplace equation (6.1), we obtain

$$\Delta\varphi + 2\kappa(i\varphi_{x'} + \varphi_z) + \mathcal{O}(K^0) = 0. \quad (6.29)$$

We stretch the coordinates by $Y = K^{1/2}y'$, $\kappa = Kr$, where K is the large parameter, r is the solution of the plate dispersion relation, $r = \mathcal{O}(1)$. Next, the z -derivative can be expressed via x' - and YY -derivatives in the following form

$$\varphi_z = -i\varphi_{x'} - \frac{\varphi_{YY}}{2r}, \quad (6.30)$$

and then eliminated from the equations.

We consider large values of K and expand the potential in power series of K . The first two equations then become

$$\mathcal{O}(K^0): \quad (\mathcal{D}r^4 - \mu + 1) \left(-i\varphi_{x'} - \frac{\varphi_{YY}}{2r} \right) + \mathcal{D}(-2r^3\varphi_{YY} - 4ir^4\varphi_{x'}) = 0, \quad (6.31)$$

and

$$\mathcal{O}(K^1) : \quad (\mathcal{D}r^4 - \mu + 1)r = 1. \quad (6.32)$$

Equation (6.32) is the dispersion relation of the problem. The elastic coefficients \mathcal{D} and μ are constant, and therefore r is constant too and the rays are straight lines. Next, the partial differential equation

$$2ir\varphi_{x'} + \varphi_{YY} = 0 \quad (6.33)$$

has to be considered. Two terms in (6.33) are equal in order of magnitude when $x' = \mathcal{O}(1)$ and $Y = \mathcal{O}(1)$, then $y' = \mathcal{O}(K^{-1/2})$. This in fact defines the area of validity of the parabolic approximation.

Use of Laplace transform

$$\psi(s, Y) = \int_0^\infty \varphi(x', Y) e^{-sx'} dx'$$

leads to the equation

$$2irs\psi + \psi_{YY} = 2ir\varphi(0, Y), \quad (6.34)$$

and the following initial conditions are required, see Mei and Tuck [76], changing with the change of the Y -sign,

$$\varphi(0, Y) = A_s, \quad Y < 0, \quad (6.35)$$

$$\varphi(0, Y) = 0, \quad Y > 0. \quad (6.36)$$

A value of the constant A_s can be obtained from the second part of our solution, using the results for the function w_2 .

From the general solution of (6.34), we obtain the following equations

$$\psi^-(s, Y) = \alpha_1(s) e^{\sqrt{2irs}Y} + \frac{A_s}{s}, \quad Y < 0, \quad (6.37)$$

$$\psi^+(s, Y) = \beta_2(s) e^{-\sqrt{2irs}Y}, \quad Y > 0, \quad (6.38)$$

with the following notation of the amplitude functions and their transforms: φ^- and ψ^- in the region $Y < 0$, and φ^+ and ψ^+ in the region $Y > 0$. The constants can be determined by use of the matching (transition) conditions (6.37–6.38), they are: $\alpha_1 = -\beta_2 = -A_s/2s$. Applying Laplace inverse transform and using the transition conditions

$$\varphi^+ = \varphi^-, \quad \varphi_Y^+ = \varphi_Y^- \quad (6.39)$$

at $Y = 0$, we derive the following results for the amplitude functions, according to [20],

$$\varphi^-(x', Y) = -\frac{A_s}{\sqrt{\pi}} \left(\int_0^\infty e^{-\lambda^2} d\lambda - \int_0^{-q} e^{-\lambda^2} d\lambda \right) + A_s, \quad (6.40)$$

$$\varphi^+(x', Y) = \frac{A_s}{\sqrt{\pi}} \left(\int_0^\infty e^{-\lambda^2} d\lambda - \int_0^q e^{-\lambda^2} d\lambda \right), \quad (6.41)$$

where the upper limit of the second integral is given by

$$q = \frac{Y\sqrt{ir}}{\sqrt{2x'}}. \quad (6.42)$$

Each of the integrals multiplied by coefficients in (6.40–6.41) is an error function $\operatorname{erf} q$ (the upper limit of integration is its argument); the error function with argument ∞ equals 1.

Calculating the integrals in (6.40–6.41), we may obtain the value of the potential in the plate area and, correspondingly, the value of the deflection w_s . The analysis presented in this section is valid in the whole area of the plate, so like the function $w_s(x', y')$ exists in the whole plate area.

Finally, the total deflection of the quarter-infinite plate is written in the original coordinates (x, y) as the following sum

$$w(x, y) = w_1(x, y) + w_s(x, y) \quad (6.43)$$

for the whole plate area, where the first term is the main part of the solution and the second part represents the solution along the rays by stretching the coordinates. The function w_1 can be computed by formula (6.13) and the function w_s by formula (6.28).

6.6 Numerical results

In this section we show the numerical results for the deflection of the quarter-infinite plate and the inner reflection on the far edge of the plate.

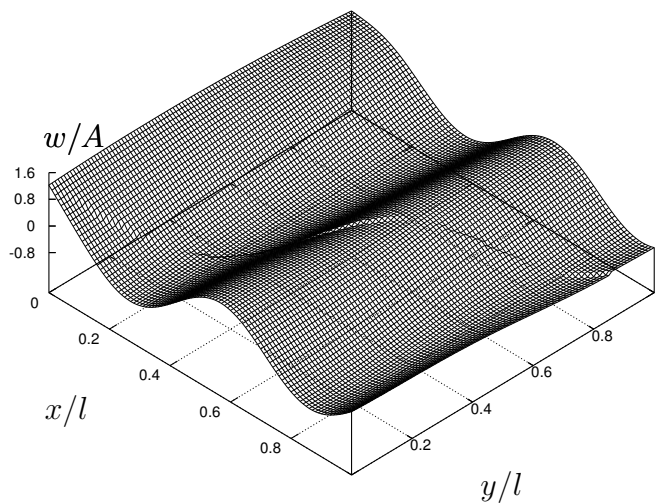


Figure 6.5: Deflection of the QIP, for $\lambda = 0.5l$, $\beta = 5^\circ$, then $\theta \approx 49.9^\circ$.

In figures 6.5–6.7, results are presented for the total plate deflection w , normalized by the wave amplitude $A = 1$ m. The results are shown for different angles of incidence and

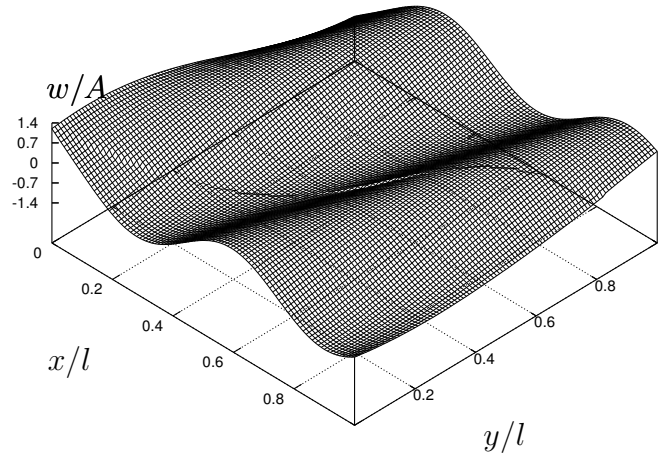


Figure 6.6: Deflection of the QIP, for $\lambda = 0.5l$, $\beta = 15^\circ$, then $\theta \approx 50.5^\circ$.

wavelengths. Calculations are based on the constant flexural rigidity $\mathcal{D} = 10^5 \text{ m}^4$, water depth $h = 100 \text{ m}$, Poisson's ratio $\nu = 0.3$, and ratio $m/\rho_w = 0.25 \text{ m}$. The number of roots of the dispersion relation (6.15) taken into account is $N = 15$. The length and width of part of the plate shown in the figures equal to $l = 300 \text{ m}$.

The difference of the deflection in the main zone \mathcal{P}_1 and in the zone \mathcal{P}_2 can be seen in the figures. The values of the reflection angle θ are presented for corresponding situations. Solutions in the zones \mathcal{P}_1 and \mathcal{P}_2 match each other well, as shown in figures 6.5–6.7, so there is a smooth transition between these zones along the border.

Numerical results for the inner reflection are given in figure 6.8. As was expected, the value of w_s is quite small compared to the main deflection w_1 . For rather long waves we can neglect the contribution of inner reflection w_s in the total deflection (6.43), but for short waves this term has to be taken into account.

6.7 Conclusions

An analytical study has been presented for the problem of interaction between an elastic floating plate of quarter-infinite planform and water waves. The solution consists of three parts. The first part is the solution in the main zone of the plate. It is based on the approach given in chapter 3 and papers [43, 5] for a semi-infinite plate. The integro-differential equation, geometrical-optics approach, Green's function, thin-plate theory, boundary (free surface and bottom) and plate free-edge conditions are used for the solution.

We have taken into account a finite number of roots of the plate dispersion relation, which represent one traveling wave mode and several damped wave modes. We were especially interested in the propagation of the traveling mode — the main ray (ray Ansatz) of the solution. Its reflection (inner reflection) on the plate far edge results in additional plate deflection. Special matching conditions were derived along the border which split up the plate area into zones where inner reflection does exist and where it does not, i.e.,

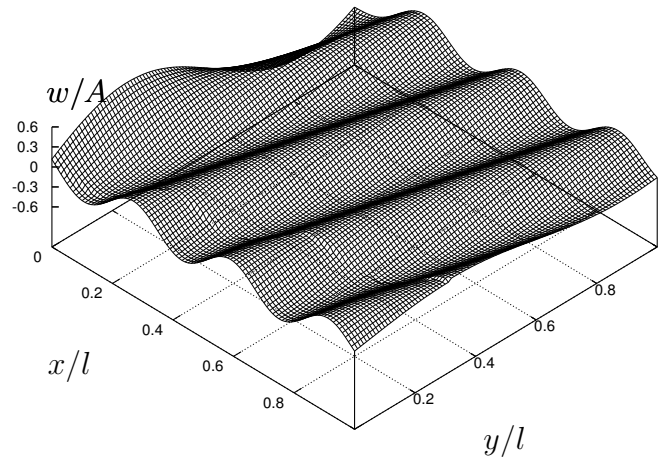


Figure 6.7: Deflection of the QIP, for $\lambda = 0.1l$, $\beta = 5^\circ$, then $\theta \approx 72.3^\circ$.

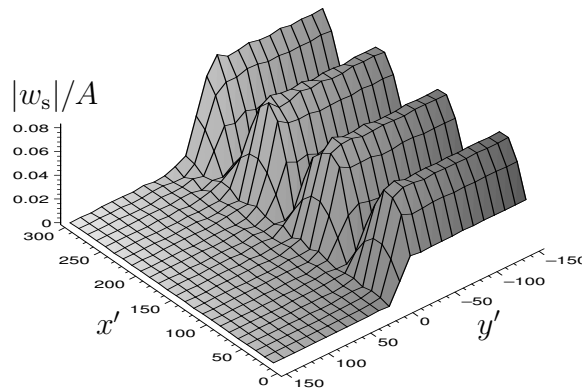


Figure 6.8: Absolute value of inner reflection w_s , for $\lambda = 0.5l$.

in the main zone and the zone close to the plate edge.

First, the deflection was represented as a sum of the main deflection w_1 and the product of inner reflection w_2 . Using the ray method, stretching the coordinates, and using derived matching and initial conditions, we obtained the deflection function w_s existing in the whole plate area to substitute w_2 . Numerical results for the plate deflection and inner reflection were presented. Solutions in two zones match each other well.

The approach presented can also be used to study the free-surface elevation, reflection and transmission of incident waves. The case of perpendicular incident waves has been studied by Takagi [121] and Ohkusu and Namba [95]; in the latter paper the problem was solved for shallow water. The influence of the waves traveling along the edge $y = 0$ has to be studied for this case. For shallow water, the problem can be solved using transition conditions for the potential, as was demonstrated in chapter 3. The effect of the corner point was ignored in the analysis presented. Hence, it may also be interesting to study its effect on the results.

6.8 Extensions

The analytical study presented in this chapter may be developed further. We can extend the presented approach to the case of incident waves propagating from the third quadrant as shown in figure 6.9, i.e. from $(-\infty, -\infty)$.

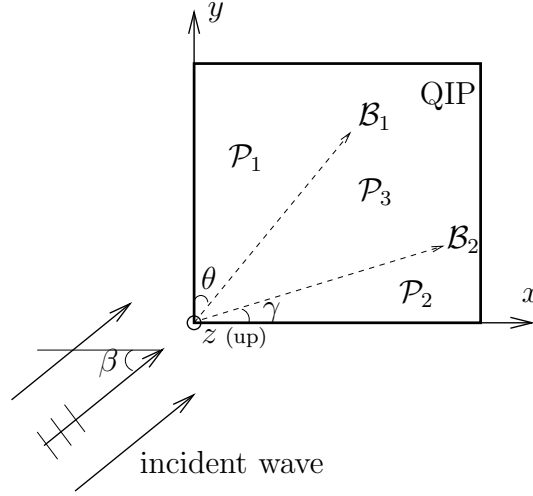


Figure 6.9: QIP and waves coming from third quadrant.

The technique used for the situation where waves are coming from the second quadrant is extended to this situation in the following way. First, the main deflection of the plate is determined. Then we can find the additional deflections in the zones \mathcal{P}_1 and \mathcal{P}_2 . Using these results and the matching conditions derived along the borders \mathcal{B}_1 and \mathcal{B}_2 , we can determine the influence of the inner reflection products in the zones \mathcal{P}_1 and \mathcal{P}_2 , respectively, on the 'shadow' region \mathcal{P}_3 . Also, Bessel or Hankel functions can be used to study the wave propagation in the shadow region \mathcal{P}_3 .

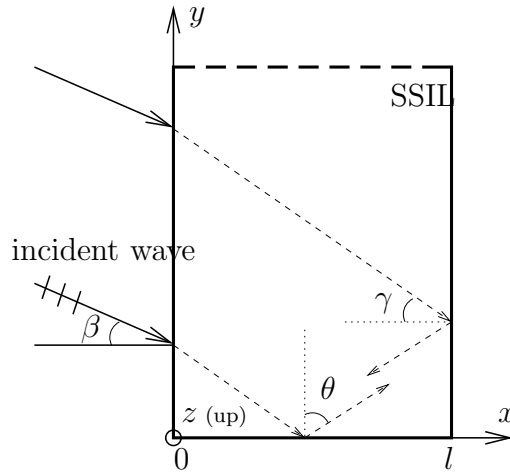


Figure 6.10: Waves incident on a strip of semi-infinite length.

The analysis presented can also be extended to two other planforms of the elastic floating plate which is a model of the VLFS: a strip of semi-infinite length and a plate

of finite dimensions. The latter is the realistic case. These problems can be solved with our approach: first, we derive the main result in the whole plate area; next, we study the inner reflection of the wave modes on the plate edges. Further, we can derive the matching conditions as has been shown in this chapter. To increase the accuracy of the results, one can also study a 'second inner reflection' — the reflection of the reflected traveling wave mode on the next edge of the plate, etc.

The geometry of the problem for a strip of semi-infinite length (SSIL) is shown in figure 6.10. In this case we have to study the reflection of the traveling wave mode (ray Ansatz) on two edges: $y = 0$, $0 < x < l$ and $x = l$, $0 < y < \infty$, which are shown in figure 6.10. The deflection of the SSIL can be written in the following form

$$w(x, y) = w_1(x, y) + w_2(x, y) + w_3(x, y),$$

where w_1 and w_2 are the same as in the QIP case and w_3 is the additional deflection appearing due to the reflection of the traveling mode on the edge $x = l$. The relation between the inner reflection angles is $\gamma = \pi/2 - \theta$, and the angle γ is defined by $\tan \gamma = \kappa_1/k_0$.

To increase the accuracy of the approach, we can consider two more terms, such as: the traveling wave mode reflected on $x = l$, which was previously reflected on the edge $y = 0$, and the traveling wave mode previously reflected on the edge $x = l$. Results for these terms can be obtained with the amplitude a_1^* .

In the case of a plate of finite dimensions, the plate occupies the finite element of the free surface. Let us assume that the waves propagate from the third quadrant in the direction of the first quadrant, where the plate covers the region $0 \leq x \leq l$, $0 \leq y \leq b$. We can consider separately the main ray crossing the edge $x = 0$, $0 < y < b$ and that crossing the edge $y = 0$, $0 < x < l$, which are reflected on three other edges of the plate. Further, we may also study the second inner reflection of the traveling wave mode.

Chapter 7

Hydroelastic behavior of a plate of finite draft

In this chapter the diffraction of incident surface water waves by a very large floating platform of finite thickness and draft is under consideration. The platform of finite, but small, draft is modeled by a thin elastic isotropic plate. An analytical and numerical study of the hydroelastic behavior of the plate is presented. The problem is solved for the main case of finite water depth. To simplify the equations involved, the half-plane problem is considered. Recommendations are given for other horizontal planforms of the plate and possible extensions of the method developed. Although here the half-plane problem is considered, the approach may be extended to plates of other horizontal planforms. The deflection of the plate is represented as a series of solutions with respect to the plate draft; we present and use first and second terms. Each of these terms can be written as a series of exponential functions. The integro-differential formulation and equation obtained, the dispersion relations in the plate region and open water, the Green's theorem, geometrical-optics approach and Lindstedt (PLK) method are used to determine reduced wavenumbers of zero and first draft order. Further, sets of equations are derived to find the corresponding wave-mode amplitudes. Results obtained for the plate of finite draft are compared to those for a plate with zero thickness.

7.1 Introduction

Fluid-structure interaction is an important subject of hydrodynamics. The subject is widely studied and many papers devoted to it have been published in recent years. A very detailed literature survey of hydroelastic analysis of VLFS has been published by Watanabe et al. [143]. Our general survey is given in chapter 1. A number of different approaches has been developed for the problem of interaction between VLFS and surface water waves. The VLFS is modeled by a thin elastic plate; generally, the plate is assumed to have zero thickness, e.g. [5, 41, 91, 115, 126]. In chapters 3–6, too, the solutions for different horizontal planforms of the floating plate were derived using the zero-thickness assumption. Horizontal force on a plate of small draft was studied in [94].

In contrast to previous chapters, here, our technique is extended to a plate having nonzero (constant) draft, which is a realistic problem of the highest interest. Hence,

in this section we derive the solution for a plate of finite draft (PFD) based on our integro-differential formulation, IDE and the solution derived for the zero-thickness case using the geometrical-optics approach, and the Lindstedt method. The details on the integro-differential formulation are given in chapter 2; the derivation of IDE for particular problems and its solution are presented in chapters 3–6. The Lindstedt or PLK (Poincaré-Lighthill-Kuo) method is described in [53]. Our ideas and preliminary results for the problem were presented in [10].

The key idea of our approach is the representation of the plate deflection (vertical displacement in the plate region) as a sum of the zero-thickness result obtained in section 3.4, a zero draft order solution, and a correction term, a first draft order solution. Having nonzero thickness, the plate has two wetted surfaces: a horizontal (bottom) and vertical (side) one, the latter was not considered in the previous sections.

After the introduction, we formulate the problem in the second section. The problem is treated in the frequency domain. In the third section, we point the direction of an analysis and describe the form of deflection chosen. The amplitudes and reduced wavenumbers, which are related to the roots of the dispersion relations in the plate region and open-water region, may be represented as a power series with respect to the plate draft. As in the previous chapters, we apply the Green's theorem for the velocity potential in both the plate and open-water regions. The Green's function is introduced for the finite water depth case. Next, we derive an integral equation for the potential and an integro-differential equation for the plate deflection. As will be noticed, the left-hand side of the IDE derived coincides with one derived with the zero-thickness assumption, while the right-hand side includes terms of zero and first draft order.

The next step of the analysis for the problem studied is the use of expanded forms for the amplitudes and reduced wavenumbers. Then, the terms of zero draft order are identified and studied separately. In the fourth section we derive the solution for the zero draft order problem, following the approach derived for the semi-infinite plate in chapter 3. Using the set of equations derived, we determine the amplitudes and deflection of zero draft order. In the fifth section we consider the equation of first draft order extracted from the governing IDE. It is expected and will be justified that the reduced wavenumbers of first draft order can be expressed via the wavenumbers of zero draft order, which are the roots of the dispersion relation in the plate region. Knowing the amplitudes and wavenumbers used in this step, we can derive a set of equations to determine the amplitudes of the first-draft-order deflection. This completes our analytical study.

The sixth section gives numerical results for different values of the plate draft and wavelength. In addition it compares the numerical results for the total deflection, the solution obtained with the zero-thickness assumption and the deflection functions of zero and first draft order. In the seventh section, possible extensions of the method are demonstrated, and the direction of an analysis is pointed. Concluding remarks are given in the eighth section.

7.2 Formulation

A plate of finite small draft, semi-infinite in horizontal planform, covers part of the water surface. Water is assumed to be an ideal incompressible fluid of finite and constant depth.

The plate deflection is generated by incoming surface waves propagating in the positive x -direction. The geometry of the problem and the coordinate system chosen are shown in figure 7.1.

In the chapter the plate has the following parameters and material characteristics: ρ_p – density, h_p – thickness, d – draft, m – mass per unit area, D – flexural rigidity. The water and wave parameters are: ρ_w – density, h – depth, λ – wavelength, k_0 – wavenumber, ω – wave frequency, A – wave height. The introduced structural parameters $\mathcal{D} = D/\rho_w g$, $\mu = m\omega^2/\rho_w g$ are constant as an isotropic plate is considered; the flexural rigidity and bending stiffness of the plate are constant.

The wave height A is smaller than the plate thickness h_p . Therefore, there is no cavity between the wetted surface of the plate and water surface. The normal incidence of water waves is studied. This assumption is by no means necessary — the problem would not be difficult to deal with if this simplifying assumption was not made. Hence, the angle of incidence β is zero; the geometry of our problem becomes two-dimensional (x, z). However, the problem is formulated for the general three-dimensional case. A transition to the case of oblique waves is described in section 7.7.

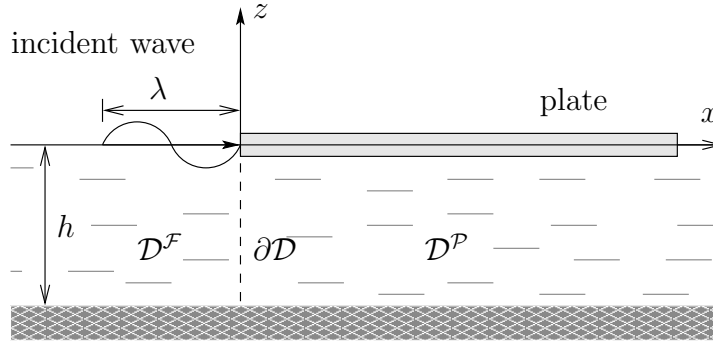


Figure 7.1: Definition sketch of the problem.

With the usual assumptions of an ideal fluid and small amplitudes, see sections 2.2 and 3.2, the velocity potential can be written in the form (2.7) $\Phi(x, y, z, t) = \phi(x, y, z)e^{-i\omega t}$. The potential $\phi(x, y, z)$ is governed by the Laplace equation in the fluid, $-h < z < 0$,

$$\Delta\phi(x, y, z) = 0. \quad (7.1)$$

The velocity potential must satisfy the boundary conditions on the free surface $z = 0$

$$\frac{\partial\phi(x, y, 0)}{\partial z} - K\phi(x, y, 0) = 0, \quad \text{on } \mathcal{F}, \quad (7.2)$$

on the bottom $z = -h$ (2.21), and on the plate wetted surfaces which are horizontal \mathcal{P} ($x > 0, z = -d$) surface and vertical \mathcal{S}_s ($x = 0, -d < z < 0$), see section 2.4 and [10, 143]. The condition on the horizontal surface (plate bottom) has the form

$$\frac{\partial\phi(x, y, -d)}{\partial z} = -i\omega w(x, y), \quad \text{on } \mathcal{P}, \quad (7.3)$$

and the condition on the vertical wetted surface (the side)

$$\frac{\partial\phi(0, y, z)}{\partial x} = 0, \quad \text{on } \mathcal{S}_s, \quad (7.4)$$

as the direction of the normal vector pointing from the fluid domain to the plate coincides with the z -direction in the former case, and with the x -direction in the latter. The radiation condition for the scattering and radiation potential at $R \rightarrow \infty$ is written in the form (2.26). In two-dimensional (x, z) analysis, the horizontal distance R simply becomes x .

Using thin plate theory, see section 2.3, we can obtain the differential equation for the plate deflection and, correspondingly, the following expression for the total potential ϕ at the plate area

$$(\mathcal{D}\Delta^2 - \mu + 1) \frac{\partial \phi}{\partial z} - K\phi = 0, \quad (7.5)$$

where $K = \omega^2/g$. As the geometry of our problem is two dimensional (x, z) , this expression takes the form

$$\left(\mathcal{D} \frac{d^4}{dx^4} - \mu + 1 \right) \frac{\partial \phi}{\partial z} - K\phi = 0, \quad (7.6)$$

For the potential open water area \mathcal{F} we have the condition (7.2). The potential of the undisturbed incident wave ϕ^{inc} is given by

$$\phi^{\text{inc}}(x, y, z) = \frac{\cosh k_0(z+h)}{\cosh k_0 h} \frac{gA}{i\omega} e^{ik_0(x \cos \beta + y \sin \beta)}, \quad (7.7)$$

which in 2D becomes

$$\phi^{\text{inc}}(x, z) = \frac{\cosh k_0(z+h)}{\cosh k_0 h} \frac{gA}{i\omega} e^{ik_0 x}. \quad (7.8)$$

For water of finite depth, the wavenumber k_0 is the only real solution of the water dispersion relation

$$k_i \tanh k_i h = K. \quad (7.9)$$

The wavelength of the incoming waves is $\lambda = 2\pi/k_0$. The diffraction potential, which equals $\phi - \phi^{\text{inc}}$, must satisfy the Sommerfeld radiation condition at infinity.

The linearized free surface kinematic condition (7.3), which in 2D has the form

$$\frac{\partial \phi}{\partial z}(x, z) = -i\omega w(x), \quad (7.10)$$

expresses the relation between the velocity potential and the plate deflection. The horizontal edge of the plate is free of vertical forces, bending and twisting moments, and the free edge conditions at $y = 0$ are

$$\frac{d^2 w}{dx^2} = 0; \quad (7.11)$$

$$\frac{d^3 w}{dx^3} = 0, \quad (7.12)$$

as the direction of the normal n coincides with that of the x -axis and the geometry of the problem is two-dimensional.

7.3 Solution

Following section 2.7, here, with the use of thin plate theory and Green's theorem we obtain an integral equation for the potential and, further, an integro-differential one for the plate deflection. The key idea of our approach is adding a correction which is dependent on draft to the solution obtained for the SIP with the zero-thickness assumption, given in section 3.4.

7.3.1 Deflection

As in the case of zero draft, see p.50, we represent the deflection of the plate with constant draft in the form

$$w(x) = \sum_{n=0}^{\infty} a_n e^{i\kappa_n x}, \quad (7.13)$$

where the amplitudes a_n and reduced wavenumbers κ_n are unknown. Each term of the series represents the corresponding wave mode. Due to the convergence of the series in (7.13), a finite number of wave modes, M , is taken into account. However, now we will write the amplitude as a power series with respect to small value of the draft as follows:

$$a_n = a_n^{(0)} + d a_n^{(1)} + \mathcal{O}(d^2). \quad (7.14)$$

To avoid secular behavior of the amplitudes, as in the Lindstedt (PLK) method [53], we also expand the reduced wavenumber κ_n as a power series

$$\kappa_n = \kappa_n^{(0)} (1 + d \kappa_n^{(1)}) + \mathcal{O}(d^2). \quad (7.15)$$

The plate deflection (7.13) may be rewritten as the sum of the zero draft order (with a correction term in the exponential function) and first draft order solutions

$$w(x) = w^{(0)}(x) + d w^{(1)}(x), \quad (7.16)$$

where the function $w^{(q)}(x)$, $q = 0, 1$ is given by

$$w^{(q)}(x) = \sum_{n=0}^M a_n^{(q)} e^{i\kappa_n^{(0)} (1 + d \kappa_n^{(1)}) x}. \quad (7.17)$$

Terms containing $a_n^{(0)}$ and $a_n^{(1)}$ of the corresponding series are of the zero (with a correction) and first draft order, respectively. In fact the term of the zero draft order is the first term of the asymptotics, and the term of the first draft order is the second asymptotical term.

For the case where the plate thickness is assumed to be zero, see sections 2.6, 3.4 and [5], the deflection $w^{(0*)}(x)$ is represented in the form

$$w^{(0*)}(x) = \sum_{n=0}^M a_n^{(0)} e^{i\kappa_n^{(0)} x}. \quad (7.18)$$

This deflection function will be used to compare the results obtained for the current problem with those obtained using the zero-thickness assumption.

7.3.2 Derivation and analysis of IDE

Here the main integro-differential equation for the problem is derived. We follow the derivation of the IDE presented in sections 2.7 and 3.3. The Green's function $\mathcal{G}(\mathbf{x}, \boldsymbol{\xi})$ is introduced for a source within the fluid (see section 2.5). We apply the Green's theorem for the potential in the open water and plate regions as for the previous problems.

The total potential $\phi(\mathbf{x})$ satisfies the equation derived

$$2\pi\phi(x, z) = 2\pi\phi^{\text{inc}}(x, z) + \int_{S_s} \left(\phi \frac{\partial \mathcal{G}}{\partial n} - \mathcal{G} \frac{\partial \phi}{\partial n} \right) d\zeta + \int_{\mathcal{P}} \left(\phi \frac{\partial \mathcal{G}}{\partial n} - \mathcal{G} \frac{\partial \phi}{\partial n} \right) d\xi, \quad (7.19)$$

where we have the first integral as the vertical side surface is considered now; it is a new term compared to zero-thickness analysis. Because the normal coincides with the x -axis, the normal derivative of the potential, ϕ_n , for the vertical surface of the plate, becomes ϕ_x , equaling zero due to the condition (7.4). Hence, the second term in the first integral in (7.19) vanishes. For the horizontal surface, where the normal coincides with the z -axis, the potential normal derivative becomes ϕ_z .

Thus, from (7.19) we obtain

$$2\pi\phi(x, z) = 2\pi\phi^{\text{inc}}(x, z) + \int_{-d}^0 \phi(0, \zeta) \frac{\partial \mathcal{G}(x, -d; 0, \zeta)}{\partial \xi} d\zeta + \int_0^\infty \left(\phi(\xi, -d) \frac{\partial \mathcal{G}(x, -d; \xi, -d)}{\partial \zeta} - \mathcal{G}(x, -d; \xi, -d) \frac{\partial \phi(\xi, -d)}{\partial \zeta} \right) d\xi. \quad (7.20)$$

The Green's function \mathcal{G} may be rewritten as

$$\mathcal{G}(x, -d; \xi, -d) = \mathcal{G}(x, 0; \xi, 0) - d \left(\frac{\partial \mathcal{G}(x, 0; \xi, 0)}{\partial z} + \frac{\partial \mathcal{G}(x, 0; \xi, 0)}{\partial \zeta} \right) + \mathcal{O}(d^2). \quad (7.21)$$

Then, rewriting the integrals in the integral equation for the potential (7.20), we arrive at the following approximate integral equation:

$$\begin{aligned} 2\pi\phi(x, -d) &= 2\pi\phi^{\text{inc}}(x, -d) + d\phi(0, 0) \frac{\partial \mathcal{G}(x, 0; 0, 0)}{\partial \xi} \\ &+ \int_0^\infty \left(\phi(\xi, -d) \frac{\partial \mathcal{G}(x, 0; \xi, 0)}{\partial \zeta} - \mathcal{G}(x, 0; \xi, 0) \frac{\partial \phi(\xi, -d)}{\partial \zeta} \right) d\xi \\ &- d \int_0^\infty \phi(\xi, -d) \left(\frac{\partial^2 \mathcal{G}(x, 0; \xi, 0)}{\partial z \partial \zeta} + \frac{\partial^2 \mathcal{G}(x, 0; \xi, 0)}{\partial \zeta^2} \right) d\xi \\ &+ d \int_0^\infty \frac{\partial \phi(\xi, -d)}{\partial \zeta} \left(\frac{\partial \mathcal{G}(x, 0; \xi, 0)}{\partial z} + \frac{\partial \mathcal{G}(x, 0; \xi, 0)}{\partial \zeta} \right) d\xi + \mathcal{O}(d^2), \end{aligned} \quad (7.22)$$

for the potential in the plate area \mathcal{P} , where the first term represents the incident field. Here and in the sequel we neglect terms of order $\mathcal{O}(d^2)$. The total potential ϕ will be

rewritten as Taylor expansion series. The incident potential $\phi^{\text{inc}}(x, -d)$ can be derived from (7.8) at $z = -d$. Alternatively, the incident potential ϕ^{inc} might also be rewritten as Taylor expansion series at $z = 0$.

The two-dimensional Green's function at the free surface ($z = \zeta = 0$) has the following form, see section 2.5 and [10, 43]:

$$\mathcal{G}(x, 0; \xi, 0) = - \int_0^\infty \frac{\cosh kh}{k \sinh kh - K \cosh kh} e^{ik(x-\xi)} dk, \quad (7.23)$$

while the general forms of the two-dimensional Green's function are

$$\mathcal{G}(x, z; \xi, \zeta) = - \int_{-\infty}^\infty \frac{1}{k} \frac{K \sinh k\zeta + k \cosh k\zeta}{k \sinh kh - K \cosh kh} \cosh k(z+h) e^{ik(x-\xi)} dk \quad (7.24)$$

for $z < \zeta$, and

$$\mathcal{G}(x, z; \xi, \zeta) = - \int_{-\infty}^\infty \frac{1}{k} \frac{K \sinh kz + k \cosh kz}{k \sinh kh - K \cosh kh} \cosh k(\zeta+h) e^{ik(x-\xi)} dk \quad (7.25)$$

for $z > \zeta$. In our analysis we will use formula (7.24) for the Green's function in the general case and formula (7.23) at the free surface. In the three-dimensional case, the Green's function at the free surface is written in the form (2.53).

We introduce the function F_0 , which contains terms of the right-hand side of (7.22) (except of the third one):

$$\begin{aligned} 2\pi F_0 &= 2\pi \phi^{\text{inc}}(x, -d) + d\phi(0, 0) \frac{\partial \mathcal{G}(x, 0; 0, 0)}{\partial \xi} \\ &- d \int_0^\infty \phi(\xi, -d) \left(\frac{\partial^2 \mathcal{G}(x, 0; \xi, 0)}{\partial z \partial \zeta} + \frac{\partial^2 \mathcal{G}(x, 0; \xi, 0)}{\partial \zeta^2} \right) d\xi \\ &+ d \int_0^\infty \frac{\partial \phi(\xi, -d)}{\partial \zeta} \left(\frac{\partial \mathcal{G}(x, 0; \xi, 0)}{\partial z} + \frac{\partial \mathcal{G}(x, 0; \xi, 0)}{\partial \zeta} \right) d\xi. \end{aligned} \quad (7.26)$$

The relations between the potential and its derivatives and the plate deflection can be derived from the conditions (7.10) and (7.6). Then, combining the left-hand side and the first integral in the right-hand side of (7.22), we obtain the following integro-differential equation for the plate deflection:

$$\left\{ \mathcal{D} \frac{d^4}{dx^4} - \mu + 1 \right\} w(x) - \frac{K}{2\pi} \int_0^\infty \mathcal{G}(x, 0; \xi, 0) \left\{ \mathcal{D} \frac{d^4}{d\xi^4} - \mu \right\} w(\xi) d\xi = F_0, \quad (7.27)$$

analogously to chapters 3–6. If we insert expressions for the deflection (7.13) and the Green's function (7.23) into the IDE (7.27), keeping a_n and κ_n in the general forms, the

following equation is derived

$$\begin{aligned} & \sum_{n=0}^M (\mathcal{D}\kappa_n^4 - \mu + 1) a_n e^{i\kappa_n x} + \frac{K}{2\pi} \int_0^\infty \sum_{n=0}^M (\mathcal{D}\kappa_n^4 - \mu) a_n e^{i\kappa_n \xi} \\ & \times \int_0^\infty \frac{\cosh kh}{k \sinh kh - K \cosh kh} e^{ik(x-\xi)} dk d\xi = F_0. \end{aligned} \quad (7.28)$$

The modified form of the function F_0 will be discussed later.

Next, the integration with respect to ξ has to be carried out. The k -integral can be solved by means of the residues at the poles $k = \kappa_n$ and $k = k_i$ of the complex plane (as described in section 3.4). Then we obtain

$$\begin{aligned} & \sum_{n=0}^M (\mathcal{D}\kappa_n^4 - \mu + 1) a_n e^{i\kappa_n x} + K \sum_{n=0}^M (\mathcal{D}\kappa_n^4 - \mu) a_n \\ & \times \left(\frac{e^{i\kappa_n x}}{\kappa_n \tanh \kappa_n h - K} + \sum_{i=0}^{M-2} \frac{k_i e^{ik_i x}}{(\kappa_n - k_i) \mathcal{K}_i} \right) = F_0, \end{aligned} \quad (7.29)$$

where the function \mathcal{K}_i introduced is

$$\mathcal{K}_i = K(1 - Kh) + k_i^2 h \quad (7.30)$$

for $i = 0, \dots, M-2$. To function F_0 , the right-hand side of (7.27–7.28), the same operations have been applied.

Now we rewrite the amplitudes a_n in the form (7.14) and obtain the following extended expression from (7.29):

$$\begin{aligned} & \sum_{n=0}^M (\mathcal{D}\kappa_n^4 - \mu + 1) (a_n^{(0)} + da_n^{(1)}) e^{i\kappa_n x} \\ & + K \sum_{n=0}^M (\mathcal{D}\kappa_n^4 - \mu) (a_n^{(0)} + da_n^{(1)}) \frac{e^{i\kappa_n x}}{\kappa_n \tanh \kappa_n h - K} = F, \end{aligned} \quad (7.31)$$

where the function F has been derived from the original function F_0 as the contribution of the poles $k = \kappa_n$ and $k = k_i$ in the complex plane, analogously to the derivation of the

left-hand side in (7.29). It has the following form

$$\begin{aligned}
F = & A e^{ik_0 x} \frac{\cosh k_0(h-d)}{\cosh k_0 h} - K \sum_{n=0}^M (\mathcal{D}\kappa_n^4 - \mu) (a_n^{(0)} + da_n^{(1)}) \sum_{i=0}^{M-2} \frac{k_i e^{ik_i x}}{(\kappa_n - k_i) \mathcal{K}_i} \\
& - d \sum_{i=0}^{M-2} \frac{k_i^2 e^{ik_i x}}{\mathcal{K}_i} \left(A + K \sum_{n=0}^M (\mathcal{D}\kappa_n^4 - \mu) (a_n^{(0)} + da_n^{(1)}) \sum_{j=0}^{M-2} \frac{k_j}{(\kappa_n - k_j) \mathcal{K}_j} \right) \\
& + K d \sum_{n=0}^M (\mathcal{D}\kappa_n^4 - \mu + 1) (a_n^{(0)} + da_n^{(1)}) \left(\frac{\kappa_n \tanh \kappa_n h e^{i\kappa_n x}}{\kappa_n \tanh \kappa_n h - K} + \sum_{i=0}^{M-2} \frac{K k_i e^{ik_i x}}{(\kappa_n - k_i) \mathcal{K}_i} \right) \\
& + d \sum_{n=0}^M (\mathcal{D}\kappa_n^4 - \mu + 1) (a_n^{(0)} + da_n^{(1)}) \left(\frac{\kappa_n^2 e^{i\kappa_n x}}{\kappa_n \tanh \kappa_n h - K} + \sum_{i=0}^{M-2} \frac{k_i^3 e^{ik_i x}}{(\kappa_n - k_i) \mathcal{K}_i} \right) \\
& - K d \sum_{n=0}^M (a_n^{(0)} + da_n^{(1)}) \left(\frac{\kappa_n \tanh \kappa_n h e^{i\kappa_n x}}{\kappa_n \tanh \kappa_n h - K} + \sum_{i=0}^{M-2} \frac{K k_i e^{ik_i x}}{(\kappa_n - k_i) \mathcal{K}_i} \right) \\
& - K^2 d \sum_{n=0}^M (a_n^{(0)} + da_n^{(1)}) \left(\frac{e^{i\kappa_n x}}{\kappa_n \tanh \kappa_n h - K} + \sum_{i=0}^{M-2} \frac{k_i e^{ik_i x}}{(\kappa_n - k_i) \mathcal{K}_i} \right). \quad (7.32)
\end{aligned}$$

To found the third term in (7.32) we have used the value of the potential in open water area at $x = 0$.

From now on we will separately continue the analysis for zero and first draft order equations. We will use the product of the incident potential, the first term in (7.32), only in zero draft order equations.

7.4 Zero draft order

First, we distinguish terms of zero draft order in (7.31–7.32), which allows us to find $\kappa_n^{(0)}$ and, later, $a_n^{(0)}$. Analyzing the left-hand side of (7.31) and collecting terms of $\mathcal{O}(d^0)$, we obtain the governing equation of the zero draft order

$$\sum_{n=0}^M \mathcal{F}(\kappa_n^{(0)}) a_n^{(0)} e^{i\kappa_n x} = A e^{ik_0 x} - K \sum_{n=0}^M (\mathcal{D}\kappa_n^4 - \mu) a_n^{(0)} \sum_{i=0}^{M-2} \frac{k_i e^{ik_i x}}{(\kappa_n - k_i) \mathcal{K}_i}, \quad (7.33)$$

where the function $\mathcal{F}(\kappa_n)$ has the form

$$\mathcal{F}(\kappa_n) = \frac{(\mathcal{D}\kappa_n^4 - \mu + 1) \kappa_n \tanh \kappa_n h - K}{\kappa_n \tanh \kappa_n h - K}. \quad (7.34)$$

In the numerator of the function $\mathcal{F}(\kappa_n)$, we have the dispersion relation in the plate region, which is

$$\left(\mathcal{D}\kappa_n^{(0)4} - \mu + 1 \right) \kappa_n^{(0)} \tanh \kappa_n^{(0)} h = K. \quad (7.35)$$

The dispersion relation (7.35) is of zero draft order and it allows us to find the reduced wavenumbers $\kappa_n^{(0)}$, which coincide with the roots of (7.35) because of the two-dimensional geometry of the problem.

Making M the truncation parameter of the problem, we take into account $M + 1$ roots $\kappa_n^{(0)}$ of the plate dispersion relation (7.35) and $M - 1$ roots k_i of the water dispersion relation (7.9). All the roots have the same location in the complex plane as was described in section 3.4. The plate dispersion relation (7.35) has the following solutions: two at the real axis $\pm\kappa_0^{(0)}$, and four complex roots $\pm\kappa_1^{(0)}$, $\pm\kappa_2^{(0)}$ (the position of these six roots in the complex plane was shown in figure 3.3), and $\pm\kappa_n^{(0)}$, $n = 3, 4, \dots$ at the imaginary axis. The four complex roots are symmetrically placed with respect to both the real and imaginary axes. We take into account M roots of the dispersion relation (7.35) located in the upper half-plane, the real positive root $\kappa_0^{(0)}$, which represents the traveling wave mode, two complex roots $\kappa_1^{(0)}$ and $\kappa_2^{(0)}$ with equal imaginary parts and equal but opposite-signed real parts, which represent damped wave modes, and imaginary roots $\pm\kappa_n^{(0)}$, $n = 3, 4, \dots, M$. From the roots of the water dispersion relation (7.9), $M - 1$ roots are taken into account: the only real positive root k_0 and $M - 2$ imaginary roots k_i , $i = 1, \dots, M - 2$.

The set of equations to determine the amplitudes $a_n^{(0)}$ can be obtained by considering the coefficients of the exponential function $e^{ik_i x}$; the procedure is described in detail in section 3.4. We obtain $M - 1$ equations

$$\sum_{n=0}^M \left(\mathcal{D}\kappa_n^{(0)4} - \mu \right) \frac{K k_i a_n^{(0)}}{\left(\kappa_n^{(0)} - k_i \right) \mathcal{K}_i} = A_i, \quad (7.36)$$

where $i = 0, \dots, M - 2$, and

$$A_0 = -A \frac{\cosh k_0(h - d)}{\cosh k_0 h},$$

$A_i = 0$ for $i = 1, \dots, M - 2$. The rest of the equations are obtained from the free edge conditions (7.11–7.12):

$$\sum_{n=0}^M \kappa_n^{(0)2} a_n^{(0)} = 0; \quad (7.37)$$

$$\sum_{n=0}^M \kappa_n^{(0)3} a_n^{(0)} = 0. \quad (7.38)$$

In such a way, the set of equations for the amplitudes $a_n^{(0)}$ consists of $M + 1$ equations (7.36–7.38) and has exactly the same form as that derived for the case of zero-thickness assumption in chapter 3 ($A_0 = -A$ when $d = 0$). Hence, the deflection function $w^{(0*)}(x)$ can be computed by formula (7.18).

7.5 First draft order

In this section, we consider the terms of first draft order in the extended IDE (7.31). Terms which contain $\kappa_n - k_i$ in the denominator in formula (7.32) result in extra terms of $\mathcal{O}(d^1)$. The first-draft-order governing equation becomes

$$\sum_{n=0}^M \left(\mathcal{F}(\kappa_n^{(0)}) a_n^{(1)} + \frac{\partial \mathcal{F}(\kappa_n^{(0)})}{\partial \kappa_n} \kappa_n^{(0)} \kappa_n^{(1)} a_n^{(0)} \right) \frac{e^{i\kappa_n x}}{\kappa_n \tanh \kappa_n h - K} = F^{(1)}, \quad (7.39)$$

where the function $F^{(1)}$, according to formulas (7.31–7.32), has the following form

$$\begin{aligned}
F^{(1)} = & -K \sum_{n=0}^M \left(\mathcal{D}\kappa_n^{(0)4} - \mu \right) \sum_{i=0}^{M-2} \frac{k_i e^{ik_i x}}{\left(\kappa_n^{(0)} - k_i \right) \mathcal{K}_i} \left(a_n^{(1)} - \frac{\kappa_n^{(0)} \kappa_n^{(1)} a_n^{(0)}}{\left(\kappa_n^{(0)} - k_i \right)} \right) \\
& -K \sum_{n=0}^M \left(4\mathcal{D}\kappa_n^{(0)4} \kappa_n^{(1)} - \mu \right) \sum_{i=0}^{M-2} \frac{k_i e^{ik_i x}}{\left(\kappa_n^{(0)} - k_i \right) \mathcal{K}_i} a_n^{(0)} \\
& - \sum_{i=0}^{M-2} \frac{k_i^2 e^{ik_i x}}{\mathcal{K}_i} \left(A + K \sum_{n=0}^M \left(\mathcal{D}\kappa_n^{(0)4} - \mu \right) a_n^{(0)} \sum_{j=0}^{M-2} \frac{k_j}{\left(\kappa_n - k_j \right) \mathcal{K}_j} \right) \\
& + K \sum_{n=0}^M \left(\mathcal{D}\kappa_n^{(0)4} - \mu + 1 \right) \left(\frac{\kappa_n \tanh \kappa_n h e^{i\kappa_n x}}{\kappa_n \tanh \kappa_n h - K} + \sum_{i=0}^{M-2} \frac{K k_i e^{ik_i x}}{\left(\kappa_n^{(0)} - k_i \right) \mathcal{K}_i} \right) a_n^{(0)} \\
& + \sum_{n=0}^M \left(\mathcal{D}\kappa_n^{(0)4} - \mu + 1 \right) \left(\frac{\kappa_n^2 e^{i\kappa_n x}}{\kappa_n \tanh \kappa_n h - K} + \sum_{i=0}^{M-2} \frac{k_i^3 e^{ik_i x}}{\left(\kappa_n^{(0)} - k_i \right) \mathcal{K}_i} \right) a_n^{(0)} \\
& - K \sum_{n=0}^M \left(\frac{\kappa_n \tanh \kappa_n h e^{i\kappa_n x}}{\kappa_n \tanh \kappa_n h - K} + \sum_{i=0}^{M-2} \frac{K k_i e^{ik_i x}}{\left(\kappa_n^{(0)} - k_i \right) \mathcal{K}_i} \right) a_n^{(0)} \\
& - K^2 \sum_{n=0}^M \left(\frac{e^{i\kappa_n x}}{\kappa_n \tanh \kappa_n h - K} + \sum_{i=0}^{M-2} \frac{k_i e^{ik_i x}}{\left(\kappa_n^{(0)} - k_i \right) \mathcal{K}_i} \right) a_n^{(0)}, \tag{7.40}
\end{aligned}$$

after some manipulations. All terms in (7.40) are of the first draft order.

The function $\mathcal{F}(\kappa_n)$, which was written in the form (7.34), can be expanded in the following way

$$\mathcal{F}(\kappa_n) = \mathcal{F}(\kappa_n^{(0)}) + d \frac{\partial \mathcal{F}(\kappa_n^{(0)})}{\partial \kappa_n} \kappa_n^{(0)} \kappa_n^{(1)} + \mathcal{O}(d^2). \tag{7.41}$$

Doing some operations and considering the coefficients of $e^{i\kappa_n x}$, we obtain the following relation for reduced wavenumbers of the first draft order $\kappa_n^{(1)}$

$$\kappa_n^{(1)} = \frac{\left(\mathcal{D}\kappa_n^{(0)4} - \mu + 1 \right) \kappa_n^{(0)} - K \tanh \kappa_n^{(0)} h}{\mathcal{Q}(\kappa_n^{(0)})} \tag{7.42}$$

with

$$\mathcal{Q}(\kappa_n^{(0)}) = \left(\mathcal{D}\kappa_n^{(0)4} - \mu + 1 \right) \kappa_n^{(0)} h + \left(5\mathcal{D}\kappa_n^{(0)4} - \mu + 1 \right) \tanh \kappa_n^{(0)} h - K h \tanh \kappa_n^{(0)} h. \tag{7.43}$$

Thus, the reduced wavenumbers $\kappa_n^{(1)}$ are now expressed via $\kappa_n^{(0)}$, which are the roots of the plate dispersion relation (7.35). It is seen from (7.42) that $\kappa_n^{(1)} \sim \mathcal{O}(1/h)$, and also that $d\kappa_n^{(1)} < 1$ for realistic values of the draft and wavelength as was expected.

The nature of the wavenumbers of first draft order $\kappa_n^{(1)}$ is the same as for the corresponding wavenumbers $\kappa_n^{(0)}$ for $n = 0, 1, 2$: they are purely real when $n = 0$, and are complex when $n = 1, 2$. For $n = 3, 4, \dots, M$, however, the wavenumbers $\kappa_n^{(1)}$ are purely real, while the wavenumbers $\kappa_n^{(0)}$ are pure imaginary roots of the dispersion relation (7.35).

It can be shown that $\kappa_n = \kappa_n^{(0)}(1 + d\kappa_n^{(1)})$ fulfills the following dispersion relation

$$(\mathcal{D}\kappa_n^4 - \mu + 1) \kappa_n \tanh \kappa_n(h - d) = K \quad (7.44)$$

up to $\mathcal{O}(d^2)$.

Knowing $\kappa_n^{(1)}$ and $a_n^{(0)}$, we can compute the deflection function $w^{(0)}$ by formula (7.17). Then, the amplitudes $a_n^{(1)}$ may be found with the use of equations (7.39–7.40), the amplitudes $a_n^{(0)}$, and the wavenumbers $\kappa_n^{(0)}$ and $\kappa_n^{(1)}$. For this we use the technique with which we also found the amplitudes in the previous section and in chapters 3–5. The equations for determining the amplitudes $a_n^{(1)}$ have the following form

$$\begin{aligned} & K \sum_{n=0}^M \left(\mathcal{D}\kappa_n^{(0)4} - \mu \right) \frac{k_i}{(\kappa_n^{(0)} - k_i) \mathcal{K}_i} a_n^{(1)} \\ &= K \sum_{n=0}^M \left(\mathcal{D}\kappa_n^{(0)4} - \mu \right) \frac{\kappa_n^{(0)} \kappa_n^{(1)} k_i}{(\kappa_n^{(0)} - k_i)^2 \mathcal{K}_i} a_n^{(0)} \\ &\quad - K \sum_{n=0}^M \left(4\mathcal{D}\kappa_n^{(0)4} \kappa_n^{(1)} - \mu \right) \sum_{i=0}^{M-2} \frac{k_i}{(\kappa_n^{(0)} - k_i) \mathcal{K}_i} a_n^{(0)} \\ &\quad - \frac{k_i^2}{\mathcal{K}_i} A - \frac{k_i^2}{\mathcal{K}_i} K \sum_{n=0}^M \left(\mathcal{D}\kappa_n^{(0)4} - \mu \right) a_n^{(0)} \sum_{j=0}^{M-2} \frac{k_j}{(\kappa_n - k_j) \mathcal{K}_j} \\ &\quad + K \sum_{n=0}^M \left(\mathcal{D}\kappa_n^{(0)4} - \mu + 1 \right) \frac{k_i (K + k_i)}{(\kappa_n^{(0)} - k_i) \mathcal{K}_i} a_n^{(0)} - 2K^2 \sum_{n=0}^M \frac{k_i}{(\kappa_n^{(0)} - k_i) \mathcal{K}_i} a_n^{(0)}, \end{aligned} \quad (7.45)$$

for $i = 0, \dots, M-2$. As in the previous section, $M-1$ equations (7.45) are supplemented by the equations derived from the free edge conditions (7.11–7.12):

$$\sum_{n=0}^M \kappa_n^{(0)2} a_n^{(1)} = -2 \sum_{n=0}^M \kappa_n^{(0)2} \kappa_n^{(1)} a_n^{(0)}, \quad (7.46)$$

$$\sum_{n=0}^M \kappa_n^{(0)3} a_n^{(1)} = -3 \sum_{n=0}^M \kappa_n^{(0)3} \kappa_n^{(1)} a_n^{(0)}. \quad (7.47)$$

We may note that the coefficients of the amplitudes $a_n^{(0)}$ and $a_n^{(1)}$ are the same in the corresponding sets of equations, the left-hand sides of the sets (7.36–7.38) and (7.45–7.47), respectively. The set of $M+1$ equations (7.45–7.47) of the first draft order allows us to find the amplitudes $a_n^{(1)}$ and, correspondingly, the deflection term $w^{(1)}$ with the use of (7.17).

Hence, the total deflection can be computed by formula (7.13).

7.6 Numerical results and discussion

Here numerical results are presented for the total deflection of the plate with finite draft. We obtain results for practically relevant cases. The results for different values of the plate draft, water depth and wavelength are compared. The results are also compared with those obtained with the zero-thickness assumption in chapter 3 and with those obtained in [45] for the case of small finite draft. Also, we study the influence of the correction of the nonzero draft on the results for the plate deflection.

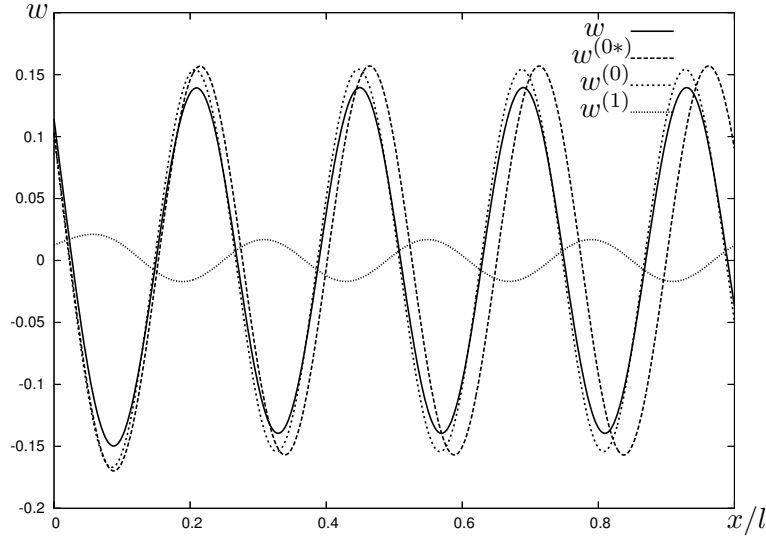


Figure 7.2: Deflections w , $w^{(0*)}$, $w^{(0)}$, $w^{(1)}$; for $h = 10$ m, $\mathcal{D} = 10^7$ m⁴, $l = 1000$ m, $\lambda = 200$ m, $d = 2$ m.

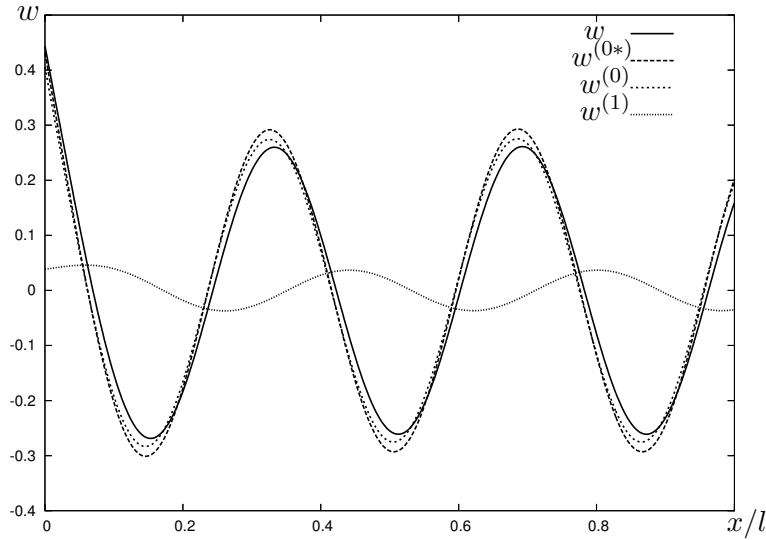


Figure 7.3: Deflections w , $w^{(0*)}$, $w^{(0)}$, $w^{(1)}$; as in figure 7.2, for $h = 100$ m.

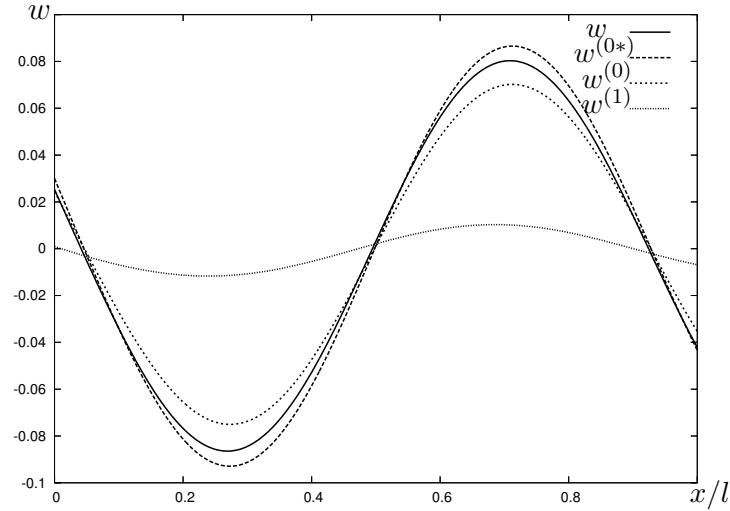


Figure 7.4: Deflections w , $w^{(0*)}$, $w^{(0)}$, $w^{(1)}$; for $h = 100$ m, $\mathcal{D} = 10^7$ m⁴, $l = 300$ m, $\lambda = 60$ m, $d = 2$ m.

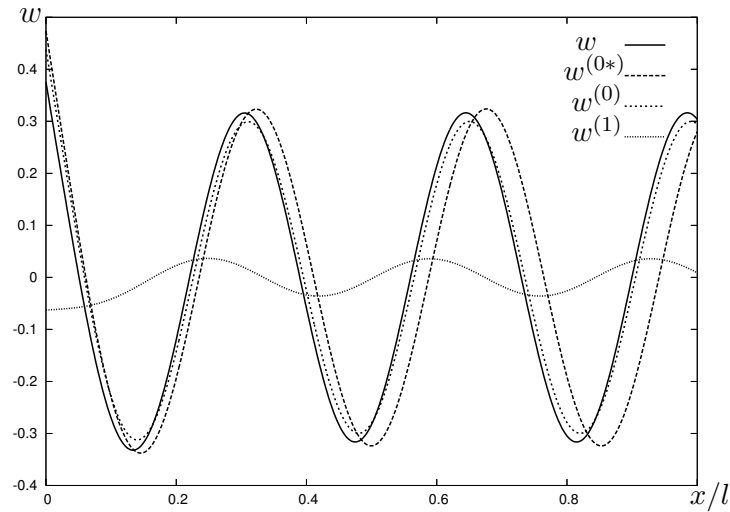


Figure 7.5: Deflections w , $w^{(0*)}$, $w^{(0)}$, $w^{(1)}$; for $h = 10$ m, $\mathcal{D} = 10^5$ m⁴, $l = 300$ m, $\lambda = 90$ m, $d = 2$ m.

The number of the roots $\kappa_n^{(0)}$ and, correspondingly, that of the roots $\kappa_n^{(1)}$ which are taken into account for the computations is $M = 30$. It provides sufficient accuracy, as was also reported in chapters 3–6. We take the Poisson's ratio $\nu = 0.25$, ratio $m/\rho_w = 0.25$ m, and wave height $A = 1$ m as constant. Hence, results shown are for the real part of the deflection, normalized by the wave height. Results for w are plotted against x/l , where l is the length of the plate part considered.

The four curves in figures 7.2–7.5 represent the total deflection w , deflection for the case of zero draft (zero-thickness assumption) $w^{(0*)}$, the deflection terms of zero $w^{(0)}$ and first $w^{(1)}$ draft order.

In figures 7.2–7.4, results are shown for realistic values of the plate rigidity (as for

a VLFS) for shallow and rather deep water. In figure 7.5, results are plotted for low rigidity (as for an ice field). The vertical and horizontal shifts can be seen when w , $w^{(0*)}$ and $w^{(0)}$ are compared. The difference between the total deflection w for finite draft and the deflection function $w^{(0*)}$, and the direction and value of the shifts, the differences between w , $w^{(0)}$ and $w^{(0*)}$, are highly dependent on the draft value and water depth. The plate deflection decreases (vertical shift) with increasing draft value. The direction of the horizontal shift may differ for shallow and deep water (to the left and to the right, respectively).

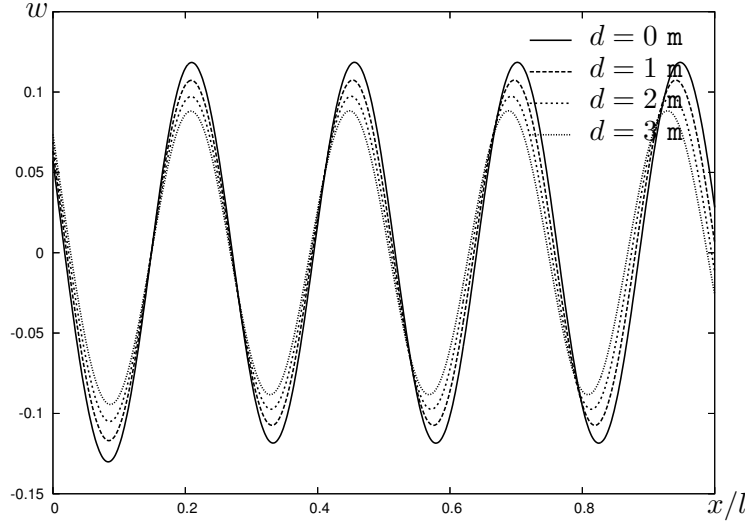


Figure 7.6: PFD deflection w ; for different draft values and $h = 20$ m, $\mathcal{D} = 10^7$ m⁴, $l = 1000$ m, $\lambda = 100$ m.

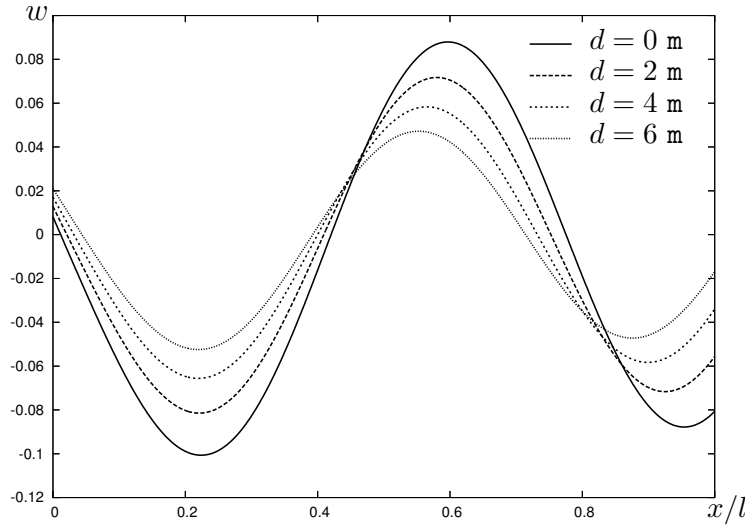


Figure 7.7: PFD deflection w ; for different draft values and $h = 10$ m, $\mathcal{D} = 10^7$ m⁴, $l = 300$ m, $\lambda = 90$ m.

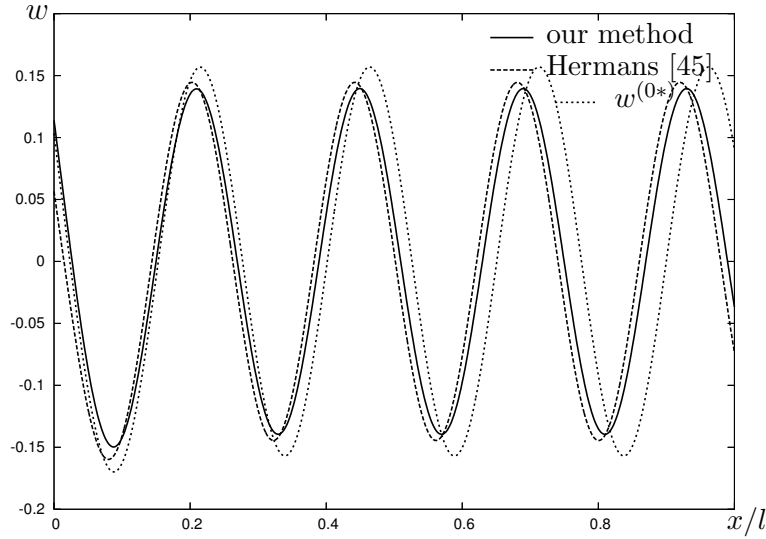


Figure 7.8: Comparison of the results for deflection w with those of Hermans [45];
 $h = 10$ m, $\mathcal{D} = 10^7$ m⁴, $l = 1000$ m, $\lambda = 200$ m, $d = 2$ m.

Results for the total deflection w for different values of the draft are given in figures 7.6–7.7. With increase of the draft value, the total deflection of the floating plate decreases as expected, that is prominent in figures presented. The draft has sufficient influence on the results, especially for shallow water and, also, for the plate of low rigidity. For realistic values of the plate rigidity and draft (as for VLFS), water depth and wavelength, however, the influence is not too large.

The solution for plate of finite small draft is derived in this chapter by expansions of all terms with respect to draft d . Hermans in [45] obtained the solution for this problem straightforwardly by use of conditions at $z = -d$. The comparison of numerical results for deflection of two approaches is given in figure 7.8 and shows good agreement. Also, the deflection obtained with zero-thickness assumption is depicted in the same figure to see the influence of draft. Here we have both horizontal and vertical shifts.

7.7 Extensions

Here we describe how the approach presented in this chapter may be extended to other geometries of the problem. For the case of water waves with oblique incidence, we can represent the deflection of the PFD having a semi-infinite horizontal shape in the form

$$w(x, y) = \sum_{n=0}^M (a_n^{(0)} + da_n^{(1)}) \exp \{ i\kappa_n^{(0)} (1 + d\kappa_n^{(1)}) x \cos \beta + ik_0 \sin \beta \}. \quad (7.48)$$

In general we follow the analysis presented in sections 7.3–7.5 with some minor modifications (in this case the geometry is three-dimensional).

Furthermore, the approach presented may be extended to the strip case: a PFD of finite width and infinite length. We assume that the wavelength λ is smaller than the

strip width l . The deflection is represented in the following way:

$$w(x, y) = \sum_{n=0}^M \left[(a_n^{(0)} + da_n^{(1)}) \exp \{i\kappa_n^{(0)} (1 + d\kappa_n^{(1)}) x \cos \beta\} + (b_n^{(0)} + db_n^{(1)}) \exp \{-i\kappa_n^{(0)} (1 + d\kappa_n^{(1)}) x \cos \beta\} \right] \exp \{ik_0 \sin \beta\} \quad (7.49)$$

for the case of oblique waves.

Also, the approach can be extended to a floating plate with another horizontal planforms considered in the thesis.

7.8 Conclusions and discussion

This chapter solved the problem of the diffraction of surface water waves on the floating flexible plate of a finite small draft. The analytical and numerical study of the plate's hydroelastic behavior has been presented. The problem has been solved with the use of thin plate theory, the Green's theorem, integro-differential formulation, governing equations of the zero and first draft order derived. Our approach is based on the integro-differential equation method, the modified geometrical-optics approach, and the Lindstedt method. The plate deflection is represented as a series of solutions with respect to the draft. The effect of the correction for the nonzero thickness has been studied. With growth of the draft (thickness), the plate deflection decreases. Other unknown parameters of the problem, such as the free-surface elevation, reflection and transmission coefficients may be determined by the approach presented as well.

For the case of shallow water, this problem may be solved with the Stoker approximation theory [107]. However, the case of finite water depth is the general case, and the solution presented can be used for all water depths, as was previously reported in chapters 3–5, [5, 8, 9, 88].

This is a new application of our method, which in chapters 3–6 was applied to plates of (assumed) zero thickness. The approach presented can be extended to the case of oblique incident waves or to a strip of finite width and infinite length, shown in section 7.7, and to plates of other horizontal planforms.

Although our main goal was to study the interaction between water waves and very large floating structures, the method is also valid for small- and middle-sized floating structures. In addition, it can be used to study the interaction between ice sheets and water waves.

The study presented in this chapter is a practically relevant extension of those given in the previous chapters. Here we derived the solution by expansions of all terms with respect to draft d (except for the incident potential, that is also can be done), while Hermans in [45] obtained the solution straightforwardly using conditions at $z = -d$. Future work could focus on the plate of variable thickness and draft; some information can be found in [101]. Also, it might be interesting to study the hydroelastic motion of a plate on water of varying depth [16, 17].

Chapter 8

General conclusions and recommendations

All general conclusions are given in this chapter. First, it gives a brief overview of the problems solved in the thesis. Then the key ideas, important details, basic characteristics and advantages of the method developed are described. Further, recommendations are given concerning future study of plate-water interaction, and VLFS analysis and design. Our view on very large floating structures in and for the future is given at the end of this chapter.

8.1 Main conclusions

In this section, the main conclusions of the thesis are presented. Detailed concluding remarks, together with the analysis, mathematical operations, numerical results and a discussion were given for particular problems in chapters 3–7.

VLFS-water interaction has been treated in this thesis. We studied the behavior of the very large floating structure in water waves. A thin elastic plate served as a model of the very large floating structure, which can be used for different purposes in the offshore zone or open sea. The hydroelastic motion of a floating plate and its response to surface waves was also studied. The problem was solved analytically for six different shapes of the floating plate. A new method for modeling plate-water interaction, the integro-differential equation method, was developed. Results were obtained for three models: of infinite, finite, and shallow water depth.

The complete study and details of the analysis were presented for each particular problem in corresponding sections of chapters 3–7. Analytical solutions and numerical results were obtained for: the plate deflection, free-surface elevation, initiated wave pattern, and the reflection and transmission of incident waves.

The influence of the water depth, wave parameters (wavelength, amplitude, frequency), plate properties (rigidity) and length parameters on the behavior of the floating plate and its hydroelastic response to an incident field has been investigated. Numerical results were obtained for practically relevant and important cases. For the computations mainly the packages developed in Fortran were used.

For realistic values of the plate rigidity and mass, the plate deflections were found to

be very small. This means in practice that the VLFS is very stable and so that it will not unbalance people walking on the floating platforms, or move structures/facilities located on them.

The influence of plate motion on wave propagation has been investigated. With decreasing water depth, the results for the plate deflection and free-surface elevation change gradually, while the influence of the water depth itself on the results increases.

On the plate contour, the vertical displacements of the plate and the free surface may differ because the transition conditions imposed require continuity of mass and energy fluxes, but not continuity of the free surface and plate elevations. All length and other parameters of the problem can be normalized by the plate length (diameter); then we use dimensionless parameters to ensure the correctness and accuracy of numerical study.

We have obtained numerical results for a floating plate having properties of the VLFS, behaving in water waves nearly as a rigid body; if the properties of ice are used, the plate is much more flexible.

8.2 Method

A new method to solve the problem of the interaction between a floating flexible plate and water waves has been proposed. The key idea of our approach is derivating an integral equation for the velocity potential and, further, an integro-differential equation for the vertical displacement, the plate deflection or the free-surface elevation. We named the proposed method **the integro-differential equation method**. Standard equations of hydrodynamics, namely the Laplace equation and boundary conditions, Green's theorem and thin plate theory have been used to derive the general integro-differential equation (IDE) for the problem.

After the derivation of the IDE, we proceeded with the complex integration and operations on the integrand and the Green's and deflection functions involved. Using different techniques for particular problems (various plate shapes and water depth models were considered), we found a set of equations for the amplitudes of wave modes. Then, the plate deflection could be determined as the superposition of exponential or Bessel functions multiplied by the amplitudes, defined as in the geometrical-optics approach. Our approach can also be used to determine parameters of the water field, the free-surface elevation, initiated wave pattern generated by the plate motion, and reflection and transmission of incident surface waves.

As shown in chapters 3–7, the integro-differential equation method allows us to solve the plate-water interaction problem for different planforms of the floating plate (having either a rectangular or an arbitrary shape). The method is also suitable for all three water depth models: for infinite, finite, and shallow depth.

Due to the properties of the VLFS and its thickness, which is small compared to its length parameters, the floating structure is modeled by a thin elastic plate. Therefore the Kirchhoff thin plate theory was applied to describe the motion of the plate. The plate deflection was represented as a superposition of exponential or Bessel functions for different problems solved in chapters 3–7. For the case of a three-dimensional plate, the deflection was represented as a combination of power series with respect to the constant draft, which is a small parameter of the problem. Such a choice and following truncations

of the series due to their decaying behavior were verified for all problems considered.

Modified forms of the Green's functions were derived for different situations in section 2.5 using the standard forms [146] for infinite and finite water-depth cases. The Green's function and the velocity potential satisfy the boundary conditions at the free surface and bottom and radiation condition. We combined the kinematic and dynamic conditions at the free surface with equations of the thin plate theory and applied the Green's theorem to obtain an integral equation for the potential and an integro-differential equation for the plate deflection, which is our main interest.

Two dispersion relations were used, one in the open fluid domain, and the second one in the domain covered by the plate. The governing IDE derived is valid at the free surface, which reduces the initial three-dimensional problem to a two-dimensional one. Next, the integration in the complex plane was carried out using different operations and methods for particular problems. The poles of the integrand in the IDE are at the solutions of the plate dispersion relation. Application of the residue theorem at these poles yields equations for determining the amplitudes of wave modes. The set of equations for the amplitudes is completed by the free edge conditions. When the amplitudes and reduced wavenumbers corresponding to the roots of the dispersion relations are known, the plate deflection can be computed.

The advantage of the approach presented is that it derives one common set of equations for the plate and open-water regions, in contrast to other methods. With the integral equation for the potential and following the analysis, we can derive expressions for both vertical displacements in the plate and open-water regions, the plate deflection and the free-surface elevation, respectively. Hence, we can determine the plate deflection and free-surface elevation using one common set of equations. Our approach can also determine other unknowns of the problem, such as the reflection and transmission coefficients.

8.2.1 Extensions

First, we developed a method based on the integro-differential equation and asymptotic theory of the geometrical-optics approach for the simplest geometry of the problem, a half-plane horizontal planform of a floating plate (chapter 3). Then the technique was extended to other planforms of the floating plate, such as a strip-shaped plate (chapter 3), a circular plate (chapter 4), a ring-shaped plate (chapter 5), a quarter-infinite plate (chapter 6), and, finally, a plate of finite thickness (chapter 7).

The method can also be extended to the case of multiple strips; the solution for this problem is presented in [44], and to a plate of variable thickness. An extension to the latter case is straightforward for shallow water.

As the approach proposed is valid for both short and long waves, it can be used to study the interaction of water waves and middle- or small-sized floating structures. Our method can be applied for the ice-water interaction problem as well.

In the next sections, recommendations and a discussion on the future of VLFSs are given.



Figure 8.1: An application of our study: VLFS-water interaction.

8.3 Recommendations

Our approach is a large but only a first step to studying the behavior of real very large floating structures. Many different parameters and effects have to be considered. In our analyses, the bottom surface of the VLFS and the sea bed were assumed to be flat, however, in the analysis of a real floating structure they must have realistic non-flat shapes. Analytical approaches can be used/extended for the analysis of the realistic offshore structures.

Direct numerical methods can be used for real floating structures as well. In literature, a few numerical approaches can be found. The integral and integro-differential equations derived for the velocity potential and vertical displacement, respectively, in the thesis can also be solved numerically.

The approach developed may be also applied for offshore structures with piles; then an additional condition is needed: a zero for the plate deflection at each pile.

Despite the great interest in and many studies on the hydroelastic analysis of mat-like very large floating structures, there is still much work to be done. Directions for future study are also indicated by Watanabe et al. [143, 144].

Arbitrary (non-rectangular) shaped VLFSs should be analyzed further. In fact, the planform of the VLFS may be of any shape, which depends on its future purpose, location, sea/ocean currents, etc.

The effect of nonlinear waves has to be considered. The analysis based on linear waves is not valid in extreme situations such as large storms. These situations have to be considered in design for safety and survivability reasons. More research on the impact of tsunamis and typhoons on floating structures is expected.

VLFSs with an uneven (non-flat) bottom or hull have to be studied. Up to now, the bottom of VLFSs has usually been assumed to be flat. A non-uniform sea bed topography



Figure 8.2: An application of our study: ice-water interaction.

must also be taken into account. More work is needed on a realistic sea bed (non-flat) topography.

In addition, more studies are and knowledge is required on the use of mooring facilities [104, 151] and anti-motion devices [143] presented in figures 1.2 and 1.4, e.g., the use of smart active anti-motion control devices (so far, only passive anti-motion devices have been used).

It is expected that more studies will be done in the coming years on specific purposes for and, correspondingly, specific designs and shapes of the VLFS. Also, various new concepts of the VLFS system are/will be proposed, for instance a joined-separated VLFS design [104], which makes it multifunctional and easily movable.

8.4 Future of VLFS and VLFS for the future

Here we present our view on the future of VLFSs and the future VLFSs. Other opinions on their future can be found in [81, 104, 144, 151].

Coastal zones will continue to be developed in the next years, and so will very large floating structures.

Floating structures have been and will continue to be constructed mostly in bays, lakes or sea areas sheltered by islands and peninsulas. Since in these regions waves and wind do not act so strongly on the floating structures, the motions of the VLFSs are not so large either and they can easily be moored/held there [151]. When floating structures are located in the open sea, the design of mooring facilities is crucial for the safety of people and the structures themselves. More VLFSs are expected to be located far from the shore.

We think that VLFS have a great future. As predicted, VLFSs will be used for floating piers, docks, bridges, storage facilities, rescue bases, breakwaters, power plants, etc.; see

chapter 1, [143, 144, 141]. Also, already in 21st century, we may expect the construction of the first floating airport(s) or other huge artificial floating islands, and wide use of mobile offshore structures.

Other applications of very large floating structures are huge living complexes and even floating cities, first predicted by Jules Verne in his novel "A Floating City" (1871). This may become a reality sooner than one would expect.

Thus, in reply to Mark Twain and Jerome K. Jerome (see chapter 1), we may say that the production of land is resumed, and not only through land reclamation works, but also by the construction of new artificial floating islands in the sea, which can be used for many different purposes.

Bibliography

- [1] ABRAMOWITZ M. and STEGUN I.A. (1964). Handbook of Mathematical Functions with Formulas, Graphs, and Mathematical Tables. U.S. Government Printing Office, Washington, 1046p.
- [2] AMOS D.E. (1986). A Portable Package for Bessel Functions of a Complex Argument and Nonnegative Order. *ACM Transactions on Mathematical Software*, vol.12, p.265-273.
- [3] ANDRIANOV A.I. and HERMANS A.J. (2002a). A VLFP on Infinite, Finite and Shallow Water. *Proceedings of the 17th International Workshop on Water Waves and Floating Bodies*, Cambridge, UK, p.1-4.
- [4] ANDRIANOV A.I. and HERMANS A.J. (2002b). Diffraction of Surface Waves by VLFP on Infinite, Finite and Shallow Water. *Proceedings of the International Seminar Day on Diffraction' 2002*, Saint Petersburg, p.13-23.
- [5] ANDRIANOV A.I. and HERMANS A.J. (2003a). The Influence of Water Depth on the Hydroelastic Response of a Very Large Floating Platform. *Marine Structures*, vol.16, iss.5, p.355-371.
- [6] ANDRIANOV A.I. and HERMANS A.J. (2003b). Hydroelasticity of Quarter-Infinite Plate on Water of Finite Depth. *Proceedings of the 18th International Workshop on Water Waves and Floating Bodies*, Le Croisic, France, p.1-4.
- [7] ANDRIANOV A.I. and HERMANS A.J. (2004). Hydroelasticity of Elastic Circular Plate. *Proceedings of the 19th International Workshop on Water Waves and Floating Bodies*, Cortona, Italy, p.7-10.
- [8] ANDRIANOV A.I. and HERMANS A.J. (2005a). Hydroelasticity of a Circular Plate on Water of Finite or Infinite Depth. *Journal of Fluids and Structures*, vol.20, iss.5, p.719-733.
- [9] ANDRIANOV A.I. and HERMANS A.J. (2005b). Hydroelastic Behavior of a Floating Ring-Shaped Plate. *Journal of Engineering Mathematics*, *accepted*.
- [10] ANDRIANOV A.I. and HERMANS A.J. (2005c). Hydroelastic Analysis of Floating Plate of Finite Draft. *Proceedings of the 20th International Workshop on Water Waves and Floating Bodies*, Longyearbyen, Spitsbergen, Norway, p.13-16.

-
- [11] ATHANASSOULIS G.A. and BELIBASSAKIS K.A. (1999). A Consistent Coupled-Mode Theory for the Propagation of Small-Amplitude Water Waves over Variable Bathymetry Regions. *Journal of Fluid Mechanics*, vol.389, p.275-301.
- [12] BABICH V.M. and BULDYREV V.S. (1990). Short-Wavelength Diffraction Theory. Springer-Verlag, Berlin, 445p.
- [13] BABICH V.M. and KIRPICHNIKOVA N.YA. (1979). The Boundary-Layer Method in Diffraction Problems. Springer-Verlag, Berlin, 140p.
- [14] BALLARD R.D. (2001). Adventures in Ocean Exploration. National Geographic Society, Washington, 288p.
- [15] BALMFORTH N.J. and CRASTER R.V. (1999). Ocean Waves and Ice Sheets. *Journal of Fluid Mechanics*, vol.395, p.89-124.
- [16] BELIBASSAKIS K.A. and ATHANASSOULIS G.A. (2004). Three-Dimensional Green's Function for Harmonic Water Waves over a Bottom Topography with Different Depths at Infinity. *Journal of Fluid Mechanics*, vol.510, p.267-302.
- [17] BELIBASSAKIS K.A. and ATHANASSOULIS G.A. (2005). A Coupled-Mode Model for the Hydroelastic Analysis of Large Floating Bodies over Variable Bathymetry Regions. *Journal of Fluid Mechanics*, vol.531, p.221-249.
- [18] CHEUNG K.F., PHADKE A.C., SMITH D.A., LEE S.K and SEIDL L.H. (2000). Hydrodynamic Response of a Pneumatic Floating Platform. *Ocean Engineering*, vol.27, iss.12, p.1407-1440.
- [19] CHUNG H. and LINTON C.M. (2003). Interaction between Water Waves and Elastic Plates. *Proceedings of the 18th International Workshop on Water Waves and Floating Bodies*, Le Croisic, France, p.37-40.
- [20] CHURCHILL R.V. (1958). Operational Mathematics. McGraw-Hill Book Company, New York, 337p.
- [21] COLTON D. (1988). Partial Differential Equation (An Introduction). The Random House, New York, 308p.
- [22] COLTON D. and KRESS R. (1983). Integral Equation Methods in Scattering Theory. John Wiley & Sons, New York, 272p.
- [23] DAVIS J.L. (2000). Mathematics of Wave Propagation. Princeton University Press, Princeton, 395p.
- [24] DINGEMANS M.W. (1997). Water Wave Propagation over Uneven Bottoms. Part I. Linear Wave Propagation. World Scientific, Singapore, 471p.
- [25] DINGEMANS M.W. (1997). Water Wave Propagation over Uneven Bottoms. Part II. Non-linear Wave Propagation. World Scientific, Singapore, 495p.

- [26] DOETSCH G. (1950). Handbuch der Laplace-Transformation, Part I. Birkhäuser Verlag, Basel, 581p.
- [27] DORONIN YU.P. and KHEISIN D.E. (1977). Sea Ice. Amerind Publishing, New Delhi, 323p.
- [28] EATOCK TAYLOR R. and OHKUSU M. (2000). Green Functions for Hydroelastic Analysis of Vibrating Free-Free Beams and Plates. *Applied Ocean Research*, vol.22, iss.5, p.295-314.
- [29] ENDO H. (2000). The Behaviour a VLFS and an Airplane during Takeoff/Landing Run in Wave Condition. *Marine Structures*, vol.13, iss.6, p.477-491.
- [30] EVANS D.V. and DAVIES T.V. (1968). Wave-Ice Interaction. *Report 1313*, Davidson Lab – Stevens Institute of Technology, New Jersey.
- [31] EVANS D.V. and PORTER R. (2003). Wave Scattering by Narrow Cracks in Ice Sheets Floating on Water of Finite Depth. *Journal of Fluid Mechanics*, vol.484, p.143-165.
- [32] FOX C. and SQUIRE V.A. (1994). On the Oblique Reflexion and Transmission of Ocean Waves at Shore Fast Sea Ice. *Philosophical Transactions of the Royal Society of London, series A*, vol.347, iss.1682, p.185-218.
- [33] GAKHOV F.D. (1966). Boundary Value Problems. Pergamon Press, London, 564p.
- [34] GEHRING F. (1860). De Aequationibus Differentialibus Quibus Aequilibrium et Motus Laminae Crystallinae Definiuntur. Doctorate Thesis, Universität Berlin, Schultz, Berlin, 30p.
- [35] GOL'DSHTEIN R.V. and MARCHENKO A.V. (1989). The Diffraction of Plane Gravitational Waves by the Edge of an Ice Cover. *Journal of Applied Mathematics and Mechanics*, vol.53, iss.6, p.731-736.
- [36] GUÉRET R.A.M. and HERMANS A.J. (2001). Air Cushion under Floating Offshore Structure. *Proceedings of the 16th International Workshop on Water Waves and Floating Bodies*, Hiroshima, Japan, p.45-48.
- [37] GUÉRET R.A.M. (2002). Interaction of Free Surface Waves with Elastic and Air-Cushion Platforms. Doctorate Thesis, Delft University of Technology, ISBN 90-407-2357-5, 119p.
- [38] HAMAMOTO T. and FUJITA K. (2002). Wet-Mode Superposition for Evaluating the Hydroelastic Response of Floating Structures with Arbitrary Shape. *Proceedings of the 12th International Offshore and Polar Engineering Conference*, Kitakyushu, Japan, p.290-297.
- [39] HAVELOCK T.H. (1955). Waves Due to a Floating Sphere Making Periodic Heaving Oscillations. *Proceedings of the Royal Society of London, series A*, vol.231, p.1-7.

-
- [40] HERMANS A.J. (2000). A Boundary Element Method for the Interaction of Free-Surface Waves with a Very Large Floating Flexible Platform. *Journal of Fluids and Structures*, vol.14, iss.7, p.943-956.
- [41] HERMANS A.J. (2001a). A Geometrical-Optics Approach for the Deflection of a Floating Flexible Platform. *Proceedings of the 16th International Workshop on Water Waves and Floating Bodies*, Hiroshima, Japan, p.53-56.
- [42] HERMANS A.J. (2001b). A Geometrical-Optics Approach for the Deflection of a Floating Flexible Platform. *Applied Ocean Research*, vol.23, iss.5, p.269-276.
- [43] HERMANS A.J. (2003). The Ray Method for the Deflection of a Floating Flexible Platform in Short Waves. *Journal of Fluids and Structures*, vol.17, iss.4, p.593-602.
- [44] HERMANS A.J. (2004). Interaction of Free-Surface Waves with Floating Flexible Strips. *Journal of Engineering Mathematics*, vol.49, iss.2, p.133-147.
- [45] HERMANS A.J. (2005). Free-Surface Wave Interaction with a Thick Flexible Dock. *To be published*.
- [46] HORIKAWA K. and MARUO H. (editors) (1988). Nonlinear Water Waves. *IUTAM Symposium, Tokyo, 1987*. Springer-Verlag, Berlin, 466p.
- [47] ISOBE E. (1999). Research and Development of Mega-Float. *Proceedings of the 3rd International Workshop on Very Large Floating Structures*, Honolulu, USA, p.7-13.
- [48] JOHN F. (1949). On the Motion of Floating Bodies, I. *Communications on Pure and Applied Mathematics*, vol.2, p.13-57.
- [49] JOHN F. (1950). On the Motion of Floating Bodies, II. *Communications on Pure and Applied Mathematics*, vol.3, p.45-101.
- [50] JONES D.S. (1964). The Theory of Electromagnetism. Pergamon Press, Oxford, 807p.
- [51] KASHIWAGI M. (1998). A B-spline Galerkin Scheme for Calculating Hydroelastic Response of a Very Large Floating Structure in Waves. *Journal of Marine Science and Technology*, vol.3, iss.1, p.37-49.
- [52] KASHIWAGI M. (2000). Research on Hydroelastic Responses of VLFS: Recent Progress and Future Work. *International Journal of Offshore and Polar Engineering*, vol.10, iss.2, p.81-90.
- [53] KEVORKIAN J. and COLE J.D. (1996). Multiple Scale and Singular Perturbation Methods. Springer-Verlag, New York, 633p.
- [54] Khabakhpasheva T.I. and Korobkin A.A. (2001). Reduction of Hydroelastic Response of Floating Platform in Waves. *Proceedings of the 16th International Workshop on Water Waves and Floating Bodies*, Hiroshima, Japan, p.73-76.

-
- [55] Khabakhpasheva T.I. and Korobkin A.A. (2002). Exact Solutions of Floating Elastic Plate Problem. *Proceedings of the 17th International Workshop on Water Waves and Floating Bodies*, Cambridge, UK, p.81-84.
- [56] Kim J.W. and Ertekin R.C. (1998). An Eigenfunction-Expansion Method for Predicting Hydroelastic Behavior of a Shallow-Draft VLFS. *Proceedings of the 2nd International Conference on Hydroelasticity in Marine Technology*, Fukuoka, Japan, p.47-59.
- [57] Kirchhoff G.R. (1876). Vorlesungen über Mathematische Physik: Part I, Mechanik. Teubner, Leipzig, 466p.
- [58] Kline M. and Kay I.W. (1965). Electromagnetic Theory and Geometrical Optics. Interscience, New York, 527p.
- [59] Kochin N.E., Kibel I.A. and Roze N.V. (1964). Theoretical Hydromechanics. Interscience, New York, 577p.
- [60] Korn G.A. and Korn T.M. (1968). Mathematical Handbook for Scientists and Engineers: Definitions, Theorems and Formulas for Reference and Review. McGraw-Hill Book Company, New York, 831p.
- [61] Korobkin A.A. (2000). Numerical and Asymptotic Study of the Two-Dimensional Problem on Hydroelastic Behavior of a Floating Plate in Waves. *Journal of Applied Mechanics and Theoretical Physics*, vol.41, iss.2, p.286-293.
- [62] Kouzov D.P. (1963a). Diffraction of a Plane Hydroacoustic Wave on the Boundary of Two Elastic Plates. *Journal of Applied Mathematics and Mechanics*, vol.27, iss.3, p.806-815.
- [63] Kouzov D.P. (1963b). Diffraction of a Plane Hydro-Acoustic Wave at a Crack in an Elastic Plate. *Journal of Applied Mathematics and Mechanics*, vol.27, iss.6, p.1593-1601.
- [64] Lamb H. (1945). Hydrodynamics. Dover Publications, New York, 738p.
- [65] Landau L.D. and Lifshitz E.M. (1959). Fluid Mechanics. Pergamon Press, London, 536p.
- [66] Le Méhauté B. (1976). An Introduction to Hydrodynamics and Water Waves. Springer-Verlag, New York, 320p.
- [67] Lewis R.M. and Keller J.B. (1964). Asymptotic Methods for Partial Differential Equations: The Reduced Wave Equation and Maxwell's Equation. New York University, 68p.
- [68] Li R., Shu Z. and Wang Z. (2003). A Numerical and Experimental Study on the Hydroelastic Behavior of the Box-Typed Very Large Floating Structure in Waves. *Proceedings of the 13th International Offshore and Polar Engineering Conference*, Honolulu, USA, vol.I, p.113-120.

-
- [69] LIGHTHILL J. (1978). *Waves in Fluids*. Cambridge University Press, 504p.
- [70] LINTON C.M. and CHUNG H. (2003). Reflection and Transmission at the Ocean/Sea-Ice Boundary. *Wave Motion*, vol.38, p.43-52.
- [71] LOVE A.E.H. (1906). *A Treatise on the Mathematical Theory of Elasticity*. Cambridge University Press, 551p.
- [72] LUNEBURG R.K. (1964). *Mathematical Theory of Optics*. University of California Press, Berkeley, 448p.
- [73] MAGNUS W. and OBERHETTINGER F. (1949). *Formulas and Theorems for the Functions of Mathematical Physics*. Chelsea Publishing, New York, 172p.
- [74] MAMIDIPUDI P. and WEBSTER W.C. (1994). The Motions Performance of a Mat-Like Floating Airport. *Proceedings of the International Conference on Hydroelasticity in Marine Technology*, Trondheim, Norway, p.363-375.
- [75] MEI C.C. and BLACK J.L. (1969). Scattering of Surface Waves by Rectangular Obstacles in Waters of Finite Depth. *Journal of Fluid Mechanics*, vol.38, iss.3, p.499-511.
- [76] MEI C.C. and TUCK E.O. (1980). Forward Scattering by Long Thin Bodies. *SIAM Journal of Applied Mathematics*, vol.39, iss.3, p.178-191.
- [77] MEYLAN M.H. and SQUIRE V.A. (1996). Response of a Circular Ice Floe to Ocean Waves. *Journal of Geophysical Research*, vol.101, iss.C4, p.8869-8884.
- [78] MEYLAN M.H. (2001). A Variational Equation for the Wave Forcing of Floating Thin Plates. *Applied Ocean Research*, vol.23, iss.4, p.195-206.
- [79] MEYLAN M.H. (2002). Wave Response of an Ice Floe of Arbitrary Geometry. *Journal of Geophysical Research*, vol.102, iss.C1, p.5/1-5/11.
- [80] MINDLIN R.D. (1951). Influence of Rotatory Inertia and Shear on Flexural Motion of Isotropic Elastic Plates. *ASME Journal of Applied Mechanics*, vol.13, p.31-38.
- [81] MOAN T. (2003). *Marine Structures for the Future. CORE Report 2003-01*, Singapore, 52p.
- [82] MOLIN B. (2001). On the Piston and Sloshing Modes in Moonpools. *Journal of Fluid Mechanics*, vol.430, p.27-50.
- [83] MORSE P. and FESHBACH H. (1953). *Methods of Theoretical Physics*. McGraw-Hill Book Company, New York, Part I, 998p.
- [84] MORSE P. and FESHBACH H. (1953). *Methods of Theoretical Physics*. McGraw-Hill Book Company, New York, Part II, 980p.
- [85] MURAI M., INOUE Y. and NAKAMURA T. (2002). On the Prediction Method of a Hydroelastic Response of a VLFS Considering a Seabed Topography. *Journal of The Society of Naval Architects of Japan*, vol.192, p.309-318.

- [86] NAGATA S., YOSHIDA H., FUJITA T. and ISSHIKI H. (1998). Reduction of the Motion of an Elastic Floating Plate in Waves by Breakwaters. *Proceedings of the 2nd International Conference on Hydroelasticity in Marine Technology*, Fukuoka, Japan, p.229-238.
- [87] NAGATA S., YOSHIDA H., NIIZATO H., OHKAWA Y. and KOBAYASHI K. (2003). Effects of Breakwaters on Motions of an Elastic Plate in Waves. *International Journal of Offshore and Polar Engineering*, vol.13, iss.1, p.43-51.
- [88] NEWMAN J.N. (1977). *Marine Hydrodynamics*. The MIT Press, Cambridge, USA, 402p.
- [89] NOBLE B. (1958). *Methods Based on the Wiener-Hopf Technique*. Pergamon Press, Belfast, 246p.
- [90] NOBLESSE F. (1982). The Green Function in the Theory of Radiation and Diffraction of Regular Water Waves by a Body. *Journal of Engineering Mathematics*, vol.16, iss.2, p.137-169.
- [91] OHKUSU M. and NAMBA Y. (1996). Analysis of Hydroelastic Behaviour of a Large Floating Platform of Thin Plate Configuration in Waves. *Proceedings of the International Workshop on Very Large Floating Structures*, Hayama, Japan, p.143-148.
- [92] OHKUSU M. and NAMBA Y. (1998). Hydroelastic Behaviour of a Large Floating Platform of Elongated Form on Head Waves in Shallow Water. *Proceedings of the 2nd International Conference on Hydroelasticity in Marine Technology*, Fukuoka, Japan, p.177-183.
- [93] OHKUSU M. (1999). Hydroelastic Interaction of a Large Floating Platform with Head Seas. *Proceedings of the 14th International Workshop on Water Waves and Floating Bodies*, Port Huron, USA, p.119-122.
- [94] OHKUSU M. (2004). Horizontal Force on a Very Thin Plate in Waves. *Proceedings of the 19th International Workshop on Water Waves and Floating Bodies*, Cortona, Italy, p.151-154.
- [95] OHKUSU M. and NAMBA Y. (2004). Hydroelastic Analysis of a Large Floating Structure. *Journal of Fluids and Structures*, vol.19, iss.4, p.543-555.
- [96] OHMATSU S. (2001). Numerical Calculation Method for the Hydroelastic Response of a Pontoon-Type Very Large Floating Structure Close to a Breakwater. *Journal of Marine Science and Technology*, vol.5, iss.4, p.147-160.
- [97] PETER M.A., MEYLAN M.H. and CHUNG H. (2003). Wave Scattering by a Circular Plate in Water of Finite Depth: a Closed Form Solution. *Proceedings of the 13th International Offshore and Polar Engineering Conference*, Honolulu, USA, vol.I, p.180-185.

- [98] PETER M.A. and MEYLAN M.H. (2004). The Eigenfunction Expansion of the Infinite Depth Free Surface Green Function in Three Dimensions. *Wave Motion*, vol.40, p.1-11.
- [99] PHILLIPS O.M. (1966). The Dynamics of the Upper Ocean. Cambridge University Press, 261p.
- [100] PINKSTER J.A., FAUZI A., INOUE Y. and TABETA S. (1998). The Behaviour of Large Air Cushion Supported Structures in Waves. *Proceedings of the 2nd International Conference on Hydroelasticity in Marine Technology*, Fukuoka, Japan, p.497-505.
- [101] PORTER D. and PORTER R. (2004). Approximations to Wave Scattering by an Ice Sheet of Variable Thickness over Undulating Bed Topography. *Journal of Fluid Mechanics*, vol.509, p.145-179.
- [102] SEDOV L.I. (1965). Two-Dimensional Problems in Hydrodynamics and Aerodynamics. John Wiley & Sons, New York, 427p.
- [103] SETO H. and OCHI M. (1998). A Hybrid Element Approach to Hydroelastic Behaviour of a Very Large Floating Structure in Regular Waves. *Proceedings of the 2nd International Conference on Hydroelasticity in Marine Technology*, Fukuoka, Japan, p.185-193.
- [104] SHUKU M., HORIBA S., INOUE S., KOBAYASHI E. and SIMAMUNE S. (2001). Overview of Mega-Float and Its Utilization. Mitsubishi Heavy Industries, Ltd., *Technical Review*, vol.38, iss.2, p.39-46.
- [105] SLEPYAN L.I. and FADEEV V.M. (1988). Reflection, Refraction, and Emission of Waves in a Piecewise-Uniform Elastic System Interacting with a Fluid. *Doklady Physics*, vol.33, iss.3, p.236-238.
- [106] SOMMERFELD A. (1964). Optics. Academic Press, New York, 383p.
- [107] STOKER J.J. (1957). Water Waves. Interscience Publishers, New York, 567p.
- [108] STUROVA I.V. (2000). Diffraction of Shallow-Water Waves on a Floating Elastic Platform. *Journal of Applied Mathematics and Mechanics*, vol.64, p.1004-1012.
- [109] STUROVA I.V. (2001). The Diffraction of Surface Waves by an Elastic Platform Floating on Shallow Water. *Journal of Applied Mathematics and Mechanics*, vol.65, iss.1, p.109-117.
- [110] STUROVA I.V. (2002). The Action of Periodic Surface Pressures on a Floating Elastic Platform. *Journal of Applied Mathematics and Mechanics*, vol.66, iss.1, p.71-81.
- [111] STUROVA I.V. (2003). Response of Unsteady External Load on the Elastic Circular Plate Floating on Shallow Water. *Proceedings of the 18th International Workshop on Water Waves and Floating Bodies*, Le Croisic, France, p.177-180.

- [112] SVESHNIKOV A.G. and TIKHONOV A.N. (1982). The Theory of Functions of a Complex Variable. Mir, Moscow, 333p.
- [113] TAKAGI K. (1996). Interaction between Tsunami and Artificial Floating Island. *International Journal of Offshore and Polar Engineering*, vol.6, iss.3, p.171-176.
- [114] TAKAGI K. (1999). Hydroelastic Behavior of a Very Large Floating Structure. *Proceedings of the 14th International Workshop on Water Waves and Floating Bodies*, Port Huron, USA, p.137-140.
- [115] TAKAGI K., SHIMADA K. and IKEBUCHI Y. (2000). An Anti-Motion Device for a Very Large Floating Structure. *Marine Structures*, vol.13, p.421-436.
- [116] TAKAGI K. and KOHARA K. (2000). Application of the Ray Theory to Hydroelastic Behavior of VLFS. *Proceedings of the 10th International Offshore and Polar Engineering Conference*, Seattle, USA, p.72-77.
- [117] TAKAGI K. (2001a). Parabolic Approximation of the Hydro-Elastic Behavior of a Very Large Floating Structure in Oblique Waves. *Proceedings of the 16th International Workshop on Water Waves and Floating Bodies*, Hiroshima, Japan, p.153-156.
- [118] TAKAGI K. and NAGAYASU M. (2001b). Hydroelastic Behavior of a Mat-Type Very Large Floating Structure of Arbitrary Geometry. *Proceedings of the MTS/IEEE Conference and Exhibition Oceans 2001*, Honolulu, USA, vol.3, p.1923-1929.
- [119] TAKAGI K. (2002). Hydroelastic Response of a Very Large Floating Structure in Waves — a Simple Representation by the Parabolic Approximation. *Applied Ocean Research*, vol.24, p.175-183.
- [120] TAKAGI K. (2003). Analysis of Hydroelastic Behavior of a Very Large Mobile Offshore Structure in Waves. *Proceedings of the 18th International Workshop on Water Waves and Floating Bodies*, Le Croisic, France, p.181-184.
- [121] TAKAGI K. (2004). Quarter-Plane Problem of a Floating Elastic Plate. *Journal of Engineering Mathematics*, vol.48, iss.2, p.105-128.
- [122] TAKAGI K. and NOGUCHI J. (2005). PFFT-NASTRAN Coupling for Hydroelastic Problem of VLMOS in Waves. *Proceedings of the 20th International Workshop on Water Waves and Floating Bodies*, Longyearbyen, Spitsbergen, Norway, p.241-244.
- [123] TIKHONOV A.N. (1963). Equations of Mathematical Physics. Pergamon Press, Oxford, 781p.
- [124] TIMOSHENKO S.P. and WOINOWSKY-KRIEGER S. (1959). Theory of Plates and Shells. McGraw-Hill, New York, 580p.
- [125] TIMOSHENKO S.P., YOUNG D.H. and WEAVER W. (1974). Vibration Problems in Engineering. John Wiley & Sons, New York, 521p.
- [126] TKACHEVA L.A. (2001a). Surface Waves Diffraction on a Floating Elastic Plate. *Fluid Dynamics*, vol.36, iss.5, p.776-789.

- [127] TKACHEVA L.A. (2001b). Scattering of Surface Waves by the Edge of a Floating Elastic Plate. *Journal of Applied Mechanics and Technical Physics*, vol.42, p.638-646.
- [128] TKACHEVA L.A. (2001c). Hydroelastic Behavior of a Floating Plate in Water. *Journal of Applied Mechanics and Technical Physics*, vol.42, p.991-996.
- [129] TKACHEVA L.A. (2002). Diffraction of Surface Waves at a Thin Elastic Plate. *Proceedings of the 17th International Workshop on Water Waves and Floating Bodies*, Cambridge, UK, p.175-178.
- [130] TKACHEVA L.A. (2003). Plane Problem of Surface Wave Diffraction on a Floating Elastic Plate. *Fluid Dynamics*, vol.38, iss.3, p.465-481.
- [131] TRANTER C.J. (1968). Bessel Functions with Some Physical Applications. The English Universities Press, London, 148p.
- [132] TSUBOGO T. (2001). The Motion of an Elastic Disk on Shallow Water in Waves. *Proceedings of the 11th International Offshore and Polar Engineering Conference*, Stavanger, Norway, vol.I, p.229-233.
- [133] USHA R. and GAYATHRI R. (2005). Wave Motion over a Twin-Plate Breakwater. *Ocean Engineering*, vol.32, iss.8-9, p.1054-1072.
- [134] UTSUNOMIYA T., WATANABE E. and EATOCK TAYLOR R. (1998). Wave Response Analysis of a Box-Like VLFS Close to a Breakwater. *Proceedings of the 17th International Conference on Offshore Mechanics and Arctic Engineering*, p.1-8.
- [135] UTSUNOMIYA T. and WATANABE E. (2001). Accelerated Green's Function Method for Wave Response of Very Large Floating Structures. *Proceedings of the 16th Ocean Engineering Symposium*, The Society of Naval Architects of Japan, p.313-320.
- [136] UTSUNOMIYA T., WATANABE E. and NISHIMURA N. (2001). Fast Multipole Method for Hydrodynamic Analysis of Very Large Floating Structures. *Proceedings of the 16th International Workshop on Water Waves and Floating Bodies*, Hiroshima, Japan, p.161-164.
- [137] VAN DYKE M. (1964). Perturbation Methods in Fluid Mechanics. Academic Press, New York, 229p.
- [138] WANG C.D. and MEYLAN M.H. (2004). A Higher-Order-Coupled Boundary Element Method and Finite Element Method for the Wave Forcing of a Floating Elastic Plate. *Journal of Fluids and Structures*, vol.19, p.557-572.
- [139] WANG C.M., XIANG Y., WATANABE E. and UTSUNOMIYA T. (2004). Mode Shapes and Stress-Resultants of Circular Mindlin Plates with Free Edges. *Journal of Sound and Vibration*, vol.276, p.511-525.
- [140] WATANABE E., MARUYAMA T., TANAKA M. and TAKEDA S. (2000). Design and Construction of a Floating Swing Bridge in Osaka. *Marine Structures*, vol.13, iss.4-5, p.437-458.

-
- [141] WATANABE E. (2003) Floating Bridges: Past and Present. *Structural Engineering International*, vol.13, no.2, p.128-132.
- [142] WATANABE E., UTSUNOMIYA T., WANG C.M. and XIANG Y. (2003). Hydroelastic Analysis of Pontoon-Type Circular VLFS. *Proceedings of the 13th International Offshore and Polar Engineering Conference*, Honolulu, USA, vol.I, p.93-99.
- [143] WATANABE E., UTSUNOMIYA T. and WANG C.M. (2004). Hydroelastic Analysis of Pontoon-Type VLFS: a Literature Survey. *Engineering Structures*, vol.26, iss.2, p.245-256.
- [144] WATANABE E., WANG C.M., UTSUNOMIYA T. and MOAN T. (2004). Very Large Floating Structures: Applications, Analysis and Design. *CORE Report 2004-02*, Singapore, 30p.
- [145] WATSON G.N. (1944). A Treatise on the Theory of Bessel Functions. Cambridge University Press, 804p.
- [146] WEHAUSEN J.V. and LAITONE E.V. (1960). Surface Waves. *Encyclopedia of Physics*, vol.9, Springer-Verlag, Berlin, p.446-814 (*also at* <http://www.coe.berkeley.edu/SurfaceWaves>).
- [147] WHITHAM G.B. (1974). Linear and Nonlinear Waves. John Wiley & Sons, New York, 636p.
- [148] WHITTAKER E.T. and WATSON G.N. (1920). A Course of Modern Analysis. Cambridge University Press, 608p.
- [149] WU C., WATANABE E. and UTSUNOMIYA T. (1995). An Eigenfunction Matching Method for Analyzing the Wave Induced Responses of an Elastic Floating Plate. *Applied Ocean Research*, vol.17, p.301-310.
- [150] YEUNG R.W. and KIM J.W. (2000). Effects of a Translating Load on a Floating Plate-Structural Drag and Plate Deformation. *Journal of Fluids and Structures*, vol.14, iss.7, p.993-1011.
- [151] YONEYAMA H., HIRAISHI T. and UEDA S. (2004). Recent Technological Advances of Ship Mooring Analysis and Construction of Floating Structures in Japan. *PIANC Bulletin*, vol.116, p.79-89.
- [152] YOSHIMOTO M., HOSHINO K., OHMATSU S. and IKEBUCHI T. (1997). Slamming Load Acting on a Very Large Floating Structure with Shallow Draft. *Journal of Marine Science and Technology*, vol.2, iss.3, p.163-172.
- [153] ZILMAN G. and MILOH T. (2000). Hydroelastic Buoyant Circular Plate in Shallow Water: a Closed Form Solution. *Applied Ocean Research*, vol.22, p.191-198.

Conferences' proceedings

- [154] Proceedings of the International Conference(s) on Offshore Mechanics and Arctic Engineering (OMAE), annual, <http://www.omae.org>.
- [155] Proceedings of the International Offshore and Polar Engineering Conference(s) (ISOPE), annual, <http://www.isope.org>.
- [156] Proceedings of the International Workshop(s) on Water Waves and Floating Bodies (IWWF), annual. <http://www.rina.org.uk/showarticle.pl?id=6330&n=560>.

Also:

Proceedings of the International Conference(s) on Hydroelasticity in Marine Technology (also known as series 'Hydroelasticity in Marine Technology').

Proceedings of the International Workshop(s) on Very Large Floating Structures.

Websites (VLFS, Mega-Float)

- [157] Introduction of Mega-Float.
http://www.srcj.or.jp/html/megafloat_en/.
- [158] National Maritime Research Institute of Japan.
<http://www.nmri.go.jp>
- [159] Structurae: International Database and Gallery of Structures.
<http://www.structurae.de>

Also:

http://www.mlit.go.jp/english/maritime/mega_float.html
<http://www.riam.kyushu-u.ac.jp/ship/>
<http://str.kuciv.kyoto-u.ac.jp/>
<http://www.centrair.jp>
http://www.city.kobe.jp/cityoffice/39/port/airport/airport_e.htm
<http://www.hongkongairport.com>
<http://www.airport.or.kr>
<http://www.floatinc.com>
<http://www.noort-innovations.nl>
<http://www.flyland.nl>
<http://www.jsce-int.org/Publication/CivilEng/2000/realizing.pdf>
<http://www.eng.nus.edu.sg/core/>
<http://www.eng.nus.edu.sg/EResnews/0406/>
<http://www.uh.edu/engines/epi1638.htm>
<http://oe.ore.hawaii.edu/~vlfs/>
<http://xtreme.eng.hawaii.edu/research-projects/vlfs/>
<http://www.seastead.org>
<http://www.kordi.re.kr>

Index

- Circular plate 67
 - finite depth 77
 - infinite depth 73
- Deflection 36
 - circular plate 37, 73
 - plate of finite draft 38, 125
 - quarter-infinite plate 38, 110
 - ring-shaped plate 37, 93
 - semi-infinite plate 36, 54
 - strip 37, 51
- diffraction 28
- Elastic plate 26
- Free edge conditions 27
- free-surface elevation 41, 79, 92
- Geometrical-optics approach 110
- Green's function 32, 50
 - in Cartesian coordinates 33, 50, 55, 127
 - in polar coordinates 35, 71, 92
- Green's theorem 39, 49
- Incident waves 22
 - potential, finite depth 31
 - potential, infinite depth 30
 - potential, shallow depth 32
- integral equation (IE) 39
- integro-differential equation (IDE) 41
- integro-differential equation method (IDEM)
 - 18, 140
- initiated wave pattern 80, 100
- Laplace equation 24, 28, 46, 69, 89, 108, 123
- Lindstedt method 125
- Mega-Float 9
- Plate deflection, *see* deflection
- plate of finite draft 121
- Purposes of VLFS 5
- Quarter-infinite plate 107
- Radiation 29
- Reflection 32, 53
 - coefficient 32, 53, 56, 59
- recommendations 142
- ring-shaped plate 87
 - finite depth 98
 - infinite depth 96
- Semi-infinite plate 45
- strip of infinite length 45
- Thin plate theory 26
- transmission 32, 54
 - coefficient 32, 54, 56, 59
- Velocity potential 24, 28, 46, 69, 89, 108, 123
- VLFP 2, 45
- VLFS 2, 3, 5, 45, 139
- VLFS system 8
- Water depth 28
 - finite 31
 - infinite 30
 - shallow 31

Summary

Hydroelastic Analysis of Very Large Floating Structures

Alexey Andrianov

Due to the growth of their population, urban development and the corresponding expansion of land use, several countries have decided to build artificial islands in the sea space (and other water space) to decrease the pressure on the heavily used land space. The traditional method, reclamation of the land from the sea, is already widely applied, but there is also an attractive new alternative: construction of very large floating structures, proposed by researchers, naval and civil architects and engineers. Very large floating structures can and are already being used for storage facilities, industrial space, bridges, ferry piers, docks, rescue bases, breakwaters, airports, entertainment facilities, military purposes, even habitation, and other purposes. The floating structure can be speedily constructed, exploited, and easily relocated, expanded, or removed. These structures are reliable, cost-effective, and environmentally friendly floating artificial islands, that obey multistage reliability principle.

The subject of this thesis is hydroelastic analysis of a very large floating structure, i.e., the study of the motion of a floating structure and its response to surface water waves. The main idea in the concepts proposed is to build a very large mat-like structure whose thickness is very small compared to its horizontal length parameters. Various problems of the interaction between this very large floating structure and water waves are treated in the thesis. The main objective of our study is to derive an analytical solution and numerical results for various shapes and dimensions of the floating plate. The geometrical sketches of the plate considered are rectangular and arbitrary horizontal planforms.

The plate deflection and free-surface elevation, which are the vertical displacements in the plate and the open-water regions, respectively, and the reflection and transmission of water waves are studied using different theories of applied mathematics, mechanics and hydrodynamics, e.g., water wave propagation and diffraction theories, Kirchhoff's theory of thin plates, and the Green's theorem. New approaches for the hydroelastic analysis of the VLFSs are proposed; they are based on a general integro-differential equation method, which is developed in chapter 2 and applied in the following chapters, and on the geometrical-optics approach, the ray method (chapter 6), and the Lindstedt method (chapter 7). Three different models of water depth are considered: shallow water for a floating structure quite close to the shore, the general and universal case of finite water depth, which is of main interest, and 'infinitely' deep water for structures located far into

the open sea.

The problem background and introduction, literature survey and information on current and future floating structures are given in chapter 1. Chapter 2 describes the general theory, the basic equations and conditions, introduces and formulates particular problems considered, and proposes a method of solution. The problems for the following models and horizontal shapes of a very large floating platform are solved in the thesis: a semi-infinite plate and a strip of infinite length in chapter 3, a circular plate in chapter 4, a ring-shaped plate in chapter 5, a quarter-infinite plate in chapter 6, and a plate of finite thickness in chapter 7. Analytical solutions together with representations and operations for specific cases are described in the corresponding chapters. Chapters 3–7 also give concluding remarks, possible method extensions and suggestions for other plate planforms. General conclusions, recommendations and a discussion on very large floating structures in and of the future are given in chapter 8. Numerical results are obtained for practically important and relevant situations for different values of wavelength, water depth, plate characteristics and other physical parameters of the problem.

The research carried out in the thesis may be applied to predict the behavior of floating structures and their hydroelastic response to water waves. Also the interaction between large ice sheets or fields and surface waves can be described with the method presented.

Samenvatting

Hydroelastische analyse van zeer grote drijvende structuren

Alexey Andrianov

Verscheidene landen hebben, wegens groei van de bevolking, stedelijke ontwikkeling en overeenkomstige uitbreiding van het gebruikte land, beslist de ruimte op zee (en andere waterruimte) te gebruiken om kunstmatige eilanden aan te leggen om de druk op intensief gebruikte landruimte te verminderen. Dit kan op een traditionele manier worden gedaan, terugwinning van het land op de zee, tegenwoordig breed toegepast, of op een nieuwe aantrekkelijke alternatieve manier: bouw van zeer grote drijvende structuren, voorgesteld door onderzoekers, maritieme en civiele ingenieurs. De zeer grote drijvende structuren kunnen en worden reeds gebruikt voor opslagfaciliteiten, industriële ruimte, als bruggen, ferry pieren, dokken, noodhavens, golfbrekers, luchthavens, vermaak faciliteiten, voor militaire doeleinden, wonen, en andere doeleinden. De drijvende structuur kan snel worden geconstrueerd, geëxploiteerd, en gemakkelijk worden verplaatst, uitgebreid of verwijderd. Deze drijvende kunstmatige eilanden zijn betrouwbaar, voldoen ook een 'multilevel' betrouwbaarheidsprincipe, rendabel en milieuvriendelijk.

Het onderwerp van dit proefschrift is een hydroelastische analyse van een zeer grote drijvende structuur, i.e. de studie van de bewegingen van een drijvende structuur en zijn reactie op oppervlaktewatergolven. Het belangrijkste idee in voorgestelde concepten is een zeer grote mat-vormige structuur te bouwen waarbij de dikte van de structuur zeer klein is in vergelijking met de horizontale lengteparameters. Diverse problemen van de interactie tussen de zeer grote drijvende structuur en watergolven worden behandeld in het proefschrift. De belangrijkste doelstelling van onze studie is een afleiding van een analytische oplossing met numerieke resultaten voor diverse vormen en afmetingen van de drijvende plaat. De beschouwde horizontale geometrie van de plaat is rechthoekig of willekeurig.

De deflectie van de plaat en de vrije-oppervlakteverhoging, welke respectievelijk de verticale verplaatsingen van de plaat en van de open-watergebieden zijn de terugkaatsing en de transmissie van watergolven worden bestudeerd met gebruik van verschillende theorieën uit de toegepaste wiskunde, mechanica en hydrodynamica, zoals de propagatie en de diffractietheorieën van watergolven, Kirchhoff theorie van dunne platen, Greense theorema's. Nieuwe benaderingen voor de hydroelastische analyse van drijvende structuren worden voorgesteld; zij zijn gebaseerd op een algemene integraal-differentiaal vergelijking methode, die in hoofdstuk 2 wordt ontwikkeld en in het volgende hoofdstukken wordt

toegepast, de geometrische optica benadering, stralenmethode (hoofdstuk 6), en Lindstedt methode (hoofdstuk 7). Drie verschillende gevallen van waterdiepte worden beschouwd: ondiep water wanneer de drijvende structuur dichtbij de kust is, het algemene geval van eindige waterdiepte (het moeilijkste en belangrijkste geval), en 'oneindig' diep water wanneer de structuur zich in open zee ver van de kust bevindt.

De probleem achtergrond en inleiding, het literatuur onderzoek en informatie over bestaande en voorgestelde drijvende structuren worden gegeven in hoofdstuk 1. Vervolgens beschrijft de auteur in hoofdstuk 2 de algemene theorie, basis vergelijkingen en voorwaarden, inleiding en formulering van speciale gevallen, voorgestelde methode van oplossing. De problemen voor de volgende vormen van het zeer grote drijvende platform worden opgelost in het proefschrift: een half-oneindige plaat en een strook van oneindige lengte in hoofdstuk 3, een cirkelplaat in hoofdstuk 4, een ringvormige plaat in hoofdstuk 5, een kwart-oneindige plaat in hoofdstuk 6, een plaat van eindige dikte in hoofdstuk 7. Hoofdstukken 3–7 geven naast analytische oplossingen, mogelijke methode uitbreidingen en suggesties voor andere plaatvormen, en ook numerieke resultaten; de numerieke resultaten zijn verkregen voor in de praktijk belangrijke en relevante situaties voor verschillende waarden van de golflengte, waterdiepte, kenmerken van het platform en andere parameters van dit probleem. In hoofdstuk 8 staan algemene conclusies, aanbevelingen en bespreking van zeer grote drijvende structuren in en voor toekomst.

Het onderzoek dat in het proefschrift is uitgevoerd, kan worden toegepast om het gedrag van drijvende structuren en hun hydroelastische reactie op watergolven te voorspellen. De interactie tussen grote ijsbladen of ijsgebieden en oppervlaktegolven kan ook met gebruik van de voorgestelde methode worden beschreven.

Résumé

Аннотация

Гидроупругий анализ больших плавающих структур

Алексей Андрианов

Япония, Нидерланды и другие страны, в связи с ростом численности населения, ускоренным развитием промышленности и соответствующим уменьшением свободных сухопутных территорий, активно используют морское пространство для строительства искусственных островов. Для этого существуют два способа. Первый, традиционный – создание насыпных островов; второй, относительно новый – строительство больших плавающих структур (БПС). БПС могут использоваться в качестве промышленных и складских сооружений, нефтехранилищ, пристаней, доков, спасательных баз, волнорезов, аэропортов, военных баз, жилых помещений, и т.д. БПС могут быть быстро построены и введены в эксплуатацию, а также легко перемещены, расширены или разобраны. БПС надежны, дешевы по сравнению с насыпными островами, экологически безопасны для окружающей среды. Инженерный расчет, на котором базируется проектирование БПС, требует детального теоретического анализа их взаимодействия с волнами на поверхности жидкости. Гидроупругому анализу БПС и посвящена настоящая диссертация.

Поскольку толщина БПС существенно меньше её горизонтальных размеров, в принятой расчетной схеме она заменяется тонкой упругой пластиной, которую можно рассматривать в рамках теории Кирхгоффа. Жидкость считается идеальной.

Целью исследования является получение аналитических решений и численных результатов для различных геометрических форм и размеров плавающих пластин, что позволяет сделать некоторые общие выводы о поведении БПС при взаимодействии их с волнами на поверхности жидкости.

Вертикальные отклонение пластины и свободной поверхности воды, отражение и прохождение волн исследуются при помощи методов математики, прикладной математики, теоретической механики и гидродинамики. В частности, применяются ТФКП, теории интегральных преобразований и интегральных уравнений, распространения и дифракции волн.

Предложены новые подходы для гидроупругого анализа взаимодействия пластин с жидкостью, основанные на интегро-дифференциальном уравнении, описанном в главе 2, и методах геометрической оптики (глава 6) и Линдстедта (глава 7). Рассматриваемые задачи решены для трех моделей жидкости: теории мелкой воды,

бесконечной и конечной глубин. Последний случай представляет основной интерес, поскольку именно он наиболее характерен для практических приложений.

Введение, обзор литературы и информация о БПС, уже построенных и проектируемых, приведены в главе 1.

В главе 2 описаны общая теория, основные уравнения и граничные условия, формулировки рассматриваемых частных задач, а также предложенный метод решения.

Далее рассмотрены задачи для следующих моделей пластины: полуплоскость и полоса бесконечной длины в главе 3, круговая пластина в главе 4, кольцеобразная пластина в главе 5, четвертьплоскость в главе 6. Во всех этих случаях глубина погружения пластины в жидкость не учитывается. Исследованию этого вопроса посвящена глава 7. Наряду с аналитическими решениями получены численные результаты для практически реальных значений параметров. В главах 3–7 приведены следующие из результатов исследования выводы и обсуждены возможности применения развитых методов к другим задачам, например, для исследования взаимодействия между большими ледяными полями и поверхностными волнами на воде.

Общие выводы, предложения и обсуждение будущего БПС содержатся в главе 8.

Résumé

Резюме

Гідропружний аналіз великих плаваючих структур

Олексій Андріанов

Японія, Нідерланди та інші країни, у зв'язку із зростанням чисельності населення, прискореним розвитком промисловості і відповідним зменшенням вільних сухопутних територій, активно використовують морський простір для будівництва штучних островів. Для цього існують два способи. Перший, традиційний – створення насипних островів; другий, відносно новий – будівництво великих плаваючих структур (ВПС). ВПС можуть використовуватися як промислові та складські споруди, нафтосховища, мости, пристані, доки, рятувальні бази, хвилерізи, аеропорти, військові бази, житлові приміщення, і т.ін. ВПС можуть бути швидко побудовані та введені в експлуатацію, а також легко переміщені, розширені або розібрані. ВПС надійні, екологічно безпечні для навколишнього середовища, дешеві відносно насипних островів. Інженерний розрахунок, на якому базується проектування ВПС, вимагає детального теоритичного аналізу їх взаємодії з хвилями на поверхні рідини. Гідропружному аналізу ВПС і присвячена ця дисертація.

Оскільки товщина ВПС істотно менша за її горизонтальні розміри, у прийнятій розрахунковій схемі вона замінюється тонкою пружною пластиною, яку можна розглядати в рамках теорії Кірхгофа. Рідина вважається ідеальною.

Метою дослідження є отримання аналітичних рішень і чисельних результатів для різних геометричних форм і розмірів плаваючих пластин, що дозволяє зробити деякі загальні висновки про поведінку ВПС при взаємодії їх з хвилями на поверхні рідини.

Вертикальні відхилення пластини та вільної поверхні води, відраження і проходження хвиль досліджуються за допомогою методів математики, прикладної математики, теоретичної механіки та гідродинаміки. Зокрема, застосовуються ТФКП, теорії інтегральних перетворень та інтегральних рівнянь, розповсюдження і дифракції хвиль.

Запропоновані нові підходи для гідропружного аналізу взаємодії пластин з рідиною, засновані на інтегро-диференційному рівнянні, описаному у розділі 2, методі геометричної оптики (розділ 6) і метода Ліндстедта (розділ 7). Дані задачі розв'язані для трьох моделей: теорії мілкої води, нескінченної і кінцевої глибин. Останній випадок представляє основний інтерес, оскільки саме він найбільш характерний для практичних застосувань.

Вступ, огляд літератури та інформація про ВПС, вже побудовані і проєктовані, приведені у розділі 1.

У розділі 2 описані загальна теорія, основні рівняння та граничні умови, формулювання частинних задач, а також запропонований метод розв'язання.

Далі розглянути задачі для наступних моделей пластини: напівплощина та смуга нескінченної довжини у розділі 3, кругова пластина у розділі 4, кільцеподібна пластина у розділі 5, чвертьплощина у розділі 6. У всіх цих випадках глибина занурення пластини в рідину не враховується. Дослідженню цього питання присвячений розділ 7. Разом з аналітичним розв'язанням одержані чисельні результати для практично реальних значень параметрів. У розділах 3–7 також приведені наступні з результатів дослідження висновки і обговорені можливості застосування розвинутих методів до інших задач.

Загальні висновки, пропозиції і обговорення майбутнього ВПС містяться у розділі 8.

Запропонований у дисертації метод може також застосовуватися для дослідження взаємодії між великими крижаними полями і поверхневими хвилями на воді.

Acknowledgements

We all have dreams. Doing and completing Ph.D. in interesting modern field, under supervision of an excellent scientist and teacher, at a nice department of a world-famous university was one of my dreams. This dream became a reality in Delft University of Technology. I have spent four and half excellent, fruitful and interesting years in small beautiful Delft, where I have met a lot of nice people, who became real friends for me and who helped me. At the same time, I felt strong support and understanding from my family and old friends. Acknowledgements are one of the most important part of my thesis because I really desire to thank all people whose friendship, favour, leadership, support and interest helped me in general and, in particular, to complete my Ph.D. study...

First of all, my greatest thanks go to my supervisor Professor Aad Hermans, for his education, ideas, inspiration, advises, prompt and clear comments about our work, answers on many questions, and constant enthusiasm and interest. I consider myself as a very happy person to work with such an outstanding researcher as a supervisor. And I learned a lot about research, scientific philosophy and other things, for instance, how to get joy from the equations and problems (of course, after they are solved). Being 38th Ph.D. of Aad is not only a pleasure, but a big responsibility, hence, I hope this thesis conformed his constantly high research standards. Dank je wel, Aad, for guiding me in worlds of Hydrodynamics and Applied Mathematics, that are nice but not the easiest to walk on and to work on.

I am deeply grateful to my first scientific supervisor Professor Vladimir Loboda from Dnepropetrovsk National University. My first steps in science were made under his outstanding and inimitable supervision and I have learned a lot from him.

Next, I am grateful to Professors Gregory Zilman, Alexander Korobkin, Ken Takagi, Izolda Sturova, Larisa Tkacheva, Gerassimos Athanassoulis, Makoto Ohkusu, Touviah Miloh, Marshall Tulin and other researchers from different institutions of The Netherlands, Russia, Japan, Israel, England, USA and other countries for valuable and useful discussions, information, comments. Special thanks to Ken for providing numerical data for a comparison and JSPS affairs. Attending the conferences is one of the best parts of Ph.D. study. Here, I also want to acknowledge many people which attended the conferences: International Workshops on Water Waves and Floating Bodies (IWWWFB), Days on Diffraction, and Advanced Problems in Mechanics (APM), for great atmosphere, interesting meetings, scientific and general discussions. I am also thankful to colleagues in many countries whom I was in contact with because of research.

My acknowledgements go to Wim van Horsen for organizing and arranging many

things, helping me with coming to Delft, talks and advises. To Kees Lemmens I am very thankful because of his help with computers, different software, advises and conversations. Thanks to Eef Hartman on the same matter. Next, I would like to thank the secretaries of our department, Judith Ormskerk, Mirjam Nielsen, and Evelyn Sharabi, for organizing and help on different things. For help with papers, visas, etc., I am thankful to CICAT project assistants, Durk Jellema, Martine van der Laag-Hoogendijk, and Manon Post. To Manon, especially, for 'heads up!' and our talks.

I received a lot of different help during my Ph.D. study, so as at the time of writing the thesis. I am very grateful to Mirjam Nieman who improved the English of the thesis significantly and made a lot of suggestions. Thanks to Henric Corstens who checked my Dutch in 'samenvatting en stellingen'.

After previous acknowledgements of more or less scientific and professional origin, I would like to thank my friends. I am really grateful to many people for their friendship, support, our contacts and conversations. To Ayşe Kaslilar special thanks for her openness and kindness, our discussions and talks about everything during smoking together tours. Great thanks go to Dwi Riyanti, in particular, for her optimism, talks and advises, and to Xander Campman for his 'introduction into Dutch life', hiking, conversations, and help. Dwi and Xander, extra thanks for agreeing to be my paranimfen (*paranymphs*) on 9/9/2005. I am deeply grateful to Svetlana Ponomaryeva, especially for her smile, beauty, nice mood, and encouragement. To her, Daria Spivakovskaya, for our friendship in particular, and Maria Zarubinskaya for help, interest, common events and talks (*all in Russian!*). I am thankful to Remus Hanea, also for talks and watching football together, to Renaud Guéret for scientific discussions and excellent flat on de Vlouw with view on Nieuwe Kerk, and to other colleagues, which also became friends for me. And, of course, our common parties, intellectual, sport, celebration and drinking activities, hiking tours, trips, days out were just great.

I want to thank my colleagues from the Mathematical Physics group and all the Department of Applied Mathematics (TW) for many scientific, about- and non-scientific discussions, seminars, useful advises and information, and for their assistance. Also, I thank all of my colleagues whose names are already mentioned, and Gérard Herman, Auke Ditzel, Gerrit van Ballegooijen, Peter van Beek, Marleen Keijzer, Kees Korving, Hai Xiang Lin, Gede Suweken and all other present and former members of the department for friendly atmosphere on our 3rd/5th floor. Some very good traditions of the department were supplemented by new ones introduced by us; hopefully, they all will be kept. Working together with such interesting, competent and energetic people was a big pleasure for me. Thanks a lot / dank je wel / спасибо! Words of gratitude are also addressed to Anna Dall'Acqua, Blagoy Iliev and many others from Delft Institute of Applied Mathematics, Faculty of Electrical Engineering, Mathematics and Computer Science (EWI), and TU Delft.

In 4.5 years at TU I had eight roommates at office HB 03.270/05.260, which always was an international (and multi-lingual) room with a nice atmosphere, jokes, and help to each other. My words of gratitude correspond to Darmawijoyo, Timber Haaker, Valeriy Gayko, Chris Chartrand, Saad Ibrahim, Nengah Suparta, Veselin Vavrek, and Alina Barbu.

My thanks go to Svetlana Trofimova, Timofey Gerasimov, Inna Gitman, Yuliya Efimova, those who mentioned above and all other members of 'Russian Club of Delft' for

time and fun together.

I would like to thank colleagues, lecturers and professors from the Department of Applied and Theoretical Mechanics of the Faculty of Mechanics and Mathematics of the Dnepropetrovsk National University for their lectures, knowledges, and help. To all my groupmates from group MH-94-1 of DNU I am very grateful for our friendship, common and always young spirit, and good memories.

I am deeply grateful to my dear friends in Dnepropetrovsk whose friendship, openness, support, optimism, advises, emotions helped and will help me. Vlad Ivanik, Anna Ilyenko, Andrey Sergeev, Vyacheslav Chudakov, Evgeniy Karakash, Alexandr Peschanskiy, Konstantin Voytsekhovskiy, Konstantin Dovgopolo, Olga Vasilyeva, many others... thank you all / спасибо / дякую! For our unforgettable conversations, disputes, activities, trips to Crimea and other places, parties, for so many things. I am very thankful to many other my friends and colleagues in Dnepropetrovsk and Ukraine, in Moscow, especially Larisa Lesnichaya, St. Petersburg, especially Alexandr Lesnichi and his family, Elena Grekova and Sergey Gavrilov, and Russia, and in many different places of the world. To Victoria Olenich, in particular, I am thankful for her openness, cheerfulness, interest and support. Special thanks go to Olga Shipilova.

Sport and, of course, football are very important for me. Football team 'Op het Randje' (*On the Edge*), where I have been playing in last 4.5 years, is the best team, at least in Holland, and almost always winning. Here I want to express my special gratitude to Robbert Kleerebezem, Fulco Kramer, Martijn Hoebe, Bart Ebus, Jelle Hijmisen, Taco Dekker, Alexey Cherepanov, Roelco Kleijn, Victor Papavasileiou, Antonio Martins, all former and present players of 'Op 't Randje' (<http://www.ophetrandje.tk>). Guys, I thank you all not only for playing football together, great team spirit, fantastic victories, titles collected, passes obtained and goals scored, but also for your friendship, help, all our events, talks and discussions. *Actually, my stay in Delft results not only in this thesis, but also in 153 goals in 108 matches in University championships.*

Great thanks to all people with whom I played badminton, tennis, volleyball, basketball, did many other sports in these years. And thanks a lot to all who joined me for traveling through different cities and places in Europe, hiking, mountain climbing, sight-seeing, laying on beaches, swimming, cycling, playing snowballs, who visited me here, in Delft, or whom I visited in these years...

In addition, I am grateful to L.N. Tolstoy, F.M. Dostoevsky, P. Coelho, O. Mityaev, Y. Shevchuk and to many other people whom I do not know personally, but whose books, music or ideas helped me a lot in my life.

I am deeply grateful to beautiful and charming ladies who inspired and encouraged me, and stimulated me to move forward in the last years, also for inimitable feelings, emotions and the joy of living.

I am infinitely grateful to my family for their love, kindness, cheerfulness, inspiration, understanding, support, 'lightness', time and trips together, and for everything they did, do, and will do for me. How can I express what I feel for you in words?.. I love you so much. Расстояние между близкими людьми не может быть измерено в километрах!

To my dear brother Vladimir Belenko I am especially thankful for his enthusiasm, support, music, and jokes, and much more. Спасибо, Володя!

My thesis is dedicated to my parents, both of them are very good persons and excellent scientists. Following their track, I entered Mathematics and Mechanics faculty and decided to stay in research. I am very thankful to my parents for their guidance and advises, activity and motivation.

To my father, Igor Andrianov, I am especially grateful for his help, understanding, always right and clear analysis, and encouragement. Папа, спасибо!

My very greatest thanks go to my mother, Valentina Lesnichaya, in particular for her education, teaching, encouragement, all kinds of support, ideas and spirit, composure and optimism, and for everything. Мама, спасибо!

Thanks a lot! Спасибо!

*Alexey Andrianov
Delft, July 2005*

Curriculum Vitae

Alexey Andrianov was born on 16th October 1977 in Dnepropetrovsk, Ukraine, former USSR. He lived and studied in primary and secondary schools in Ukraine and Russia.

In 1994 he obtained the school-leaving certificate and entered at the Dnepropetrovsk National University. In 1995 he started a research work in the field of Fracture Mechanics under supervision of Prof. Vladimir V. Loboda at the Department of Theoretical and Applied Mechanics. In June 1999 Alexey Andrianov defended his Master thesis "The Investigation of a Strip with Interface Cracks along the Fixed Edges under Bending Load" and obtained M.Sc. degree in Mechanics and Applied Mathematics. He continued the research work in Dnepropetrovsk National University till December 2000.

From January 2001 Alexey Andrianov follows a Ph.D. research program at the Department of Applied Mathematics, Delft University of Technology in Delft, The Netherlands. He works on the project "The Interaction between Very Large Floating Structures and Water Waves" under supervision of Prof. Aad J. Hermans. The research is related to Hydrodynamics and Applied Mathematics and concerning the problems of fluid-structure interaction. The work which has been done in January 2001 – July 2005 results in the thesis entitled "Hydroelastic Analysis of Very Large Floating Structures", to be defended on 9th September 2005 in Delft.



Alexey Andrianov

alex@andrianov.org

alexey@andrianov.org

<http://www.andrianov.org>

a.i.andrianov@ewi.tudelft.nl

<http://ta.twi.tudelft.nl/users/andrianov>

Names explanation.

My first name 'Alexey' is written in Ukrainian passport as 'Olexiy' (my official first name) and as shortified 'Alex' in some of publications and documents.

Dnepropetrovsk is Dnipropetrovsk (Dnipropetrovs'k) in Ukrainian.

Dnepropetrovsk State University became Dnepropetrovsk National University in 2000.